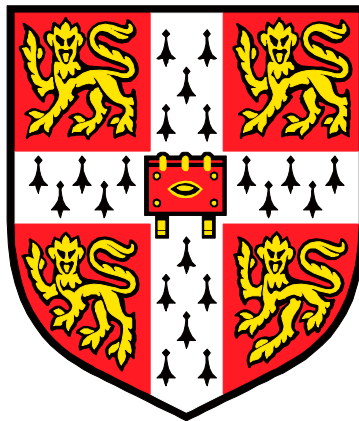


**ROLE OF TWO GENES,
CACNA1D AND *CADM1*, WITH
COMMON OR RARE
MUTATIONS IN ALDOSTERONE
PRODUCING ADENOMAS OF
THE ADRENAL.**

SUMEDHA GARG

GONVILLE AND CAIUS COLLEGE



UNIVERSITY OF CAMBRIDGE

DECEMBER 2018

This dissertation is submitted for the degree of Doctor of Philosophy

ROLE OF TWO GENES, *CACNA1D* AND *CADM1*, WITH COMMON OR RARE MUTATIONS IN ALDOSTERONE PRODUCING ADENOMAS OF THE ADRENAL

Submitted By – Ms Sumedha Garg

Primary aldosteronism (PA) accounts for 5-10% of all hypertension. One of the major causes of PA is sporadic formation of aldosterone-producing adenomas (APAs). These benign tumours develop in the cortical region of adrenal glands and autonomously secrete excessive amounts of aldosterone. This hormone increases sodium retention and water reabsorption by the kidneys, leading to high blood pressure. Landmark discoveries of somatic mutations in APAs led to better understanding of molecular mechanisms causing autonomous aldosterone secretion. The first mutations were found in *KCNJ5*, followed by *ATP1A1*, *ATP2B3* and *CACNA1D*, all encoding cation-channels or transporters. Several *in vitro* studies showed disruption of cellular ion-balance leading to the phenotype of hyper-aldosterone secretion from APAs.

Following our lab's discovery of initial four somatic mutations by whole exome sequencing, over 30 single-base change mutations have been reported in the *CACNA1D* gene, which encodes the α_1 subunit of an L-type Ca^{2+} channel (LTCC), $\text{Ca}_v1.3$. Initial and several subsequent mutations cause electrophysiological gain-of-function with increased activation and/or slowed inactivation of $\text{Ca}_v1.3$. Prior to the discovery of these mutations, L-type Ca^{2+} channels were not considered important in regulation of aldosterone production. In the first part of my thesis, I investigated two of the mutations and showed that the gain-of-function results in increased aldosterone secretion from an adrenocortical carcinoma cell line, H295R, when transiently transfected with the mutants. I also showed that $\text{Ca}_v1.3$ can play a role in physiological aldosterone secretion, finding that CYP11B2 expression is reduced by 50% in the adrenals of $\text{Ca}_v1.3$ knockout mice. The discovery of mutations in *CACNA1D* led to a [REDACTED] Award from [REDACTED] in which high-throughput screening of $\text{Ca}_v1.3$ -expressing cells was undertaken against [REDACTED] 1.8M compound library. I identified the adrenal isoforms of the channel's alpha and beta subunits (*CACNA1D* and *CACNB2*), and helped development of the stable HEK293 cell line used for screening. This led to 3 tool compounds (A, B & C) that were selective antagonists for $\text{Ca}_v1.3$ over [REDACTED] in high-throughput electrophysiological experiments using [REDACTED] and [REDACTED] platforms. I showed compound B to effectively inhibit aldosterone secretion in both H295R and primary adrenal cells isolated from a normal adrenal. This finding is a significant step in developing compound B further into a $\text{Ca}_v1.3$ -selective drug for treating PA patients without cardiovascular side effects as in the case of existing dihydropyridine class of Ca^{2+} channel blockers.

The second part of my thesis focused on genotyping and whole exome sequencing of 59 APAs from 52 patients, in order to identify further genes underlying primary aldosteronism. Mutations in previously reported genes were identified in 34 of the APAs (57.6%). *CACNA1D* was the most commonly mutated gene (20.3%) in this cohort, but not *KCNJ5* (16.9%) as previously reported. This variation in the frequencies observed is perhaps due to the different

methods used for screening PA. For example, many of our patients were detected by renin measurement in resistant hypertension, and their APA identified by a unique PET-CT (using C¹¹ metomidate), in place of adrenal vein sampling.

In addition to this, novel somatic mutation was found in a gene not encoding an ion channel, however, this protein was previously linked to cell-cell adhesion and tumour suppression. The gene identified is *CADM1*, a cell adhesion molecule 1, and the mutation found leads to substitution of valine by aspartate [REDACTED] in the single transmembrane domain of this cell surface protein. The likely significance of this discovery was greatly enhanced when we ascertained that one of the 'private' somatic mutations found on whole exome sequencing of APAs in Munich was in fact a similar substitution in the adjacent amino acid [REDACTED] of the membrane-spanning domain.

High expression of *CADM1* in zona glomerulosa (ZG) was found, the site of aldosterone synthesis in the adrenal cortex and in the APAs, as well as the aldosterone producing cell clusters (APCCs) within the ZG. *In vitro* experiments using H295R cells showed both mutations in *CADM1* lead to 10-20 fold upregulation of *CYP11B2* transcription, on qPCR, resulting in 2-4-fold increase of aldosterone secretion, compared to the wild-type *CADM1*. Despite the introduction of a negative charge into the transmembrane domain, both mutants could translocate to the cell surface. The evidence to date, points to the loss of cell-cell adhesion in the presence of mutant *CADM1* as the cause of uncontrolled aldosterone synthesis. Silencing of *CADM1* in H295R cells revealed downregulation of aldosterone synthesis and secretion. Transcriptome analysis by RNAseq, of H295R cells expressing wild-type or mutant *CADM1* or silenced *CADM1* showed a large number of differentially expressed genes. Mutant *CADM1* upregulated genes involved in steroidogenesis and ACTH response pathways. A possible role of *CADM1* was found to be in the regulation of inter-cell communication via gap junction protein, connexin-43 (Cx43). This was upregulated with higher expression on plasma membrane in the *CADM1* silenced cells. TSG101, a protein involved in lysosomal degradation of Cx43 was downregulated in the absence of *CADM1* and possibly the mechanism for increased Cx43 expression. Also, immunostaining of adrenal sections showed internalised para-nuclear staining localisation of Cx43 in the ZG, APAs and APCCs, regions with high *CADM1* expression compared to membranous localisation of Cx43 in ZF.

In contrast to the common and numerous mutations in *CACNA1D*, mutations in *CADM1* are rare. Nonetheless, they may enhance our understanding of the functional significance of glomerular structure of the outer zone of adrenal cortex, where cell-cell adhesion and intercellular communication appear critical for the regulation of aldosterone secretion.

DECLARATION

This dissertation is the result of my own work and includes nothing which is the outcome of work done in collaboration except as declared in the Preface and specified in the text.

It is not substantially the same as any that I have submitted, or, is being concurrently submitted for a degree or diploma or other qualification at the University of Cambridge or any other University or similar institution except as declared in the Preface and specified in the text. I further state that no substantial part of my dissertation has already been submitted, or, is being concurrently submitted for any such degree, diploma or other qualification at the University of Cambridge or any other University or similar institution except as declared in the Preface and specified in the text.

It does not exceed the prescribed word limit (60,000 words) for the relevant Degree Committee (Clinical Medicine and Clinical Veterinary Medicine).

Sumedha Garg

December 2018

CONTENTS

THESIS SUMMARY	7
PREFACE	9
ACKNOWLEDGEMENTS.....	10
ABBREVIATIONS.....	12
LIST OF FIGURES	14
LIST OF TABLES.....	17
CHAPTER 1 - INTRODUCTION	18
1.1 Hypertension and Primary aldosteronism.....	18
1.2 Adrenal gland and steroidogenesis	20
1.3 Aldosterone	21
1.3.1 Regulation of aldosterone synthesis	21
1.3.2 Mechanism of aldosterone action.....	24
1.3.3 Effects of aldosterone excess	24
1.4 Identification, diagnosis and management of PA.....	25
1.4.1 Lateralisation of APAs.....	26
1.4.2 Management of PA.....	27
1.5 APAs: subtypes, somatic mutations and prevalence	28
1.5.1 Prevalence of mutations in known genes	32
1.6 Aims of the study.....	34
CHAPTER 2 - MATERIALS AND METHODS	35
2.1 General methods	35
2.1.1 Reagents and antibodies	35
2.1.2 Human adrenal tissue collection and processing.....	36
2.1.3 H295R and primary cell culture	37
2.1.4 Genomic DNA extraction	37
2.1.5 Sanger sequencing.....	37
2.1.6 RNA extraction from human tissues.....	38
2.1.7 RNA extraction from cultured cells	38

2.1.8	cDNA synthesis	38
2.1.9	Real Time – quantitative PCR and data analysis.....	39
2.1.10	Immunohistochemistry	39
2.1.11	Plasmids used and their propagation.....	40
2.1.12	Lentivirus production and titration	41
2.1.13	Lentivirus transduction.....	42
2.1.14	Immunocytochemistry and confocal imaging	43
2.1.15	Drug treatments on H295R and primary cells.....	43
2.1.16	Aldosterone assay.....	43
2.1.17	Protein assay and Western blotting	44
2.1.18	Statistics analysis	44

CHAPTER 3 - ROLE OF L-TYPE CALCIUM CHANNEL, Cav1.3 IN ALDOSTERONE SECRETION .. 45

3.1	Abstract.....	45
3.2	Introduction	47
3.2.1	L-type calcium channels	47
3.2.2	Regulation of Cav1.3 channel kinetics	48
3.2.3	Expression and pathophysiology of Cav1.3	49
3.2.4	Role as transcription factor	50
3.2.5	Calcium channels in adrenals	51
3.2.6	Cav1.3 antagonists.....	52
3.2.7	Cav β_2 subunit.....	53
3.2.8	Aims and Hypotheses	55
3.3	Materials and methods.....	56
3.3.1	Molecular cloning and site directed mutagenesis.....	56
3.3.2	Electrophysiology.....	60
3.3.3	Transfection of H295R cells by electroporation	62
3.3.4	Western blotting.....	62
3.3.5	RNA extraction from mice adrenals	63
3.3.6	High-throughput compound screening at [REDACTED]	63
3.4	Results.....	70
3.4.1	Isoform and expression analysis of Cav1.3 in normal adrenal cortex & APAs ...	70

3.4.2	Isoform and expression analysis of β subunit in normal adrenal cortex & APAs ..	71
3.4.3	Mutant Cav1.3 upregulates aldosterone secretion	71
3.4.4	Whole-cell patch-clamp electrophysiology	73
3.4.5	Localisation of endogenous Cav1.3 in H295R cells.....	79
3.4.6	Cleaved C-terminus of Cav1.3 translocates to nucleus and upregulates aldosterone secretion.....	80
3.4.7	Cav1.3 is a substrate for calpain proteases	82
3.4.8	Silencing of Cav1.3 in H295R cells.....	84
3.4.9	Cav1.3 knockout mice show down-regulated <i>CYP11B2</i> expression.....	85
3.4.10	Effect of Cav1.3 selective inhibition by compounds A, B & C on aldosterone secretion	86
3.5	Discussion	88

CHAPTER 4 - GENOTYPING AND WHOLE EXOME SEQUENCING OF APAs TO FIND NEW SOMATIC MUTATIONS..... 92

4.1	Abstract.....	92
4.2	Introduction	94
4.2.1	Aim and Hypotheses	94
4.3	Materials and methods.....	95
4.3.1	Sample gDNA preparation and selection	95
4.3.2	Samples/patients in the study	95
4.3.3	Targeted hotspot sequencing - primers and PCR conditions	97
4.3.4	WES sample preparation and QC	98
4.3.5	WES methodology	98
4.3.6	Somatic mutation detection-Mutect2 pipeline.....	98
4.4	Results.....	100
4.4.1	Sample workflow and mutation detection.....	100
4.4.2	New cases with mutations in known genes	101
4.4.3	Novel somatic mutations - <i>CADM1</i>	102
4.5	Discussion	104

CHAPTER 5 - NOVEL MUTATIONS IN CELL ADHESION MOLECULE, *CADM1* FOCUS ATTENTION ON THE SIGNIFICANCE OF CELL-CELL COMMUNICATION IN ALDOSTERONE SECRETION.. 106

5.1	Abstract.....	106
5.2	Introduction.....	108
5.2.1	CADM1 gene discovery and structure.....	108
5.2.2	CADM1 protein structure and processing.....	109
5.2.3	Physiological function in various tissues.....	110
5.2.4	Pathological roles of CADM1.....	113
5.2.5	<i>CADM1</i> expression in human adrenal.....	115
5.2.6	Connexin-43/ <i>GJA1</i> in human adrenal.....	116
5.2.7	Case report of patient 184, CADM1mutant APA.....	117
5.2.8	Aims and Hypotheses.....	122
5.3	Materials and methods.....	123
5.3.1	RNA extraction from FFPE sections of 184NT.....	123
5.3.2	RT-PCR primers and conditions.....	123
5.3.3	CADM1 cloning and mutagenesis.....	123
5.3.4	CADM1 shRNA cloning.....	124
5.3.5	Cell culture media concentration.....	125
5.3.6	Western blotting.....	126
5.4	Results.....	127
5.4.1	CADM1 transcripts in H295R cells, human adrenal and APAs.....	127
5.4.2	CADM1 protein localisation in human adrenal and APAs.....	128
5.4.3	Confirmation of mutant allele expression in 184T cDNA.....	132
5.4.4	Mutant CADM1 proteins are processed differentially by proteases.....	133
5.4.5	Mutant CADM1 upregulates aldosterone synthesis.....	135
5.4.6	Aldosterone secretion is not regulated by ICD of CADM1.....	139
5.4.7	Mutant CADM1 disrupts inter cellular adhesion.....	143
5.4.8	CADM1 silencing downregulates aldosterone synthesis.....	145
5.4.9	Possible link between CADM1 & a gap junction protein, Connexin-43.....	147
5.4.10	RNAseq for CADM1-WT vs mutants overexpressing H295R cells.....	152
5.4.11	RNAseq for CADM1 silenced H295R cells.....	153
5.4.12	RNAseq for CADM1 APA vs other ZG-like APAs.....	155

5.5	Discussion	158
CHAPTER 6 - CONCLUSIONS		163
Appendix	164
Buffer recipes		164
REFERENCES		165

THESIS SUMMARY

Primary aldosteronism (PA) accounts for 5-10% of all hypertension. One of the major causes of PA is sporadic formation of aldosterone-producing adenomas (APAs). These benign tumours develop in the cortical region of adrenal glands and autonomously secrete excessive amounts of aldosterone. This hormone increases sodium retention and water reabsorption by the kidneys, leading to high blood pressure. Landmark discoveries of somatic mutations in APAs led to better understanding of molecular mechanisms causing autonomous aldosterone secretion. The first mutations were found in *KCNJ5*, followed by *ATP1A1*, *ATP2B3* and *CACNA1D*, all encoding cation-channels or transporters. Several *in vitro* studies showed disruption of cellular ion-balance leading to the phenotype of hyper-aldosterone secretion from APAs.

Following our lab's discovery of initial four somatic mutations by whole exome sequencing, over 30 single-base change mutations have been reported in the *CACNA1D* gene, which encodes the α_1 subunit of an L-type Ca^{2+} channel (LTCC), $\text{Ca}_v1.3$. Initial and several subsequent mutations cause electrophysiological gain-of-function with increased activation and/or slowed inactivation of $\text{Ca}_v1.3$. Prior to the discovery of these mutations, L-type Ca^{2+} channels were not considered important in regulation of aldosterone production. In the first part of my thesis, I investigated two of the mutations and showed that the gain-of-function results in increased aldosterone secretion from an adrenocortical carcinoma cell line, H295R, when transiently transfected with the mutants. I also showed that $\text{Ca}_v1.3$ can play a role in physiological aldosterone secretion, finding that CYP11B2 expression is reduced by 50% in the adrenals of $\text{Ca}_v1.3$ knockout mice. The discovery of mutations in *CACNA1D* led to a [REDACTED] [REDACTED] from [REDACTED] in which high-throughput screening of $\text{Ca}_v1.3$ -expressing cells was undertaken against [REDACTED] 1.8M compound library. I identified the adrenal isoforms of the channel's alpha and beta subunits (*CACNA1D* and *CACNB2*), and helped development of the stable HEK293 cell line used for screening. This led to 3 tool compounds (A, B & C) that were selective antagonists for $\text{Ca}_v1.3$ over [REDACTED] in high-throughput electrophysiological experiments using [REDACTED] and [REDACTED] platforms. I showed compound B to effectively inhibit aldosterone secretion in both H295R and primary adrenal cells isolated from a normal adrenal. This finding is a significant step in developing compound B further into a $\text{Ca}_v1.3$ -selective drug for treating PA patients without cardiovascular side effects as in the case of existing dihydropyridine class of Ca^{2+} channel blockers.

The second part of my thesis focused on genotyping and whole exome sequencing of 59 APAs from 52 patients, in order to identify further genes underlying primary aldosteronism. Mutations in previously reported genes were identified in 34 of the APAs (57.6%). *CACNA1D* was the most commonly mutated gene (20.3%) in this cohort, but not *KCNJ5* (16.9%) as

previously reported. This variation in the frequencies observed is perhaps due to the different methods used for screening PA. For example, many of our patients were detected by renin measurement in resistant hypertension, and their APA identified by a unique PET-CT (using C¹¹ metomidate), in place of adrenal vein sampling.

In addition to this, novel somatic mutation was found in a gene not encoding an ion channel, however, this protein was previously linked to cell-cell adhesion and tumour suppression. The gene identified is *CADM1*, a cell adhesion molecule 1, and the mutation found leads to substitution of valine by aspartate [REDACTED] in the single transmembrane domain of this cell surface protein. The likely significance of this discovery was greatly enhanced when we ascertained that one of the 'private' somatic mutations found on whole exome sequencing of APAs in Munich was in fact a similar substitution in the adjacent amino acid [REDACTED] of the membrane-spanning domain.

High expression of *CADM1* in zona glomerulosa (ZG) was found, the site of aldosterone synthesis in the adrenal cortex and in the APAs, as well as the aldosterone producing cell clusters (APCCs) within the ZG. *In vitro* experiments using H295R cells showed both mutations in *CADM1* lead to 10-20 fold upregulation of *CYP11B2* transcription, on qPCR, resulting in 2-4-fold increase of aldosterone secretion, compared to the wild-type *CADM1*. Despite the introduction of a negative charge into the transmembrane domain, both mutants could translocate to the cell surface. The evidence to date, points to the loss of cell-cell adhesion in the presence of mutant *CADM1* as the cause of uncontrolled aldosterone synthesis. Silencing of *CADM1* in H295R cells revealed downregulation of aldosterone synthesis and secretion. Transcriptome analysis by RNAseq, of H295R cells expressing wild-type or mutant *CADM1* or silenced *CADM1* showed a large number of differentially expressed genes. Mutant *CADM1* upregulated genes involved in steroidogenesis and ACTH response pathways. A possible role of *CADM1* was found to be in the regulation of inter-cell communication via gap junction protein, connexin-43 (Cx43). This was upregulated with higher expression on plasma membrane in the *CADM1* silenced cells. TSG101, a protein involved in lysosomal degradation of Cx43 was downregulated in the absence of *CADM1* and possibly the mechanism for increased Cx43 expression. Also, immunostaining of adrenal sections showed internalised para-nuclear staining localisation of Cx43 in the ZG, APAs and APCCs, regions with high *CADM1* expression compared to membranous localisation of Cx43 in ZF.

In contrast to the common and numerous mutations in *CACNA1D*, mutations in *CADM1* are rare. Nonetheless, they may enhance our understanding of the functional significance of glomerular structure of the outer zone of adrenal cortex, where cell-cell adhesion and intercellular communication appear critical for the regulation of aldosterone secretion.

PREFACE

Parts of this PhD work have been featured in following publications-

1. Xie, C. B., Shaikh, L. H., **Garg, S.**, Tanriver, G., Teo, A. E. D., Zhou, J., Maniero, C., Zhao, W., Kang, S., Silverman, R. B., Azizan, E. A. B., and Brown, M. J. (2016) Regulation of aldosterone secretion by Cav1.3. *Sci. Rep.* 6, 24697.

During this PhD I have co-authored following publications-

1. Teo, A. E. D., **Garg, S.**, Haris Shaikh, L., Zhou, J., Karet Frankl, F. E., Gurnell, M., Happerfield, L., Marker, A., Bienz, M., Azizan, E. A. B., and Brown, M. J. (2015) Pregnancy, Primary Aldosteronism, and Adrenal CTNNB1 Mutations. *N. Engl. J. Med.* 10.1056/NEJMoa1504869.
2. Shaikh, L. H., Zhou, J., Teo, A. E. D., **Garg, S.**, Neogi, S. G., Figg, N., Yeo, G. S., Yu, H., Maguire, J. J., Zhao, W., Bennett, M. R., Azizan, E. a B., Davenport, A. P., McKenzie, G., and Brown, M. J. (2015) LGR5 activates non-canonical Wnt-signaling and inhibits aldosterone production in the human adrenal. *JCEM.* 10.1210/jc.2015-1734.
3. Maniero, C., **Garg, S.**, Zhao, W., Johnson, T. I., Zhou, J., Gurnell, M., and Brown, M. J. (2017) NEFM (Neurofilament Medium) Polypeptide, a Marker for Zona Glomerulosa Cells in Human Adrenal, Inhibits D1R (Dopamine D1 Receptor)-Mediated Secretion of Aldosterone. *Hypertension.* 70, 357–364.
4. Teo, A. E. Der, **Garg, S.**, Johnson, T. I., Zhao, W., Zhou, J., Gomez-Sanchez, C. E., Gurnell, M., and Brown, M. J. (2017) Physiological and Pathological Roles in Human Adrenal of the Glomeruli-Defining Matrix Protein NPNT (Nephronectin). *Hypertension.* 10.1161/HYPERTENSIONAHA.117.09156.

Parts of this PhD work have been presented in the form of posters at following conferences-

1. Progress in Primary Aldosteronism (PiPA) Biennial Meeting 2015 (Munich, Germany) – **Travel award for best abstracts.**
2. British Heart Foundation Fellows Meeting 2017 (Cambridge, UK).

ACKNOWLEDGEMENTS

Undertaking this PhD would have not been possible without the support and encouragement I received from many people. This has been a truly exceptional journey not only in my scientific career but also on a personal front.

I would like to express my sincere thanks to my supervisors, Prof Morris Brown and Prof Mark Gurnell for their guidance and support. They gave me an opportunity to conduct research in their group and mentored my scientific knowledge and skills for which I will always be grateful.

I would also like to acknowledge the support and encouragement I received from Prof Sadaf Farooqi in pursuing my research interest. Without the time spent and skills learnt in her research group prior to this PhD, I would have not been able to complete this phase of my career with such success.

I would like to thank my fellow research students, especially Dr Ada Teo and Dr Carmen Maniero who not only contributed routinely to collection of surgical adrenal tissues from Human Tissue Bank, but also for our lively discussions. I am glad I had their company to share and get through the periods of uncertainty we had during our PhD. Ada's friendly nature in the department gave me a smooth start and this friendship will be cherished for a long time.

I am sincerely grateful to Ms Sarah Cleary & Dr Yasmin for making my time in the department truly enjoyable and memorable. They helped and supported me unconditionally when I needed it the most. I can never imagine myself to have seen through the completion of this work without their kindness, which uplifted my spirits at some of the most difficult times.

I dedicate this thesis to my parents who have always taught me to work hard and supported me in every phase of my life. My mother always motivated and believed in me even when I doubted myself. My sister always brought so much laughter and joy in my life and kept me going. Above all, I cannot describe in words the support and love that my best friend and husband Chetan showered upon me at all times. His sacrifices and constant support during this phase of my career made it possible for me to achieve my PhD. Lastly, with the arrival of our most precious daughter 'Mishka' in our life on 16 May 2018, motivated me to complete the PhD dissertation on time, so I can spend more time with her!

I would also like to thank British Heart Foundation for funding this work (FS/14/75/31134), and Gonville and Caius College for their help and financial support all these years.

Acknowledgments of specific help and support-

I would like to thank Prof Annette Dolphin at UCL for welcoming me in her laboratory where Dr Wojciech Margas taught and helped me with electrophysiology experiments with expertise and a lot of patience.

Hard work put in by the team of scientists at [REDACTED], led by [REDACTED] & [REDACTED] for the [REDACTED] project and shortlisting of 3 tool compounds selective for Cav1.3 over [REDACTED].

Adrenals from Cav1.3 knockout mice were provided by Dr Petronel Tuluc, University of Innsbruck. Dr Lu Long, EMIT and Mrs Debra Rimmington, Institute of Metabolic Sciences provided the adrenals for age and gender matched wild-type mice of the same strain.

Teams of Dr Chaz Mein at Barts and the London Genome Centre & Dr Roger Foo at Genome Institute of Singapore performed the whole exome sequencing of our DNA samples. Transcriptome analysis by RNAseq for CADM1 project was also done by Dr Chaz Mein's team.

Dr Claudia Cabrera at Centre for Translational Bioinformatics, QMUL & Dr Roger Foo's team conducted the Mutect2 analysis for sequencing data.

Dr Wanfeng Zhao at Human Tissue Bank for optimising and performing immunohistochemistry for aquaporin 2, AQP2.

Mouse monoclonal CYP11B2 antibody was a kind gift from Dr Celso Gomez Sanchez, University of Mississippi.

Mr Gregory Strachan, provided the training and access to microscopy facilities (Leica SP8 confocal microscope and Zeiss Axioscan slide scanner) at the Institute of Metabolic Sciences

Dr Anna Petrunkina and her team at NIHR Cambridge BRC Cell Phenotypic hub provided training and access to flow cytometer FACS Canto II.

Dr Cassie Ragnauth and Mr Carl Spickett at Department of Medical Genetics for access and help with the use of Pherastar plate reader required for aldosterone HTRF assay.

ABBREVIATIONS

ACE	Angiotensin Converting Enzyme
ACTH	Adrenocorticotrophic Hormone
ADH	Antidiuretic Hormone
AngII	Angiotensin II
APA	Aldosterone producing adenoma
APPCC	Aldosterone producing cell clusters
ARR	Aldosterone-Renin-ratio
AVS	Adrenal Vein Sampling
BAH	Bilateral Adrenal Hyperplasia
CaM	Calmodulin
CAMK	Calmodulin kinase
CCB	Calcium channel blocker
CDI	Calcium dependent inactivation
CT	C-terminal
CT/PET-CT	Computed Tomography/Positron Emission Tomography-CT
CTM	C-terminal modulatory domain (of Cav1.3)
DCRD	Distal C-terminal regulatory domain (of Cav1.3)
DHP	Dihydropyridine
ENaC	Epithelial sodium channel
EV	Empty vector
FLIPR	Fluorescence Imaging Plate Reader
GATK	Genome Analysis Tool Kit
GJIC	Gap junctional intercellular communication
█	█
HTRF	Homogeneous Time Resolved Fluorescence
LTCC	L-type calcium channel
mAb	Monoclonal antibody

MR	Mineralocorticoid receptor
MRI	Magnetic Resonance Imaging
NT	N-terminal
PA	Primary Aldosteronism
pAb	Polyclonal antibody
PAC	Plasma aldosterone concentration
PASNA	Primary Aldosteronism with Seizures and Neurologic Abnormalities
PCRD	Proximal C-terminal regulatory domain (of Cav1.3)
pM	picoMolar
PMA	Phorbol-12-myristate-13-acetate
qPCR	Quantitative-PCR
RT-PCR	Reverse Transcriptase PCR
s.e.m.	Standard error of mean
SAN	Sino atrial node
SANDD	Sino atrial node dysfunction and deafness
shRNA	Short-hairpin RNA
UT	Untreated/Untransfected/Untransduced
VDI	Voltage dependent inactivation
VGCC	Voltage-gated calcium channel
WES	Whole exome sequencing
WT	Wild-type
ZF	Zona fasciculata
ZG	Zona glomerulosa
ZR	Zona reticularis

LIST OF FIGURES

Fig. 1: Categorisation of hypertension and underlying causes.....	18
Fig. 2: Categorisation of hyperaldosteronism and their underlying causes.....	19
Fig. 3: Haematoxylin and eosin (H&E) staining of human adrenal gland showing its histology	20
Fig. 4: Steroidogenesis in human adrenal gland.....	21
Fig. 5: Renin-angiotensin-aldosterone system (RAAS)	22
Fig. 6: Molecular pathways for aldosterone secretion in ZG cells.....	23
Fig. 7: Effects of aldosterone excess on various tissues/systems.....	25
Fig. 8: Schematic representation of diagnosis and treatment of primary aldosteronism.	26
Fig. 9: Proposed model for constitutive aldosterone secretion from APAs with somatic mutations.....	30
Fig. 10: Alternative splicing of β_2 subunit transcripts.....	54
Fig. 11: Sequences for scrambled (a) and Cav1.3 (b) shRNAs in pLVTH	60
Fig. 12: [REDACTED]	65
Fig. 13: [REDACTED]	66
Fig. 14: [REDACTED]	67
Fig. 15: [REDACTED]	67
Fig. 16: [REDACTED]	68
Fig. 17: Endogenous calcium subunit expression in normal adrenal and APAs.....	70
Fig. 18: AngII stimulation of aldosterone secretion from transfected H295R cells.....	71
Fig. 19: Subcellular localisation of transfected Cav1.3 WT or mutants (GFP-tagged) in H295R cells.	72
Fig. 20: Exemplary IV-traces for all Cav1.3 WT and mutants expressed with β_3 and $\alpha_2\delta$ -1 subunits.....	73
Fig. 21: Current-voltage (IV) relationship (I_{Ca}) of Cav1.3 WT or mutants in presence of β_3 ...	74
Fig. 22: Exemplary IV-traces for Cav1.3 WT expressed with β_3 , β_{2d} or β_{2e} and $\alpha_2\delta$ -1 subunits.	75
Fig. 23: Current-voltage (IV) relationship (I_{Ca}) of Cav1.3 WT in presence of β_{2d} , β_{2e} or β_3	75
Fig. 24: Exemplary IV-traces for Cav1.3 WT or V259D expressed with β_{2d} or β_{2e} and $\alpha_2\delta$ -1 subunits.....	76
Fig. 25: Exemplary steady-state inactivation traces for Cav1.3 WT or V259D expressed with β_{2d} or β_{2e} and $\alpha_2\delta$ -1 subunits.....	77
Fig. 26: Exemplary 1 sec inactivation traces for Cav1.3 WT or V259D expressed with β_{2d} or β_{2e} and $\alpha_2\delta$ -1 subunits.....	77

Fig. 27: Activation and inactivation of Ca _v 1.3 WT or mutant, V259D in the presence of β _{2d} or β _{2e} .	78
Fig. 28: Immunostaining of endogenous Ca _v 1.3 in H295R cells.	79
Fig. 29: Western blot for overexpressed Ca _v 1.3-CT in HEK293 cells.	80
Fig. 30: Immunostaining of Ca _v 1.3-CT overexpressed in H295R cells.	81
Fig. 31: Aldosterone secretion from H295R cells overexpressing C-terminal of Ca _v 1.3	81
Fig. 32: Aldosterone secretion from H295R cells treated with calpeptin	82
Fig. 33: Western blot for Ca _v 1.3 in H295R cells treated with calpeptin.	83
Fig. 34: Aldosterone secretion and Ca _v 1.3 expression in H295R cells treated with calpeptin.	83
Fig. 35: shRNA mediated Ca _v 1.3 knockdown in H295R cells and aldosterone secretion.	84
Fig. 36: RT-PCR for Ca _v 1.3 expression in adrenal cDNA of WT and knockout mice.	85
Fig. 37: Expression of CYP11B2 in adrenals of WT and Ca _v 1.3 knockout mice.	85
Fig. 38: Dose response curve for compounds A-C on aldosterone secretion in H295R cells.	86
Fig. 39: Effects of compounds A-C on aldosterone secretion from primary adrenal cells.	87
Fig. 40: Best Practices for Somatic SNVs and Indels calling in whole genome or exome sequencing data by Mutect2, GATK.	99
Fig. 41: Chromatograms for CADM1 sequencing for normal adrenal and APA gDNA samples of patient 184T showing single nucleotide variant, c. 1139 T>A, p. V380D.	102
Fig. 42: Chromatograms for CADM1 sequencing for normal adrenal and APA gDNA samples of Munich patient showing single nucleotide variant, c. 1136 G>A, p. G379D.	103
Fig. 43: Alternative splicing and transcripts of human CADM1	109
Fig. 44: Schematic representation of CADM1 structure.	110
Fig. 45: Microarray expression analysis of CADM1 in adrenal cortex and APAs	115
Fig. 46: Microarray expression analysis of gap junction proteins in adrenal cortex	116
Fig. 47 Microarray expression analysis of GJA1 in adrenal cortex and APAs	117
Fig. 48: Abdominal CT scan of patient 184.	118
Fig. 49: Sliced right adrenal of patient 184. Adenoma is indicated by black arrow.	119
Fig. 50: Immuno-staining for CYP11B2, KCNJ5 & CYP11B1 and H&E staining for patient 184 tumour and adjacent normal adrenal.	120
Fig. 51: H&E staining for APA and APCC in adrenal section of 184.	121
Fig. 52: Sequences for scrambled (a) and CADM1 (b) shRNAs in pLVTH.	125
Fig. 53: RT-PCR for CADM1 expression in H295R cells.	127
Fig. 54: RT-PCR for CADM1 expression in human normal adrenal and APA samples.	128
Fig. 55: Immunohistochemistry for CADM1 and CYP11B2 in normal adrenal gland.	129
Fig. 56: Immunohistochemistry for CADM1 and CYP11B2 in adrenal cortex next to APA.	129
Fig. 57: Immunohistochemistry for CADM1 and CYP11B2 in APAs.	130
Fig. 58: Immunohistochemistry for CADM1 and CYP11B2 in patient 184's adrenal sections.	131
Fig. 59: Chromatograms for CADM1 sequencing in the cDNA of patient 184 normal adrenal and APA samples showing expression of mutant allele, c. 1139 T>A.	132

Fig. 60: Western blot analysis for expression of CADM1 WT or mutants in transduced H295R cells.	134
Fig. 61: Mutant CADM1 upregulates CYP11B2 mRNA expression and aldosterone secretion.	136
Fig. 62: Confocal images for H295R cells transduced with CADM1-SP4 WT or mutants, G379D or V380D.	137
Fig. 63: Angiotensin II stimulation on H295R cells expressing CADM1-WT or mutants.....	138
Fig. 64: CADM1-WT reduces the effects of mutants on CYP11B2 and aldosterone upregulation.	140
Fig. 65: Effect of γ -secretase inhibitor, LY-411,575 on α -CTF of CADM1 and aldosterone secretion from H295R cells.	141
Fig. 66: γ -secretase inhibition in H295R cells overexpressing CADM1-WT or mutants.	142
Fig. 67: Sub-cellular localisation of overexpressed CADM1-WT or mutants in H295R cells.	143
Fig. 68: Loss of cell-cell adhesion in HEK293 cells expressing mutant CADM1.	144
Fig. 69: Aldosterone secretion from H295R cells cultured in monolayer or suspension.	144
Fig. 70: Silencing of CADM1 in H295R cells using shRNA lentivirus.	145
Fig. 71: Effect of CADM1 knockdown on aldosterone synthesis in H295R cells.	146
Fig. 72: Angiotensin II treatment of CADM1 silenced cells.	147
Fig. 73: Expression of connexin-43 in CADM1 silenced H295R cells.	148
Fig. 74: Immunofluorescence for GJA1, CADM1 and CYP11B2 expression in adrenal cortex and APCC.....	149
Fig. 75: Immunofluorescence for GJA1 and CADM1 expression in APAs.	149
Fig. 76: Aldosterone secretion and transcriptional analysis of H295R cells treated with Angiotensin II and PMA.....	150
Fig. 77: Effect of Angiotensin II and PMA on expression of connexin-43 in H295R cells.	151
Fig. 78: Heatmap for selected genes differentially expressed in H295R cells expressing CADM1-mutants.	152
Fig. 79: Heatmap for granin family of genes differentially expressed in H295R cells expressing CADM1-mutants.	153
Fig. 80: Heatmap for genes significantly differentially expressed in H295R cells with CADM1 knockdown compared to control shRNA cells.	153
Fig. 81: Heatmap for selected genes differentially expressed in H295R cells with CADM1 knockdown compared to control shRNA cells.	154
Fig. 82: Heatmap for granin family of genes differentially expressed in H295R cells with CADM1 knockdown compared to control shRNA cells.....	154
Fig. 83: Dot-plot for genes' expression in CADM1 mutant, 184T versus average of 2 other ZG-like APAs.....	155
Fig. 84: Immunohistochemistry for AQP2 in APAs	157

LIST OF TABLES

Table 1: Reported somatic mutations in APAs.	31
Table 2: Reported prevalence of somatic mutations in different cohorts.	33
Table 3: List of TaqMan Probes used for expression analysis	35
Table 4 : List of primary antibodies used	36
Table 5: List of plasmids and vectors used.	41
Table 6: Microarray expression data for Ca ²⁺ channel subunits in ZG and ZF of adrenal cortex.	51
Table 7: Tissue distribution of β_2 subunit transcripts.....	54
Table 8: Primers used for Ca _v 1.3 cDNA amplification	56
Table 9: Primers used for Ca _v 1.3 Gibson Assembly.....	57
Table 10: List of Ca _v 1.3 mutagenesis primers	58
Table 11: List of β_2 mutagenesis primers.....	58
Table 12: Ca _v 1.3 C-terminal cloning primers.....	59
Table 13: Ca _v 1.3 shRNA cloning primers	60
Table 14: [REDACTED]	64
Table 15: [REDACTED]	68
Table 16: [REDACTED]	68
Table 17: List of samples.....	95
Table 18: List of primers for genotyping of hotspot regions.	97
Table 19: Sample workflow and mutations found.	100
Table 20: Mutant samples per gene	102
Table 21: Summary of CADM1 promoter methylation in cancers	113
Table 22: AVS results of patient 184.....	117
Table 23: List of CADM1 RT primers.	123
Table 24: CADM1 cloning primers.	124
Table 25: CADM1 mutagenesis primers	124
Table 26: CADM1 shRNA cloning primers.....	125
Table 27: AQP2 expression from RNAseq analysis of 3 APAs/Normal pairs	156
Table 28: AQP2 expression from RNAseq analysis of H295R cells overexpressing CADM1..	156

CHAPTER 1

CHAPTER 1 - INTRODUCTION

1.1 Hypertension and Primary aldosteronism

Hypertension or high blood pressure (>140mm of Hg systolic or \geq 90mm of Hg diastolic pressure) is a major, but treatable risk factor for cardiovascular diseases, accounting for up to 40% of the world's population. It is one of the major cause of premature morbidity and mortality in today's world. If an obvious single cause of elevated blood pressure cannot be identified, it is categorised as primary or essential hypertension. 80-90% of hypertensive cases fall in this category. Remaining cases can be attributed to an identifiable cause and termed as secondary hypertension. The underlying causes for secondary hypertension can be divided into two categories, depending on increased cardiac output or increased systemic vascular resistance (Fig. 1). Increase in blood volume due to increased aldosterone, vasopressin, and renal disease etc. fall into this category. Increased vascular resistance is the outcome of conditions such as atherosclerosis, diabetes, thyroid dysfunction, stress, cerebral ischemia etc.

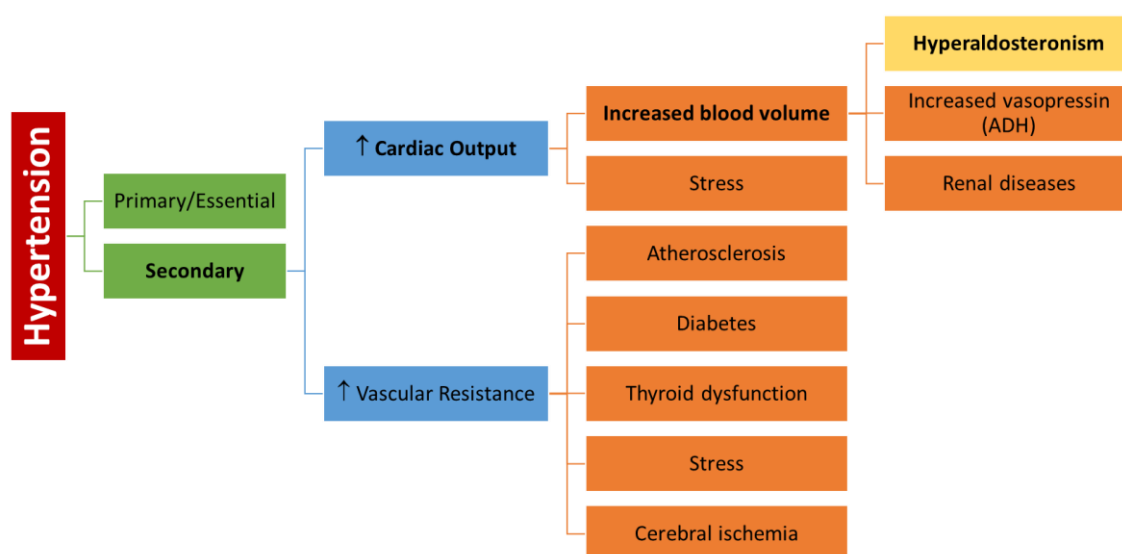


Fig. 1: Categorisation of hypertension and underlying causes.

Several pathophysiologies related to adrenal glands are the underlying cause of secondary hypertension including Cushing's syndrome (increased cortisol), pheochromocytoma (increased catecholamines), and Conn's syndrome (increased aldosterone). Hyperaldosteronism can also be categorised as primary or secondary hyperaldosteronism depending on whether aldosterone secretion is renin independent or autonomous of renin stimulation respectively (Fig. 2).

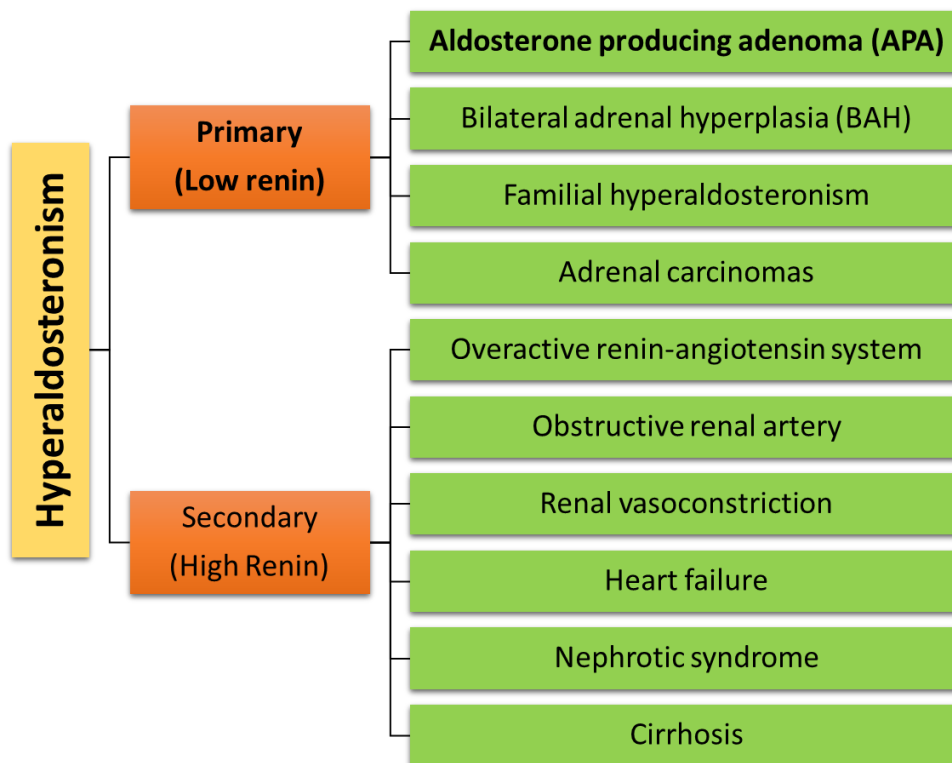


Fig. 2: Categorisation of hyperaldosteronism and their underlying causes.

Conn's syndrome, one of the major causes of primary aldosteronism (PA) is characterised by hypersecretion of hormone aldosterone by the adrenal glands due to an adenoma in adrenal cortex. It was first described in 1955 by Dr Jerome W. Conn in a patient with episodes of muscular weakness, intermittent tetany (muscular spasm), paraesthesia (abnormal tingling and pricking sensation), polyuria (excess urination), polydipsia (excess thirst), hypokalaemia (low plasma potassium), hypernatremia (high plasma sodium), alkalosis (alkaline serum), and hypertension (Conn, 1955). These symptoms were caused by renin-independent hypersecretion of aldosterone from the aldosterone producing adenoma (APA), after surgical removal of which, the condition was cured.

Since then a number of similar hypertension cases have been identified, with PA accounting for 5-13% of all hypertensive cases (Mulatero et al., 2004). PA also accounts for 20% of treatment resistant hypertensive cases (Mulatero et al., 2004; Rossi et al., 2006) and is the most common curable form of secondary hypertension by adrenalectomy. Diagnosis of PA was earlier restricted to hypokalaemic patients, but was revised a decade ago to high value for plasma aldosterone/renin ratio (ARR) (Young, 2003). Management of PA varies depending on the underlying subtype of the condition, unilateral or bilateral adrenal hyperplasia, adenoma or adrenocortical carcinoma (Funder et al., 2008; Stowasser and Gordon, 2003).

1.2 Adrenal gland and steroidogenesis

Adrenal glands are a pair of small endocrine glands present on top of the two kidneys. They are the site of several steroid hormones' synthesis. Adrenals are formed of 2 distinct regions, outer cortex and inner medulla, covered with a capsule of connective tissue (Fig. 3). Adrenal cortex produces steroid hormones and medulla secretes stress hormones, adrenaline and noradrenaline that are catecholamine in nature. Cortex is further divided into three distinct zones - outermost zona glomerulosa (ZG), middle zona fasciculata (ZF) and innermost zona reticularis (ZR). All these cortical layers have distinct histology and secretory functions. As the name suggests, cells in ZG are arranged in a glomerular or "nests" like structures. ZG cells have high nucleus to cytoplasmic volume ratio, compared to cells in ZF region. ZF cells have lipid rich cytoplasm and are arranged in column like structures. ZG is the site of steroidogenesis of the mineralocorticoid, aldosterone. ZF cells produce the glucocorticoid hormone, cortisol that plays a role in increasing blood glucose level in the conditions of stress by gluconeogenesis. The inner most region of cortex, ZR is the site of androgens' synthesis like testosterone.

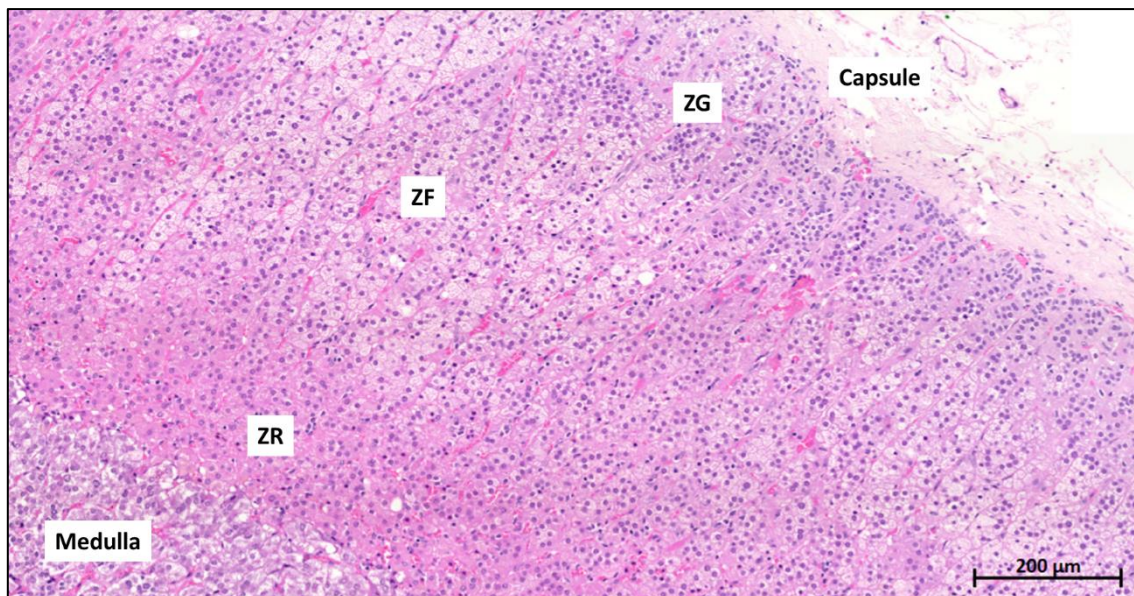


Fig. 3: Haematoxylin and eosin (H&E) staining of human adrenal gland showing its histology

This figure shows outer capsule, three concentric layers of adrenal cortex and inner-most medulla. Haematoxylin and eosin (H&E) staining of a section shows different zones in adrenal structure.

Aldosterone is a steroid hormone, synthesised and secreted by ZG cells of adrenal cortex. It is a product of long steroidogenesis process (Fig. 4) that begins with the translocation of cholesterol molecule from outer mitochondrial membrane to inner mitochondrial membrane, facilitated by steroidogenic acute regulatory protein, StAR. The last 3 reactions of this process

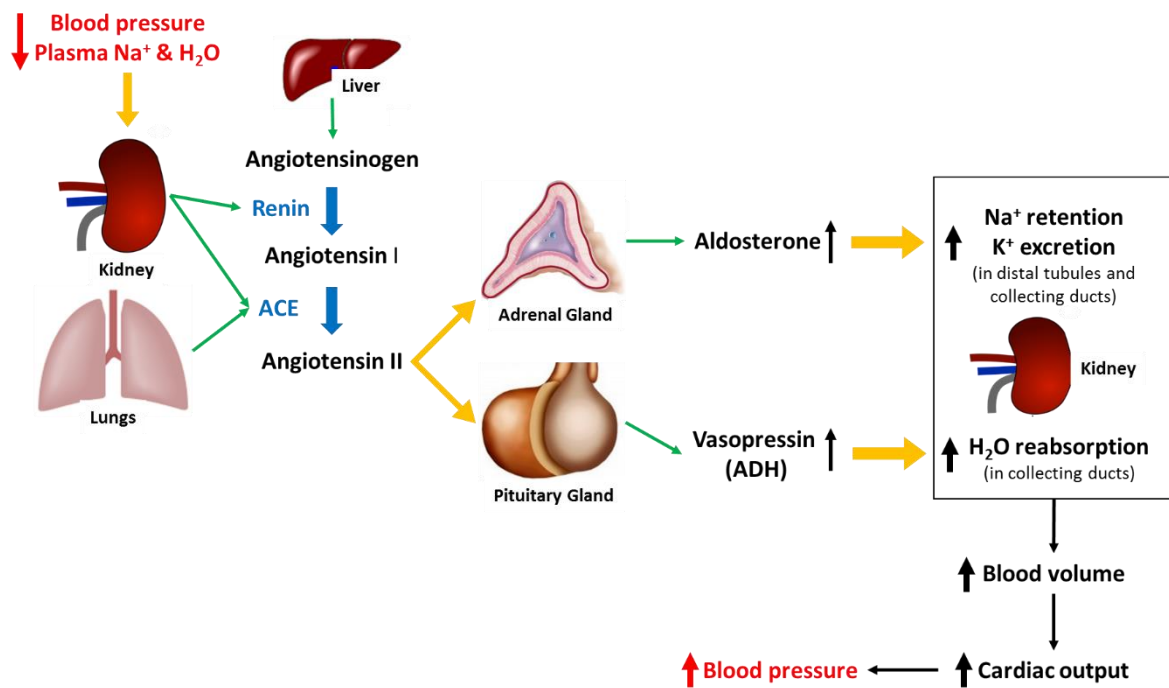


Fig. 5: Renin-angiotensin-aldosterone system (RAAS)

Green arrows indicate enzyme/hormone secretion, blue arrows represent enzymatic conversions, and orange arrows show stimulatory effects on the target organ.

At cellular level, aldosterone secretion is primarily stimulated by increase in plasma concentration of three factors: angiotensin II (AngII), potassium (K⁺) and adrenocorticotrophic hormone (ACTH) (Fig. 6) (Spät and Hunyady, 2004). ACTH activates adenylyl cyclase pathway via its receptor, MC2R leading to rise in cAMP levels that in turn increases cholesterol transport to mitochondria and transcription of several steroidogenic enzymes. On the other hand, though via different mechanisms both AngII and elevated extracellular K⁺ concentration stimulate aldosterone synthesis by raising cytoplasmic calcium levels. AngII binds to its G-protein coupled receptor, AT₁R and activates IP₃/Ca²⁺-calmodulin pathway. IP₃ receptors on endoplasmic reticulum release internally stored calcium into cytoplasm. High extracellular [K⁺] depolarises membrane potential activating and opening voltage-gated calcium channels (T- and L-type) (Spät, 2004). Influx of calcium ions through these channels elevates [Ca²⁺]_i and expression of aldosterone synthase (*CYP11B2*) via its main transcriptional regulator NURR1 (*NR4A2*).

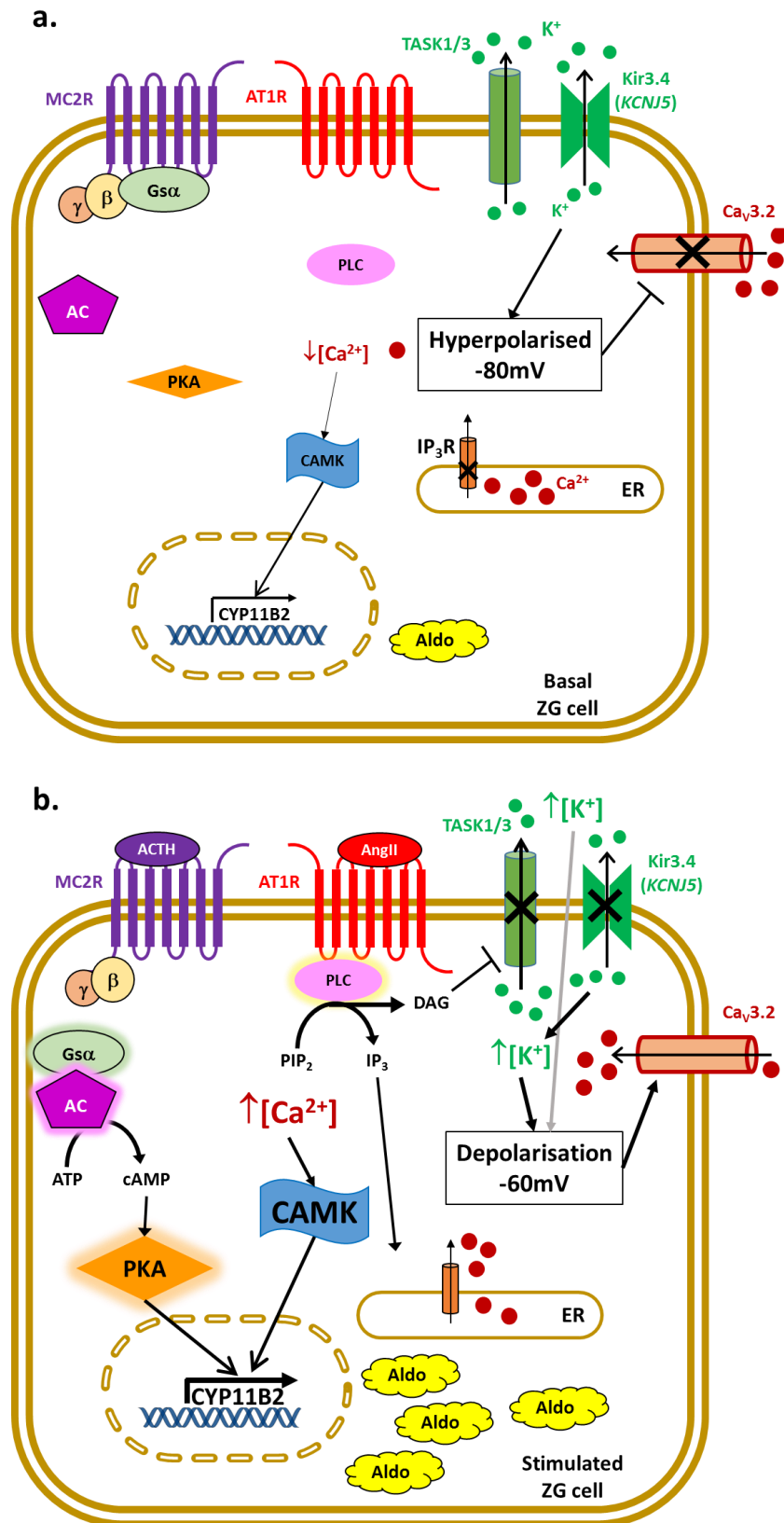


Fig. 6: Molecular pathways for aldosterone secretion in ZG cells.

a. Basal ZG cell. **b.** ZG cells on stimulation with ACTH, AngII or increased plasma K⁺ concentration. AC: Adenylyl cyclase; PKA: Protein kinase A; PLC: Phospholipase C; CAMK: Calmodulin dependent protein kinase; ER: Endoplasmic reticulum.

1.3.2 Mechanism of aldosterone action

Secreted in the blood stream, aldosterone acts on the cytosolic mineralocorticoid receptors (MR) in distal tubular and collecting duct cells of kidneys, leading to its translocation to nucleus. MR upregulates transcription of serum glucocorticoid-induced kinase 1 (SGK1), which increases ENaC (epithelial Na⁺ channels) expression on the luminal membranes of collecting ducts, NCC (sodium chloride channels) in distal convoluted tubules and Na⁺/K⁺ ATPase pumps in both. These upregulated channels function to increase sodium retention, potassium excretion and water reabsorption from the blood resulting in increased total blood volume and blood pressure. As MR is not only present in the epithelial cells of distal renal tubules but also in colon and sweat glands, aldosterone mediated sodium retention, potassium and hydrogen ion excretion occurs in these tissues as well. This action of aldosterone on epithelial cells to increase blood pressure is termed as its “genomic” effect because of MR induced target gene transcriptional upregulation. Similar genomic effects are seen in non-epithelial, endothelial cells, cardiomyocytes and vascular smooth muscle cells.

Aldosterone is reported to exert its “non-genomic” effects by activation of several signalling pathways in tissues expressing MR or other GPCRs on cell surface rather than cytosol in epithelial cells. These non-genomic effects mediated by second messengers like Ca²⁺, cAMP, IP₃/DAG are much quicker than the genomic effects.

1.3.3 Effects of aldosterone excess

Aldosterone excess in PA does not only exert its effect due to uncontrolled blood pressure but also has adverse effects by end organ damage independent of increased blood pressure (Fig. 7). Aldosterone causes increased mesangial cell proliferation and podocyte injury in kidneys by increasing oxidative stress and inflammatory pathways. These effects lead to chronic kidney disease augmenting hypertension even further. In cardiovascular system, aldosterone excess induces hypertrophy, fibrosis and inflammation which is partly dependent on its action of increasing blood pressure (Milliez et al., 2005; Savard et al., 2013). High salt intake has been shown to exaggerate these deleterious effects of aldosterone excess on cardiovascular system and require to be restricted to manage the symptoms while on medical therapy including MR antagonists, ACE inhibitors and angiotensin receptor blockers. Aldosterone excess has also been implicated in increasing insulin resistance leading to diabetes and adding to its cardio-metabolic risks (Briet and Schiffrin, 2010). This is well documented in several studies showing increased morbidity and mortality among PA patients with age and blood pressure matched essential hypertension patients. Meta-analysis of these studies have shown increased risk of cardiovascular events such as coronary artery disease, atrial fibrillation, heart failure and stroke in PA patients (Hundemer et al., 2017; Monticone et al., 2017). Among all current treatments available, MR antagonism has been observed to minimise these risk factors most effectively.

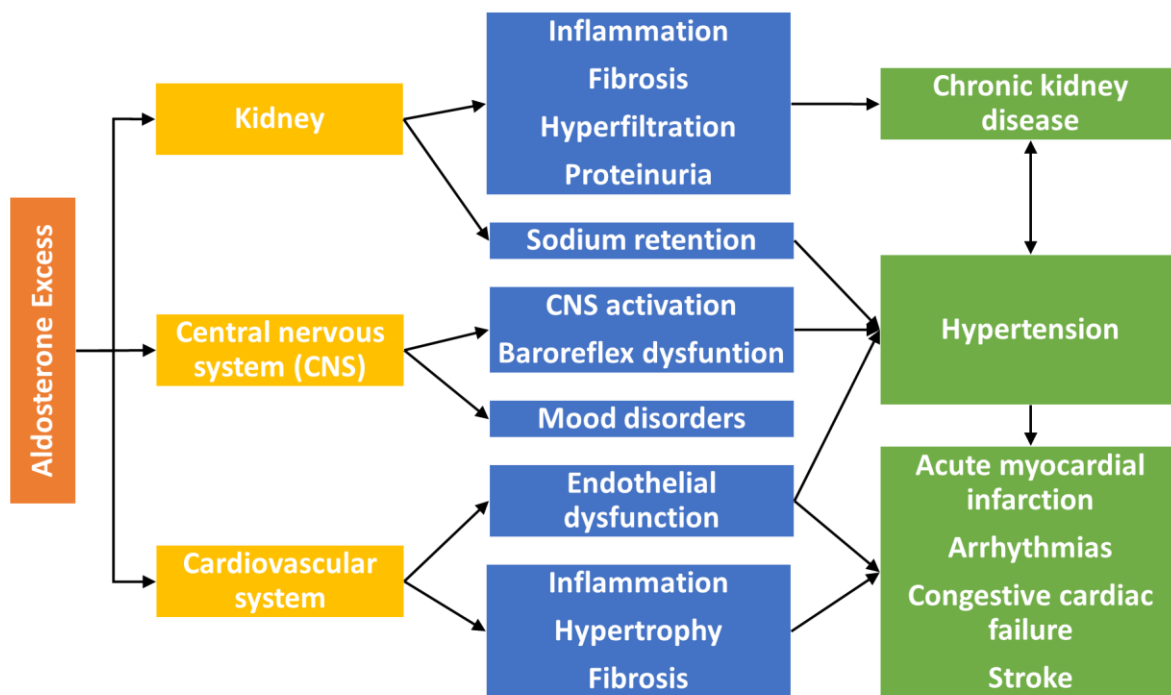


Fig. 7: Effects of aldosterone excess on various tissues/systems.

Adapted from (Stowasser and Gordon, 2016).

1.4 Identification, diagnosis and management of PA

With increasing evidences of deleterious effects of aldosterone excess, it is more than ever important to diagnose for primary aldosteronism. Funder et al. have proposed clinical practice guidelines for patient identification, screening and confirmatory tests, subtype testing and management of PA (Fig. 8). Identification of potential PA patients involves symptoms like severe hypertension which is drug resistant, young age at presentation of hypertension or family history of hyperaldosteronism (Funder et al., 2016). High plasma aldosterone to renin ratio (ARR), meaning hyper aldosterone secretion despite suppressed renin in circulation, in such potential cases is the first indication of possible PA. ARR ratio ≥ 20 ng/dl per ng/ml per hour (555 pmol/l per ng/ml per hour) along with a plasma aldosterone concentration (PAC) of ≥ 15 ng/dl (416 pmol/l) is the criteria for positive screening of primary aldosteronism (Mattsson and Young, 2006). If required, these patients then undergo further confirmatory tests such as oral sodium intake, SIT, Captopril (ACE inhibitor) and FST, followed by lateralisation of PA.

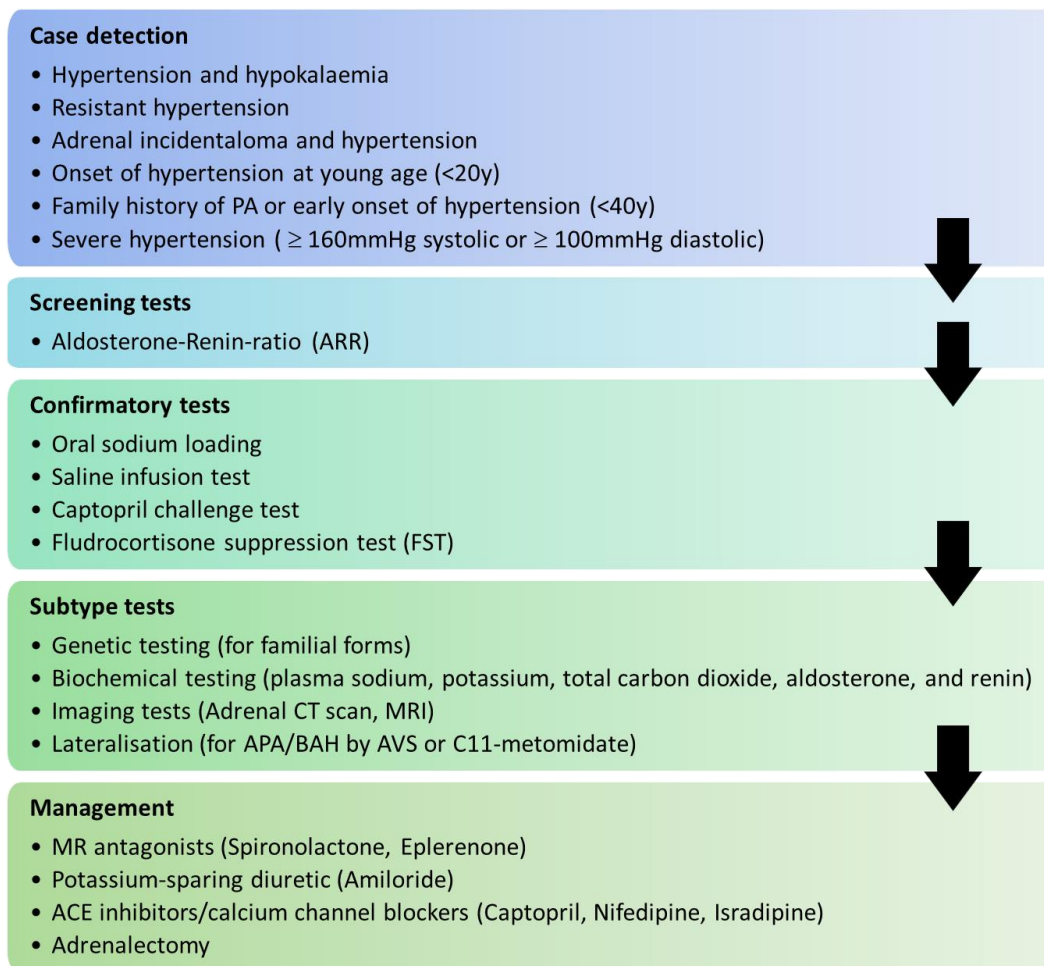


Fig. 8: Schematic representation of diagnosis and treatment of primary aldosteronism.

CT: Computed tomography, MRI: Magnetic resonance imaging, APA: aldosterone producing adenoma; BAH: Bilateral adrenal hyperplasia; ACE: Angiotensin converting enzyme. Summarised from (Funder et al., 2016; Stowasser and Gordon, 2016).

1.4.1 Lateralisation of APAs

Traditionally abdominal thin-slice CT and MRI were used to detect adenomas in adrenal for PA diagnosis, but are more suitable only for classical Conn's adenomas larger than 1cm in diameter and cannot differentiate between an APA and non-functioning incidentalomas common in patients >40 years of age. Also, if adenomas are within the whole adrenal are very commonly missed with these detection methods. To overcome these limitations, adrenal vein sampling (AVS) for both adrenals is the gold standard for detecting functioning adenomas and lateralisation to either side (Funder et al., 2008). Aldosterone to cortisol ratio is analysed for both left and right adrenal veins in addition to that in peripheral blood from inferior vena cava (IVC). High aldosterone to cortisol ratio confirms diagnosis for PA and unilateral or bilateral condition. Despite its merits over CT/MRI imaging techniques, AVS also has limitations. It is invasive, technically challenging especially for the right side due to its small size, and expensive. Stress prior to procedure induces ACTH levels which can fall down at the time of

sampling leading to underestimated aldosterone and cortisol secretion and the ratio. Also presence of APA co-secreting both aldosterone and cortisol can skew the AVS results missing the PA diagnosis. Recently, detection of sub-centimetre APAs has become easier by PET-CT using C¹¹-labelled metomidate, a potent inhibitor of both CYP11B1 and CYP11B2 (Azizan et al., 2013; Burton et al., 2012; Powlson et al., 2015). Lateralisation of APAs by this method was found to be in consistency with that from AVS. Its utility was first demonstrated by specific uptake of C¹¹-metomidate in adrenals of several primates (Bergström et al., 1998). In humans, only cortical tumours were shown to be positive for C¹¹-metomidate labelling as compared to non-cortical tumours (Bergström et al., 2000). This method is non-invasive and faster than AVS with only limitation that is the short half-life of only 20min of the label C¹¹. To overcome this issue, some centres are testing more stable radio-labelled I¹²³-metomidate (Hahner et al., 2008; Kreissl et al., 2013).

1.4.2 Management of PA

Surgical removal of unilateral APAs and adjacent adrenal gland is the first choice of curing primary aldosteronism as it improves hypertension in almost 100% of the cases. It has been shown to significantly reduce proteinuria and left ventricular size, improving cardiovascular events (Funder et al., 2016). If the condition is diagnosed not to be unilateral (that's BAH or bilateral APA) or patient is not fit or willing for adrenalectomy, it needs to be managed medically. First line of recommended drugs in such cases is MR antagonists - spironolactone or eplerenone (Funder et al., 2016) to reduce the cardiovascular morbidity because of aldosterone excess. Combined therapy of spironolactone with amiloride (ENaC blocker) is also recommended so as to minimise the dose-dependent side-effects of spironolactone such as gynecomastia in males, menstrual irregularity, breast inflammation, erectile dysfunction etc. because ultimately synthesis of aldosterone in ZG cells require opening of calcium channels to raise intracellular Ca²⁺ levels, calcium channel blockers seem like good candidates for managing PA, but again selective Ca_v1.3 blocker would be needed to prevent cardiovascular Ca_v1.2 blockage with existing dihydropyridines (DHP).

1.5 APAs: subtypes, somatic mutations and prevalence

Aldosterone-producing adenoma (APAs) are benign tumours originating in adrenal cortex and account for more than one-third of PA cases (Young, 2007). Existence of histologically distinct types of APAs (ZG-like and ZF-like APAs) has been known for long time (Ganguly, 1992; Tunny et al., 1991) but it was not until recently that somatic mutations in specific genes (Table 1) were associated with the two subtypes (Azizan et al., 2012a, 2013). APAs resembling ZF of adrenal cortex have large, lipid-laden cells and are generally larger (>2cm) than ZG-like APAs, which are smaller (≤ 1 cm) and comprised of compact, lipid-sparse cells. Somatic mutations in the gene *KCNJ5* were first reported by Choi et al. (Choi et al., 2011) and have since been found in various cohorts around the world with varying prevalence (Table 2). The mutations lie in *KCNJ5* or near the selectivity filter of the G-protein regulated inward rectifying K^+ channel, Kir3.4 through which K^+ ions move freely. Histologically, APAs with *KCNJ5* mutations resemble those in the ZF-like category. On the other hand, smaller ZG-like APAs frequently possess somatic mutations in *CACNA1D*, *ATP1A1* & *ATP2B3*. The ZG-like and ZF-like APAs not only differ histologically and genetically, but also in their transcriptomes (Azizan et al., 2013). Despite this homogenous cellular composition of most APAs, very recently steroidogenic enzyme expression and genetic heterogeneity within the APAs has been found and studied (Nakamura et al., 2015; Nanba et al., 2016). Nearly in all cohorts *KCNJ5* mutant, ZF-like large APAs tend to be more common in females, patients presenting at younger age compared to ATPases and *CACNA1D* mutant APAs that are more frequently found in male patients (Azizan et al., 2013; Beuschlein et al., 2013; Boulkroun et al., 2012).

A regulated aldosterone secretion from ZG cells is maintained by highly regulated Ca^{2+} concentration in the cytoplasm, mainly by Ca^{2+} entry via L- and T-type calcium channels on the cell membrane. These voltage-gated calcium channels (VGCCs) open in response to cell membrane depolarisation as a result of several stimuli. These include inhibition of TASK (K^+ channels) via AngII activated AT1R receptor, resulting in elevated intracellular K^+ levels and membrane depolarisation. Efflux of K^+ via Kir3.4/GIRK4 (*KCNJ5*), a G-protein activated inward rectifier K^+ channel, maintains resting membrane potential to hyperpolarised states at which calcium channels remain closed (Fig. 9a). Mutations in or near the selectivity filter of Kir3.4/GIRK4 lead to unselective Na^+ influx, depolarisation and calcium channel opening (Fig. 9b). Mutations in Na^+/K^+ ATPase subunit α -1 (*ATP1A1*) cause the loss of its physiological function of maintaining the concentration gradient of Na^+ and K^+ ions and hence results in depolarisation (Fig. 9) (Azizan et al., 2013; Beuschlein et al., 2013). Ca^{2+} ATPase3 (*ATP2B3*) maintains low cytoplasmic calcium concentration by pumping Ca^{2+} ions out of the cell (Fig. 9a), but mutations in this protein also lead to its loss of function and increase in intracellular calcium (Fig. 9b) (Beuschlein et al., 2013). Most of the studied mutations in *CACNA1D* result in gain-of-function of the pore-forming α_1 -subunit of L-type calcium channel $Ca_v1.3$. Mutated $Ca_v1.3$ channels exhibit higher calcium conductance and altered current-voltage relationship

reflected by channel opening even at hyperpolarised membrane potentials (Fig. 9b) (Azizan et al., 2013; Scholl et al., 2013). As a result APA cells with mutations in any of these genes have persistent Ca^{2+} entry and upregulated CYP11B2 transcription.

In addition to somatic mutations in APAs, germline mutations in *KCNJ5*, *CACNA1D* and *CACNA1H*, encoding the T-type calcium channel $\text{Ca}_v3.2$, have been associated with the familial forms of primary aldosteronism. Several germline mutations in *KCNJ5* reported in cases of familial hyperaldosteronism III are same as the somatic mutations in APAs, for example E145Q, G151R and T158A (Monticone et al., 2013, 2015; Scholl et al., 2012). Those never reported in APAs and only germline include G151E and Y152C. Two *de novo* *CACNA1D* germline mutations, G403D and I750M both in the residues reported somatically in APAs were found in 2 patients with hypertension from birth and are associated with the multi organ syndrome known as primary aldosteronism, seizures and neurologic abnormalities (PASNA) (Scholl et al., 2013). Five cases of early onset of hypertension were found to be heterozygous for gain-of-function M1549V variant in *CACNA1H* (Fig. 9b), which leads to hyper aldosterone secretion *in vitro* but the mutation did not segregate with the phenotype (Reimer et al., 2016; Scholl et al., 2015).

Very recently two independent groups reported novel germline mutations in gene *CLCN2*, encoding a voltage gated chloride channel in cases of familial hyperaldosteronism type II and early onset of primary aldosteronism (Fernandes-Rosa et al., 2018; Scholl et al., 2018). Altogether, 6 variants were reported in 9 probands and those studied *in vitro* showed gain-of-function phenotype in mutant ClC-2 channels with increased efflux of Cl^- ions leading to membrane depolarisation and hyper aldosterone secretion.

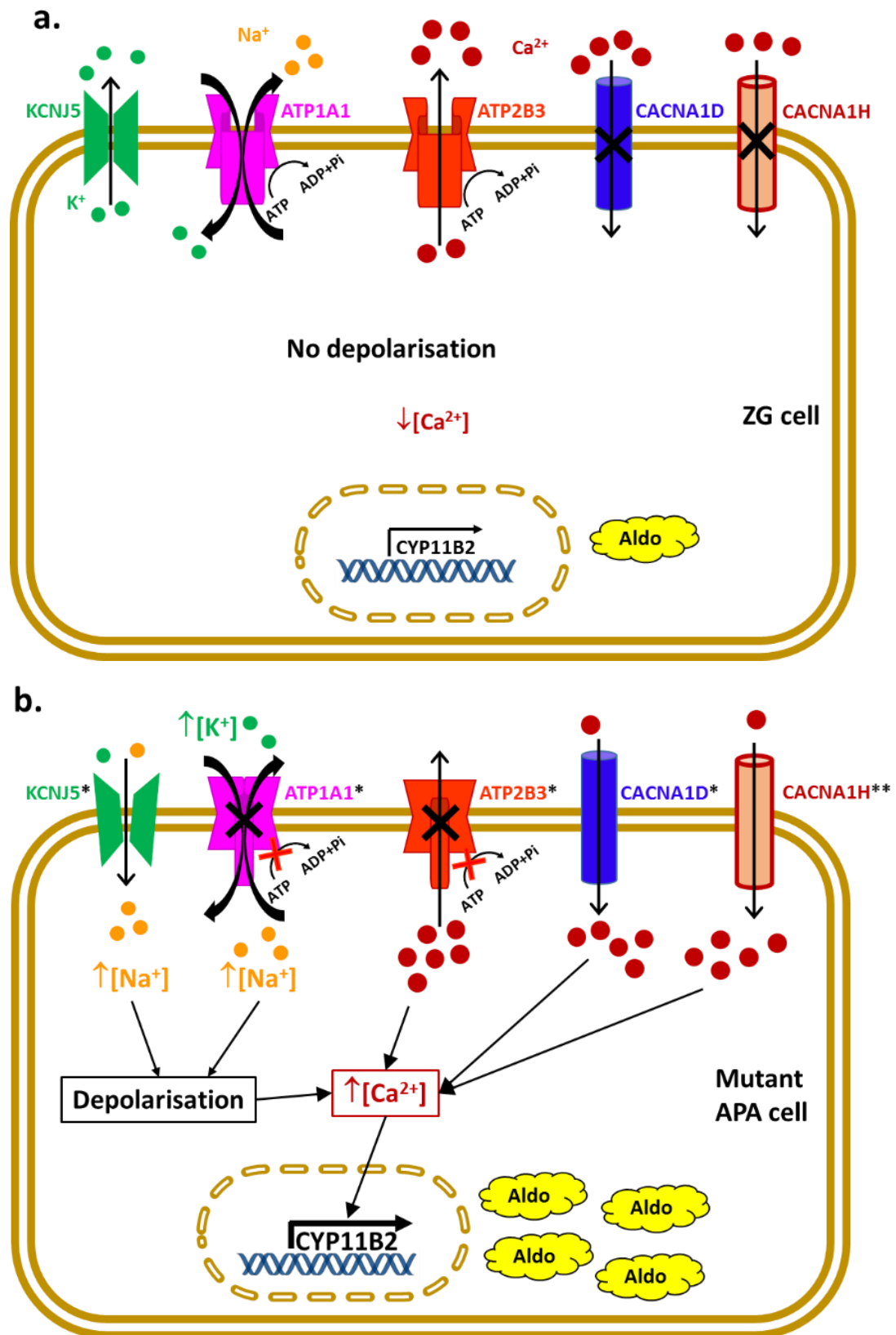


Fig. 9: Proposed model for constitutive aldosterone secretion from APAs with somatic mutations.
a. Physiological roles of wild-type *KCNJ5*, *ATP1A1*, *ATP2B3*, *CACNA1D* & *CACNA1H* channels/transporters in a normal ZG cell. **b.** Effect of somatic mutations* in APAs and germline only mutations** in *CACNA1H* (Cav3.2) in early onset primary aldosteronism is shown. Adapted from (Monticone et al., 2014).

Table 1: Reported somatic mutations in APAs.

Gene	Mutation	Reference
<i>KCNJ5</i>	G151R	(Choi et al., 2011)
	T158A	(Choi et al., 2011)
	L168R	(Choi et al., 2011)
	I157del	(Azizan et al., 2012b)
	E145K	(Azizan et al., 2013)
	W126R	(Fernandes-Rosa et al., 2014)
	A139_F142dup	(Hardege et al., 2015)
	E147Q	(Wang et al., 2015)
	149_150insTTT	(Wang et al., 2015)
	A153_F164dup	(Wang et al., 2015)
<i>ATP1A1</i>	F100_L104del	(Beuschlein et al., 2013)
	L104R	(Beuschlein et al., 2013)
	V332G	(Beuschlein et al., 2013)
	EETA963S	(Azizan et al., 2013)
	G99R	(Fernandes-Rosa et al., 2014)
	M102_I106del	(Åkerström et al., 2015)
	F959_E961del	(Åkerström et al., 2015)
	E960_L964del	(Åkerström et al., 2015)
	F956_E961del	(Åkerström et al., 2015)
	M102_L103del	(Åkerström et al., 2015)
L103_M104del	(Åkerström et al., 2015)	
<i>ATP2B3</i>	L425_V426del	(Beuschlein et al., 2013)
	V426_V427del	(Beuschlein et al., 2013)
	L424_V425del	(Fernandes-Rosa et al., 2014)
	T423_L425del	(Åkerström et al., 2015)
	L424_V426del	(Åkerström et al., 2015)
	V426_V429del	(Åkerström et al., 2015)
<i>CACNA1D</i>	V259D	(Azizan et al., 2013)
	G403R (8A)	(Azizan et al., 2013)
	I750M/I770M	(Azizan et al., 2013; Scholl et al., 2013)
	F747L	(Azizan et al., 2013)
	R990H	(Azizan et al., 2013)
	P1336R	(Azizan et al., 2013)
	M1354I	(Azizan et al., 2013)
	G403R (8B)	(Scholl et al., 2013)
	G403D (8B)	(Scholl et al., 2013)
	L655P	(Fernandes-Rosa et al., 2014)
	S652L	(Fernandes-Rosa et al., 2014)
	Y741C	(Fernandes-Rosa et al., 2014)
	F747V	(Fernandes-Rosa et al., 2014)
	I750F	(Fernandes-Rosa et al., 2014)
	V979D	(Fernandes-Rosa et al., 2014)
	K981N	(Fernandes-Rosa et al., 2014)
	A998I	(Fernandes-Rosa et al., 2014)
	A998V	(Fernandes-Rosa et al., 2014)
	V1151F	(Fernandes-Rosa et al., 2014)
	I1152N	(Fernandes-Rosa et al., 2014)
	V1338M	(Fernandes-Rosa et al., 2014)
	V401L	(Åkerström et al., 2015)
V748I	(Wang et al., 2015)	

1.5.1 Prevalence of mutations in known genes

Prevalence rates of somatic mutations in APA candidate genes have been reported in several studies in different cohorts (Table 2). *KCNJ5* is the first causative gene discovered in APAs (Choi et al., 2011), and is therefore, the most sequenced gene in all cohorts with nearly complete prevalence estimates, ranging from 36-80%. A study by Lenzini et al. employed meta-analysis of 13 such reports to find overall prevalence of *KCNJ5* mutations in APAs and any associated clinical features that might help predicting *KCNJ5* genotype for a patient pre-operatively (Lenzini et al., 2015). They reported overall prevalence of 44% *KCNJ5* mutant APAs, which varied significantly between Caucasian and Asian (China and Japan) cohorts with prevalences of 35% and 63%, respectively. This huge difference among populations was attributed to high dietary salt intake in Asian population compared to Caucasian diet, probably predisposing them to more frequent genetic alterations and somatic mutations. Among clinical features, no significant differences in the blood pressure and serum K⁺ levels were found in patients with *KCNJ5* mutant APAs compared to non-mutants, except for confirming some of the previous observations that *KCNJ5* mutant APAs were larger in size and more often found in females, younger patients, and led to higher aldosterone levels in plasma compared to the non-mutants (Azizan et al., 2013; Beuschlein et al., 2013; Boulkroun et al., 2012).

Prevalence data of mutations in other genes is not as much complete because they are not sequenced for in most studies and hence less reliable to make any conclusions. When sequenced, mutations in *CACNA1D* gene has been reported in up to 10% cases, *ATP1A1* in 5.3% and *ATP2B3* in <2% cases in a combined European cohort (ENSAT, excluding UK) (Fernandes-Rosa et al., 2014). One possible reason for apparent low prevalence of these genes could be cases that go undetected on routine CT/MRI scans due to their small size.

Table 2: Reported prevalence of somatic mutations in different cohorts.

Centre	Sample size (n)	Mutant APAs (%)					Reference
		<i>KCNJ5</i>	<i>ATP1A1</i>	<i>ATP2B3</i>	<i>CACNA1D</i>	<i>CTNNB1</i>	
Uppsala	22	36.0	NS	NS	NS	NS	(Choi et al., 2011)
UK	46	43.5	NS	NS	NS	NS	(Azizan et al., 2012b)
Australia	27	37.0	NS	NS	NS	NS	
US	47	38.0	NS	NS	NS	NS	(Monticone et al., 2012)
ENSAT	474	38.0	5.3	1.7	9.3	NS	(Fernandes-Rosa et al., 2014)
Uppsala	36	69.4	2.8	5.6	0.0	NS	(Åkerström et al., 2015)
Dusseldorf	33	45.5	3.0	0.0	0.0	NS	
Halle	8	50.0	0.0	0.0	0.0	NS	
Lubeck	20	65.0	10.0	5.0	0.0	NS	
Sydney	34	41.2	5.9	0.0	8.8	NS	
Stockholm	34	55.9	11.8	5.9	5.9	NS	
China	114	75.4	0.0	0.0	0.9	NS	(Wang et al., 2015)
China	168	76.8	2.4	0.6	0.6	NS	(Zheng et al., 2015)
Taiwan	148	59.5	1.4	0.7	0.0	NS	(Wu et al., 2015)
Taiwan	219	52.9	1.4	0.5	0.0	3.7	(Wu et al., 2017)
Japan	23	65.2	NS	NS	NS	NS	(Taguchi et al., 2012)
Japan	47	78.7	NS	NS	NS	NS	(Okamura et al., 2017)
Meta-analysis	1636	44.3	NA	NA	NA	NA	(Lenzini et al., 2015)
Europe		35.0	NA	NA	NA	NA	
Asia		63.0	NA	NA	NA	NA	

ENSAT: European Network for the Study of Adrenal Tumours; NS: Not sequenced; NA: Not analysed

1.6 Aims of the study

The somatic mutations in *CACNA1D* have been shown to cause gain-of-function phenotype in the electrophysiological properties of Cav1.3. It is hypothesised that expression of these mutant Cav1.3 channels would increase intracellular calcium and aldosterone secretion *in vitro* by human adrenocortical carcinoma cell line, H295R. Role of endogenous Cav1.3 in non-mutated state has not been studied previously. The primary aim of this project was to investigate if and how it regulates physiological aldosterone secretion. Determination of Cav1.3 as the main source of sustained calcium entry for regulated and/or autonomous aldosterone secretion led our interest towards its potential as a valuable and novel therapeutic target for treatment of primary aldosteronism. [REDACTED] project with [REDACTED] aimed at screening millions of compounds that would selectively block Cav1.3 over other ion channels, especially [REDACTED] to minimise unwanted cardiovascular side-effects. This selective molecule would be expected to block aldosterone production in APAs. This would be of significant value in treating patients with resistant hypertension driven by APAs, not only with *CACNA1D* mutations, but also those without *CACNA1D* mutations, by blocking unregulated Ca²⁺ influx altogether despite membrane depolarisation due to other dysfunctional ion channels.

And the secondary aim, was to genotype all APAs in the available cohort that is enriched for smaller ZG-like APAs and likely to have fewer ZF-like APAs with *KCNJ5* mutations. This study included 59 APAs from 52 patients (7 patients had 2 nodules). Genotyping was done partially by Sanger sequencing for known genes and by next-generation sequencing of whole exomes in genomic DNA extracted from paired normal adrenal and APAs. As we could detect many small APAs by PET-CT scans using C¹¹-metomidate which are usually missed on routine CT scans, we expected to find more cases of *CACNA1D*, *ATP2B3* or *ATP1A1* mutants compared to *KCNJ5* and hence differences in the mutational prevalence of these genes as reported globally. We also envisaged to find some novel genes with somatic mutations which would be of interest, to understand the phenotype of hyper aldosterone secretion. Discovery of novel somatic mutation in *CADM1* gene led to an investigation of its role in aldosterone producing adrenal cells.

CHAPTER 2

CHAPTER 2 - MATERIALS AND METHODS

2.1 General methods

2.1.1 Reagents and antibodies

Table 3: List of TaqMan Probes used for expression analysis

Gene Symbol	Target Isoform	Assay ID	Pre-designed or Custom made
<i>CACNA1D</i>	Cav1.3 (Total)	Hs01073321_m1	Pre-designed
<i>CACNA1D</i>	Cav1.3-2137	Hs01080346_m1	Pre-designed
<i>CACNA1D</i>	Cav1.3-2181	Hs01073303_m1	Pre-designed
<i>CACNA1C</i>	Cav1.2 (Total)	Hs00167681_m1	Pre-designed
<i>CACNB2</i>	β_2 (Total)	Hs00167861_m1	Pre-designed
<i>CACNB2</i>	β_{2a}	Hs01100746_m1	Pre-designed
<i>CACNB2</i>	β_{2d}	AJ39RUG	Custom made
<i>CACNB2</i>	β_{2e}	Hs01110867_m1	Pre-designed
<i>CACNB3</i>	β_3	Hs00893804_g1	Pre-designed
<i>CADM1</i>	-	Hs00942509_m1	Pre-designed
<i>GJA1</i>	-	Hs00748445_s1	Pre-designed
<i>18s rRNA</i>	-	4319413E	Pre-designed
<i>CYP11B2</i>	mouse	Mm01204955_g1	Pre-designed

Human CYP11B2 probe and primers –

Probe: [FAM]-CTGCACCACGTGCTGAAGCACT-[TAM]

Forward primer: 5'-GCAGAGGCAGAGATGCTG-3'

Reverse primer: 5'-CTTGAGTTAGTGTCTCCACCAGGA-3'

Drugs and reagents - Angiotensin II (Sigma, A9525), Calpeptin (Sigma, C8999), PMA (Calbiochem, 524400), LY-411,575 (Sigma, SML0506).

Primary antibodies used are listed in Table 4.

Secondary antibodies used for immunocytochemistry were all purchased from Molecular Probes®, Life Technologies for various species (anti-mouse, anti-rabbit, anti-chicken or anti-goat) conjugated to Alexa Fluor – 405, 488, 568, 633 & 647.

Table 4 : List of primary antibodies used

Antibody against	Supplier	Cat #	Stock concentration	Species	Monoclonal/ Polyclonal	Isotype	Conc. Used*
Cav1.3 (against intracellular C-terminal domain) [named as Cav1.3-CT]	NeuroMab	N38/8	0.2mg/ml	Mouse	Mono	IgG1	1:300
Cav1.3 (against intracellular loop in pore forming domain) [named as Cav1.3-NT]	NeuroMab	L48A/9	0.2mg/ml	Mouse	Mono	IgG2a	1:300
Cav1.3 (against intracellular C-terminal domain) [named as Cav1.3-CTsc]	SantaCruz	sc-25687	0.2mg/ml	Rabbit	Poly		1:500
CADM1 (against intracellular C-terminal domain)	Sigma	S4945	1.5mg/ml	Rabbit	Poly		1:1000
CADM1 (Clone 3E1 against ectodomain)	MBL Japan	CM004-3	1mg/ml	Chicken	Mono	IgY	1:2000
Connexin-43	Sigma	C6219	0.5mg/ml	Rabbit	Poly		1:1000
Aquaporin2	Novus Biologicals	NB110-74682SS	0.16mg/ml	Rabbit	Poly		1:100
FLAG M2	Sigma	F1804	1mg/ml	Mouse	Mono	IgG1	1:2000
Myc-tag (71D10)	Cell Signalling Technology	2278	NA	Rabbit	Mono	IgG	1:1000
turboGFP	Origene	TA150041	1mg/ml	Mouse	Mono	IgG2b	1:2000
EGFP	Abcam	ab5450	0.5mg/ml	Goat	Poly		1:2000
β -Actin	Sigma	A2066	0.5mg/ml	Rabbit	Poly		1:5000
GAPDH	Sigma	G8795	1mg/ml	Mouse	Mono		1:2000
CYP11B2	Prof Celso E. Gomez-Sanchez (Mississippi) (Gomez-Sanchez et al., 2014)			Mouse	Mono	IgG1	

* indicated dilutions were used for both immunostaining of cultured cells and tissues and western blotting.

2.1.2 Human adrenal tissue collection and processing

Adrenal tissues from patients who underwent adrenalectomy at Addenbrooke's hospital were collected via Human Tissue Bank facility. These patients were operated on following diagnosis of Primary Aldosteronism. All tissues were obtained with approval from the Cambridgeshire 2 Research Ethics Committee and written informed consent from each patient prior to surgery. APAs and corresponding adjacent normal adrenal tissue were dissected by the histopathologists and depending on the availability were collected as 3 different samples for further processing – 1) fresh frozen in liquid N₂ and stored at -80°C; 2) a piece immersed in RNALater® solution for 24hrs at 4°C to preserve total RNA and stored at -80°C after removing the solution; and 3) in complete cell culture media for isolation of primary cells by digestion with collagenase.

2.1.3 H295R and primary cell culture

H295R cells were routinely grown and maintained in DMEM F-12/HAM media supplemented with 10% fetal-calf serum, 1% ITS (insulin, transferrin & sodium selenite), 1% L-glutamine, and 1% penicillin-streptomycin at 37°C in the presence of 5% CO₂.

Human adrenal primary cells from normal or APA tissue were also cultured in fully supplemented DMEM F-12/HAM media like H295R cells. On receipt of tissue pieces post-adrenalectomy, APAs were minced finely and adjacent normal adrenal was dissected to remove fat and medulla as much as possible before mincing using sterile scalpel. Minced tissue samples were transferred to 50ml falcon tubes and digested with 3.3mg/ml collagenase in complete media. Tubes were incubated in 37°C water-bath for up to 2hr while shaking to disperse cells by digestion of connective tissue. Falcon tubes were vortexed vigorously and centrifuged at 800rpm for 3min. Pelleted cells were resuspended in fresh complete media and transferred to cell culture flasks. Primary cells take about a week to recover and attach to the surface. Cell were trypsinised and plated for any experiments that could be done at the time or frozen in liquid nitrogen for future use.

2.1.4 Genomic DNA extraction

Genomic DNA (gDNA) from normal adrenal and APA samples was extracted using QIAamp DNA Mini kit (51304, Qiagen) according to manufacturer's instructions. Up to 25mg tissue was used per sample and DNA was eluted in 200µl nuclease-free water. All DNA samples were quantified with Nanodrop ND-1000 spectrophotometer (ThermoScientific).

2.1.5 Sanger sequencing

Targeted gDNA regions were amplified using specific primers and up to 100ng total DNA in a 25µl reaction according to the instructions for GoTaq® G2 Flexi DNA Polymerase (M7805, Promega). PCRs were performed using a touchdown PCR program with decreasing annealing temperature from 68°C to 60°C over 16 cycles (TD_68_60). Amplified PCR products were analysed on agarose gel and treated with a mixture of exonuclease and shrimp alkaline phosphatase enzymes (Exo-SAP) to remove excess primers and nucleotides for 1hr at 37°C before setting up sequencing reaction. 5µl cleaned PCR product with either forward or reverse primer was amplified using BigDye® Terminator v3.1 Cycle Sequencing Kit (Applied Biosystems) in a 10µl reaction. Sequencing reaction products were cleaned using magnetic beads and analysed on 3730 DNA Analyser (Applied Biosystems). In case of plasmid DNA sequencing, initial PCR and Exo-SAP steps were not required. 50-100ng of purified plasmid was directly subjected to sequencing reaction with appropriate primer and run on the

analyser. Sequencing results were analysed using DNA variant analysis tool Mutation Surveyor (SoftGenetics).

2.1.6 RNA extraction from human tissues

Tissue samples preserved in RNALater[®] solution (Ambion[™], Life Technologies) and stored in -80°C were used for RNA extraction. Total RNA was extracted from about 50-100 mg normal adrenal tissue and APAs, using PureLink[®] RNA Mini Kit with Trizol[®] (Ambion[™], Life Technologies) according to manufacturer's protocol. Tissues were dissected and homogenised in at least 9 times the volume of Trizol[®] in TissueLyser LT (Qiagen) at 4°C. Prior to elution, RNA on column was treated with DNase (Qiagen) to digest the genomic DNA contamination. Final RNA was eluted in 50µl nuclease-free water and quantified with Nanodrop.

2.1.7 RNA extraction from cultured cells

Total RNA was extracted from freshly cultured cells using PureLink[®] RNA Mini Kit (Ambion[™], Life Technologies) according to manufacturer's protocol. Cells were lysed in the lysis buffer containing β-mercaptoethanol from the kit. Prior to elution, RNA on column was treated with DNase (Qiagen) to digest the genomic DNA contamination. Depending on the starting cell number, final RNA was eluted in 30-50µl nuclease-free water and quantified with Nanodrop.

2.1.8 cDNA synthesis

Single stranded complementary DNA (cDNA) was synthesised from total RNA extracted using AMV reverse transcriptase from Reverse Transcription System (A3500, Promega). Up to 1µg (or 8.9µl) RNA was reverse transcribed in a total 20µl reaction. In case of tissue samples, equal amount of RNA was used for every paired normal and APA samples. For cell culture experiments, equal RNA was used for all samples in an experiment in order to achieve comparative Ct values for house-keeping gene, 18s in qPCRs. Mix of 8.9µl RNA with 0.5µg of Oligo(dT)₁₅ and Random primers each in total volume of 10.9µl was incubated at 70°C for 10min and cooled to 4°C. Once cool following reagents were added to make final reaction of 20µl.

MgCl ₂ , 25mM	4.0µl
Reverse Transcription 10X Buffer	2.0µl
dNTP Mixture, 10mM	2.0µl
Recombinant RNasin [®] Ribonuclease Inhibitor	0.5µl
AMV Reverse Transcriptase (25u/µl)	0.6µl (15u/µg RNA)

This reaction was incubated in thermal cycler at 22°C for 15 min, 42°C for 1 h, and 95°C for 5 min. cDNA was diluted with nuclease-free water 5 times to final volume of 100µl prior to qPCR reaction setup.

2.1.9 Real Time – quantitative PCR and data analysis

Gene (mRNA) expression in cDNA was quantified using pre-designed or custom made TaqMan probes (Applied Biosystems) for targets listed in respective chapters. Duplicate qPCR reactions were set up for each sample with every target probe. 15µl reaction comprised of 7.5µl Fast Advanced TaqMan® Gene Expression Master Mix, 2X (Applied Biosystems), 0.75µl TaqMan probes, 20X (Applied Biosystems), 2-5µl diluted cDNA and 1.75-4.75µl nuclease-free water. qPCR plates were run on ABI 7900 Real-time PCR system.

Threshold cycle number (C_T value) was automatically calculated by the software in the exponential phase of amplification. Duplicates were averaged and ΔC_T was calculated by subtracting house-keeping gene, 18s C_T from target gene C_T for normalisation. $2^{-\Delta C_T} \times 10^7$ values were used to express relative gene expression for paired normal and APA samples and $2^{-\Delta\Delta C_T}$ method was used for analysis of gene expression in cell culture experiments.

2.1.10 Immunohistochemistry

Formalin-fixed paraformaldehyde embedded (FFPE) tissue sections of human normal adrenal and/or APA for immuno-staining were prepared at Human Tissue Bank at Addenbrooke's hospital. FFPE sections were deparaffinised before antigen retrieval was performed. This was achieved by two sequential 10min incubations of slides in Histo-Clear II solution followed by two washes in 100% methanol for 5min each. Slides were further washed in 90% and 70% methanol for 5min each. Slides were rinsed once in Milli-Q water and boiled in R-Universal antigen retrieval buffer (Aptum Biologics) placed in pressure steamer, 2100-Retriever (Aptum Biologics) for 30min followed by cooling for 2hrs before proceeding with staining procedure by either method.

2.1.10.1 DAB method

After antigen retrieval, sections were stained by colorimetric method using EnVision®+Dual Link System-HRP (DAB+) kit (K4065, Dako) according to manufacturer's instructions. This kit contains horseradish peroxidase (HRP) labelled polymer conjugated to anti-mouse and anti-rabbit secondary antibodies, making it suitable for staining with any mouse or rabbit origin primary antibodies. Briefly, endogenous peroxidase activity was blocked by incubation with

the Dual Endogenous Enzyme Block solution for 10mins, followed by a 5min wash in PBS. Sections were incubated with appropriately diluted primary antibodies in the Antibody Diluent (S0809, Dako) for 30min in a humid chamber at room temperature. Negative control slides were incubated with the diluent only. All slides were washed with PBS for 5min and incubated with HRP-labelled Polymer for 30min and washed again with PBS for 5 min. Substrate-Chromogen solution containing DAB+ chromogen was used to develop brown coloured precipitate for up to 10min under observation. No colour development was observed in the negative control slides. Chromogen solution was washed off promptly from all slides using deionised water and Haematoxylin counterstaining for nuclei was performed by incubating in Mayer's Haematoxylin solution (MHS1, Sigma) for 5min. Slides were dipped 8 times in destain solution containing 50% methanol and 1% HCl followed by dipping in tap water for development of blue nuclei stain. Slides were dehydrated in gradient methanol solutions in the reverse order as deparaffinisation and hydration. Slides were finally mounted using Histomount (National Diagnostics) and curated for 24hrs in a fume extractor hood. Slides were scanned at 40x magnification using Aperio scanner at the Tissue Bank and analysed using Aperio ImageScope (Leica Biosystems).

2.1.10.2 Immunofluorescent staining

If needed, sections were incubated with 2ug/ml wheat germ agglutinin (WGA)-Alexa Fluor®633 (W21404, ThermoFisher) for 5min at room temperature and washed twice in PBS. Sections were permeabilised using 0.05% Triton X-100 in PBS (PBST) for 5min at room temperature and washed with PBS. Non-specific binding was blocked by incubating sections in 2% BSA-PBS for 2hrs at room temperature in a humid container. Sections were washed once with PBS and incubated with appropriately diluted primary antibodies in 1% BSA-PBS overnight at 4°C in humid container. Slides were washed with PBST for 5min while agitation and incubated with 1:500 diluted different Alexa Fluor®-conjugated secondary antibodies (ThermoFisher) in 1% BSA-PBS for 2hrs at room temperature. Slides were again washed in PBST for 5mins and mounted with ProLong Diamond mounting media with DAPI (P36966, ThermoFisher). After at least 24hrs of curating slides at 4°C, slides were scanned for immunofluorescence using Axioscan Z1 Slidescanner (Zeiss) and analysed using software Zen Blue Edition (Zeiss).

2.1.11 Plasmids used and their propagation

Various vector plasmids used in this study are listed in Table 5.

Table 5: List of plasmids and vectors used.

Plasmid	Source	Use	Antibiotic resistance	E. Coli strain used
pCR-Blunt® TOPO	Zero Blunt® PCR Cloning Kit (ThermoFisher)	Initial TOPO cloning of Cav1.3 fragments which were later assembled into pcDNA3.1 vector.	Kanamycin	NEB Stable
pcDNA3.1	Prof Sadaf Farooqi's Lab (IMS)	Cloning of N-terminally Flag-tagged full-length Cav1.3 cDNA for overexpression in H295R cells.	Ampicillin	NEB Stable
pIRES2-AcGFP1	Prof Sadaf Farooqi's Lab (IMS)	Cloning of C-terminally Myc-tagged β_{2d} and β_{2e} cDNA for overexpression in tsA-201 cells. There is AcGFP cDNA expression under IRES sequence.	Kanamycin	NEB Stable
pENTR™/D-TOPO	pENTR™/D-TOPO® Cloning Kit (ThermoFisher)	Entry vector for initial cloning of CADM1 cDNA with a C-terminal Myc-tag for gateway cloning into lentiviral pLOC plasmid.	Kanamycin	OneShot Top10
pLOC	Prof Celso Gomez-Sanchez (University of Mississippi)	2nd generation lentivirus expression vector for CADM1 containing tGFP under IRES sequence as marker of transfection/transduction.	Ampicillin	NEB Stable
pLVTH	Didier Trono (Addgene# 12262)	2nd generation lentivector for expression of shRNA under H1 promoter and GFP as marker.	Ampicillin	NEB Stable
psPAX2	Didier Trono (Addgene# 12260)	2nd generation lentiviral packaging plasmid.	Ampicillin	Received as bacterial stab.
pMD2.G	Didier Trono (Addgene# 12259)	VSV-G envelope expressing plasmid for producing lentivirus.	Ampicillin	Received as bacterial stab.

2.1.12 Lentivirus production and titration

HEK293T cells were cultured in complete media (high glucose DMEM supplemented with 10% FBS, antibiotics and L-glutamine) in a 75cm² flasks up to the confluency of 60-70%. At the time of transfection culture media was gently replaced with 8ml of fresh DMEM F-12/HAM media supplemented with 10% FBS, but no antibiotics (media appropriate for the target H295R or primary adrenal cells). Cells were co-transfected with 2 μ g of psPAX2 (packaging plasmid), 1 μ g of pMD2.G (VSV-G envelope expressing plasmid) and 4 μ g of pLOC (over-expression of cDNA) or pLVTH (shRNA) constructs using 21 μ l of 1mg/ml PEI transfection reagent (Polyethylenimine-Max, 24765, Polysciences). The mix of plasmid DNAs and PEI were diluted into 800 μ l of serum-free DMEM media and incubated at room temperature for 15min before adding to the cells dropwise. As both pLOC and pLVTH plasmids contained GFP coding sequence as markers of transfection efficiency, GFP fluorescence was observable at 24hrs. 48hrs from transfection, lentivirus containing culture media was collected from the flask and

stored in fridge. Fresh 8ml antibiotic-free DMEM F-12/HAM was gently added to the cells for another 24hr incubation to enhance lentivirus production. At 72hrs, media from the flask and media collected at 48hrs were pooled for lentivirus concentration procedure.

About 16ml of lentivirus containing media was centrifuged at 2,000rpm for 5min at 4°C and supernatant was filtered through 0.45µM PVDF filters using a 20ml syringe. Cleared supernatant was concentrated about 70-fold to 230µl lentivirus stock by centrifugation in Amicon-15 30k filters (Millipore) at 4,000xg for 30min at 4°C. Concentrated lentivirus was stored at -80°C as 20-30µl aliquots.

Prepared lentivirus was titrated using flow cytometry to estimate the concentration of transducing units in the stock by calculating percentage of GFP positive cells using method described by Kutner and colleagues as a guideline (Kutner et al., 2009). H295R cells were plated at a density of 8×10^4 cells/well in 24-well plates. 24hrs later, total number of cells in a well were counted by trypsinising 3-4 wells. This number is the number of cells at the time of transduction. Media in rest of the wells was replaced with 250µl of complete media containing 8µg/ml Polybrene (Hexadimethrine bromide, 107689, Sigma). 15, 10, 5, 2 or 1µl each of lentivirus to be titrated was added to a well. Some wells were kept un-transduced as controls. Transduced cells were incubated at 37°C for 20hrs and lentivirus containing media was replaced with fresh complete media. Cells were incubated for another 2 days, by when transduced cells expressed GFP and fluorescence was observed. All transduced and un-transduced control cells were trypsinised and resuspended in 150µl PBS. This cell resuspension was subjected to flow cytometry on BD FACSCanto II (BD Biosciences) to collect data for every condition and percentage of GFP+ cells was analysed using Flowing software (Perttu Terho, Turku Centre for Biotechnology, Finland). Finally, lentivirus titre was expressed as transducing units (TU)/ml using formula $TU/ml = (F \times N \times 1000) / V$, where F is the percentage of GFP+ cells, N is the number of cells at the time of transduction and V is the volume (µl) of lentivirus added to each well for transduction.

2.1.13 Lentivirus transduction

H295R or primary adrenal cells were plated in 48 or 96-well plates at a density of 5×10^4 cells/well in 250µl or 2×10^4 cells/well in 100µl complete media respectively. 24hrs later, lentiviral particles were added at multiplicity of infection (MOI) of 2-5 in the presence of 8µg/ml Polybrene in complete media. Culture media containing lentivirus was replaced with fresh complete media after 20hrs incubation. Depending on the experiment, transduced cells were either starved overnight at 72hrs with nil media for drug stimulations or harvested for RNA or protein at the time point of 96hrs.

2.1.14 Immunocytochemistry and confocal imaging

H295R cells were grown on coverslips and transfected/transduced with appropriate constructs. When required, plasma membrane marker WGA-Alexa Fluor® 633 was used at 2ug/ml in complete media for 10 mins at 37°C and rinsed with PBS twice. Cells were fixed with 4% paraformaldehyde (PFA) or chilled methanol for 10mins at room temperature and washed with PBS thrice. Cells were permeabilised using 0.1% Triton X-100 in PBS (PBST) for 5min at room temperature and washed twice with PBS. Cells were blocked with 3% BSA-PBST for 1hr at room temperature and washed once with PBS. Cells were incubated with appropriately diluted primary antibodies in 3% BSA-PBST for overnight at 4°C. Cells were washed thrice with PBS and incubated with appropriate secondary antibody diluted in 3%BSA-PBST for 1hr at room temperature. Cells were washed thrice with PBS and coverslips were mounted in Vectashield with DAPI (Vector Laboratories) on slides. After at least 24hrs of curating slides at 4°C, confocal imaging was performed on 510 Meta (Zeiss) or SP8 (Leica) confocal microscopes.

2.1.15 Drug treatments on H295R and primary cells

Drug treatments on H295R and primary adrenal cells were always performed after an overnight starvation step in the serum-free media. Starved cells were incubated with appropriately diluted drugs and corresponding vehicle controls for 24hr, unless indicated otherwise. In the experiments of drug treatments on H295R cells transduced with lentivirus, starvation was performed at 72hrs from transduction followed by addition of drugs for 24hrs. Except for angiotensin II, all drugs used were dissolved in DMSO of which the final concentration in cell culture media was kept to 0.1% or less, if possible. Angiotensin II stock at 1mM was prepared in sterile water and further dilutions were made in PBS.

2.1.16 Aldosterone assay

Conditioned media from cultured cells was collected into fresh plates and centrifuged to remove any dead cells. 10µl of cleared media sample was assayed for aldosterone concentration using HTRF based Aldo assay kit (Cisbio Bioassays) according to manufacturer's instructions. When required, cell lysis buffer was added to original cell culture plate for total protein estimation by BCA assay for normalisation of aldosterone concentrations and represented as pM/ug. Within an experiment, aldosterone assays data is represented as aldosterone levels relative to control condition.

2.1.17 Protein assay and Western blotting

H295R or HEK293 cells in plates were rinsed with PBS and lysed in minimum volume of the chilled cell lysis buffer required. Lysis buffer used contained freshly added protease inhibitor cocktail solution. Cells were incubated in lysis buffer on ice briefly to ensure complete lysis and lysates were transferred to 1.5ml microfuge tubes. Lysates were cleared of any cell debris by centrifugation at 13,000xg for 20min at 4°C. Cleared supernatant was transferred to fresh tubes and total protein concentration was estimated.

In case of adrenal tissues (normal adrenal and APAs), samples were minced in lysis buffer as much as possible and transferred to 2ml microfuge tubes. Tissue samples were homogenised by brief shaking periods in the TissueLyser LT (Qiagen) using 5mm Stainless Steel Beads (Qiagen) at 4°C. Homogenised lysate was transferred to fresh 1.5ml tubes and centrifuged at 13,000xg for 20min at 4°C. Supernatant was transferred to fresh tubes and total protein concentration was estimated.

Total protein concentration was estimated by using Pierce™ BCA Protein Assay Kit (23227, ThermoFisher) according to manufacturer's instructions. The assay is a colorimetric assay using detection of cuprous ions (Cu^{1+}) by bicinchoninic acid (BCA). Briefly, most cell lysates were diluted 10-15 times in lysis buffer for the protein assay. Protein standards were prepared by 1:2 serial dilutions of 2mg/ml BSA stock solution. 10 μ l protein standards or diluted samples were added to flat bottom 96-well plate. Reagent A was diluted in Reagent B at a concentration of 1:50 and mixed well. 80 μ l of this protein assay reagent was added to each well of standards or samples. Plates were sealed and incubated at 37°C for 20min for purple colour development. The assay plate was analysed in the plate reader for absorbance at 562nm wavelength. Sample protein concentration was calculated by interpolated values from the linear standard curve obtained.

Depending on the protein of interest, SDS-PAGE and western blotting protocols were optimised and varied to obtain best possible results. These variable protocols are explained in relevant sections.

2.1.18 Statistics analysis

Analysis was performed using GraphPad Prism 7 software. All data are presented as the mean \pm standard error or mean (s.e.m.). Differences among the groups were analysed using a one- or two-way ANOVA, followed by the Dunnett's test to determine whether the groups were different from a control group, or the Sidak's test to compare multiple pairs in groups.

CHAPTER 3

CHAPTER 3 - ROLE OF L-TYPE CALCIUM CHANNEL, $Ca_v1.3$ IN ALDOSTERONE SECRETION

3.1 Abstract

Prior to the discovery of *CACNA1D* mutations, L-type Ca^{2+} channels were not considered important in regulation of aldosterone production. Since our lab's discovery of four somatic mutations in *CACNA1D*, over 30 single-base change mutations have been reported in this gene, which encodes the α_1 subunit of an L-type Ca^{2+} channel (LTCC), $Ca_v1.3$. All mutations found initially, and several subsequent mutations cause gain-of-function in the electrophysiological properties with increased activation and/or slowed inactivation of $Ca_v1.3$. I investigated if the mutations in $Ca_v1.3$ influence aldosterone production, and whether the role of the $Ca_v1.3$ is confined to states of aldosterone excess, or crucial in physiological aldosterone regulation too.

Firstly, the most predominant transcripts for $Ca_v1.3$ and the auxiliary β -subunit in the human adrenals, APAs and the adrenocortical carcinoma cell line, H295R was determined. This was necessary to study the functional consequences of $Ca_v1.3$ mutants in the presence of appropriate β -subunit. $Ca_v1.3$ transcript that is 2137 amino acids long and contains exon 8A makes most of the channel expressed. β_{2d} splice variant of β_2 subunit encoded by *CACNB2* was found to be the most predominant isoform expressed in normal adrenals and APAs. Compared to the adjacent normal adrenal glands of the same patients, $Ca_v1.3$ -2137aa and β_2 expression was upregulated only in the ZG-like APAs, and not in ZF-like APAs. β_{2e} was upregulated in the ZG-like APAs. Due to differences in their N-termini sequences β_{2d} and β_{2e} exert distinct modulatory effects on α_1 channel kinetics. No significant differences were found in β_2 subunit mediated voltage dependence of activation of WT or mutant V259D $Ca_v1.3$, but only inactivation properties were influenced by the type of β_2 variant co-expressed. β_{2e} , the membrane-associated subunit, abolished the fast inactivation of only V259D $Ca_v1.3$, compared to that seen in the presence of non-membrane associated β_{2d} subunit. Two of the $Ca_v1.3$ mutations studied led to increased aldosterone secretion in H295R cells.

Secondly, the role of endogenous, non-mutant $Ca_v1.3$ in aldosterone secretion was investigated. Nuclear localisation of intracellular c-terminal of $Ca_v1.3$ in H295R brought our attention to its potential role as transcription factor. Its susceptibility to calpain-mediated cleavage was confirmed by increased levels of full-length $Ca_v1.3$ protein detected in H295R cells treated with calpeptin, a calpain inhibitor. Calpeptin treatment also inhibited

aldosterone secretion. Consistent with these observations was the nuclear localisation of overexpressed C-terminal chain of Cav1.3 resulting in increased aldosterone secretion. Though target genes for Cav1.3's C-terminal as transcription factor were not investigated, its significant role in aldosterone secretion was ascertained by 50% reduction in *CYP11B2* expression in the adrenals of Cav1.3^{-/-} mice compared to wild-type animals.

Lastly, with the [REDACTED] project, scientists at [REDACTED] conducted a high-throughput screening of Cav1.3-expressing cells against their 1.8 million compound library. The lower resting membrane potential of -80mV to -60mV in aldosterone producing adenoma cells (especially with *CACNA1D* mutation) that is more negative than other tissues was exploited in the compound screen. This screen led to 3 tool compounds (A, B & C) that were selective antagonists for Cav1.3 over [REDACTED] in high-throughput electrophysiological experiments. Of these 3 compounds, I found compound B the most effective in inhibiting aldosterone secretion in both H295R and primary cells isolated from normal adrenals. This finding is a significant step in developing compound B further into a Cav1.3-selective drug for treating PA patients without cardiovascular side effects as in the case of existing dihydropyridine class of Ca²⁺ channel blockers.

In this study, we have not only shown Cav1.3 is crucial for physiological aldosterone secretion, but also discovered a novel mechanism that it might fulfil this significant role by acting as a transcription factor in addition to calcium entry point. Discovery of compound B, a potential selective antagonist for Cav1.3 proves promising as a translational application of *CACNA1D* mutations in primary aldosteronism and possibly other Cav1.3 channelopathies like Parkinson's disease and autism.

3.2 Introduction

3.2.1 L-type calcium channels

As the name suggests, voltage-gated calcium channels (VGCCs) are ion channels through which Ca^{2+} ions enter the cells from external medium. These channels open in response to depolarisation of the membrane potential and are present in all excitable cells, like neurons and endocrine cells. For the Ca_v1 (L-type) and Ca_v2 (P/Q-, N- & R-types) families, the functional calcium channel is a heteromeric protein structure formed by a principal pore-forming α_1 subunit with auxiliary β (β_1 - β_4) and $\alpha_2\delta$ ($\alpha_2\delta$ -1 - $\alpha_2\delta$ -4) subunits. These auxiliary subunits regulate channel trafficking to the cell membrane and modulate its electrophysiological properties. Ca_v3 (T-type) channels are believed not to require these auxiliary subunits. Depending on the presence of one of the many α_1 subunit types present, the voltage-dependence (high or low voltage activation) and kinetics of the channel are determined. All channels exhibit distinct properties and are differentially expressed in various cell/tissue types, from neurons to skeletal and cardiac muscles to endocrine glands.

$\text{Ca}_v1.3$ is the α_1 subunit that forms an L-type calcium channel, where L stands for long-lasting inward calcium currents through these channels. Like every α_1 subunit, $\text{Ca}_v1.3$ also has a 4 homologous repeat structure (I-IV), with each repeat consisting of 6 transmembrane α -helices. The fourth transmembrane helix (S4), containing positively charged amino acids, of each repeat along with S1-S3 act as the voltage sensor domain of the channel, whereas S5 & S6 together with their linker loop, line the pore of the channel.

β subunits, encoded by *CACNB1-CACNB4*, are cytoplasmic proteins containing a Src homology 3 (SH3) and an inactive guanylate kinase (GK)-like domain (McGee et al., 2004). They interact with the α_1 subunit at the intracellular loop between repeats I and II. This interaction is required not only for increased channel trafficking to the plasma membrane, but also for channel activation and inactivation (Findeisen and Minor, 2009; Yamaguchi et al., 2000).

$\alpha_2\delta$ subunits, encoded by genes *CACNA2D1-CACNA2D4*, interact with the α_1 subunit at its extracellular domains. Post-translation, $\alpha_2\delta$ subunits are cleaved into α_2 and δ subunits in a proteolytic reaction. The α_2 subunit localises extracellularly but remains bound by a disulphide bond to the δ subunit that is itself anchored to the plasma membrane either by a short transmembrane domain or glycosyl-phosphatidylinositol (GPI)-anchor. Expression of $\alpha_2\delta$ has an additive effect on the enhanced membrane expression and channel conductance of α_1 subunit in the presence of β subunits (Yamaguchi et al., 2000).

3.2.2 Regulation of Ca_v1.3 channel kinetics

Alternative splicing of any expressed gene is a well-recognised phenomenon that adds to molecular diversity of structural and functional proteins. Of all Ca_v1 channels, alternative splicing of rat Ca_v1.3 at its C-terminal is best described. Depending on the length and specific domains present in the C-terminal splice variant, it can be categorised as a “long” or “short” isoform (Xu and Lipscombe, 2001). In addition to pre-IQ and IQ domains, the “long” isoforms also contain proximal C-terminal regulatory domain (PCRD) and distal C-terminal regulatory domain (DCRD) domains forming C-terminal modulatory domain (CTM), that is lacking in “short” isoforms (Singh et al., 2008). Calcium-free calmodulin (apoCaM) binds to the IQ domain that is followed by calcium binding to apoCaM/IQ complex when intracellular or local intracellular Ca²⁺ concentration increases, initiating a negative feedback mechanism described as calcium-dependent inactivation (CDI) of the channel. Inactivation of channels is of critical importance in protection of cells from Ca²⁺ overload in conditions of long depolarisation. The DCRD competes with CaM for binding to the IQ domain resulting in weak CDI in the transcripts containing the full length CTM domain.

Compared to Ca_v1.2, Ca_v1.3 is 20-fold less sensitive to nimodipine, a dihydropyridine (DHP) and activates at 25mV more hyperpolarised potentials (Xu and Lipscombe, 2001). These differences are further exaggerated due to alternative splicing in the C-terminal domain of Ca_v1.3 that not only regulates its CDI, but also extends to DHP sensitivity (Huang et al., 2013) and voltage-dependent activation characteristics (Singh et al., 2008) of various transcripts. DHP sensitivity was reported to be inversely related to CaM/IQ binding mediated CDI. Long variants with weak CDI (e.g. Ca_v1.3₄₂) are more prone to DHP blockade compared to short variants with strong CDI (e.g. Ca_v1.3_{42a}) (Huang et al., 2013). Ca_v1.3_{42a}, with truncated C-terminal domains activates much faster at more negative voltages compared to Ca_v1.3₄₂ (Singh et al., 2008). This is more likely due to the absence in short transcripts of the inhibitory effect that CTM has on coupling of voltage-sensor S4 movement with the S5-S6 lined pore opening (Lieb et al., 2014).

Another form of regulation of CDI of Ca_v1.3 was reported by Huang *et al.* in rodent brain and isolated primary neurons. This unique mechanism, RNA editing is the post-transcriptional modification of adenosine-to-inosine (A to I) in mRNA sequence which translates into alternative amino acids. This phenomenon is reported in many proteins and recently in Ca_v1.3 too. It occurs in the IQ domain of Ca_v1.3 producing proteins with modified amino acid sequences like MQDY, IQDC or MQDC as opposed to unedited IQDY. Ca_v1.3 channels with edited IQ domain sequences were shown to exhibit weakened CDI by reducing the CaM affinity for PCRD in the C-terminus (Huang et al., 2012).

In addition to calcium-dependent inactivation calcium channels exhibit voltage-dependent inactivation (VDI) which is triggered by the same membrane depolarisation that initially activates and opens the channel. As the name suggests VDI reduces the open probability of calcium channels during long or subsequent membrane depolarisations. Similar to CDI, one of the major regulators of VDI is the associated β subunit (Cens et al., 1999). All β subunits, except for membrane bound β_2a , have been demonstrated to promote VDI of the channels (Buraei and Yang, 2010).

3.2.3 Expression and pathophysiology of $Ca_v1.3$

Along with $Ca_v1.2$, $Ca_v1.3$ is expressed in many excitable cells in brain and heart. Platzter et al. generated $Ca_v1.3$ null mice by inserting neomycin resistance gene within the exon 2 in the reverse strand by homologous recombination. This led to introduction of multiple stop codons in all 3 frames and hence translation into a truncated peptide.

These $Ca_v1.3$ knockout mice showed abnormal cochlear morphology due to degeneration of outer hair cells of ears. Complete loss of Ca^{2+} currents in inner hair cells led to complete hearing loss in the absence of $Ca_v1.3$ (Platzter et al., 2000). It is also expressed in the heart, particularly in the pacemaker cells of sinoatrial node (SAN) and atrioventricular node (AVN) where it plays a significant role in the pace-making activity as revealed by reduced heart rate and cardiac arrhythmia in $Ca_v1.3$ null mice (Mangoni et al., 2003). These phenotypes are replicated in humans suffering from SAN dysfunction and deafness (SANDD) syndrome due to a loss of function mutation, G403dup in *CACNA1D* (Baig et al., 2011).

In addition to the somatic mutations in 5 APAs, Scholl et al. reported 2 cases of *de novo* germline mutations, G403D and I770M in *CACNA1D*. These patients were diagnosed with neurological disorders and hypertension from birth, with elevated aldosterone levels despite suppressed plasma renin activity (PRA) (Scholl et al., 2013). This multi organ syndrome has been termed as primary aldosteronism, seizures and neurologic abnormalities (PASNA). Three *de novo* mutations in *CACNA1D* - G407R, A749G and V401L were reported in the patients suffering from autism spectrum disorder and epilepsy (Pinggera et al., 2015, 2017). Similar to the most somatic mutation in APAs, all these *de novo* germline mutations result in gain of function of $Ca_v1.3$ with a shift in voltage dependence of activation and inactivation to more negative voltages and reduced channel inactivation.

Increased mitochondrial oxidative stress due to $Ca_v1.3$ -mediated increased Ca^{2+} currents in the dopaminergic neurons has been implicated in cell death associated with Parkinson's

disease. Surmeier et al. presented some evidence of preventing cell death in the substantia nigra neurons (SNc) by using low doses of dihydropyridines to inhibit Cav1.3 as a potential therapeutic target for treatment of Parkinson's disease (Surmeier et al., 2011).

Cav1.3 probably plays a role in the regulation of aldosterone secretion but its endocrine function is studied in more detail in pancreas and adrenal medulla. It plays a critical role in the proliferation of pancreatic β cells (Namkung et al., 2001), but there are no evidences of impaired insulin secretion or difference in the plasma glucose levels of the knockout mice, which could be due to compensatory increased expression of Cav1.2 (Platzer et al., 2000). Cav1.3's pace-making role was also evident in the normal firing of action potentials in mouse chromaffin cells (MCCs), which was reduced in the MCCs from Cav1.3 knockout mice (Marcantoni et al., 2010). This pace-making activity of chromaffin cells is essential for normal secretion of catecholamines from adrenal medulla.

3.2.4 Role as transcription factor

It has been reported that the C-terminal of Cav1.2 is cleaved to generate calcium channel associated transcription factor (CCAT) which translocates to nucleus regulating expression of itself and various other proteins in neurons and cardiomyocytes (Gomez-Ospina et al., 2006, 2013; Schroder et al., 2009). A similar phenomenon is recently reported for Cav1.3 acting as transcriptional regulator in atrial myocytes, where its cleaved C-terminal translocates to nucleus in a directly regulated manner by levels of intracellular Ca^{2+} . Cav1.3 c-terminal upregulates the expression of MLC2, myosin light chain 2 (Lu et al., 2015), which plays an important role in the regulation of myosin ATPase activity and is required for the surface expression of Ca^{2+} activated K^+ channels (SK2) in myocytes. Cleaved c-terminal is believed to be exported out of nucleus when intracellular calcium increases, possibly to inhibit the channel activity and also to alter gene transcription. The proteolytic cleavage of Cav1.1 in skeletal muscles and Cav1.2 in hippocampal neurons is mediated by proteases of calpain family (Hell et al., 1996) at an alanine residue downstream of PCRD (Hulme et al., 2005). Calpain2, *CAPN2* is the most predominantly expressed of all calpains in the adrenal cortex (Shaikh et al., 2015; Zhou et al., 2015). It is important to note that despite high conservation of putative cleavage site sequence among Cav1.1, Cav1.2 and Cav1.3, there was no evidence of proteolytic cleavage of Cav1.3 in mice brain homogenates (Scharinger et al., 2015). The cleavage of c-terminal domain modulates the channel activity by removal of DCRD which normally competes with calmodulin for binding to PCRD. Properties of the residual Cav1.3 channel activity were not studied (Lu et al., 2015), but cleaved Cav1.2 is reported to carry more current due to lack of auto-inhibitory c-terminal domain (Hulme et al., 2006).

3.2.5 Calcium channels in adrenals

Microarray analysis for calcium channels' subunits expression in human adrenals revealed α_1D (Ca_v1.3), $\alpha_2\delta$ -1 and β_2 to be the most predominant of all types (Table 6) (Shaikh et al., 2015; Zhou et al., 2015). Until recently, the low voltage activated T-type calcium channel Ca_v3.2 was thought to be the primary mode of Ca²⁺ entry into the ZG cells, activating downstream pathways for aldosterone synthesis and secretion (Cohen et al., 1988; Payet et al., 1994). But discovery of gain-of-function somatic mutations in the gene *CACNA1D* provided evidence for critical role of the L-type calcium channel, Ca_v1.3 in this system (Azizan et al., 2013; Scholl et al., 2013). More recently, a germline gain-of-function mutation M1549V in *CACNA1H*, the gene encoding Ca_v3.2 was discovered in 5 patients with the onset of hypertension with PA by the age of 10 years (Scholl et al., 2015). The mutated channel exhibited slower activation and inactivation resulting in increased calcium entry.

Table 6: Microarray expression data for Ca²⁺ channel subunits in ZG and ZF of adrenal cortex.

Subunit Type	Gene ID	log ₂ expression
α_1 (Ca _v 1.3)	<i>CACNA1D</i>	6.36
$\alpha_2\delta$ -1	<i>CACNA2D1</i>	6.15
β_2	<i>CACNB2</i>	5.90
α_1 (Ca _v 3.2)	<i>CACNA1H</i>	3.83
γ_8	<i>CACNG8</i>	3.58
α_1 (Ca _v 3.3)	<i>CACNA1I</i>	3.15
β_3	<i>CACNB3</i>	3.12
β_1	<i>CACNB1</i>	2.99
β_4	<i>CACNB4</i>	2.84
$\alpha_2\delta$ -4	<i>CACNA2D4</i>	2.74
γ_7	<i>CACNG7</i>	2.73
γ_4	<i>CACNG4</i>	2.72
γ_1	<i>CACNG1</i>	2.64
γ_6	<i>CACNG6</i>	2.63
α_1 (Ca _v 2.2)	<i>CACNA1B</i>	2.53
α_1 (Ca _v 1.4)	<i>CACNA1F</i>	2.52
α_1 (Ca _v 2.3)	<i>CACNA1E</i>	2.52
α_1 (Ca _v 1.2)	<i>CACNA1C</i>	2.51
α_1 (Ca _v 3.1)	<i>CACNA1G</i>	2.47
α_1 (Ca _v 2.1)	<i>CACNA1A</i>	2.46
$\alpha_2\delta$ -2	<i>CACNA2D2</i>	2.44
$\alpha_2\delta$ -3	<i>CACNA2D3</i>	2.44
α_1 (Ca _v 1.1)	<i>CACNA1S</i>	2.44
γ_5	<i>CACNG5</i>	2.34
γ_2	<i>CACNG2</i>	2.25
γ_3	<i>CACNG3</i>	2.18

For a number of years ZG cells were believed to be electrically unexcitable (Quinn et al., 1987), but Hu et al. provided evidence for their electrical activity in intact glomeruli structures. They argued that Ca^{2+} release from intracellular stores is insufficient for sustained aldosterone secretion from ZG cells and continuous Ca^{2+} entry from extracellular media is essential (Hu et al., 2012). This would normally be not possible in isolated ZG cells that are too hyperpolarised (at -80mV, very close to K^+ equilibrium) in resting conditions to favour opening of any calcium channels (Quinn et al., 1987; Spät, 2004). They demonstrated ZG cells within the intact glomeruli structures in mouse adrenal slices were electrically excitable and had intrinsic oscillations of membrane potential facilitating periodic calcium entry. These oscillations in the membrane potential are sensitive to Ni^{2+} but not nifedipine, indicating a more important role of $\text{Ca}_v3.2$ over $\text{Ca}_v1.3$ in the pacemaker activity in mouse ZG cells (Barrett et al., 2016; Hu et al., 2012).

3.2.6 $\text{Ca}_v1.3$ antagonists

Various classes of calcium channel blockers (CCBs) used are dihydropyridines (nifedipine, isradipine, nimodipine, amlodipine, etc.), phenylalkylamines (e.g. verapamil) and benzothiazepines (e.g. diltiazem), which bind reversibly to different subunits of calcium channels inhibiting calcium entry. DHPs are the major class of these drugs that bind close to the pore-forming domains of the α_1 subunit of L-type calcium channels, inducing inactivated state of the channel. DHPs are not selective and inhibit all $\text{Ca}_v1.1$ – $\text{Ca}_v1.4$ with variable affinities. In general among all LTCCs, $\text{Ca}_v1.2$ is the most sensitive to DHPs, making them first choice of treatment for hypertension by targeting $\text{Ca}_v1.2$ in cardiovascular tissues. Verapamil and diltiazem also inhibit calcium channels by blocking the calcium entry pore.

In patients with resistant hypertension (PA) aldosterone receptor antagonist, spironolactone, is the only drug used at the moment but has its limitations due to its affinity for androgen and progesterone receptors. The dose and efficacy of spironolactone is limited in male patients because of its side-effects causing gynaecomastia and sexual dysfunction. It also causes menstrual irregularities in female patients. Eplerenone, also an MR antagonist is more selective with fewer sex-related side effects can also be used, but is more expensive in many countries.

3.2.6.1 *Compound 8*

The lower sensitivity of $\text{Ca}_v1.3$ for DHPs makes them less favourable for $\text{Ca}_v1.3$ specific blockade as required in conditions such as Parkinson's disease or primary aldosteronism. Higher doses of DHPs required for blocking $\text{Ca}_v1.3$ would potentially lead to deleterious cardiovascular side effects because of unwanted $\text{Ca}_v1.2$ blockade. In an attempt to find a

selective Cav1.3 antagonist, Kang et al. used a small molecular screen and discovered a pyrimidinetrione (PYT), 1-(3-chlorophenethyl)-3-cyclopentylpyrimidine-2,4,6-(1H,3H,5H)-trione, named as compound 8 to be 600-fold selective antagonist for Cav1.3 over Cav1.2 in a fluorescent imaging plate reader (FLIPR) assay on HEK293 cells stably expressing these calcium channels (Kang et al., 2012). But soon contradictory reports emerged suggesting compound 8 belongs to a new class of LTCCs agonist rather than antagonist as it increased overall Ca²⁺ currents by slowing activation, inactivation and tail currents of Cav1.3 (Ortner et al., 2014). Another group then provided evidence for selectivity of compound 8 being highly dependent on the type of β subunit present in the system (Huang et al., 2014). They found compound 8 inhibited Cav1.3 only modestly and only in the presence of non-membrane associated β subunits (β_1 , β_3 or β_4) but not the palmitoylated β_{2a} . Also currents through Cav1.2 were inhibited to greater extent in the presence of β_{2a} than those through Cav1.3 (Huang et al., 2014). Our group studied the effect of compound 8 on aldosterone secretion from H295R and primary adrenal cells (Xie et al., 2016). We found that at 1 μ M concentration, compound 8 stimulated aldosterone secretion in H295R cells which express both Cav1.3 & Cav1.2, but not in primary cells mainly expressing Cav1.3. At higher concentrations of 10 and 100 μ M aldosterone was inhibited in both cell types, similar to a commonly used dihydropyridine, nifedipine.

3.2.7 Cav β_2 subunit

Cav β_2 subunit is encoded by the *CACNB2* gene that was first cloned along with *CACNA1D* (Cav1.3) in 1992 using a human hippocampal cDNA library (Williams et al., 1992). In following years five alternatively spliced variants β_{2a} - β_{2e} were cloned and studied for their influence on functional properties of the α_1 subunit of L-type calcium channels (Allen and Mikala, 1998; Yamaguchi et al., 2000). These five transcripts vary in sequence at their N-terminal due to alternative splicing of the first and/or second exons (Fig. 10) (Takahashi et al., 2003). β_2 transcripts are expressed in all excitable tissues, like brain and heart, and are developmentally regulated (Table 7).

Heterologous expression of recombinant β_2 splice variants in HEK293 cells demonstrated their differential sub-cellular localisation to be the key factor influencing their modulatory roles on L-type calcium channel kinetics. β_{2a} and β_{2e} localise to plasma membrane constitutively even in the absence of α_1 subunit, whereas β_{2b} , β_{2c} and β_{2d} remain in the cytoplasm (Takahashi et al., 2003). This preferential localisation of β_{2a} and β_{2e} subunits slows the voltage-dependent inactivation of LTCCs as compared to when expressed with any of β_{2b} - β_{2d} . The β_{2a} variant remains plasma membrane bound due to palmitoylation of two cysteine residues present in its N-terminal (Chien et al., 1996). On the other hand, β_{2e} is recruited to plasma membrane by electrostatic forces between two amino acid residues (positively charged lysine and

hydrophobic tryptophan) in its N-terminal and anionic phospholipids of the membrane (Kim et al., 2015; Miranda-Laferte et al., 2014). Neither of these two characteristic features for plasma membrane localisation are present in the N-termini of β_2b - β_2d .

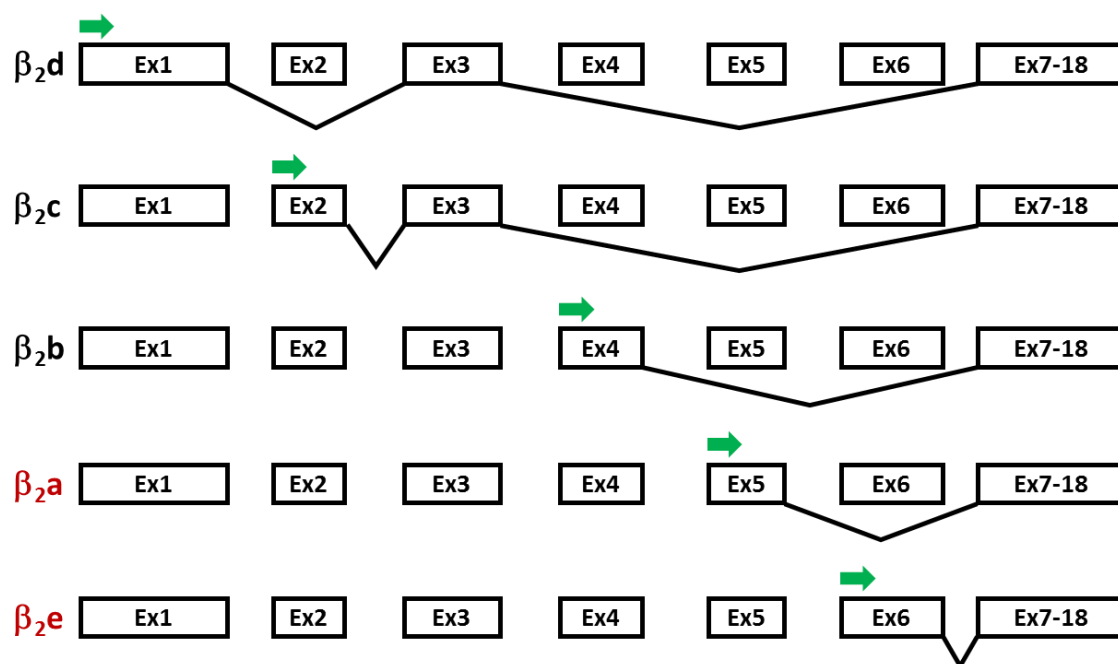


Fig. 10: Alternative splicing of β_2 subunit transcripts.

Green arrows show translational initiation sites for each transcript and membrane associated β_{2a} & β_{2e} are shown in red. Adapted from (Takahashi et al., 2003)

Table 7: Tissue distribution of β_2 subunit transcripts

(Buraei and Yang, 2010)

β_2	Tissue distribution
β_2	Expressed in brain (hippocampus—becoming the most abundant isoform there, cerebellum, pontine nucleus, substantia nigra, central grey, habenula, pineal gland, thalamic nuclei, cerebrum), heart, lung, nerve endings at the NMJ, T cells, and osteoblasts, but not in kidney, liver, pancreas, or spleen. Brain expression is constant during development.
β_{2a}	Expressed in brain, heart, and aorta; its heart and brain levels seem lower than other β subunits and isoforms.
β_{2b}	Expressed in brain, heart, and aorta. It is the most abundant β in human heart.
β_{2c}	Expressed in brain and heart, where it is the second most abundant β . Its expression declines in adults.
$\beta_{2d,e}$	Expressed in heart. β_{2e} expression is robust only in young animals.

3.2.8 Aims and Hypotheses

The somatic mutations in *CACNA1D* have been shown to cause gain-of-function phenotype in the electrophysiological properties of Ca_v1.3 (Azizan et al., 2013; Scholl et al., 2013). It is hypothesised that expression of these mutant Ca_v1.3 channels would increase intracellular calcium and aldosterone secretion *in vitro* by human adrenocortical carcinoma cell line, H295R.

Role of endogenous Ca_v1.3 in non-mutated state requires detailed investigation to establish if and how it regulates physiological aldosterone secretion.

Determination of Ca_v1.3 as the main source of sustained calcium entry for regulated and/or autonomous aldosterone secretion led our interest towards its potential as a valuable and novel therapeutic target for treatment of primary aldosteronism. [REDACTED] [REDACTED] aimed at screening millions of compounds that would selectively block Ca_v1.3 over other ion channels, especially [REDACTED] to minimise unwanted cardiovascular side-effects. This selective molecule should be able to block aldosterone production in APAs. It would be of significant value in treating patients with resistant hypertension driven by APAs, not only with *CACNA1D* mutations, but also those without *CACNA1D* mutations, by blocking unregulated Ca²⁺ influx altogether despite membrane depolarisation due to other dysfunctional ion channels.

3.3 Materials and methods

3.3.1 Molecular cloning and site directed mutagenesis

3.3.1.1 *Ca_v1.3* in *pcDNA3.1*

Total cDNA from H295R cells was used to amplify coding sequence for any one of the 3 long transcripts of *Ca_v1.3* in 3 fragments with overlapping sequences using specific primers listed in Table 8. All fragments were amplified using Q5 DNA polymerase 2X master mix and cloned into pCR-Blunt® TOPO vector of Zero Blunt® PCR Cloning Kit (Invitrogen). Several clones were screened for each fragment and sequence verified.

Table 8: Primers used for *Ca_v1.3* cDNA amplification

Amplicon	Primer Name	Sequence	Amplicon size (bp)
Amp-1	Ca _v 1.3-Start-F	ATGATGATGATGATGATGATGAAAA	2227
	Ca _v 1.3-R5	GAATATAGTTACCACAAATGAAG	
Amp-2	Ca _v 1.3R5-F	CTTCATTTGTGGTAACTATATTC	2242
	Ca _v 1.3-F11-R	CTTGCCTCAGGGTCATATTCTG	
Amp-3	Ca _v 1.3-F11	CAGAATATGACCCTGAGGCAAAG	1991
	Ca _v 1.3-Stop-R	CTACAAGGTGGTGATGCATATCA	

Coding sequence for FLAG-tag was added in the forward primer for first fragment that will produce N-terminally FLAG-tagged protein. TOPO construct with *Ca_v1.3*-Amp1 was used as template to produce FLAG-tagged fragment that was later used in Gibson assembly reaction.

<i>KpnI</i> - FLAG - <i>Bam</i> HI- Ca_v1.3 -F	GTTGGTACCGCCACCATGGATTACAAGGATGACGACGATA AGGGATCCATGATGATGATGATGATGATGAAAA
--	---

FLAG-*Ca_v1.3*-Amp1 PCR product and TOPO constructs with *Ca_v1.3*-Amp2 & *Ca_v1.3*-Amp3 were used as templates to amplify overlapping fragments compatible with the Gibson assembly kit (NEB) using primers shown in Table 9. The assembly reaction was set up using 0.25pmoles each of 3 purified PCR products and *pcDNA3.1* vector (digested with *KpnI* and *XhoI*). Total 1pmole DNA fragments were mixed with 2X Gibson Assembly mix and incubated at 50°C for 1hr followed by transformation into Stable Competent *E. coli* (NEB) according to manufacturer's instructions. Clones were screened and sequence verified to a final construct of FLAG-*Ca_v1.3* in *pcDNA3.1*. The insert cDNA of *Ca_v1.3* corresponded to 2137 amino acid long transcript (NM_001128839).

Table 9: Primers used for Cav1.3 Gibson Assembly

Amplicon	Primer Name	Sequence	Amplicon size (bp)
GAmp-1	<u>KpnI</u> -FLAG-Cav1.3-GA1_F	TTTAAACTTAAGCTTGGTACCGCCACCATGGATTACAAG	2274
	Cav1.3-GA1_R	ACAAATGAAGAGGATGATGAAGTAGATGC	
GAmp-2	Cav1.3-GA2_F	TCATCATCCTCTTCATTTGTGGTAACTATATTCTAC	2239
	Cav1.3-GA2_R	TCATATTCTGACCATATTCTTTTGAATTCATCTAAATG	
GAmp-3	Cav1.3-GA3_F	AGAATATGGTCAGAATATGACCCTGAGG	2026
	Cav1.3- <u>XhoI</u> -GA3_R	TTTAAACGGGCCCTCTAGACTCGAGCTACAAGGTGGTGATGCATATC	

3.3.1.2 Cav1.3 mutagenesis

FLAG-Cav1.3 construct was used for generating 7 mutants using Q5 site-directed mutagenesis kit (NEB). Mutagenesis primers were designed using NEBaseChanger online tool (NEB) (Table 10). Linear mutant PCR product was generated by Q5 DNA polymerase master mix, 2X (NEB) and treated with KLD enzyme mix for 5min at room temperature followed by transformation into Stable Competent E. coli (NEB) according to manufacturer's instructions.

Positive clones were selected on Ampicillin LB-Agar plates and verified by sequencing.

3.3.1.3 β_2 constructs in pIRES2-AcGFP1

Myc-FLAG-tagged β_2c construct (pCMV6-Entry vector, NM_201571) was purchased from Origene Technologies, which served as the template for β_2d (NM_201596) and β_2e (NM_201570) constructs by mutagenesis using following primers (Table 11).

Table 10: List of Ca_v1.3 mutagenesis primers

Mutagenesis Primer	Sequence (lower case = mutant nucleotide)
Ca _v 1.3_V259D_F	AGTTTACAAGaTGCCTGAACTCC
Ca _v 1.3_V259D_R	GGGCACTCCTGACACTAG
Ca _v 1.3_G403R_F	TCTTGTACTIONcGTGTATTGAGCG
Ca _v 1.3_G403R_R	TTAGTACGAAAAATGACCC
Ca _v 1.3_F747L_F	TGAATGTCTTgTTGGCCATCG
Ca _v 1.3_F747L_R	GTAGAATATAGTTACCACAAATG
Ca _v 1.3_I750M_F	TCTTGGCCATgGCTGTAGACA
Ca _v 1.3_I750M_R	AGACATTCAGTAGAATATAGTTACC
Ca _v 1.3_R990H_F	AGGGTCCTGCaTCCCCTCAGG
Ca _v 1.3_R990H_R	TAAGACCCTCAGAATCTTCACAACG
Ca _v 1.3_P1336R_F	CAGGCGCTCCgGTATGTGGCC
Ca _v 1.3_P1336R_R	AAAGGACTTAATAAAAAGTCCACAGCAATG
Ca _v 1.3_M1354I_F	TCATTGGCAtaCAGATGTTTGG
Ca _v 1.3_M1354I_R	CCGCATAGATGAAGAACAG

Table 11: List of β₂ mutagenesis primers

Primer	Sequence (Uppercase = target-specific primer)
β ₂ d insert1 F	cccacagcggcgggcggtggcgaggagTCATATGGAAAAGGAGCCAG AAGGAAAAACAGATTTAAAGG
β ₂ d insert1 R	aggcgacttgacatgtcccttggaccatGGCGATCGCGGCGGCAGA
β ₂ d insert2 F	cccggggggcgctcggagccgcccacagTCATATGGAAAAGGAGCCAG AAGGAAAAACAGATTTAAAGGATCTG
β ₂ d insert2 R	agccacgttctctagcagttccatctggatCTCCTGCGCCACCGCCGC
β ₂ e insert F	caaggaggaaggctgaagaattctgatctgtGGTTCGGCAGACTCCTAC ACTAGC
β ₂ e insert R	gctcttttcagaagcctgatccaggtggccttcatGGCGATCGCGGCGGCAGA

As before, Q5 site-directed mutagenesis kit and Stable Competent *E. coli* (NEB) were used according to manufacturer's instructions. Once clones were verified by sequencing for presence of β₂d or β₂e complete ORF, they were sub-cloned, by Gibson assembly method, into pIRES2-AcGFP1 plasmid between EcoRI and BamHI restriction sites with a C-terminal Myc-tag.

3.3.1.4 *Ca_v1.3 C-terminal cloning in pLOC*

To study the role of C-terminal of Ca_v1.3 in aldosterone secretion, this fragment was cloned in pLOC vector in 3 steps. Firstly, the pore-forming region of Ca_v1.3 was deleted from the full-length Ca_v1.3 construct in pcDNA3.1 (described in 3.3.1.1) using NEB site directed mutagenesis kit. Resulting construct contained 682 amino acids corresponding to the intracellular c-terminal peptide sequence of Ca_v1.3 2137 amino acid long transcript (NM_001128839) with a FLAG tag on N-terminal, which was amplified for directional TOPO cloning in pENTR vector. At this stage, a Myc-tag sequence was added in the 3' primer to generate "FLAG-Ca_v1.3 CT-Myc" construct in the Gateway cloning entry vector. All primers used in this cloning are listed in Table 12. Lastly, the recombination reaction was performed to transfer the ORF sequence from pENTR construct to pLOC vector using LR Clonase II enzyme mix (11791020, Invitrogen) according to manufacturer's instructions. Recombined plasmids reaction was transformed into Stable competent cells (NEB) and selected on LB agar plates containing ampicillin. Positive clones were miniprep'd and sequence verified. Clones with correct sequences were maxiprep'd and used for preparing lentivirus by transfection of HEK293T cells.

Table 12: Ca_v1.3 C-terminal cloning primers

Primer name	Primer Sequence
Ca _v 1.3-delPore-F	ACCCGGGACTGGTCTATTTT
Ca _v 1.3-delPore-R	CATGGTGGCGGTACCAAG
TOPO-FLAG-F	CACCATGGATTACAAGGATG
Ca _v 1.3-CT-Myc-R	GAATTCCTACAGATCTTCTTCGCTAATCAGTTTCTGTTCCAAGGTGGT GATGCATATCATTTC

The original pLOC plasmid which contains ccdB gene between attR cloning sites, was not recommended for transfection of mammalian cells. Therefore in addition to the Ca_v1.3CT construct in pLOC, a control vector was prepared by cloning puromycin resistance gene into pENTR and recombining with original pLOC. The PuroR-pLOC construct was used as the transfection control empty vector (EV) in this study.

3.3.1.5 *Ca_v1.3 shRNA in pLVTH*

shRNA sequences for scrambled (non-targeting control) or specific to Ca_v1.3 [shRNA1: CCGAATAGCTCCAAGCAAA and shRNA2: GGAAGACCCAGAGATACA, as used by (Samak et al., 2011)] (Fig. 11) were inserted in the pLVTH vector using Q5 site-directed mutagenesis kit (NEB). Mutagenesis primers were designed using NEBaseChanger online tool (NEB) to insert shRNA, consisting of sense, loop and antisense sequences into the vector (Table 13).



Fig. 11: Sequences for scrambled (a) and Cav1.3 (b) shRNAs in pLVTH

Table 13: Cav1.3 shRNA cloning primers

Primer Name	Primer sequence
scrambled-F	tccaacgaggttattacgtaaggtattTTTTGGAAAAGCTTATCGATAC
scrambled-R	tccaacgaggttattacgtaaggtatccGGGGATCTGTGGTCTCAT
shCav1.3-1-F	atccgtttgcttgagctattcggTTTTGGAAAAGCTTATCGATACC
shCav1.3-1-R	atcaatgtgcttgagctattcggGGGGATCTGTGGTCTCATA
shCav1.3-2-F	atccgtgtatctctgggtcttccTTTTGGAAAAGCTTATCGATACC
shCav1.3-2-R	atcaatgtatctctgggtcttccGGGGATCTGTGGTCTCATA

Mutagenesis KLD reaction was used to transform NEB Stable E.coli and selected on LB agar plates containing ampicillin. Positive clones were miniprep'd and sequence verified. Clones with correct sequences were maxiprep'd and used for preparing lentivirus by transfection of HEK293T cells.

3.3.2 Electrophysiology

3.3.2.1 tsA-201 cell culture and transfection by Fugene

tsA-201 cells were routinely grown and maintained in DMEM media (Gibco), supplemented with 10% fetal-calf serum, 1% L-glutamine and 1% penicillin-streptomycin at 37°C in the presence of 5% CO₂.

tsA-201 cells were plated in 3.5cm cell culture dishes at about 50% confluency. 3-4hrs later cells were transfected with plasmid constructs for calcium channel subunits, $\alpha_1\beta:\alpha_2\delta-1:YFP$

in the ratio of 3:2:2:0.4 μg respectively using Fugene (Promega) according to manufacturer's instructions and incubated at 37°C in the presence of 5% CO_2 .

3.3.2.2 Whole-cell patch-clamp electrophysiology

48hrs post transfection, tsA-201 cells were replated in new 3.5cm cell culture dishes in 2ml complete medium. Generally transfected cells were lifted using cell dissociation medium (Gibco) and depending on the confluency 1/8th to 1/12th of cells were plated in new dishes and incubated at 37°C in the presence of 5% CO_2 for at least 2hrs. Cells were rinsed with whole cell patch clamping external solution containing 10mM CaCl_2 or BaCl_2 as indicated. CsCl buffer was used as the internal solution to fill 2-4M Ω borosilicate glass electrodes. Cells positive for YFP fluorescence were patched for whole cell patch clamp recordings at room temperature and 70% compensated for series resistance and capacitance before any recordings were taken.

Cells were held at a holding potential of -80mV before a step protocol of 50ms to different voltages was applied to determine the current-voltage (I-V) relationship. Currents were leak subtracted using a P/8 protocol. I-V curves were fitted to the equation $I = G_{\text{max}}(V - V_{\text{rev}})/(1 + \exp(-(V - V_{50})/k))$, where V_{rev} is the reversal potential, V the test potential, I the peak current, G_{max} the maximum conductance, V_{50} the half-maximal activation voltage and k the activation slope factor. The voltage dependence of the Ca^{2+} or Ba^{2+} conductance was fitted according to a Boltzman distribution $G = G_{\text{max}}/(1 + \exp(-(V - V_{50})/k))$ using GraphPad Prism 6 (GraphPad Prism software).

The inactivation time course was measured during 1s depolarizations from -80mV to indicated voltages (-20 to 30mV) and r_{300} was calculated as the fraction of current remaining at 300ms from the start of the depolarisation step.

The steady state inactivation was measured by applying pre-sweep conditioning voltages for 5s and a subsequent 50ms test pulse to V_{max} (30 s recovery between protocols). Inactivation was calculated as the ratio between the current amplitudes of the test pulses versus current amplitude at V_{max} ($I/I_{V_{\text{max}}}$). Steady-state inactivation parameters were obtained by fitting the data to a modified Boltzmann equation $G = (1 - G_{\text{max}})/(1 + \exp(V - V_{50})/k) + G_{\text{max}}$.

3.3.3 Transfection of H295R cells by electroporation

Up to 5×10^6 cells were aliquoted and resuspended in 100 μ l Mirus Ingenio electroporation solution (Mirus) per transfection and mixed with 3 μ g of each plasmid DNA. Cells were electroporated in 0.2cm cuvettes in Amaxa Nucleofactor system (Lonza) using program T-20 and diluted in serum-containing antibiotic-free media to plate 1.5×10^5 cells in 200 μ l media/well of a 96-well plate.

3.3.4 Western blotting

According to the experiment and availability of total protein estimated by protein assay, 10-40 μ g cell lysate protein was diluted with the 4X NuPAGE™ LDS Sample Buffer (NP0007, ThermoFisher) and 10X NuPAGE® Sample Reducing Agent (NP0009, ThermoFisher). Samples were incubated at 37°C for 5 min before running on NuPAGE™ 3-8% Tris-Acetate Protein Gels (ThermoFisher) in NuPAGE™ MOPS SDS Running Buffer (NP0001, ThermoFisher) at 150V for 1hr at room temperature. 500 μ l NuPAGE™ Antioxidant (NP0005, ThermoFisher) was diluted in 200ml running buffer in the upper chamber of running tank to prevent the re-oxidation of proteins.

For western blotting, gels were removed from gel-casting plates and nitrocellulose membrane with no auto-fluorescence were equilibrated in the transfer buffer prepared from 20X NuPAGE Transfer Buffer (NP0006, ThermoFisher), 10% methanol, 0.05% SDS and 0.1% NuPAGE™ Antioxidant for 10min and 5min before setting up the transfer stacks. Protein transfer was set up at 10-15V for overnight in the cold room.

Nitrocellulose membranes with transferred proteins were blocked in 5% fat-free milk-TBS solution for 1hr at room temperature and incubated with primary antibodies diluted in 5% milk-TBST (with 0.1% Triton X-100) overnight at 4°C. Two primary antibodies from different species (mouse, rabbit or chicken) were used at the same time at this step as species-specific secondary antibodies conjugated with either IRDye 680RD or IRDye 800CW fluorophores were used for detection by Odyssey scanner, Li-Cor. Membranes incubated with primary antibodies were washed in TBST 3 times for 5min each at room temperature and incubated with secondary antibodies diluted in 5% milk-TBST for 1hr. Membranes were washed again in TBST for 30min and rinsed in deionised water before scanning for protein detection using 700nm and 800nm channels in the Odyssey scanner. Resulting images were analysed with ImageStudio Lite software (Li-Cor).

[REDACTED]

[REDACTED]

[REDACTED]

[REDACTED]	[REDACTED]
[REDACTED]	[REDACTED]
[REDACTED]	[REDACTED]
[REDACTED]	[REDACTED] [REDACTED]

[REDACTED]

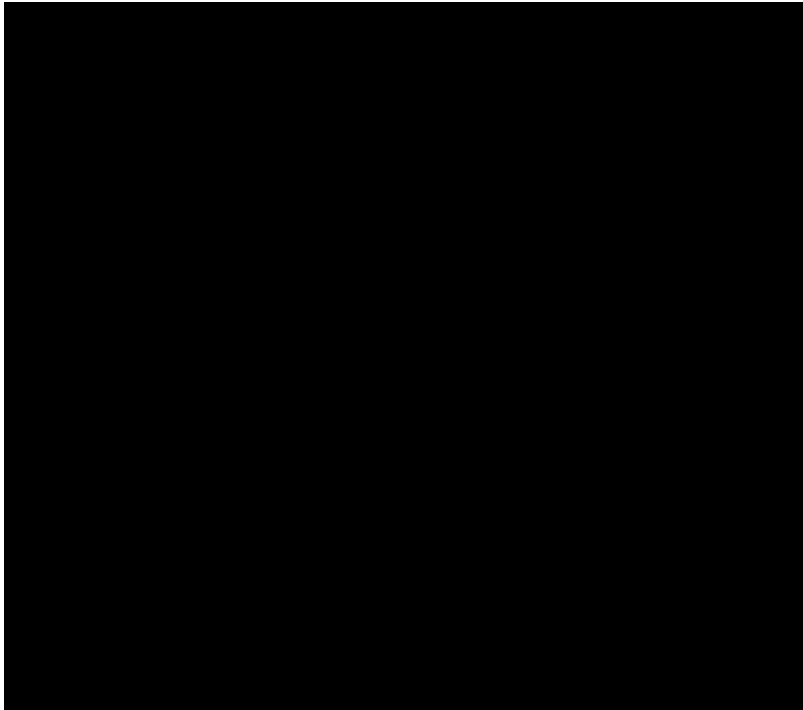
[Redacted text block]

[Redacted text block]



[Redacted text block]

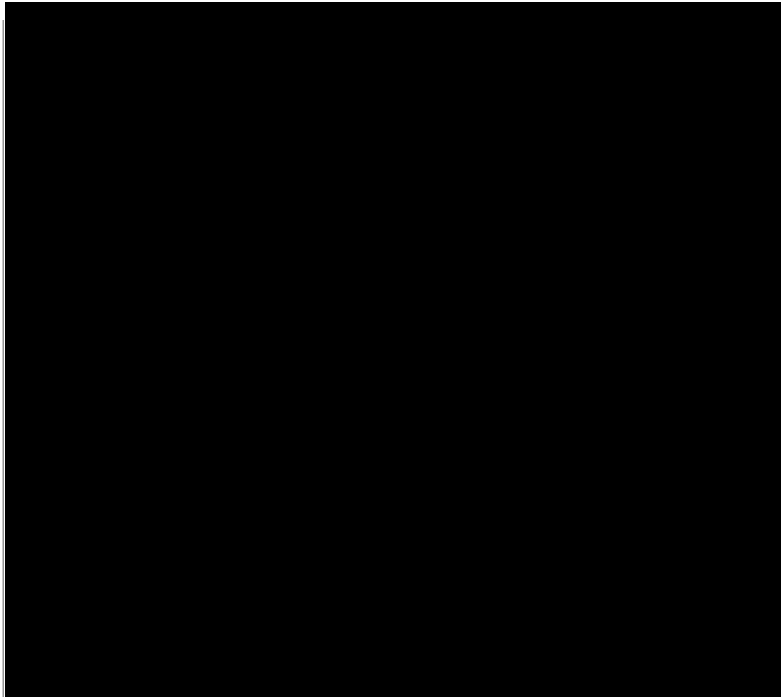
[REDACTED]



[REDACTED]

[REDACTED]

[Redacted text block]



[Redacted text block]

[Redacted text block]

[Redacted text block]

In conclusion, [REDACTED] team identified three true [REDACTED] selective molecules over [REDACTED]. The relative profile of these compounds are distinct enough that they can serve as useful tool compounds. The exact mechanism of action of these compounds could not be determined from these experiments and so further investigation would be required. I received these compounds from [REDACTED] to test their effects on aldosterone secretion from H295R and primary adrenal cells.

3.4 Results

3.4.1 Isoform and expression analysis of $Ca_v1.3$ in normal adrenal cortex & APAs

Real-time qPCR revealed significant differences in the expression levels of two LTCCs, $Ca_v1.3$ and $Ca_v1.2$. In all tissue types tested expression levels for $Ca_v1.3$ were 10-30 fold higher than $Ca_v1.2$ (Fig. 17a). $Ca_v1.3$ was highly upregulated in ZG-like APAs as compared to normal tissue adjacent to such APAs from same patients. Similar upregulation was not seen in ZF-like APAs compared to their paired normal adrenal tissue and was specific to ZG-like APAs. $Ca_v1.3$ transcripts were also analysed and 2137aa long transcript formed the most of this upregulation of $Ca_v1.3$ in ZG-like APAs (Fig. 17b).

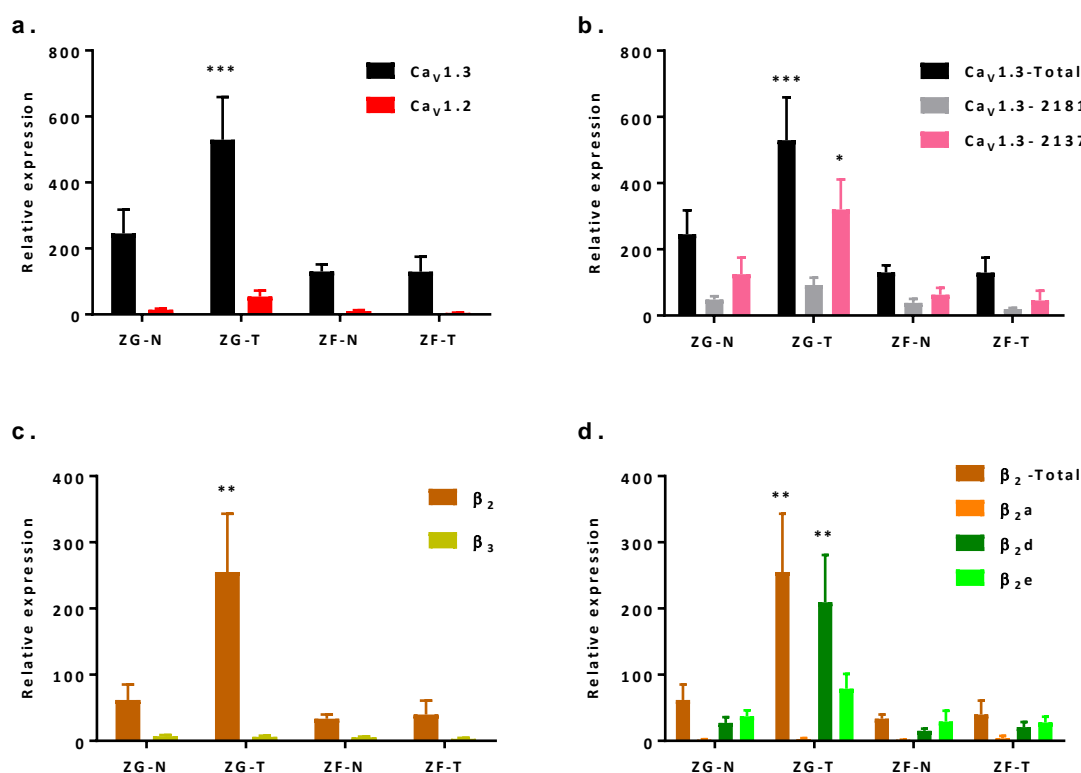


Fig. 17: Endogenous calcium subunit expression in normal adrenal and APAs.

a. Comparison of $Ca_v1.3$ and $Ca_v1.2$ expression in ZG- or ZF-like APAs and their adjacent normal adrenals. **b.** Expression data for $Ca_v1.3$ “long” transcripts, 2181 amino acid or 2137 amino acid in length. **c.** Comparison of β_2 and β_3 subunit expression. **d.** Expression data for β_2 transcripts β_2a , β_2d , β_2e . Legend, ZG-N: normal adrenal next to ZG-like APA; ZG-T: ZG-like APA; ZF-N: normal adrenal next to ZF-like APA; ZF-T: ZF-like APA. ZG-T and normal, n=11 and ZF-T and paired normal, n=3. (Two-way ANOVA, * $P \leq 0.05$, ** $P \leq 0.01$, *** $P \leq 0.001$ compared to adjacent normal tissue). Error bars represent s.e.m. Relative expression is calculated as $2^{-\Delta C_T} \times 10^7$, where $2^{-\Delta C_T} = C_T^{\text{Target gene}} - C_T^{18s}$.

3.4.2 Isoform and expression analysis of β subunit in normal adrenal cortex & APAs

Similar analysis for β subunit expression revealed β_2 as the most predominant type in adrenal, consistent with our microarray data (Fig. 17c). β_2 was also upregulated only in ZG-like APAs compared to paired normal tissue and not in ZF-like APAs. Among tested β_2 transcripts variants, β_{2d} was found to be the most predominant isoform followed by β_{2e} (Fig. 17d). β_{2a} expression was negligible in all samples.

3.4.3 Mutant Cav1.3 upregulates aldosterone secretion

H295R cells transfected with wild-type Cav1.3 showed marginally higher aldosterone secretion compared to untransfected or cells transfected with empty vector in presence of β_3 and $\alpha_2\delta-1$ constructs (Fig. 18). Cells expressing Cav1.3 mutants G403R or I750M, both of which lie in the channel activation gate towards the cytoplasmic end of S6 in pore-forming domain, secreted higher aldosterone to varying levels compared to WT. Reasonable stimulation of aldosterone secretion with angiotensin II was also observed in all groups.

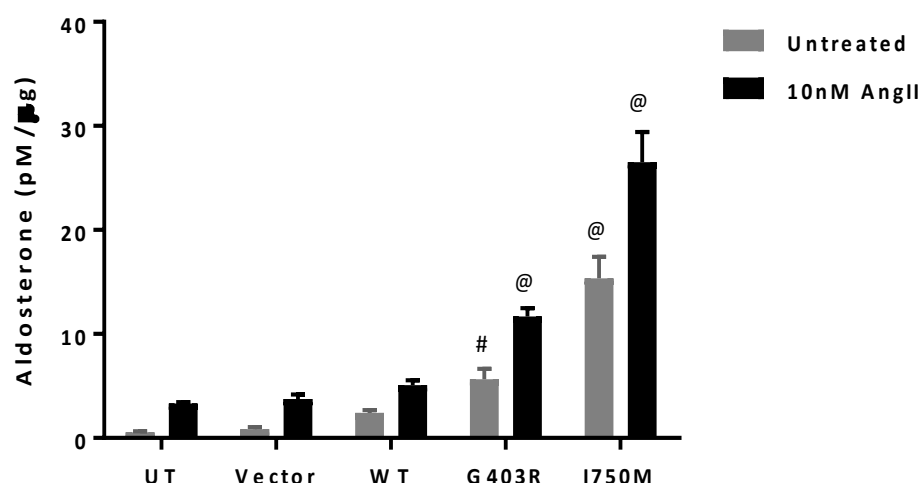


Fig. 18: AngII stimulation of aldosterone secretion from transfected H295R cells.

H295R cells were transfected by electroporation with pcDNA3.1 (Vector), FLAG-Cav1.3 wild-type (WT) or mutants G403R or I750M along with β_3 and $\alpha_2\delta-1$ constructs. UT: un-transfected. All cells were treated with 10nM angiotensin II (AngII, black bars) or vehicle only (PBS, grey bars) for 24 hrs before harvesting cells for aldosterone assay (pM) and total protein estimation (ug) (n=3 in quadruplicate). (One-way ANOVA, # P<0.001, @ P<0.0001, compared to WT). Error bars represent s.e.m.

As previously seen in electrophysiological studies, mutant Cav1.3 proteins have higher probability of channel activation at less depolarised membrane potentials and slowed inactivation, it was investigated whether these changes were solely the cause of increased aldosterone secretion or if there is any increase in membrane localisation of mutant proteins

compared to the wild-type. For this H295R cells were co-transfected with β_3 , $\alpha_2\delta$ -1 subunits and the GFP-tagged WT or mutant Cav1.3. No differences in the sub-cellular localisation of GFP-tagged Cav_v1.3 wild-type or mutants, V259D, G403R, I750M or P1336R were observed. All groups showed cells with GFP-fluorescence in both cytoplasm and cell membrane (Fig. 19).

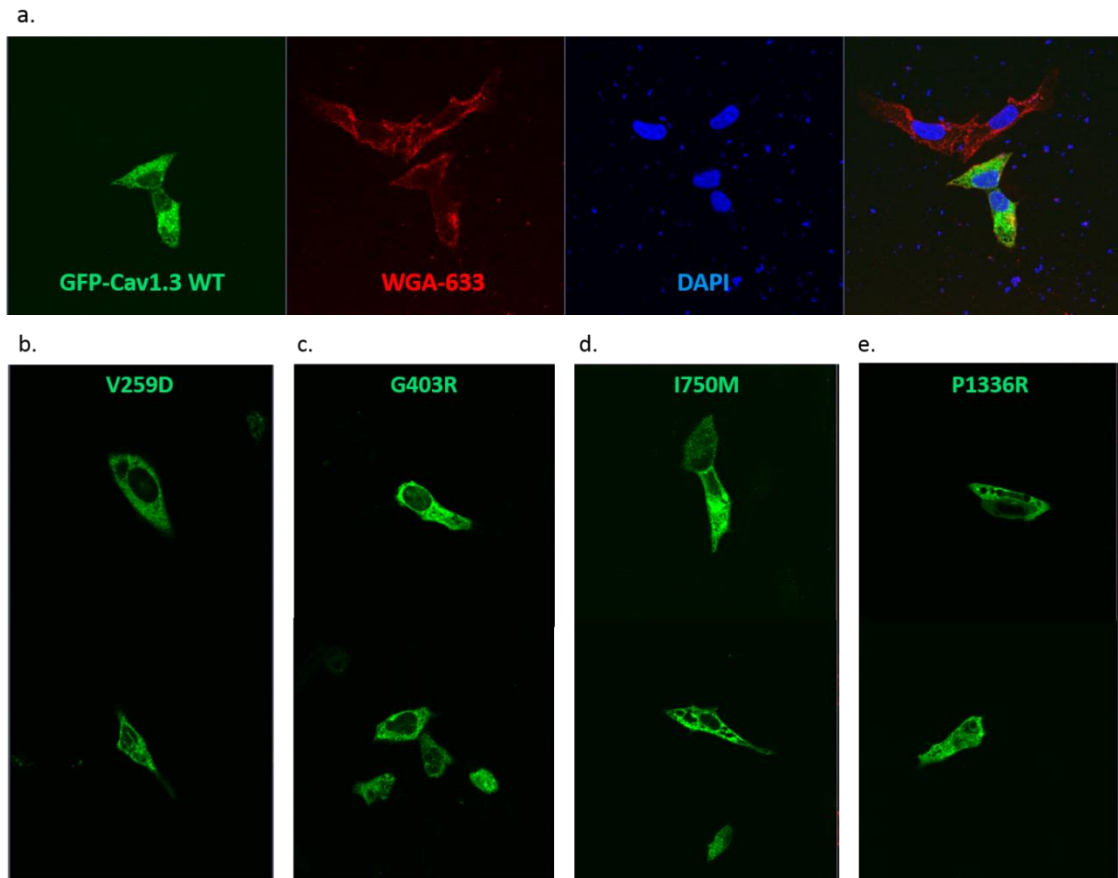


Fig. 19: Subcellular localisation of transfected Cav_v1.3 WT or mutants (GFP-tagged) in H295R cells. H295R cells were transfected using Lipofectamine with **a.** GFP-Cav_v1.3 wild-type (WT) or mutants **b.** V259D, **c.** G403R, **d.** I750M and **e.** P1336R along with β_3 and $\alpha_2\delta$ -1 constructs. Cell membranes were stained with WGA-633 (red) and nuclei with DAPI (blue). Membrane and nuclei staining not shown for the mutants (b-e).

3.4.4 Whole-cell patch-clamp electrophysiology

3.4.4.1 Current activation for $Ca_v1.3$ WT and mutants in presence of β_3 subunit

The I-V relationship was studied by whole-cell patch-clamping technique on tsA-201 cells transfected with FLAG-tagged $Ca_v1.3$ wild-type or mutants along with β_3 and $\alpha_2\delta-1$. Calcium currents were recorded using 10mM Ca^{2+} bath solution and by applying 10mV step depolarisations for 50ms each (Fig. 20i). Of the seven mutants tested, four mutants V259D, G403R, F747L and I750M showed I-V curves shifted towards more negative voltages (Fig. 20b-e & Fig. 21a). Compared to WT, mutants R990H, P1336R and M1354I showed no differences in the channel activation properties (Fig. 20f-h & Fig. 21a). The G/G_{max} as a measure of channel conductance was also calculated, which showed a similar left-ward shift for the same four mutants and no differences for other three (Fig. 21b). These data are represented as V_{50} , the voltage for half maximal conductance for each group, and summarised in Fig. 21c. A significant decrease of 10-20mV was found in V_{50} for mutants V259D, G403R, F747L and I750M $Ca_v1.3$ channel in the presence of the β_3 subunit.

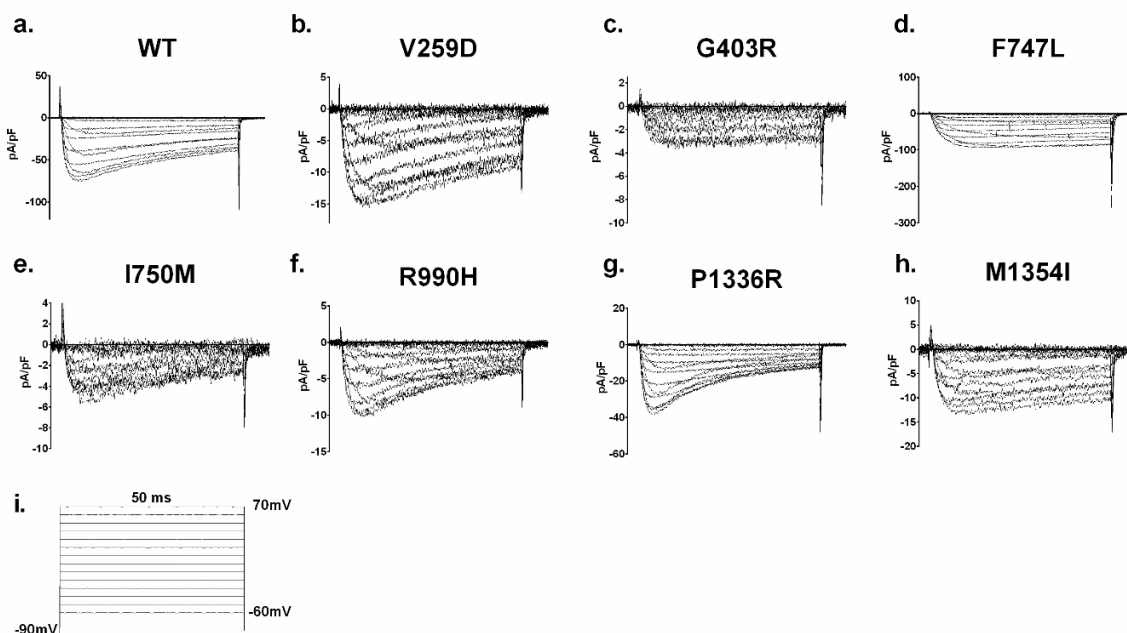


Fig. 20: Exemplary IV-traces for all $Ca_v1.3$ WT and mutants expressed with β_3 and $\alpha_2\delta-1$ subunits. a. WT, b. V259D, c. G403R, d. F747L, e. I750M, f. R990H, g. P1336R and h. M1354I. IV protocol for 10mV step depolarisation from -90mV holding potential for 50 ms is represented in i.

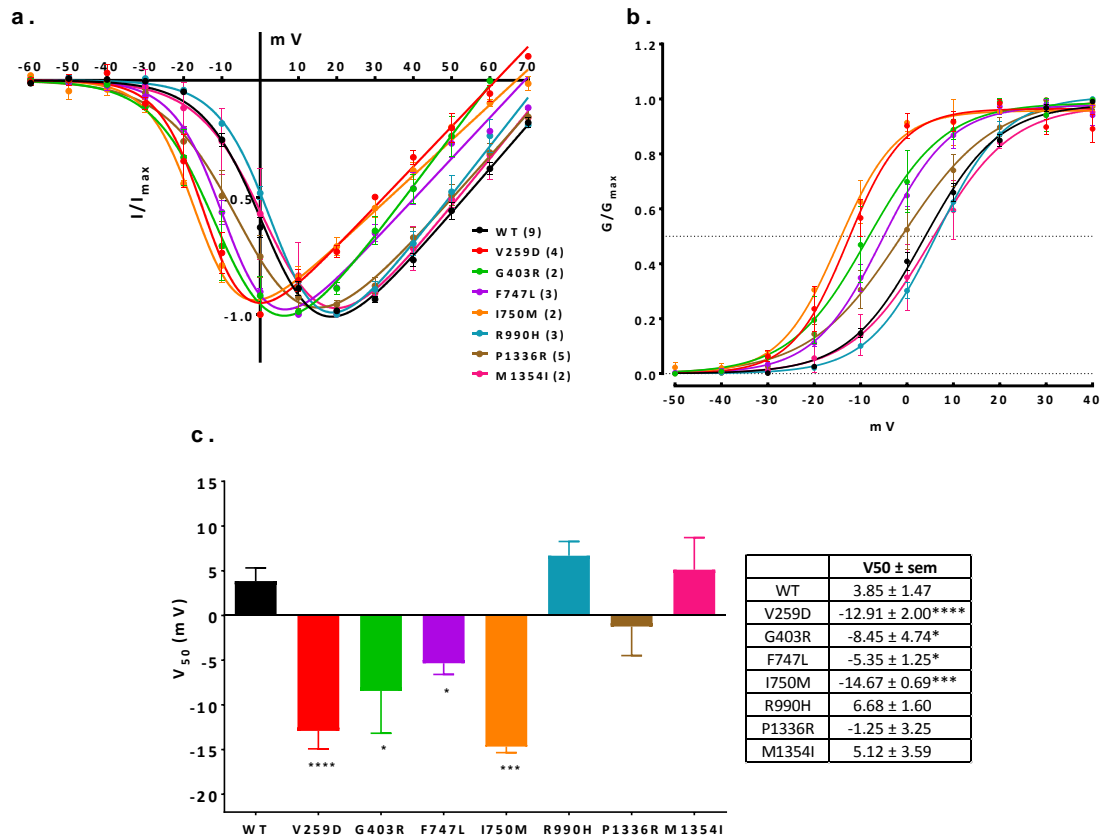


Fig. 21: Current-voltage (IV) relationship (I_{Ca}) of $\text{Ca}_v1.3$ WT or mutants in presence of β_3 .
a. Currents were recorded from 10mM Ca^{2+} in bath solution and I/I_{max} is displayed as voltage dependence of channel activation. **b.** G/G_{max} is calculated as voltage dependence of channel conductance. **c.** Voltage for half maximal conductance (V_{50}) is tabulated for each group. Number of cells (n) for each group is given in parenthesis in the figure legends. Error bars represent s.e.m. * $P \leq 0.05$, *** $P \leq 0.001$, **** $P \leq 0.0001$ compared to WT.

3.4.4.2 Effect of different β subunits on $Ca_v1.3$ WT activation

The tsA-201 cells were transfected with FLAG- $Ca_v1.3$ WT, $\alpha_2\delta-1$ and β_3 , β_{2d} or β_{2e} constructs and their I-V relationships were determined, as before in the presence of 10mM Ca^{2+} . $Ca_v1.3$ showed very similar activation and channel conductance profile in the presence of β_3 or β_{2d} (Fig. 22 & Fig. 23), whereas these properties are significantly depolarised by 10mV when β_{2e} is present.

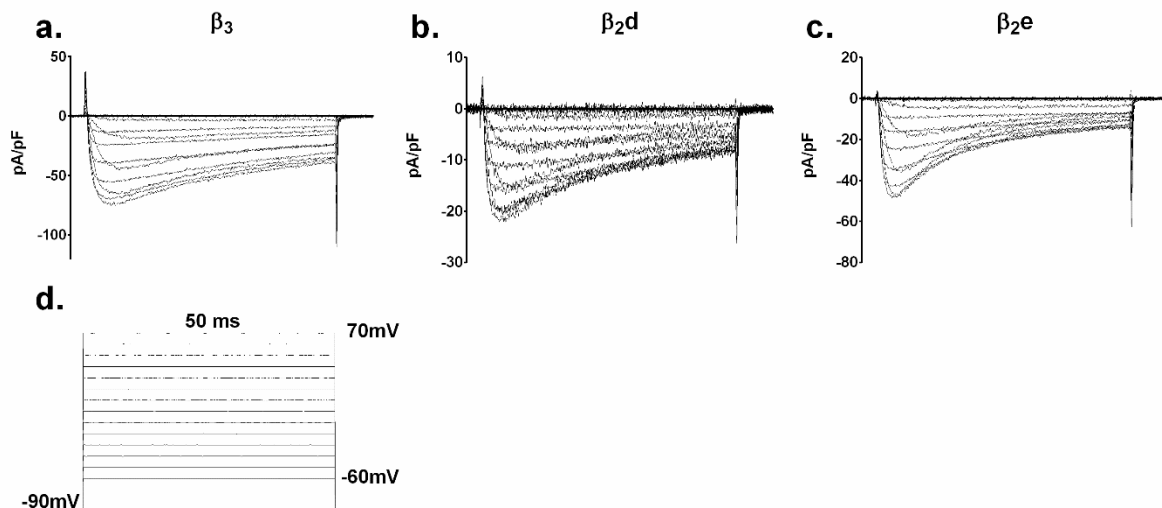


Fig. 22: Exemplary IV-traces for $Ca_v1.3$ WT expressed with β_3 , β_{2d} or β_{2e} and $\alpha_2\delta-1$ subunits.

a. β_3 , b. β_{2d} and c. β_{2e} . IV protocol for 10mV step depolarisation from -90mV holding potential for 50 ms is represented in d.

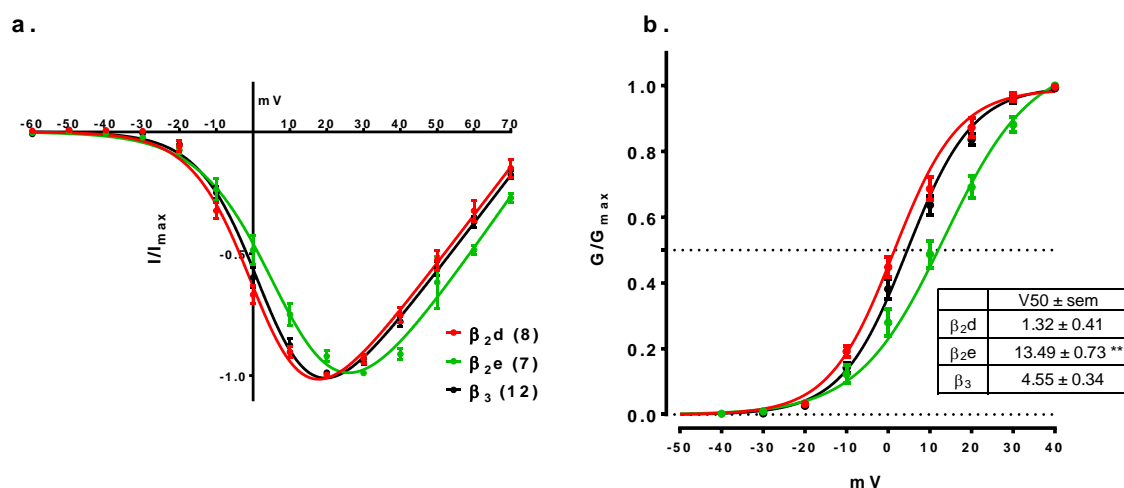


Fig. 23: Current-voltage (IV) relationship (I_{Ca}) of $Ca_v1.3$ WT in presence of β_{2d} , β_{2e} or β_3 .

a. Currents were recorded from 10mM Ca^{2+} in bath solution and I/I_{max} is displayed as voltage dependence of channel activation. b. G/G_{max} is calculated as voltage dependence of channel conductance. Voltage for half maximal conductance (V_{50}) is tabulated for each group. Number of cells (n) for each group are represented in parenthesis in figure legends. Error bars represent s.e.m. $^{**}P \leq 0.01$ compared to β_3 and β_{2d} .

3.4.4.3 β_2 subunit dependent inactivation

10mM Ba^{2+} was used as the charge carrier in these experiments to minimise the calcium-dependent inactivation of $\text{Ca}_v1.3$. The tsA-201 cells expressing $\text{Ca}_v1.3$ WT or mutant V259D with β_{2d} or β_{2e} were subjected to I-V, steady-state inactivation and time-course inactivation protocols. Independent of β_2 subunit splice variant, mutant V259D showed a hyperpolarising shift of about 12-15 mV compared to WT (Fig. 24 & Fig. 27a), similar to that seen in the experiment in which β_3 subunits were used (Fig. 21a). A modest effect on voltage dependent channel activation was induced by β_{2e} only on WT $\text{Ca}_v1.3$, compared to β_{2d} , whereas V259D activation was not affected (Fig. 27b). As expected, membrane-associated β_{2e} shifted steady-state inactivation curves to more positive voltages for both WT and V259D, compared to the non-membrane-associated β_{2d} subunit (Fig. 25 & Fig. 27c). Interestingly, as represented by r_{300} fast, inactivation of the WT channel during long depolarisations of 5 s was negligible in the presence of either β_2 subunit (Fig. 26a-b & Fig. 27d). On the other hand, the V259D channel showed significant inactivation at all tested voltages only in the presence of β_{2d} . β_{2e} subunit prevented any significant reduction in channel currents from V259D (Fig. 26c-d & Fig. 27d).

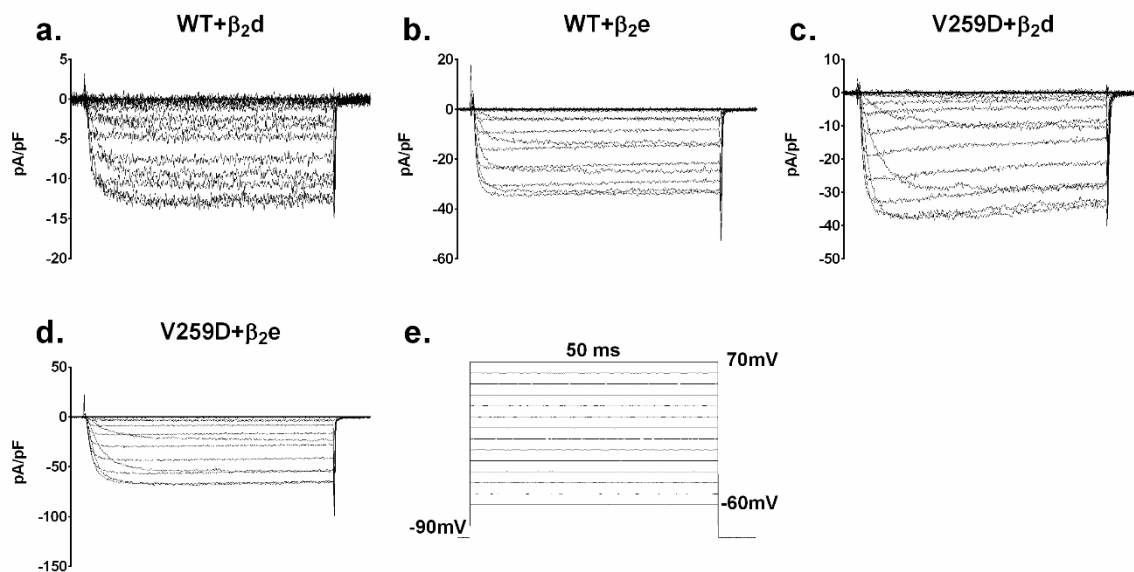


Fig. 24: Exemplary IV-traces for $\text{Ca}_v1.3$ WT or V259D expressed with β_{2d} or β_{2e} and $\alpha_2\delta-1$ subunits. a. WT+ β_{2d} , b. WT+ β_{2e} , c. V259D+ β_{2d} and d. V259D+ β_{2e} . IV protocol for 10mV step depolarisation from -90mV holding potential for 50 ms is represented in e.

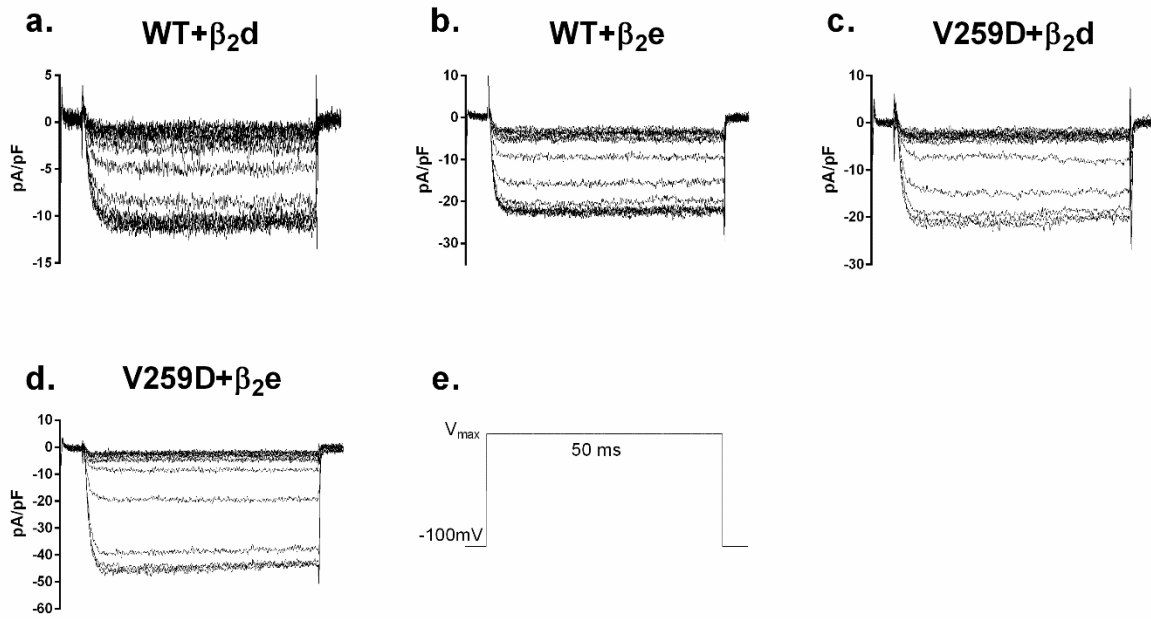


Fig. 25: Exemplary steady-state inactivation traces for $Ca_v1.3$ WT or V259D expressed with β_2d or β_2e and $\alpha_2\delta-1$ subunits.

a. WT+ β_2d , b. WT+ β_2e , c. V259D+ β_2d and d. V259D+ β_2e . After pre-conditioning at voltages of -70mV to 70mV, steady-state inactivation protocol involving depolarisation to V_{max} from -100mV holding potential for 50 ms is represented in e.

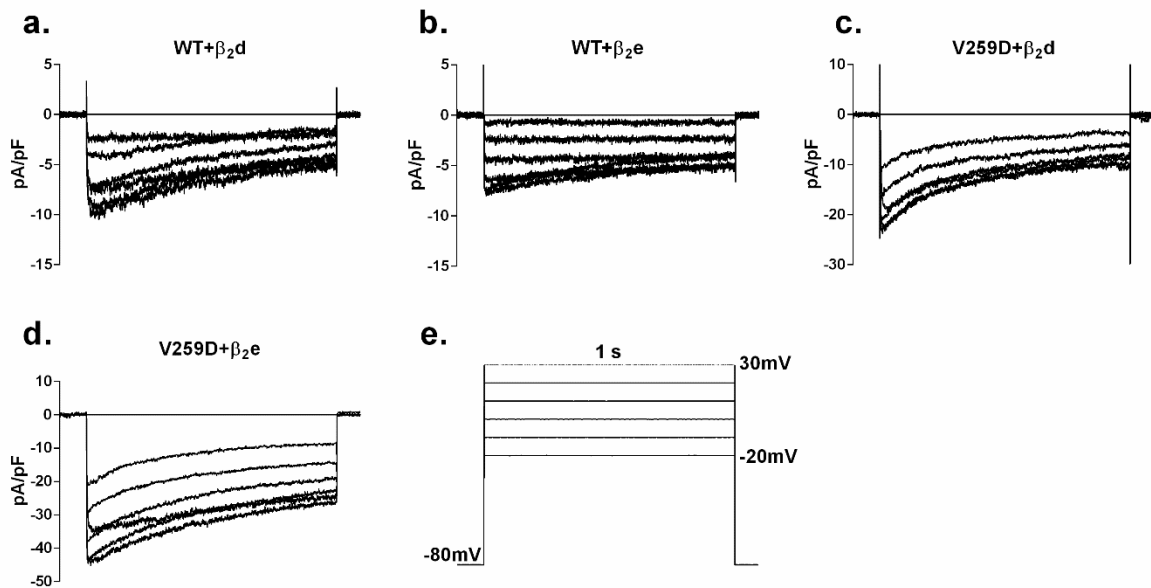


Fig. 26: Exemplary 1 sec inactivation traces for $Ca_v1.3$ WT or V259D expressed with β_2d or β_2e and $\alpha_2\delta-1$ subunits.

a. WT+ β_2d , b. WT+ β_2e , c. V259D+ β_2d and d. V259D+ β_2e . Protocol for 1 second long inactivation to 10mV step depolarisation -80mV holding potential is represented in e.

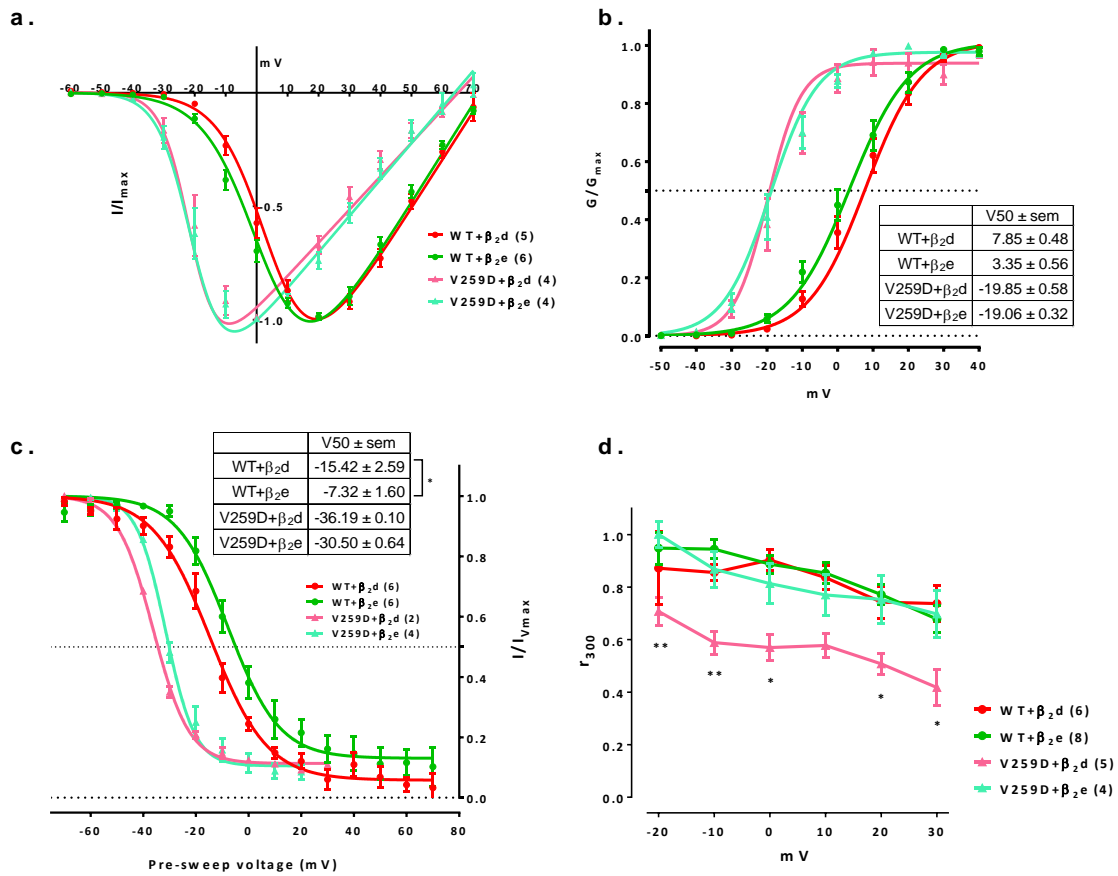


Fig. 27: Activation and inactivation of Cav1.3 WT or mutant, V259D in the presence of β_2d or β_2e .

a. Currents were recorded from 10mM Ba²⁺ in bath solution (I_{Ba}) and I/I_{max} is displayed as voltage dependence of channel activation. **b.** G/G_{max} represents channel conductance. **c.** I/I_{Vmax} is represented for steady state inactivation protocol. **d.** Fast channel inactivation is represented as r_{300} , the fraction of current remaining 300ms into the depolarisation step to indicated voltages. Number of cells (n) for each group are represented in parenthesis in figure legends. Error bars represent s.e.m. * $P \leq 0.05$ for WT+ β_2d vs WT+ β_2e in c. and * $P \leq 0.05$, ** $P \leq 0.01$ compared to V259D+ β_2e in d.

3.4.5 Localisation of endogenous $\text{Ca}_v1.3$ in H295R cells

Untransfected H295R cells were stained with different $\text{Ca}_v1.3$ antibodies against its pore-forming domain or intracellular C-terminal chain. As expected, staining with antibody towards the pore-forming domain (NeuroMab Clone L48A/9), called here as N-terminal (NT) antibody shows membranous localisation for $\text{Ca}_v1.3$ (Fig. 28a). Surprisingly, the two independent antibodies against the intracellular c-terminal (CT) chain of $\text{Ca}_v1.3$ (NeuroMab Clone N38/8 and SantaCruz sc-25687) mainly showed diffused cytoplasmic and nuclear localisation (Fig. 28 b & c). No clear membranous staining with either CT antibodies was a matter of concern suggesting doubts over specificity of these antibodies.

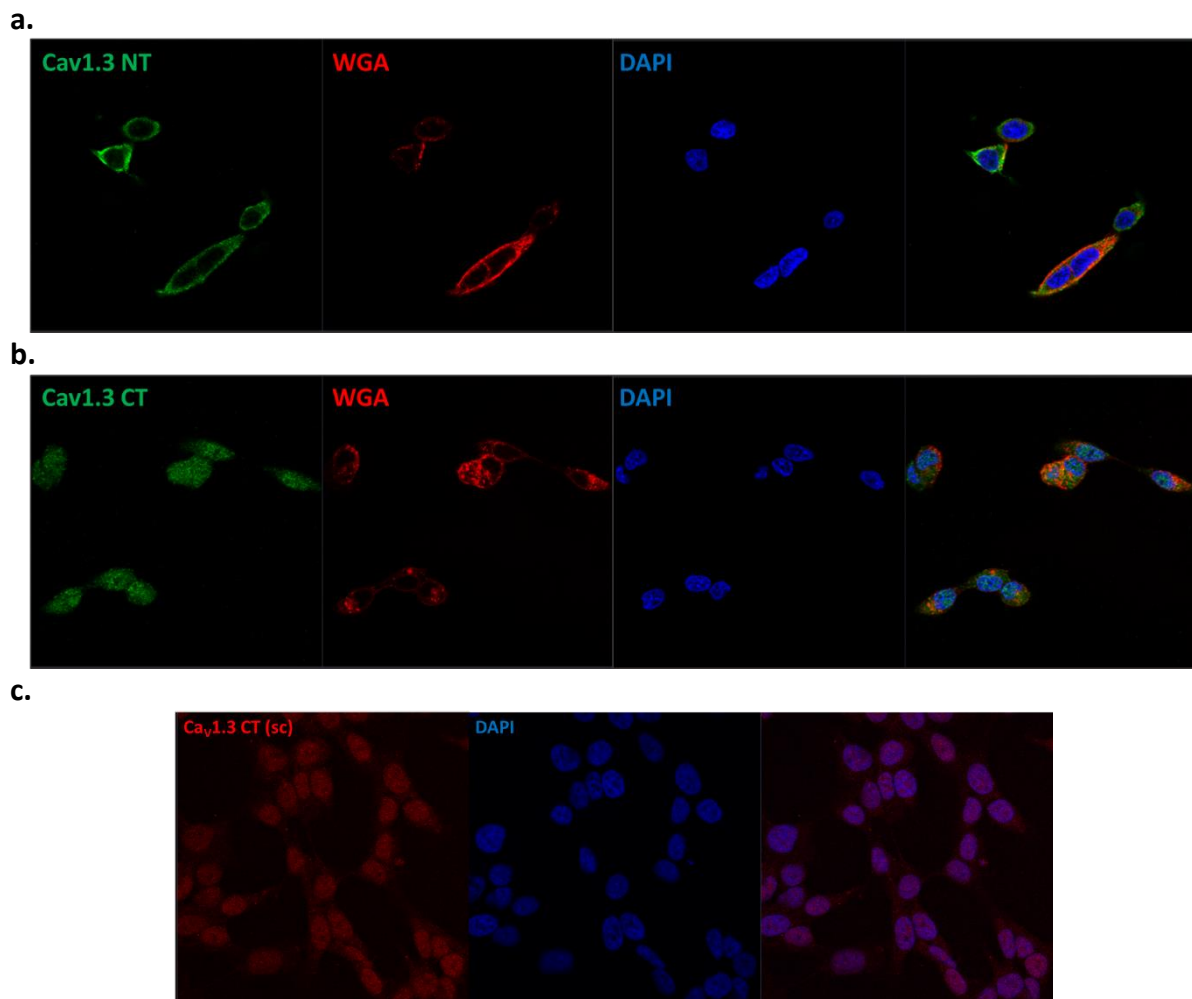


Fig. 28: Immunostaining of endogenous $\text{Ca}_v1.3$ in H295R cells.

Localisation of endogenous $\text{Ca}_v1.3$ in H295R cells by immunostaining with **a.** NeuroMab N-terminal (green); **b.** NeuroMab C-terminal (green) and **c.** SantaCruz C-terminal (red) antibodies. Plasma membranes were stained using wheat germ agglutinin (WGA, red in a. and b.) and nuclei were stained with DAPI (blue).

3.4.6 Cleaved C-terminus of Cav1.3 translocates to nucleus and upregulates aldosterone secretion

Intracellular C-terminal of Cav1.3 cloned in pLOC vector (tagged with FLAG and Myc sequences, Fig. 29a) was overexpressed in H295R cells via lentiviral transduction to study its subcellular localisation and effect on aldosterone secretion. Western blot of lysates of H295R cells expressing Cav1.3-CT using anti-Myc antibody showed the presence of 2 bands corresponding to the expected sizes of transduced C-terminal and cleaved peptide (Fig. 29b). The smaller fragment lacks the FLAG-tag sequence confirming c-terminal undergoing cleavage. Immunofluorescence with FLAG antibody showed prominent nuclear localisation of the transduced Cav1.3-CT, but unfortunately, this peptide in nucleus was not positive for myc-tag (Fig. 30). Interestingly expression of Cav1.3-CT upregulated aldosterone secretion from H295R cells compared to the control cells by 1.5 folds (Fig. 31).

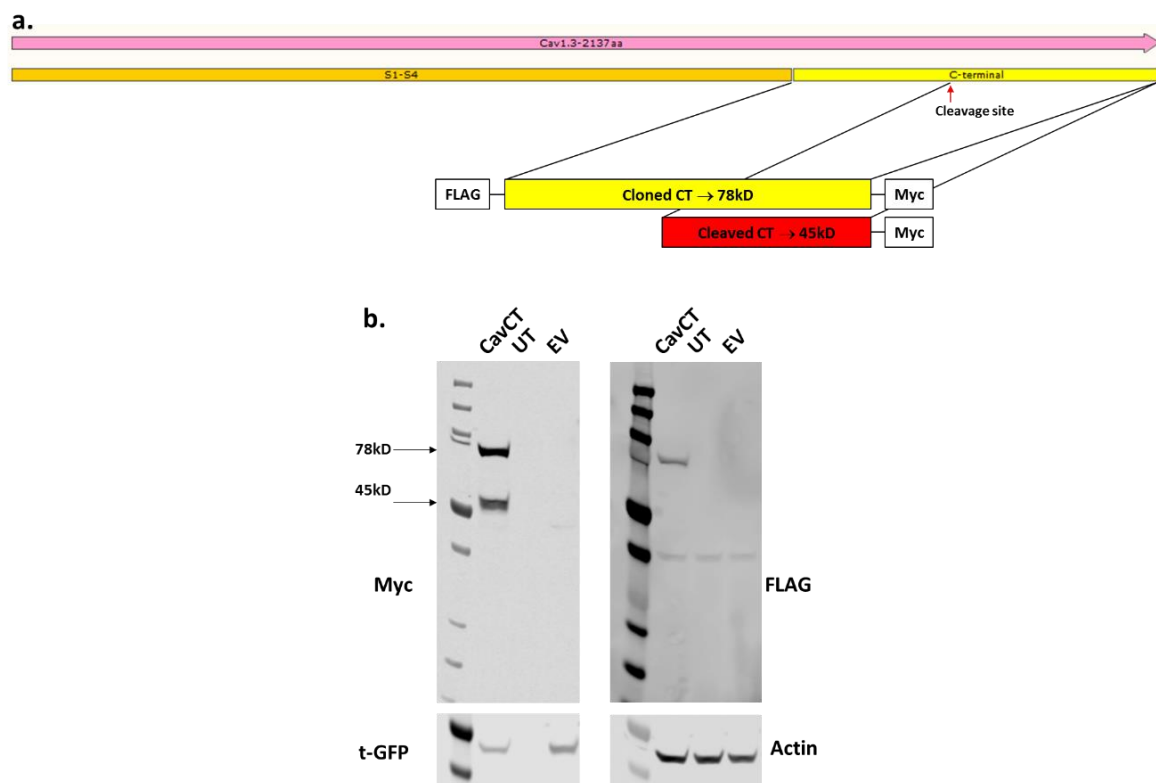


Fig. 29: Western blot for overexpressed Cav1.3-CT in HEK293 cells.

a. Schematic representation of cloned C-terminal sequence of Cav1.3 with putative calpain cleavage site indicated with a red arrow. **b.** Western blot for whole cell lysate of HEK293 cells untransfected (UT) or transfected with Cav1.3-CT (CavCT) or empty vector (EV) using PEI transfection reagent (n=3). Anti-Myc and anti-FLAG antibodies show expression of CavCT. Anti-tGFP and anti-Actin were used as loading controls.

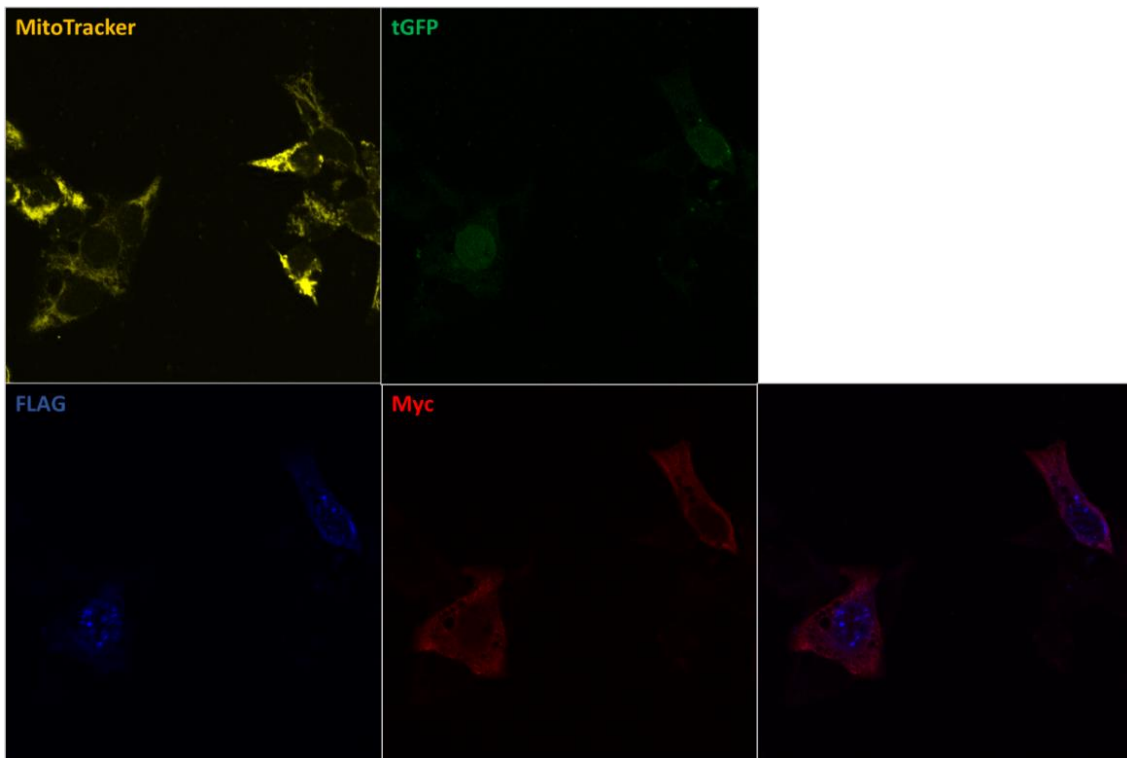


Fig. 30: Immunostaining of Cav1.3-CT overexpressed in H295R cells.

H295R cells were transduced with the lentivirus for FLAG-Cav1.3-CT-Myc and immuno-stained with anti-FLAG (blue) and anti-Myc (red) antibodies. MitoTracker (yellow) shows mitochondrial staining for all cells in the view and tGFP (green) from pLOC plasmid shows nuclei of transduced cells.

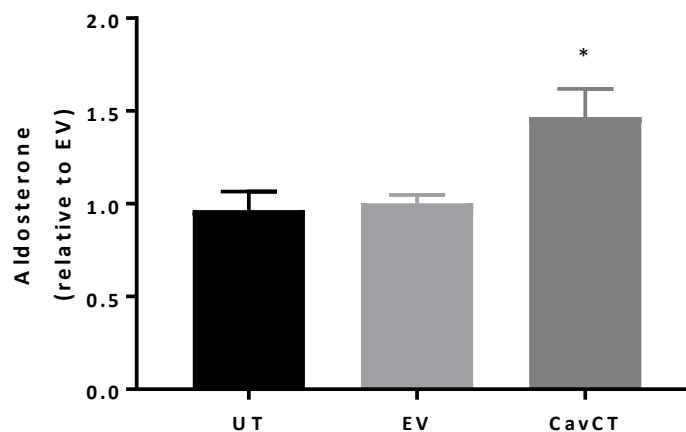


Fig. 31: Aldosterone secretion from H295R cells overexpressing C-terminal of Cav1.3

H295R cells were either untransduced (UT) or transduced with lentivirus for empty vector (EV) or C-terminal of Cav1.3 (CavCT). Aldosterone secretion was measured over 48hrs from transduction (n=3 in triplicate). (One-way ANOVA, *P=0.0243 compared to EV). Error bars represent s.e.m.

3.4.7 $\text{Ca}_v1.3$ is a substrate for calpain proteases

Unexpected localisation of C-terminal of $\text{Ca}_v1.3$ in the nuclei of H295R cells led to the hypothesis that similar to $\text{Ca}_v1.2$, intracellular domain of $\text{Ca}_v1.3$ also undergoes calpain mediated cleavage and released c-terminal chain translocates to nucleus. To test this hypothesis, first the effect of calpain inhibition on aldosterone secretion was studied. H295R cells were treated with 0-50 μM range of calpeptin and basal or AngII stimulated aldosterone secretion was measured. Calpain inhibition did not influence aldosterone secretion under basal conditions (black bars in Fig. 32), but significantly reduced the AngII stimulated aldosterone at concentrations of 5 μM or higher (red bars in Fig. 32).

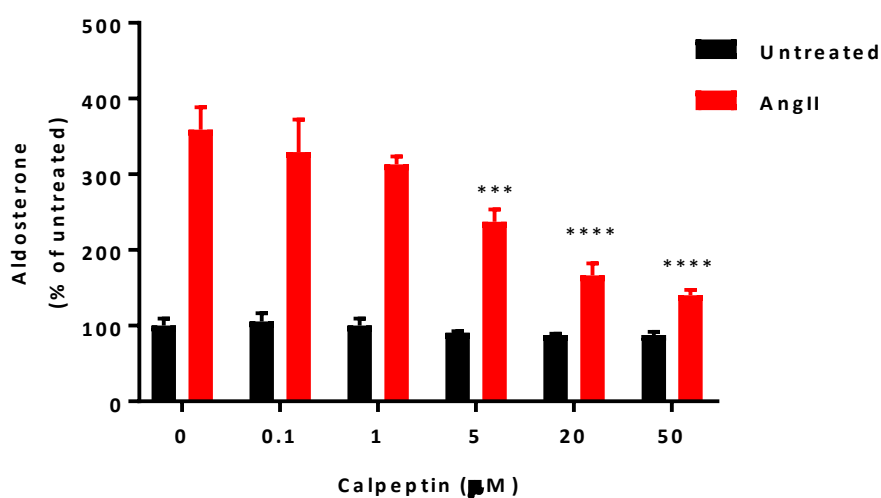


Fig. 32: Aldosterone secretion from H295R cells treated with calpeptin

H295R cells were treated with increasing dose of calpain inhibitor, calpeptin in presence or absence of 10nM angiotensin II and aldosterone secretion was measured (n=3 in triplicate). (Two-way ANOVA, ***P=0.0003 and ****P<0.0001). Error bars represent s.e.m.

Despite the uncertainty of the antibody specificity (due to the detection of multiple bands), western blot using $\text{Ca}_v1.3$ C-terminal antibody (NeuroMab, N38/8) for the lysates of calpeptin treated H295R cells showed some increase in the levels of full-length $\text{Ca}_v1.3$ (>250kD), suggesting reduction of the calpain mediated cleavage of C-terminal peptide (Fig. 33). In addition to the effect of calpeptin on $\text{Ca}_v1.3$ protein, down-regulation of $\text{Ca}_v1.3$ transcriptional expression was also observed at the concentrations that significantly reduced aldosterone secretion (Fig. 34a & b). Expression of CYP11B2 was observed to be unchanged with calpeptin treatment except for a complete knockdown at 100 μM concentration which could be a result of non-specific effect at high dose of calpeptin (Fig. 34c).

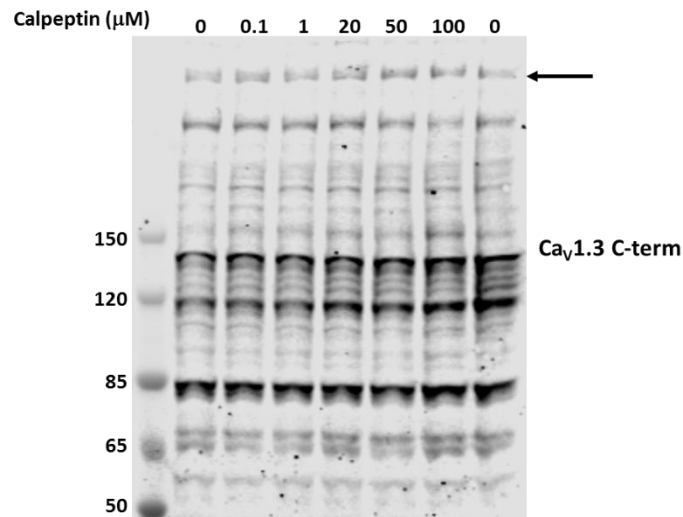


Fig. 33: Western blot for Cav1.3 in H295R cells treated with calpeptin.

Whole cell lysate of H295R cells treated with the dose range of calpeptin in the presence of AngII was western blotted with anti-Cav1.3 C-terminal antibody (NeuroMab, N38/8). Black arrow indicates the band for full-length Cav1.3 (n=2).

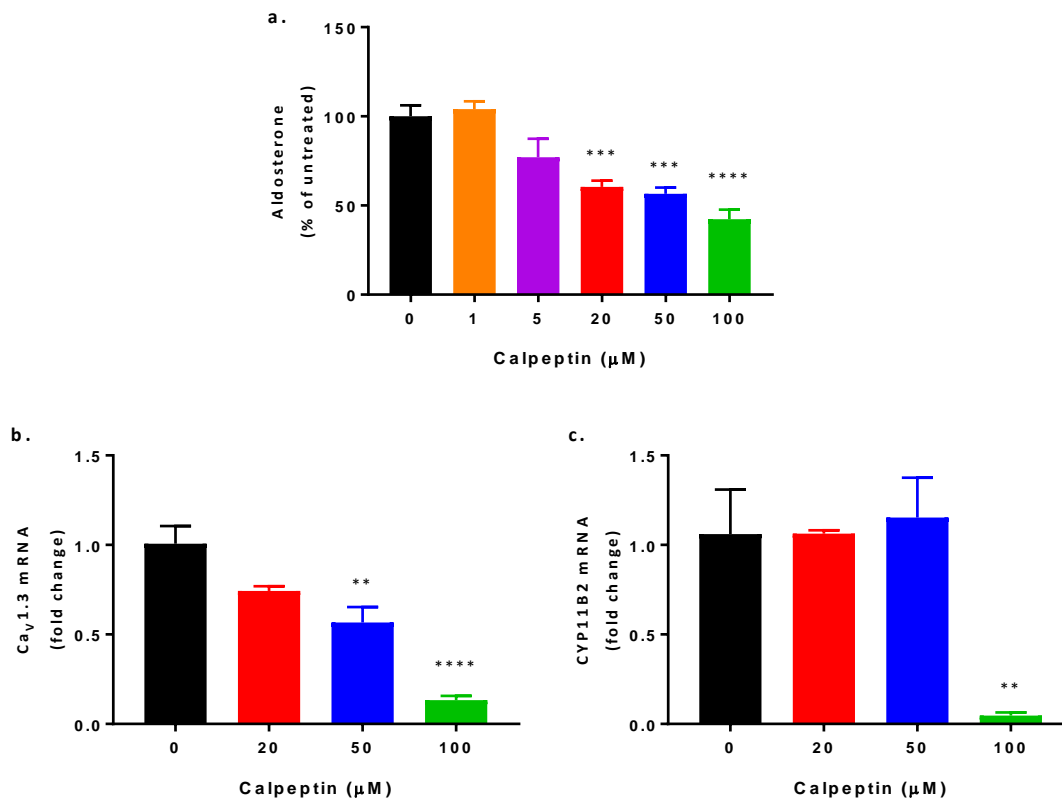


Fig. 34: Aldosterone secretion and Cav1.3 expression in H295R cells treated with calpeptin.

H295R cells were treated with 0-100μM calpeptin in the presence of 10nM angiotensin II. **a.** Aldosterone secretion was measured (One-way ANOVA, 20μM vs 0 ***P=0.0004, 50μM vs 0 ***P=0.0001, 100μM vs 0 ****P<0.0001). **b.** qPCR analysis for Cav1.3 expression in response to calpeptin at concentrations that significantly decreased aldosterone (n=3 in quadruplicate). (One-way ANOVA, **P=0.0046, ****P<0.0001). **c.** qPCR analysis for CYP11B2 expression (One-way ANOVA, **P=0.0069). Error bars represent s.e.m.

3.4.8 Silencing of Ca_v1.3 in H295R cells

To further establish the role of endogenous Ca_v1.3 in aldosterone secretion, shRNA mediated knockdown in H295R cells was performed. However, the silencing of Ca_v1.3 was not very efficient as there was no significant reduction in Ca_v1.3 mRNA levels in the shRNA transduced cells compared to the control cells (Fig. 35a), and hence no effect on aldosterone secretion was observed (Fig. 35b).

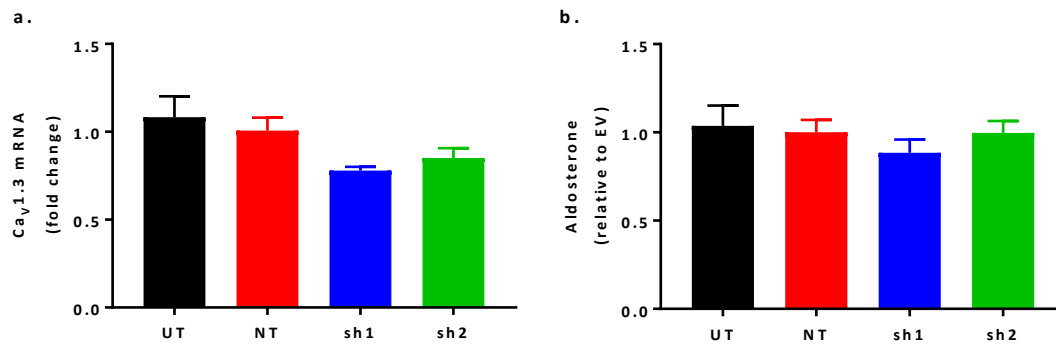


Fig. 35: shRNA mediated Ca_v1.3 knockdown in H295R cells and aldosterone secretion.

H295R cells were transduced with lentivirus for scrambled/non-targeting (NT) or two Ca_v1.3 specific shRNA sequences (sh1 & sh2). **a.** Efficiency of knockdown was measured by qPCR for Ca_v1.3. **b.** aldosterone secretion from all conditions was measured. No significant changes were observed in Ca_v1.3 levels or aldosterone secretion in either shRNA treated cells compared to untransduced (UT) or NT cells (n=3 in triplicate). Error bars represent s.e.m.

3.4.9 $Ca_v1.3$ knockout mice show down-regulated *CYP11B2* expression

Though silencing of $Ca_v1.3$ was unsuccessful in H295R cells, its significant role in aldosterone secretion *in vivo* was found. Adrenals of $Ca_v1.3$ knockout mice generated and studied by Platzer et al. were received from the collaborators (Platzer et al., 2000) and RNA was extracted. RT-PCR for $Ca_v1.3$ expression in cDNA of WT and knockout mice confirmed the complete absence of transcripts that would produce $Ca_v1.3$ proteins (Fig. 36). qPCRs showed *CYP11B2* expression was downregulated by approximately 50% in the $Ca_v1.3$ null mice compared to age-matched WT animals (all 8-weeks old), irrespective of the gender (Males: 1.00 ± 0.06 vs 0.56 ± 0.07 , $n=5$; Females: 1.00 ± 0.15 vs 0.46 ± 0.11 , $n=4$; All: 1.00 ± 0.07 vs 0.51 ± 0.06 , $n=9$) (Fig. 37).

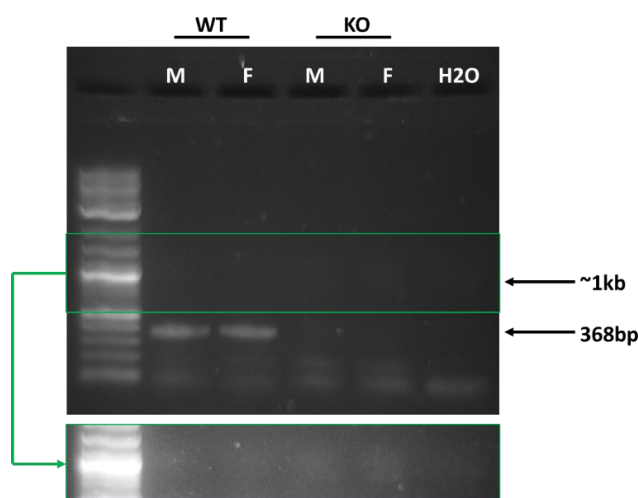


Fig. 36: RT-PCR for $Ca_v1.3$ expression in adrenal cDNA of WT and knockout mice.

RT-PCR for analysing expression of $Ca_v1.3$ in the WT and KO mice whole adrenal cDNA samples. Indicated arrows at 368bp and approximately 1kb correspond to expected amplicon sizes from WT and transgenic (KO) samples, respectively.

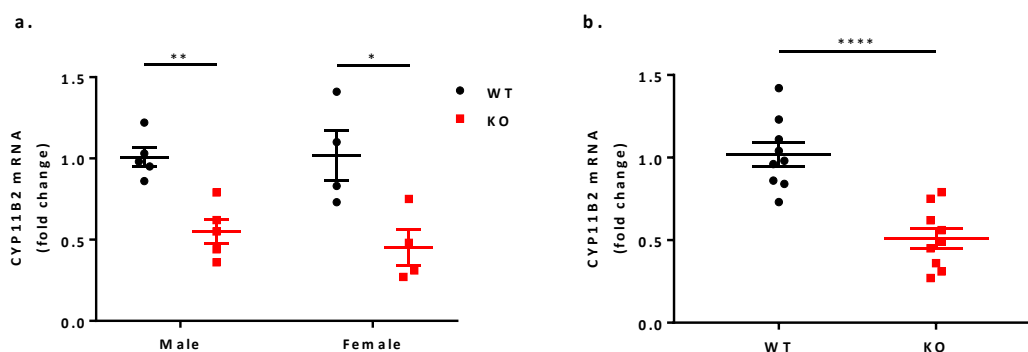


Fig. 37: Expression of *CYP11B2* in adrenals of WT and $Ca_v1.3$ knockout mice.

Expression of *CYP11B2* in the whole adrenals of age-matched WT or $Ca_v1.3$ knockout (KO) mice. **a.** *CYP11B2* mRNA fold change in WT and KO mice adrenals from males ($n=5$, 2-tailed T-Test $**P=0.0014$) and females ($n=4$, 2-tailed T-Test $*P=0.0235$). **b.** Combined data for both males and females ($n=9$, 2-tailed T-Test $****P<0.0001$). Error bars represent s.e.m.

3.4.10 Effect of Ca_v1.3 selective inhibition by compounds A, B & C on aldosterone secretion

The tool compounds A, B and C, that were found to be selective inhibitors for Ca_v1.3 (WT or mutant P1336R) over Ca_v1.2 were tested for their efficacy for inhibition of aldosterone secretion from H295R cells and primary cells isolated from human adrenals.

In H295R cells, compound A showed no inhibition of aldosterone secretion even at the highest concentration tested. There was no concern for solubility of compound A up to 100µM final concentration in the cell culture media. But compounds B & C showed cloudiness at final concentrations of 100µM and 50µM as indicated by black arrowheads in Fig. 38a. Compound C showed a mixed effect on aldosterone secretion, that's inhibition by ~50% at 1µM, but no effect at 10µM. Higher concentrations were not completely soluble and are probably too high to conclude any specific effect on aldosterone secretion. Only compound B showed a typical dose dependent inhibition on aldosterone secretion from H295R cells. its effect was observed starting at 1µM, leading up to 85% reduction in aldosterone at 50µM. IC₅₀ for compound B was calculated to be $6.6 \pm 1.4\mu\text{M}$ (Fig. 38b).

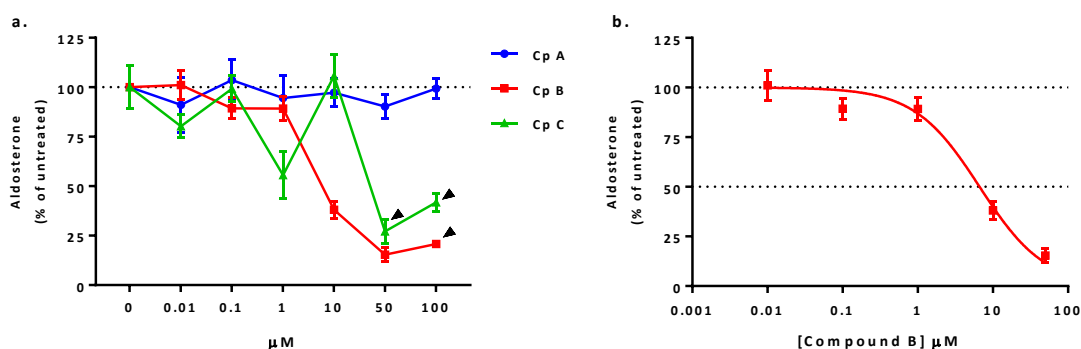


Fig. 38: Dose response curve for compounds A-C on aldosterone secretion in H295R cells.

a. Inhibition of aldosterone secretion from H295R cells treated with a dose range of 0.01-100µM concentration of compounds A, B and C for 24hrs. Aldosterone values were normalised as percent of aldosterone secreted by cells treated with DMSO only. Black arrow heads indicate incomplete solubility of compounds at the particular concentration. **b.** Dose curve for compound B only (n=3 in quadruplicate). Error bars represent s.e.m.

Primary adrenal cells from 2 patients were tested for compound A, B & C inhibitory effects on aldosterone secretion. Only 3 concentrations of 1, 10 & 50 μ M for all 3 compounds were tested. Results were variable for two patients' cells, with overall no significant activity of compound A as seen in case of H295R cells (Fig. 39 a & b). Compound B showed significant reduction on aldosterone in cells from patient-2 at 10 and 50 μ M, but its significant effect on cells from patient-1 was observed only at 1 μ M. Again no significant effect of compound C was seen in cells from patient-1, but a dose-dependent inhibition of aldosterone was observed in cells from patient-2.

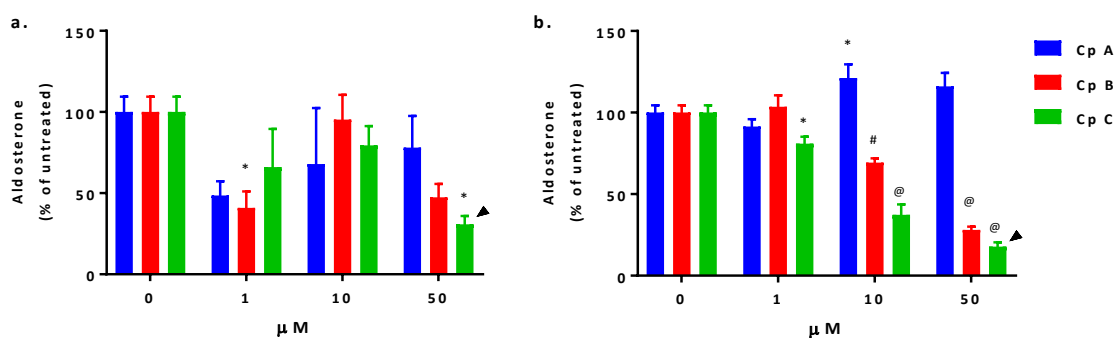


Fig. 39: Effects of compounds A-C on aldosterone secretion from primary adrenal cells.

Aldosterone secretion from primary cell of normal adrenals of 2 patients (a. and b.) on treatment with 1, 10 and 50 μ M concentrations of compounds A, B and C in quadruplicates (Two-way ANOVA, *P<0.05, #P<0.001, @P<0.0001). Black arrow heads indicate incomplete solubility of compounds at the particular concentration. Error bars represent s.e.m.

3.5 Discussion

The members of L-type calcium channel family (Ca_v1.1-Ca_v1.4) are expressed in neurons, endocrine glands, retina and skeletal and cardiac muscles. Until the discovery of somatic mutations in *CACNA1D*/Ca_v1.3 in APAs (Azizan et al., 2013; Scholl et al., 2013), Ca_v3.2 (a T-type calcium channel) was believed to be the main source of Ca²⁺ entry in the adrenal endocrine cells because resting zona glomerulosa cells are too hyperpolarised for activation of high voltage LTCCs. Microarray studies from our lab showed Ca_v1.3 to be the most predominant α_1 -subunit forming calcium channels (Shaikh et al., 2015; Zhou et al., 2015) in adrenal cortex and APAs. qPCRs for Ca_v1.3 and Ca_v1.2 confirmed the microarray findings, with 10-20 fold higher Ca_v1.3 than Ca_v1.2 in normal adrenal tissues (Fig. 17a). It was found that in ZG-like APAs, Ca_v1.3 expression levels are highly upregulated as compared to their paired adjacent normal tissue or ZF-like APAs. Further analysis of Ca_v1.3 transcripts expression showed only one of the three 'long' isoforms to be most expressed and upregulated in ZG-like APAs (Fig. 17b). This isoform, 2137 amino acid in length lacks several alternatively spliced exons compared to the longest transcript (2181 amino acids) but contains exon 8A (8B in 2181aa transcript) in which one of the common somatic mutation G403R is reported.

Expression levels of β_2 and β_3 subunits were analysed and again microarray findings were confirmed establishing β_2 as the main β subunit in adrenal tissues, which is nearly 5-fold upregulated only in ZG-like APAs compared to paired normal adrenals (Fig. 17c). It was hypothesised that constitutive aldosterone secretion from APAs could also be driven by upregulation of β_2 subunits that lead to slow inactivation of Ca_v1.3. β_2 transcript expression analysis for membrane bound β_{2a} and β_{2e} and cytoplasmic β_{2d} variants revealed data opposite to expected. None of the samples had detectable levels of β_{2a} transcript without any significant differences in β_{2d} and β_{2e} levels in the normal adrenals. Strikingly, the most predominant transcript in ZG-like APAs was β_{2d} rather than the other membrane associated β_{2e} subunit (Fig. 17d). These results could be explained by some kind of negative feedback mechanism favouring alternative splicing for β_{2d} expression over β_{2e} . These findings further support existence of very different transcriptome and underlying molecular mechanisms for aldosterone secretion in two histologically distinct ZG-like and ZF-like APAs.

This isoform analysis was crucial for the FastTrack Discovery project so the compound screening is performed using adrenal relevant transcripts of both Ca_v1.3 and β subunit, which could be different from those expressed in heart and blood vessels. This was to minimise the off-target effects of the potential compounds.

Functional studies to assess the effect of Cav1.3 mutations on aldosterone secretion from H295R cells have demonstrated their gain-of-function phenotype in electrophysiological properties (Azizan et al., 2013; Pinggera et al., 2014) translates downstream into higher aldosterone production from cells expressing mutant Cav1.3 compared to the WT (Xie et al., 2016) (Fig. 18). There are some technical issues with experiments where H295R cells had to be transfected by electroporation. I observed electroporated cells to be less healthy than the non-electroporated (un-transfected) cells and appeared to have clumped together due to loss of membrane integrity. They also appeared to be “leaky” releasing any intracellularly stored aldosterone as cells transfected just with the empty vector released more aldosterone as compared to the non-electroporated cells. Alternative method of milder transfection using Lipofectamine transfection reagent was also not ideal for achieving high transfection efficiency in case of Cav1.3 plasmids that require co-transfection of another 2 constructs for $\alpha_2\delta$ -1 and β subunits.

Application of step depolarisation protocols in whole cell patch clamping experiments on transfected tsA-201 cells showed current activation at more negative voltages for the mutants V259D (in the cytoplasmic S4-S5 linker coupling the voltage-sensing domain to the pore), G403R, F747L and I750M (in the channel activation gate) in the presence of β_3 subunit (Fig. 21). The other three mutants R990H (in the voltage sensor), P1336R (also in the cytoplasmic S4-S5 linker coupling the voltage-sensing domain to the pore) and M1354I (on the extracellular end of S5 voltage-sensing domain) did not show any significant differences in voltage dependence of channel activation compared to WT Cav1.3. Despite the different β subunit used here (β_3 vs β_{1b}), these findings are consistent with the previously reported functional studies for V259D, I750M and P1336R mutants (Azizan et al., 2013).

Subsequent to establishing the main β subunits expressed in the adrenals, whole cell patch clamping experiments were performed on tsA cells expressing Cav1.3 WT or V259D in the presence of β_{2d} or β_{2e} subunits. There were no differences found in calcium currents through WT channels in the presence of β_3 or β_{2d} , but β_{2e} led to rightward shift in the voltage-dependence of current activation, such that voltage for half maximal conductance (V_{max}) was 10mV more depolarised potentials (13.49 ± 0.73 vs 1.32 ± 0.41 mV), suggesting slower channel activation in the presence of β_{2e} subunit (Fig. 23). In the presence of Ba^{2+} as the charge carrier, type of β_2 subunit present did not influence current activation for either WT or V259D Cav1.3 channels (Fig. 27a & b).

As expected, membrane bound β_{2e} subunit led to significantly slower inactivation of Cav1.3-WT as calculated by V_{50} of inactivation compared to β_{2d} (-7.32 ± 1.60 vs -15.42 ± 2.59 mV) (Fig. 27c). The mutation V259D that shifts the voltage-dependent activation and steady-state

inactivation of $\text{Ca}_v1.3$ by 15mV to more negative voltages was not influenced by the type of β_2 subunit present. Fast channel inactivation kinetics as calculated by r_{300} values (the fraction of current remaining at 300ms from the start of the depolarisation step) of V259D, on the other hand, was influenced by the type of β_2 subunit expressed. As evident from the r_{300} values, the V259D channel expressed with β_{2d} exhibited currents inactivated by almost 50% at all voltages tested (Fig. 27d). Unexpectedly, WT channel showed almost no fast inactivation in the presence of either β_2 subunit. These results suggest that the voltage dependence of channel activation is mainly determined by the $\text{Ca}_v1.3$ subunit, i.e. WT or mutant but β subunit variants predominantly influence steady state inactivation and time constants of fast inactivation, due to their differential membrane association properties. Whole cell patch clamp experiments on tsA-201 cells provide critical evidences for modulation of channel properties under various conditions, but in the context of aldosterone synthesis, this knowledge is of limited significance unless primary cells from normal adrenal and APAs harbouring *CACNA1D* somatic mutations are studied.

Nuclear localisation of endogenous $\text{Ca}_v1.3$ in H295R cells as seen by staining with antibodies specific to cleavable c-terminal chain (Fig. 28), but not with antibody towards pore-forming domain suggests $\text{Ca}_v1.3$ to play a role as transcription factor in adrenals cells similar to that reported in mouse atrial cells (Lu et al., 2015). Here I showed that transfected c-terminal peptide translocates to nucleus of H295R cells (Fig. 30) and possibly also undergoes a protease-mediated cleavage at a site that's putatively sensitive to calpain proteases (Fig. 29). Overexpression of $\text{Ca}_v1.3$ C-terminal upregulated aldosterone secretion in H295R cells (Fig. 31). A slight puzzling observation was nuclear staining only with FLAG antibody and not with Myc antibody. There is a possibility that Myc antibody could not penetrate into the nucleus, but it needs further investigation. In order to find direct evidence of $\text{Ca}_v1.3$, like $\text{Ca}_v1.1$ and $\text{Ca}_v1.2$ in skeletal muscles, cardiomyocytes and neurons being a substrate for calpain or similar proteases (Gomez-Ospina et al., 2006, 2013; Hulme et al., 2005; Schroder et al., 2009), H295R cells were treated with a cell-permeable calpain inhibitor, calpeptin. Western blot using anti- $\text{Ca}_v1.3$ antibody towards the intracellular C-terminal showed increased levels of full-length $\text{Ca}_v1.3$ in the calpeptin treated cells compared to those in untreated cells (Fig. 33), suggesting calpain inhibition prevented proteolytic cleavage of $\text{Ca}_v1.3$ C-terminal. Interestingly, aldosterone secretion is significantly reduced in the calpeptin treated cells, where downregulation of $\text{Ca}_v1.3$ transcription was also observed (Fig. 34). These observations indicate the phenomenon of self-regulatory expression by c-terminal peptide as reported for $\text{Ca}_v1.2$. It is interesting to note that the nuclear translocation of c-terminal chain is negatively regulated by intracellular calcium concentration (Lu et al., 2015).

These experiments have provided essential insights into the role of cleaved c-terminal of $\text{Ca}_v1.3$ that is overexpressed $\text{Ca}_v1.3$ -CT upregulates aldosterone secretion up and reduced

Cav1.3-CT levels by inhibiting calpains downregulates aldosterone secretion. Despite these findings it was necessary to investigate whether Cav1.3 is a vital source of calcium entry for normal endocrine function of ZG or if it is only the gain-of-function in mutated APAs that makes Cav1.3 a target for pathological studies. To answer this question, effects of Cav1.3 knockdown by shRNA transfection in H295R cells was studied. Unfortunately only negligible knockdown of Cav1.3 transcription was achieved in this *in vitro* system (Fig. 35). For this study, only adrenal tissue was available but not the Cav1.3 knockout mice blood samples to measure plasma aldosterone levels. Quantitative PCRs showed approximately 50% downregulated expression of aldosterone synthase, *CYP11B2* in the Cav1.3 null mice compared to the age matched wild-type animals of both genders (Fig. 37). This data suggests that Cav1.3 does play a crucial role in the regulation of aldosterone secretion under normal physiological conditions of non-mutated states in the normal zona glomerulosa.

Pharmacological studies with the new tool compounds identified in the high-throughput screening at [REDACTED] also supported importance of Cav1.3 function in aldosterone secretion. Of the three Cav1.3 selective (over [REDACTED] compounds tested, compound B showed the most promising aldosterone inhibition in H295R cells (Fig. 38). Aldosterone suppression was also observed in the primary adrenal cells treated with compound B, but no definite conclusions could be drawn on the basis of only 2 sets of primary cells tested (Fig. 39). More experiments with other patients' cells are required in future studies. With recent reports of *CACNA1D* being the most commonly mutated gene in the APCCs, it is possible that either the 2 samples tested here or the one's that will be used in future, contain such somatically mutated APCCs. Knowledge of these genetic determinants would be crucial for any further development of target compounds for primary aldosteronism therapeutics.

CHAPTER 4

CHAPTER 4 - GENOTYPING AND WHOLE EXOME SEQUENCING OF APAs TO FIND NEW SOMATIC MUTATIONS

4.1 Abstract

With great technological advancements in the development of next-generation sequencing and data analysis of paired pathological and normal tissue samples discovery of somatic mutations in APAs was made possible. Since the first such report in 2011 of somatic mutations in the gene *KCNJ5*, functional mutations in several other genes encoding ion channels or transporters have been discovered. Mutations in these genes, *CACNA1D*, *ATP1A1* and *ATP2B3* and also *KCNJ5* have been implicated in membrane depolarisation in APA cells resulting in raised intracellular calcium levels and hence, autonomous aldosterone production. Another gene that is common to many cancers but rarely found in APAs is *CTNNB1*. APAs are visualised in potential PA patients or as incidentalomas by CT or MRI scan. These methods are efficient in detecting mainly large ZF-like APAs that exist outside the adrenal body. In contrast, PET-CT using C^{11} -metomidate was used in our hospital not only for lateralisation (overcoming technical difficulty associated with AVS), but also for detecting small (<1cm) ZG-like APAs within the adrenal mass.

We had a number of APAs that had not been sequenced for these known genes, so samples were genotyped and prepared for whole exome sequencing, in order to find some novel genes especially in the sub-cm adenomas. Of 59 APAs (from 52 patients) with unknown genotypes, we found mutations in 34 APAs (58% APAs or 65% patients) in the previously reported genes either by genotyping or WES. We found *CACNA1D* to be the most commonly mutated gene in our cohort accounting for 20.5% APAs (n=12 APAs, 23% patients). As expected, prevalence of *KCNJ5* mutated APAs in this study was only 17% APAs (n=10 APAs, 19% patients), which was much lower than 40% as reported in previous studies. *ATP1A1* and *ATP2B3* were mutated in 5 APAs each (8.5% APAs or 10% patients) and *CTNNB1* mutations were found in 2 APAs. We did not find any cases with a second hit in other nodule among 7 patients with 2 APAs. This difference in the prevalence of different genes probably arises from different approach to screening for PA in Addenbrooke's Hospital. Many of our patients were detected by renin measurement in resistant hypertension, and their APAs identified by the unique C^{11} -metomidate PET-CT, instead of adrenal vein sampling.

Apart from different prevalence of mutations in the known genes, we found a novel somatic mutation in a gene not encoding an ion channel/transporter, but in the gene *CADM1* encoding cell adhesion molecule that is previously linked to cell-cell adhesion and tumour suppression. The mutation we found is a single nucleotide variant leading to substitution of [REDACTED] ([REDACTED]) in the single transmembrane domain of this cell surface protein. The likely significance of this discovery was greatly enhanced when we ascertained that one of the 'private' somatic mutations found on whole exome sequencing of APAs in Munich was a similar substitution in the adjacent amino acid ([REDACTED]) of the membrane-spanning domain of *CADM1*.

4.2 Introduction

4.2.1 Aim and Hypotheses

We aimed to genotype all APAs in our cohort that is enriched for smaller ZG-like APAs and likely to have fewer ZF-like APAs with *KCNJ5* mutations. There were 59 APAs from 52 patients (7 patients had 2 nodules) analysed in the study. This was done partially by Sanger sequencing for known genes and by next-generation sequencing of whole exomes in genomic DNA extracted from paired normal adrenal and APAs. As we could detect many small APAs by PET-CT scans using C¹¹-metomidate which are usually missed on routine CT scans, we expected to find more cases of *CACNA1D*, *ATP2B3* or *ATP1A1* mutants compared to *KCNJ5* and hence differences in the mutational prevalence of these genes as reported globally. We also hoped to find some novel genes with somatic mutations which would be of interest in understanding the phenotype of hyper aldosterone secretion.

4.3 Materials and methods

4.3.1 Sample gDNA preparation and selection

All available APAs that had not been previously genotyped or whole exome sequenced in the lab were tested for known or novel somatic mutations in different batches by genotyping for hotspots, or whole exome sequencing at Barts Genome Centre and Genome Institute of Singapore. Genomic DNA for paired adjacent normal adrenal and APA(s) was extracted mainly from freshly frozen tissue samples using QIAamp DNA Mini Kit as described earlier. If such sample was not available, tissue sample preserved in RNALater was used preferably (using the same kit) over and lastly from FFPE sections dissolved in xylene using QIAamp DNA FFPE Tissue Kit (Qiagen, 56404). DNA concentration and quality for all samples was initially estimated by Nanodrop. There was good quality gDNA samples available from 59 APAs (labelled as T for tumour/APA) and 52 normal adrenals (labelled as N for normal) from 52 patients who had adrenalectomy at Addenbrooke's Hospital.

4.3.2 Samples/patients in the study

Table 17: List of samples

Sample	Source of gDNA for Normal / Tumour	APA size (mm)	Gender	Age at surgery (y)
14T	F/F		Female	
30T	F/F		Male	55
43T	FFPE/F			
96T	NA	28 or 5	Male	47
121T	FFPE/FFPE	18	Male	45
136T	F/F	12	Male	59
139T	NA	8	Male	58
141T	F/F	7	Male	53
148T	F/F	11	Male	54
156T	F/F	33	Male	66
171T	F/F	17	Female	34
176T	R/R	15	Male	64
180T	F/F	16	Female	41
181T	F/R	7	Male	44
182T	F/F	10	Male	41
183T	F/F	16	Male	56
184T	F/R	6	Male	47
185T	F/F	15	Female	42
186T1	F/F	10	Male	42
186T2	F/F	10		
187T	F/F	10	Male	33
190T	F/F	20	Female	47

191T	F/F	8	Female	39
192T	F/F	Too small	Male	63
194T	F/R	15	Male	55
195T	F/F	9.8	Female	36
196T	F/F	12	Male	63
198T	F/F	8	Female	41
200T	F/F	15	Male	59
202T	F/R	10	Male	53
204T	F/F	12	Female	28
206T	F/F	22	Female	40
206Tsmall	F/F			
207T	FFPE/F	24	Female	58
208T1	F/F	28	Female	44
208T2	F/F			
210T	F/F		Male	49
214T	F/F	7	Male	49
216T1	F/F	13	Male	42
216T2	F/F			
218T	F/F	14	Female	56
219T	F/F	19.2	Female	49
221T1	F/F	12.3	Male	63
221T2	F/F			
223T	R/R	14	Male	65
226T	F/F		Male	66
227T	F/F		Male	59
228T	F/F		Male	50
233T	F/F		Male	47
235T	F/F		Male	34
238T	R/R		Female	35
239T1	R/R		Male	
239T2	R/R			
240T	F/F		Male	57
244T	F/F		Female	55
247T	F/F		Male	61
250T	F/F		Male	69
252TL	F/F		Male	52
252TM	F/F			

F: Freshly Frozen, R: RNALater; FFPE: Formalin-fixed paraffin-embedded; NA: Info not available

4.3.3 Targeted hotspot sequencing - primers and PCR conditions

Genotyping for known mutations in the genes *ATP1A1*, *ATP2B3*, *CACNA1D*, *CTNNB1* and *KCNJ5* was performed by Sanger sequencing (Section 2.1.5) using primers aligning to gDNA sequence of frequently mutated/hotspot regions (Table 18). All primer pairs used were designed to amplify 200-600bp target sequences. PCRs were performed as described previously using GoTaq polymerase and TD_68_60 PCR program. Mutations were detected using Mutation Surveyor (SoftGenetics, USA).

Table 18: List of primers for genotyping of hotspot regions.

Target gene	Sequencing region	Primer name	Primer sequence
<i>ATP1A1</i>	Exon 4	ATP1A1_L104R_F	TCCACTGCTTCTCAGGGATT
		ATP1A1_L104R_R	GAACTCACATTATCGTTTTGAGGTT
	Exon 21	ATP1A1_960-964del_F	CTCCAAGTTTTCAAGTACAGCTAA
		ATP1A1_960-964del_R	GGGGAAAAGCCACACATACT
<i>ATP2B3</i>	Exon 8	ATP2B3_T423fs_F	GTCTGCCATCACCGTCATC
		ATP2B3_T423fs_R	CCCCAGTTTCCGAGTCTGTA
<i>CACNA1D</i>	Exon 6	CACNA1D_V259_F	GCTTTGAAATACCTCTTTGAATTTT
		CACNA1D_V259_R	ATTTTGTTTTAGATTTTCCCAAAC
	Exon 8A	CACNA1D_G403_F	TCCTCTTATTAACCCACTCTATG
		CACNA1D_G403_R	AATGTCTGGCAACCCCTCTT
	Exon 8B	CACNA1D_Ex8B_F	GGAGCACTAACCTTCAGCAAA
		CACNA1D_Ex8B_R	CATGCAGAGAAGCTGTCAGG
	Exon 15	CACNA1D_I650_F	CGGCAACCAGTCACATCC
		CACNA1D_I650_R	GGGAAATTGTCAAAGGTGCT
	Exon 17	CACNA1D_F747_F	AACACTTGGGACGGTCACTT
		CACNA1D_F747_R	CAAACACGTCAGGGGAAAAT
	Exon 24	CACNA1D_R990_F	TGTGCAGGGATACTAAAGTGAAGA
		CACNA1D_R990_R	CTCAGCTCTGCCAGAAGA
	Exon 28	CACNA1D_F1147_F	TGGTTTTTCTCTCTAGGTTGC
		CACNA1D_F1147_R	TCCTGACCAAGGGACAGAAG
	Exon 34	CACNA1D_P1336_F	CGTGAATAGAAAGGAAGCA
		CACNA1D_P1336_R	AGAGGCATTTGGCTGAAAAA
<i>CTNNB1</i>	Exon 2	CTNNB1_Ex2_F	CATCACTGAGCTAACCTGGC
		CTNNB1_Ex2_R	CTCGAGTCATTGCATACTGTCC
<i>KCNJ5</i>	Exon 1	KCNJ5_G151R_L168R_F	GCTTCATTTGGTGGCTCATT
		KCNJ5_G151R_L168R_R	GAGATGACTGCGTTGTTGGA

4.3.4 WES sample preparation and QC

About 1µg of gDNA in 20-50µl volume was sent to the laboratories performing whole exome sequencing. The samples were checked for DNA integrity and more accurate quantification by using PicoGreen DNA binding reagent (QuBit Nucleotide Quantification) before preparing libraries according to the kits used.

4.3.5 WES methodology

Following is the brief explanation of the whole exome sequencing methodology performed at Genome Centre, Barts and Genome Institute of Singapore. Extracted gDNA was run on a gel to ensure good integrity. Concentration and purity of DNA was verified and 1ug was fragmented by sonication, optimized to give a distribution of 200-500 base pairs. Libraries were prepared using Kapa DNA HTP Library Preparation Kit (KAPA Biosystems) or Nextera Rapid Capture Exome Kit (Illumina). Hybridization of the adapter ligated DNA was performed at 47°C, for 64 to 72hr, to a biotin-labelled probe included in the Nimblegen SeqCap EZ Human Exome Kit (Roche). Libraries were sequenced using the Illumina Hiseq 2500 sequencing system and paired-end 101bp reads were generated for analysis.

4.3.6 Somatic mutation detection-Mutect2 pipeline

Following bioinformatics analysis for detection of somatic mutations in the tumour samples was performed by Dr Claudia Cabrera at Centre for Translational Bioinformatics, William Harvey Research Institute, Barts and The London School of Medicine and Dentistry, Queen Mary University of London and Ms Kuan Jyn Ling in Dr Roger Foo's team at Genome Institute of Singapore, National University of Singapore. Somatic mutations were detected by following the recommended "Best Practices" algorithm for a specialised tool, Mutect2 (Fig. 40) available as part of Genome Analysis Tool Kit (GATK, Broad Institute, Massachusetts). Briefly, the exome sequences were aligned to the NCBI/build37.2 human reference genome using the Burrows-Wheeler Aligner (BWA-MEM, bwa-0.7.12). Picard Tools software (picard-tools-1.119) was used to sort alignments for each paired-exome sequence and merge bam files, followed by marking of PCR duplicates. Quality score recalibration was performed with GATK (GenomeAnalysisTK-3.6) using dbSNP, Mills, and 1000 genomes as reference resources. IndelRealigner and base quality score recalibration was also done to minimize base mismatches near indels. The final variants output were called using HaplotypeCaller for germline variants and MuTect2 for somatic variants. In Mutect2, normal and tumour DNA cross contamination estimates were calculated for each normal-tumour pair using GATK. PON (panel of normal) files were created for every normal sample which were then used to create a single PON file using CombineVariants tool in GATK. Mutect2 was then run for making single nucleotide variants (SNVs) and insertion-deletion variant calls (Indels) in each tumour sample

by running data against created PON file, COSMIC database and dbSNP. Variants were filtered on basis of quality scores, and that scored less than 0.01 in population databases including 1000G and ExAC were retained. Finally, all calls were annotated using an online annotator named Oncotator [<http://portals.broadinstitute.org/oncotator/>]. Variants were further selected for only those leading to non-synonymous, splicing and frameshift changes. Variants were also annotated by algorithms to predict pathogenicity by SIFT.

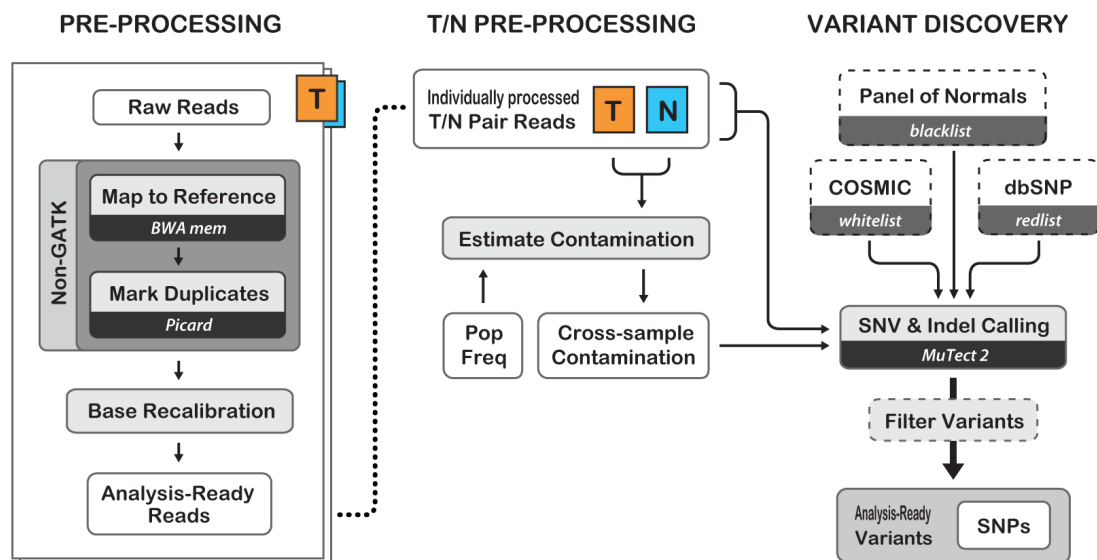


Fig. 40: Best Practices for Somatic SNVs and Indels calling in whole genome or exome sequencing data by Mutect2, GATK.

4.4 Results

4.4.1 Sample workflow and mutation detection

Of the 59 gDNA samples from APAs, some were genotyped for all hotspots in the known genes. Among 37 samples that were whole exome sequenced, some were partially genotyped by Sanger sequencing, mainly for mutations in *KCNJ5* (Table 19). Somatic mutations in the 5 candidate genes were found in 27 APAs by WES. Paired analysis by Mutect2 (GATK) for normal and APA gDNA sequencing data helped detection of a novel mutation in a gene *CADM1* in sample 184T. Of 22 samples that were not whole exome sequenced, genotyping for hotspots in the known genes and *CADM1* was done and mutations in 7 samples were detected, though none were in *CADM1*.

Table 19: Sample workflow and mutations found.

Sample	All hotspots sequenced	WES	WES Batch OR Reason for no WES	Mutant Gene	Mutation	Mutation detection method	KCNJ5 genotype
141T	No	Yes	1-Barts	<i>ATP2B3</i>	del425-426	WES	NS
184T	No	Yes	1-Barts	<i>CADM1</i>	V380D	WES	NS
187T	No	Yes	1-Barts	<i>ATP1A1</i>	L104R	WES	WT
192T	No	Yes	1-Barts	<i>ATP2B3</i>	del425-426	WES	NS
195T	No	Yes	1-Barts	<i>CACNA1D</i>	I650N	WES	NS
198T	No	Yes	1-Barts	<i>KCNJ5</i>	L168R	WES	Mutant
202T	No	Yes	1-Barts	<i>CACNA1D</i>	F1147L	WES	WT
214T	No	Yes	1-Barts	<i>CACNA1D</i>	F747L	WES	NS
14T	No	Yes	2-Singapore	<i>CTNNB1</i>	T41A	WES	WT
30T	No	Yes	2-Singapore				WT
136T	No	Yes	2-Singapore				WT
148T	No	Yes	2-Singapore	<i>ATP2B3</i>	del425-426	WES	NS
156T	No	Yes	2-Singapore	<i>ATP2B3</i>	del425-426	WES	NS
176T	No	Yes	2-Singapore	<i>ATP1A1</i>	L104R	WES	WT
181T	No	Yes	2-Singapore	<i>CACNA1D</i>	G403R-8A	WES	NS
182T	No	Yes	2-Singapore	<i>ATP1A1</i>	L104R	WES	WT
183T	No	Yes	2-Singapore				WT
185T	No	Yes	2-Singapore	<i>KCNJ5</i>	G151R	WES	Mutant
194T	No	Yes	2-Singapore	<i>CACNA1D</i>	V1338M	WES	NS
196T	No	Yes	2-Singapore	<i>CACNA1D</i>	R990G	WES	NS
200T	No	Yes	2-Singapore	<i>ATP1A1</i>	EETA963S	WES	NS
204T	No	Yes	2-Singapore	<i>KCNJ5</i>	L168R	WES	Mutant
218T	No	Yes	2-Singapore				WT
219T	No	Yes	2-Singapore	<i>KCNJ5</i>	L168R	WES	Mutant
221T1	No	Yes	2-Singapore	<i>KCNJ5</i>	L168R	WES	Mutant
223T	No	Yes	2-Singapore	<i>CACNA1D</i>	I750M	WES	WT

227T	No	Yes	3-Barts				WT
228T	No	Yes	3-Barts	<i>ATP1A1</i>	L104R	WES	WT
233T	No	Yes	3-Barts	<i>CACNA1D</i>	P1336R	WES	WT
235T	No	Yes	3-Barts				WT
238T	No	Yes	3-Barts	<i>CTNNB1</i>	S45P	WES	WT
239T1	No	Yes	3-Barts	<i>CACNA1D</i>	G403R-8B	WES	WT
240T	No	Yes	3-Barts	<i>CACNA1D</i>	F747L	WES	WT
247T	No	Yes	3-Barts				WT
250T	No	Yes	3-Barts				WT
252TL	No	Yes	3-Barts	<i>CACNA1D</i>	V1338M	WES	WT
252TM	No	Yes	3-Barts				WT
139T	Yes	No	Known mutation	<i>CACNA1D</i>	G403R-8B	Genotyping	WT
171T	Yes	No	Known mutation	<i>KCNJ5</i>	G151R	Genotyping	Mutant
190T	Yes	No	Known mutation	<i>KCNJ5</i>	G151R	Genotyping	Mutant
191T	Yes	No	Known mutation	<i>KCNJ5</i>	L168R	Genotyping	Mutant
207T	Yes	No	Known mutation	<i>KCNJ5</i>	L168R	Genotyping	Mutant
226T	Yes	No	Known mutation	<i>ATP2B3</i>	del425-426	Genotyping	WT
244T	Yes	No	Known mutation	<i>KCNJ5</i>	L168R	Genotyping	Mutant
43T	Yes	No					WT
96T	Yes	No					WT
121T	Yes	No					WT
180T	Yes	No					WT
186T1	Yes	No					WT
186T2	Yes	No					WT
206T1	Yes	No					WT
206T2	Yes	No					WT
208T1	Yes	No					WT
208T2	Yes	No					WT
210T	Yes	No					WT
216T1	Yes	No					WT
216T2	Yes	No					WT
221T2	Yes	No					WT
239T2	Yes	No					WT

WES: Whole exome sequencing; WT: Wild-type; NS: Not sequenced.

4.4.2 New cases with mutations in known genes

On compiling all genotyping and whole exome sequencing results, number of mutant APAs for the known genes were calculated (Table 20). Mutations in these genes were found in 57% of APAs (=34/59), with the most number of *CACNA1D* mutants (20%). Surprisingly, mutations in *KCNJ5* were found only in 17% APAs.

Table 20: Mutant samples per gene

Mutant gene	Mutant APAs: n	Males: n (%)	Females: n (%)	% of APAs (n=59)	% of patients (n=52)
<i>KCNJ5</i>	10	1 (10)	9 (90)	16.9	19.2
<i>ATP1A1</i>	5	5 (100)	0	8.5	9.6
<i>ATP2B3</i>	5	5 (100)	0	8.5	9.6
<i>CTNNB1</i>	2	0	2 (100)	3.4	3.8
<i>CACNA1D</i>	12	11 (92)	1 (8)	20.3	23.1
Total Mutants	34 (+1 - <i>CADM1</i>)	22 (65)	12 (35)	57.6	65.4

4.4.3 Novel somatic mutations - *CADM1*

As mentioned in Section 4.4.1, a novel mutation in the gene *CADM1* was found in one of the APAs without any variants in the known genes previously described in aldosterone producing adenomas. The mutation in tumour sample of patient 184 was confirmed to be somatic as no traces of the variant allele were seen in adjacent normal tissue gDNA sequences (Fig. 41). The mutation “c. 1139 T>A, p. V380D” lies in the exon 11 of *CADM1*, a gene encoding cell adhesion molecule 1 (Fig. 43 & Fig. 44 in next chapter). To identify more cases harbouring identical or nearby variants in *CADM1*, 22 APAs that were not whole exome sequenced and had no mutation in known genes, were genotyped for exon 11 of *CADM1*.

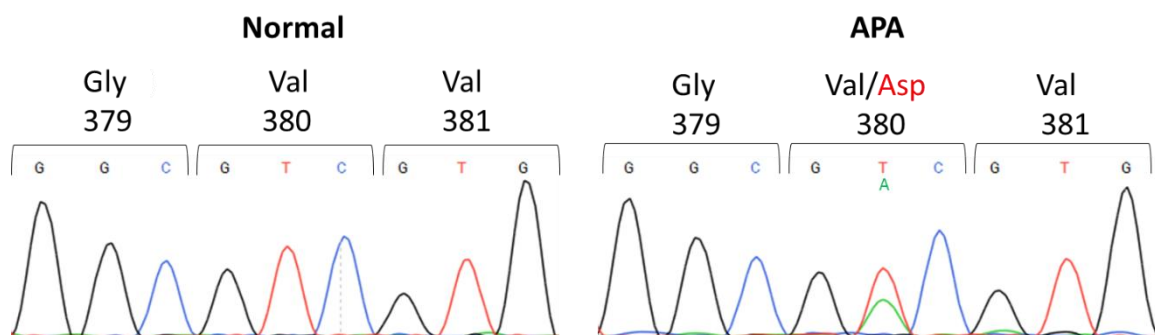


Fig. 41: Chromatograms for *CADM1* sequencing for normal adrenal and APA gDNA samples of patient 184 showing single nucleotide variant, c. 1139 T>A, p. V380D.

Though no other cases could be identified in our study cohort, collaborators at the University of Munich, Germany found only one case amongst the 70 samples used for exome sequencing for somatic mutations in *CADM1*. These 70 samples mainly harboured uncommon/unique mutations and were referred to as cases having ‘private’ mutations. This sample also harboured a single nucleotide variant “c. 1136 G>A, p. G379D”, substituting amino acid adjacent to the one in Cambridge patient (Fig. 42). The Munich patient presented at 44 years with hypokalaemic primary aldosteronism and was lateralised by adrenal vein sampling. Adrenalectomy revealed the presence of 1.5cm adenoma. Case report of patient 184 is discussed in detail in section 5.2.7 of next chapter.

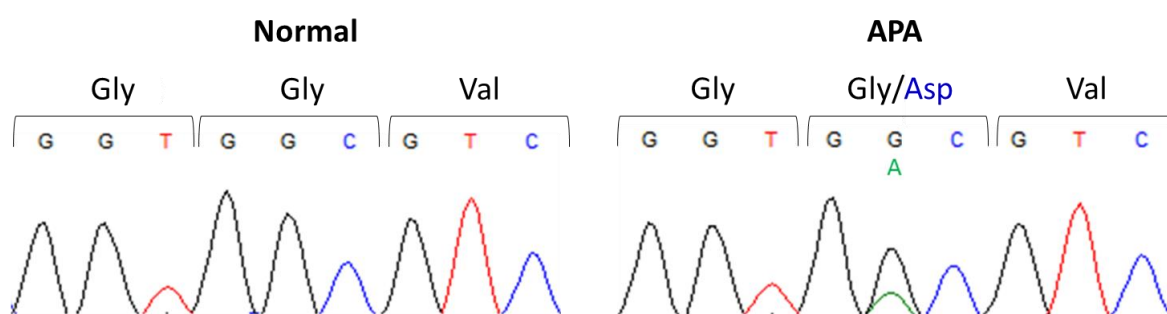


Fig. 42: Chromatograms for *CADM1* sequencing for normal adrenal and APA gDNA samples of Munich patient showing single nucleotide variant, c. 1136 G>A, p. G379D.

Both somatic mutations lead to substitution of uncharged amino acids, glycine (G) and valine (V) to negatively charged aspartate (D) residue in the single membrane spanning domain of the adhesion molecule *CADM1*. With only 2 cases of *CADM1* mutations in total 129 APAs (59 in Cambridge and 70 in Germany) it is clearly very rare but the close proximity of both substitutions made a strong case to pursue further investigation into the effects of *CADM1* mutations on its physiological function in normal adrenal and aldosterone secretion, which has not been studied previously.

4.5 Discussion

In this study we have genotyped or whole exome sequenced 59 APAs from our cohort. Genotyping involved targeted Sanger sequencing for hotspots in the known 5 candidate genes – *KCNJ5*, *CACNA1D*, *ATP1A1*, *ATP2B3* and *CTNNB1*. 37 APAs were subjected to whole exome sequencing and somatic mutations in known genes were found in 27 APAs. Mutations in 7 APAs were found by complete genotyping of 22 APAs that could not be whole exome sequenced. We found a high mutation rate of 57% among 59 APAs, or of over 65% among 52 patients. This mutation rate is comparable to that reported in large studies on Caucasian populations (Åkerström et al., 2015; Fernandes-Rosa et al., 2014). But interesting point to note here is the composition of genetic spectrum within similar overall mutation rates. We report much lower prevalence for *KCNJ5* mutant APAs, that is only 17% compared to nearly 40% in most cohorts (Table 20 vs Table 2). We found *CACNA1D* to be the most common of all candidate genes with mutations in over 20% APAs compared to the highest proportion of only 10% reported in ENSAT cohort (Fernandes-Rosa et al., 2014). This high prevalence of *CACNA1D* mutations is supported by the report of it being the most commonly mutated in APCCs, possibly the precursors of *CACNA1D* mutant APAs (unpublished data).

Interestingly, susceptibility to the mutations in different genes is much more exaggerated by gender in our study. We found only 1 (10%) male patient among 10 *KCNJ5* mutants and 1 (8%) female amongst the 12 *CACNA1D* mutants (Table 20). Additionally, 5 mutants identified for each of the *ATP1A1* and *ATP2B3* genes were all males and 2 *CTNNB1* gene mutants were females. Interestingly, the patient with the 6mm APA harbouring novel *CADM1* mutation was also a male. The reason for this huge gender bias is still unknown and would require further investigation.

We propose the differences in the prevalences of mutant genes in our study are due to different clinical practice in Addenbrooke's Hospital where PET-CT using C¹¹-metomidate has been preferred over AVS for detection of small APAs. Our findings greatly support the superiority of C¹¹-metomidate PET-CT over AVS and other imaging methods so as to not miss cases that could potentially be cured by unilateral adrenalectomy. Rather short half-life of C¹¹ is an issue in wide application of this method and development of alternative radio-labels for metomidate without losing the specificity and resolution should be pursued as a matter of urgency.

The detection of novel somatic mutation, V380D in *CADM1* made whole exome sequencing in this study even more worthwhile (Fig. 41). Apart from *CTNNB1*, which is commonly mutated in many cancers, still rarely in APAs, this is the first case of a non-ion channel or transporter

gene, but a cell-cell adhesion protein to be mutated in APAs. Our interest in pursuing functional studies on CADM1 was enhanced by identification of another case of CADM1 mutation by Munich's team of investigators. This second mutation substituted the adjacent residue (G379D) to the one that was identified by us (Fig. 42), which suggests that the two mutations lie within the single transmembrane domain of this cell surface adhesion molecule. In this report, the functional data on both these mutations is provided in the following chapter.

CHAPTER 5

CHAPTER 5 - NOVEL MUTATIONS IN CELL ADHESION MOLECULE, *CADM1* FOCUS ATTENTION ON THE SIGNIFICANCE OF CELL-CELL COMMUNICATION IN ALDOSTERONE SECRETION

5.1 Abstract

On whole exome sequencing of eight APAs up to 1cm in diameter, we found seven APAs with mutations in genes previously described in primary aldosteronism. Paired analysis of sequencing data for genomic DNA from adjacent normal adrenal and APA, using Mutect2 led us to discover a novel somatic mutation in the gene *CADM1* in the eighth sample. This somatic mutation in *CADM1* is the first instance of APA associated mutation in a gene not encoding an ion channel or ion transporter. *CADM1* is a protein previously linked to cell-cell adhesion and tumour suppression, containing three extracellular immunoglobulin-like domains, a transmembrane helix and short cytoplasmic chain. Its expression is either downregulated or absent in many cancers, hence known as a tumour suppressor gene. The mutation in the APA was a single nucleotide polymorphism leading to substitution of uncharged valine residue lying in the transmembrane domain of *CADM1* with the negatively charged aspartate, V380D. Likelihood of this somatic mutation in *CADM1* to be causative was supported by the detection of another such case in a different cohort of PA patients in Munich. This case was again a singleton among 70 paired normal and APA samples that were whole exome sequenced by our collaborators. Similar to the mutation in our patient, the second case was also the aspartate substitution of the adjacent residue within the transmembrane domain, G379D of *CADM1*.

CADM1 was found to be highly expressed in the physiological aldosterone producing zona glomerulosa (ZG), pathological aldosterone producing cell clusters (APCCs) and APAs. Overexpression of either mutant *CADM1* in H295R cells led to 10-20 fold upregulation of *CYP11B2* expression, and 2-4-fold increase in aldosterone secretion, compared to the wild-type *CADM1*. *CADM1* is a substrate for proteases and undergoes enzymatic processing at its ectodomains followed by generation of intracellular c-terminal domain (ICD) in a regulatory pathway. The increase in aldosterone was not mediated by differences in levels or composition of ICD fragments generated by mutant *CADM1* compared to WT, as γ -secretase inhibition could not reverse the hyper aldosterone secretion. Presence of negatively charged amino acid within the transmembrane domain did not affect the cell surface localisation of either mutants, but we found some evidences of loss of cell-cell adhesion in H295R cells expressing mutant *CADM1*. This loss of inter-cellular adhesion in mutant cells could be the

cause of uncontrolled aldosterone synthesis. shRNA mediated silencing of CADM1 in H295R cells downregulated aldosterone synthesis and secretion.

Transcriptome analysis, by RNAseq, of H295R cells expressing wild-type or mutant CADM1 or silenced CADM1 showed a large number of differentially expressed genes. Interestingly, most of the top genes upregulated in CADM1 silenced cells were also upregulated in mutant CADM1 expressing H295R cells. This suggests a loss-of-function phenotype for mutant proteins, except for CYP11B2 expression that goes in opposite directions. Some of the upregulated genes included ACTH receptor and several steroidogenic enzymes. An inverse relation in the absolute amounts and membrane localisation of CADM1 and Cx43 in adrenal sections and CADM1 silenced/overexpressing H295R cells was observed. This suggests CADM1 plays a role in regulating gap junctional intercellular communication (GJIC). Increased Cx43 expression could be mediated by downregulated *TSG101* expression, a protein involved in lysosomal degradation of Cx43.

It is proposed that under normal physiological conditions CADM1 acts as a crucial checkpoint in maintaining aldosterone synthesis, which is lost in silenced cells, downregulating aldosterone synthesis. In contrast, overexpressed mutants in the presence of endogenous wild-type CADM1 would interfere with trans-homophilic interactions of WT molecules and might also make trans-heterophilic interactions with WT CADM1 molecules in adjacent cells. This heterophilic interaction could act as a pseudo checkpoint for many signalling pathways including aldosterone synthesis. This hypothesis is supported by attenuated aldosterone signal from mutant expressing H295R cells in the presence of higher dose of WT CADM1.

This study has helped us to focus our attention on the previously unexplored mechanism of intercellular adhesion and communication in ZG that is essential for glomerular pace-making required for regulated aldosterone secretion.

5.2 Introduction

5.2.1 *CADM1* gene discovery and structure

CADM1, encodes a cell adhesion molecule 1 protein highly expressed in epithelial cells and maps to chromosome 11. Since its discovery it has been given several names like *IGSF4* (immunoglobulin superfamily 4), *TSLC-1* (tumour suppressor in lung cancer-1), *SynCAM1* (synaptic cell adhesion molecule-1), *NECL2* (nectin-like molecule 2), and *SgIGSF* (spermatogenic immunoglobulin superfamily) reflecting its structure, varied expression and functions via its interaction with a wide range of proteins both inter- and intra-cellularly (Section 5.2.3).

Even though the tumourigenicity of non-small cell lung cancer (NSCLC) cell line A549 cells was suppressed by micro-cell mediated chromosome transfer of chromosomes 3 and 11 in early 1990's (Sato et al., 1993), it was not until later in the decade and early millennium when two teams independently discovered the presence of a single gene in the 100kb LOH region in chromosome 11q23 containing most of tumour suppressing activity (Murakami et al., 1998) and named it *IGSF4* (Gomyo et al., 1999) or *TSLC1* (Kuramochi et al., 2001). LOH of *TSLC1* has been implicated as the cause of hepatocellular carcinoma and pancreatic cancers (Kuramochi et al., 2001).

The gene spans the sizes of 328 kilo bases on locus 11q23.3 and contains 12 exons (Biederer, 2006). Alternative splicing of *CADM1* mRNA occurs only between exon 7 and exon 11 which translate into proteins differing in extracellular sequence just upstream of the single transmembrane domain encoded within exon 11 (Fig. 43). Ectodomains of SP1, SP2 and SP6 are constitutively shed because of the presence of exon 9; SP3 lacking exons 8-10 is non-cleavable, and ectodomain of SP4 lacking exons 9-10 is shed only in response to stimuli as discussed later. SP4 is the most ubiquitously and dominantly expressed of all *CADM1* isoforms. It is involved in the homophilic cellular adhesion, which is dysregulated by expression of SP1 (Moiseeva et al., 2012). An isoform, named SP5 retains the intronic sequence between exon 7 and 8. Product of this transcript that lacks the transmembrane domain, is secreted from the cells and has an antagonistic effect on membranous *CADM1* mediated intercellular adhesion (Biederer, 2006; Koma et al., 2004).

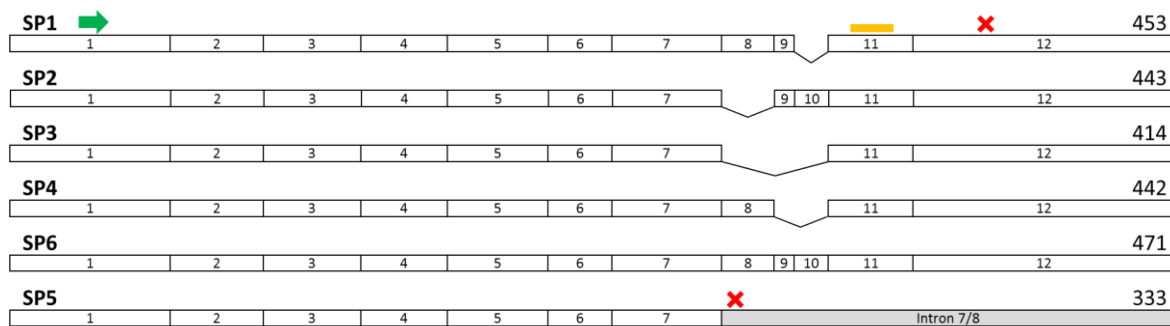


Fig. 43: Alternative splicing and transcripts of human CADM1

Six reported transcripts of human CADM1 are represented with their exonic structures. SP1-SP4 and SP6 are expressed on cell surface as indicated by the presence of exon 11 coding for transmembrane domain (yellow bar). Secreted isoform, SP5 is shown to have retained intronic sequence between exon 7 and exon 8. Green arrow indicates the common translational start site for all transcripts and red crosses indicate stop sites. Length of translated proteins in number of amino acids is indicated.

5.2.2 CADM1 protein structure and processing

CADM1 protein belongs to the immunoglobulin (Ig) like superfamily of proteins, containing N-terminal signal peptide, 3 extracellular Ig-like domains, a transmembrane helix followed by short cytoplasmic tail (Fig. 44). The cytoplasmic terminal is further characterised to contain protein 4.1-binding and PDZ type II domain binding motifs (Kuramochi et al., 2001). CADM1 Ig-like domains contain 5 sites for N-glycosylation and a juxta-membrane threonine (T) rich domain is O-glycosylated (Biederer, 2006; Biederer et al., 2002; Fogel et al., 2010). N-glycosylation of CADM1 is developmentally regulated (Kuramochi et al., 2001; Wakayama et al., 2003) and O-glycosylation is dependent on the presence of exon 8 in the expressed transcripts. CADM1 plays a vital role in cell-cell adhesion by trans-homophilic (with itself) or trans-heterophilic interaction with proteins of the same family in the adjacent cells. This inter-cell interaction is mediated by the 3 Ig-like domains of the two molecules, which is promoted by presence of N-glycans (Fogel et al., 2010). 4.1-BM and PDZ-BM are crucial for localisation of CADM1 to the lateral membranes of epithelial cells, possibly via interaction with MAGuKs, membrane-associated guanylate kinases (Masuda et al., 2005).

The extracellular domain of CADM1 undergoes proteolytic cleavage by a disintegrin and metalloprotease 10 (ADAM10) releasing the ectodomain in the extracellular space (Nagara et al., 2012) and α C-terminal fragment (α -CTF) in the membrane. α -CTF undergoes further intramembranous γ -secretase mediated cleavage releasing intracellular domain (ICD) into the cytoplasm. Both α -CTF, by internalisation and cytoplasmic ICD translocate to mitochondria, depolarising outer membrane and activating cell apoptosis. This process of CADM1 ectodomain shedding ultimately leads to loss of cell-cell adhesion and apoptosis, a process which is increased in many pathological conditions (discussed in Section 5.2.4.4).

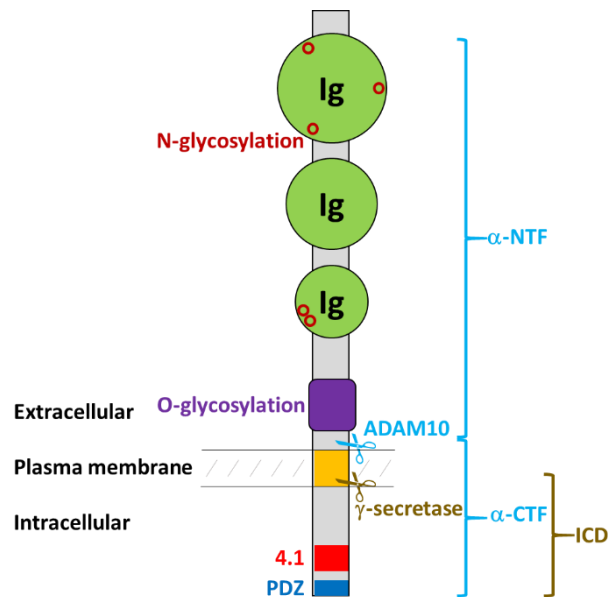


Fig. 44: Schematic representation of CADM1 structure.

Structural features of CADM1 protein are represented. Sites of proteolytic cleavage by ADAM10 and γ -secretase are shown releasing different fragments of the protein. Image adapted from (Murakami, 2005; Nagara et al., 2012)

5.2.3 Physiological function in various tissues

As discussed in the previous section, CADM1 was discovered and named independently by various research groups as a molecule performing varied roles in several mouse and human tissues. All interaction partners of CADM1, for its role of inter-cellular adhesion belong to its own family of nectin and nectin-like (Necl) proteins. Intra-cellularly it functions in signalling pathways by interacting with members of protein-4.1 family or those containing PDZ domain. Some of these are discussed briefly in this section-

5.2.3.1 Synapses

CADM1, named SynCAM by Biederer and colleagues, was reported as the homophilic cell adhesion molecule in rat brains. SynCAM was found to interact with and translocating PDZ-domain containing proteins CASK (calcium/calmodulin-dependent serine protein kinase) and syntenin to the synaptic plasma membranes in a Ca^{2+} independent manner (Biederer et al., 2002).

5.2.3.2 *Spermatogenesis*

SgIGSF/CADM1 is expressed in the mouse spermatogenic cells and essential for their adhesion to sertoli cells during the process of spermatogenesis (Wakayama et al., 2001, 2003). CADM1 null mice fail to produce mature sperms leading to male infertility (Fujita et al., 2006; van der Weyden et al., 2006; Yamada et al., 2006). This is due to abrogated trans-heterophilic adhesion of CADM1 with PVR (poliovirus receptor) molecules expressed on the surface of sertoli cells in adult mouse testis (Wakayama et al., 2007).

5.2.3.3 *Endocrine role in pancreas*

Expression of CADM1 has been reported in all of human islet cells, but restricted to only glucagon secreting alpha cells of mouse pancreas, where it promotes islet cell attachment and communication to the nerve cells (Koma et al., 2008). Though CADM1 expression is correlated with the hormonal functionality of islet cell tumours, it has an inhibitory effect on glucagon secretion in normal physiological conditions. This was demonstrated by hypersecretion of glucagon in both *in vivo* and *in vitro* models of CADM1 knockout/knockdown. Absence of CADM1 causes impaired translocation of a gap junction protein, connexin-36 to the plasma membrane resulting in loss of gap junctional intercellular communication (GJIC) (Ito et al., 2012).

5.2.3.4 *Regulation of actin cytoskeleton*

CADM1 plays a role in regulation of actin cytoskeleton in various systems. It interacts with actin filaments via direct interaction of its 4.1-BD with DAL1, also a tumour suppressor protein in lung cancer (Yageta et al., 2002). Integrity of this complex is essential for cell motility regulation and loss of any one component of the complex can lead to metastasis of lung cancer.

5.2.3.5 *Mast cell survival*

Various isoforms of CADM1 are differentially involved in the homophilic adhesion of mast cells to structural cells like fibroblasts, smooth muscle cells and nerves in the human lung (Furuno et al., 2005; Ito et al., 2003a; Moiseeva et al., 2013). SP4 isoform over-expression is essential for the survival and expansion of mast cells, which is favourable for the progression of pulmonary conditions such as asthma and allergy (Moiseeva et al., 2012).

5.2.3.6 *Epidermis and wound repair*

CADM1/Necl-2 is also expressed in the hair follicles and keratinocytes in the epidermis of both human and mice. It was shown to play an important role in the skin wound repair which was significantly delayed in the knockout mice (Giangreco et al., 2009).

5.2.3.7 *Tumour suppression by different mechanisms*

There have been a few different mechanisms reported for CADM1's tumour suppression activity. In epithelial cell cancers, also known as squamous cell carcinoma (SqCC) of lungs, head & neck, oesophagus & cervix, a phenomenon known as immune surveillance mediated by CADM1 has been studied in detail. Two research groups independently reported interaction of CADM1 with CRTAM (class I-restricted T-cell-associated molecule) which is expressed only on the surface of activated CD8+ T cells and natural killer (NK) cells (Boles et al., 2005; Galibert et al., 2005). It was observed the interaction between CADM1 on dendritic cells and CRTAM on immune cells results in the cytotoxicity of NK cells and interferon γ (IFN- γ) secretion from CD8+ T cells. Confirming these finding *in vivo*, CADM1 expression was essential for NK cells to completely reject A549 tumours induced in nude mice by lymphocyte and tumour cytotoxicity (Boles et al., 2005). In addition to NK cell mediated cytotoxicity for tumour growth and proliferation, there are some evidences supporting CADM1 mediates suppression of metastasis by sensitisation of tumour cells to the CD8+ T cells (Faraji et al., 2012).

There are also evidences from *in vitro* studies in MDCK cells that CADM1 prolongs Rac-GTP activity and lowers Rho-GTP activity resulting in suppressed epithelial-mesenchymal transition (EMT), an important phenomenon for metastasis of tumour cells (Masuda et al., 2005).

Integrin- $\alpha6\beta4$ dimers together with HER2/ERBB3 drive SqCC proliferation and metastases by inducing intracellular JAK/STAT signalling pathway. Vallath *et al.* dissected the roles of CADM1 extracellular and intracellular domains in the tumour suppression activity and found interaction of its ectodomain with HER2/ERBB3 and integrin- $\alpha6\beta4$ complex to be crucial for this role. By analysing downstream signalling pathways, they showed CADM1 expression reduces cancer cell survival by attenuating phosphorylation and activity of STAT3 and hence its cell proliferation and migration (Kawano et al., 2009; Mizutani et al., 2011; Vallath et al., 2016).

5.2.4 Pathological roles of CADM1

5.2.4.1 Role in oncogenesis by loss of expression

As discussed earlier, *CADM1/TSLC1* gene was discovered as the tumour suppressor gene due to its loss of heterozygosity in many lung, pancreatic and liver cancers or cancer-driven cell lines (Kuramochi et al., 2001) but somatic mutations did not explain the loss of CADM1 expression in majority of cases (discussed in Section 5.2.4.3). Kuramochi and colleagues investigated and using bisulphite sequencing discovered the presence of 6 CpG sites in *CADM1* gene which could be putatively methylated. These sites localised in the 93bp region of *CADM1* transcription promotor sequence. They reported a strong inverse correlation between methylation of CpG sites and CADM1 expression in normal lungs, epithelial cancers and non-cancerous/cancerous cell lines. These findings suggested *CADM1* promotor methylation is the mechanism for gene inactivation and hence, loss of its tumour suppressive properties. Gradually promotor methylation status was reported to be the second hit in addition to LOH in many other epithelial cell cancers, as summarised in Table 21.

Table 21: Summary of CADM1 promotor methylation in cancers

Tumours	Percentage of tumours with CADM1 promotor methylation	Reference
NSCLC	44 %	(Kuramochi et al., 2001)
Hepatocellular cancer	29 %	(Kuramochi et al., 2001)
Pancreatic cancer	27 %	(Kuramochi et al., 2001)
Prostate cancer	32 %	(Fukuhara et al., 2002)
Oesophageal cancer	50 %	(Ito et al., 2003b)
Nasopharyngeal cancer	34 %	(Lung et al., 2004)
Cervical cancer	58 %	(Li et al., 2005)
Breast cancer	33 %	(Allinen et al., 2002)

Adapted from (Murakami, 2005)

5.2.4.2 Role in oncogenesis by over-expression

Despite CADM1's significant role in tumour suppression of epithelial cell cancers, its overexpression has also been implicated in oncogenesis of leukaemia. It was proposed on observing ectopic expression of CADM1 in primary human adult T-cell leukaemia/lymphoma (ATLL) cells. Sasaki *et al.* demonstrated that CADM1, which is not expressed in normal or activated T-cells, was over-expressed in ATLL cells and HTLV-1 infected T-cell lines. This augmented their adhesion to the vascular endothelial cells promoting infiltration of ATL cells into other organs (Murakami, 2005; Sasaki et al., 2005). Another group later showed CADM1 interacts with Tiam1 (T-lymphoma invasion and metastasis 1), a Rac-specific guanine nucleotide exchange factor via its PDZ domain (Masuda et al., 2010) which plays a role in regulation of actin cytoskeleton. This interaction induces formation of lamellipodia in ATLL cells facilitating infiltration of leukaemic cells (Nakahata and Morishita, 2012).

Atopic dermatitis (AD) is an inflammatory skin disorder characterised by eczematous skin lesions due to increased adhesion of mast cells to sensory nerve fibres in the skin. Hagiya et al. reported it is because of over 3-fold CADM1 expression in the AD-like skin lesions from hapten-induced AD mouse model compared to normal skin (Hagiya et al., 2013). They confirmed these findings *in vitro* by overexpressing CADM1 in mouse origin mast-cell line, IC2 leading to their enhanced adhesion to dorsal root ganglion neurites in co-cultures to model the neuro-immune interactions.

5.2.4.3 Mutations in CADM1

Discovery of CADM1 as TSLC1 included reporting of 3 somatic mutations one each in NSCLC, hepatocellular carcinoma (HCC) and pancreatic cancer (PaC) in a cohort of 130 tumour samples (Kuramochi et al., 2001). The mutations in CADM1 were (1) deletion of 2bp at codon 423-424 leading to loss of stop codon and substitution of 19 amino acids with 52 amino acids in NSCLC, (2) K208X in HCC and (3) M388T in PaC. No functional studies to investigate the effects of mutations were reported. These 3 samples not only harboured the somatic mutations, but also the LOH of the wild-type TSLC1 as the second hit for complete loss of TSLC1 expression in tumour samples.

In a cohort of 195 patients with autism spectrum disorder (ASD), Zhiling et al. identified two patients with heterozygous missense mutations in CADM1 (Zhiling et al., 2008). Both mutations, H246N and Y251S, lie in the third Ig-like domain and led to impaired translocation of CADM1 to the plasma membrane *in vitro* studies. This was due to increased accumulation in the endoplasmic reticulum leading to ER stress, hence more susceptibility to proteolysis. Both mutants showed reduced homophilic interaction, resulting in shorter or no dendrites formation in the neurons. These findings highlighted the significant role of CADM1 in synaptogenesis (Fujita et al., 2010).

5.2.4.4 Increased ectodomain shedding

The phenomenon of proteolytic cleavage of extracellular domain of CADM1 or other adhesion molecules is known as ectodomain shedding. This enzymatic cleavage of CADM1 by ADAM10 results in the reduction of full-length CADM1 on the lateral membranes of epithelial cells, loss of homophilic cellular adhesion and increased cell apoptosis. In a few recent studies increased ectodomain shedding of CADM1 has been described as the main reason for pathogenesis of type 2 diabetes (Inoue et al., 2014), lung emphysema (Mimae et al., 2014) and idiopathic interstitial pneumonia (Yoneshige et al., 2015). By western blotting for CADM1 in protein extracts of pathological tissues from diseased cases, researchers observed lower levels of full-length CADM1 and increased generation of α -CTFs in pancreatic insulin-secreting islet β cells

of diabetic patients, emphysematous lungs and idiopathic interstitial pneumonia lungs compared to non-diseased tissues respectively. Reduced membranous staining, more diffused cytoplasmic staining for CADM1 was supported by significantly higher TUNEL staining as a measure for apoptosis was also observed in all pathological samples.

5.2.5 *CADM1* expression in human adrenal

CADM1's role in many tissue types and cancers is well establish but not much is known about its function in adrenal gland and aldosterone synthesis. CADM1 expression was queried in the published microarray study from our lab showing transcriptome analysis of laser captured micro-dissected (LCM) zona glomerulosa and zona fasciculata of adrenal cortex of Conn's patients along with the aldosterone-producing adenomas (APAs) in the same samples (Shaikh et al., 2015; Zhou et al., 2015). CADM1 mRNA expression was significantly higher in ZG than ZF, by 2.3-fold, but no difference was observed in expression levels in ZG or APAs (Fig. 45). Another study comparing transcriptome of whole normal adrenal and APAs not from same patients reported a 2-fold higher CADM1/IGSF4 expression in the APAs, though it is not clear if this difference was statistically significant (Williams et al., 2010).

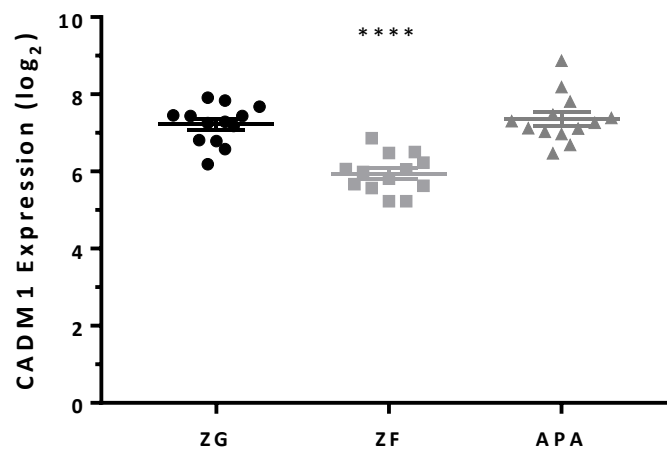


Fig. 45: Microarray expression analysis of CADM1 in adrenal cortex and APAs

Relative expression values as log₂ for CADM1 in zona glomerulosa (ZG), zona fasciculata (ZF) and aldosterone producing adenomas (APA) from same patients (n=13, One-way ANOVA, ****P<0.0001, compared to ZG). (Shaikh et al., 2015; Zhou et al., 2015).

5.2.6 Connexin-43/*GJA1* in human adrenal

Prompted by the finding of reduced cell surface expression of connexin-36 (encoded by *GJD2*) in the endocrine cells of mouse pancreas on silencing *CADM1* expression (Ito et al., 2012), I queried the expression of various gap junction proteins in adrenal cortex. This was to investigate if *CADM1* expression has a similar effect on GJIC and the regulation of aldosterone secretion from ZG in the adrenal cortex. The microarray analysis of ZG and ZF RNA samples (Shaikh et al., 2015; Zhou et al., 2015) revealed *GJA1* encoding connexin-43 to be the most predominant gap junction protein expressed (Fig. 46). *GJA1* is highly expressed in both ZG and ZF, but significantly higher (approx. 4-fold) in the ZF at mRNA level (Fig. 47). Slightly significant higher expression in matched APAs compared to ZG was also found.

In an attempt to characterise the type and role of gap junction proteins in human adrenal gland and adrenocortical tumours, Murray *et al.* reported connexin-43 to be the most predominant of the 3 types tested, connexin-43, connexin-32 (*GJB1*) and connexin-26 (*GJB2*) (Murray et al., 2000). They also reported ZF to express the highest density of gap junctions in the whole of adrenal cortex, with reduced and lowest numbers in benign and malignant adrenocortical tumours, respectively suggesting the loss of GJIC to play a role in carcinogenesis. In the same study only negligible amount of gap junctions could be detected in H295 cells (Murray et al., 2000), derived from an adrenocortical carcinoma and the parental cell line for more commonly used H295R cells with better adherent properties (Rainey et al., 1994, 2004). No connexin-43 expression was found in the adrenal medulla and pheochromocytomas (Willenberg et al., 2006).

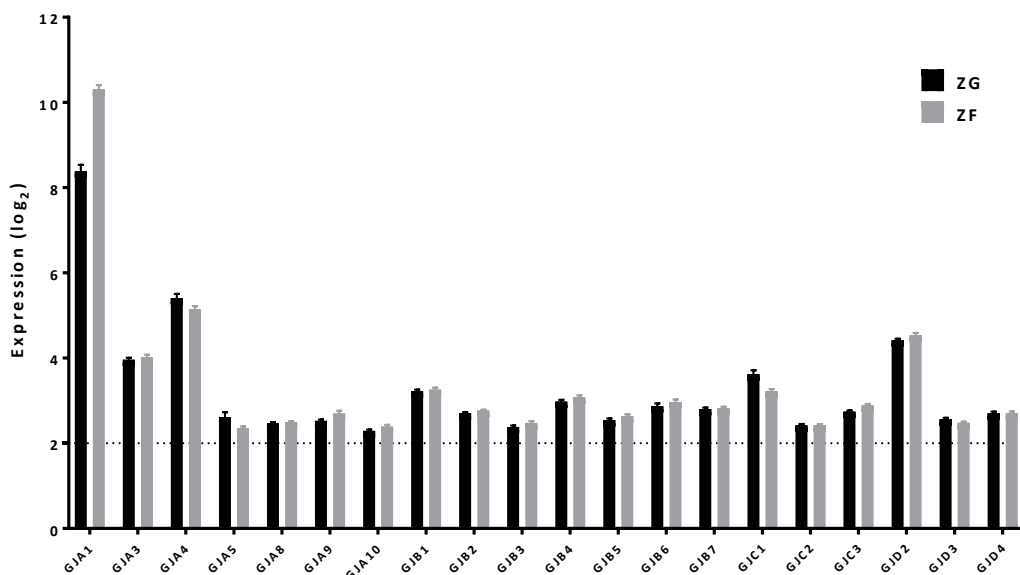


Fig. 46: Microarray expression analysis of gap junction proteins in adrenal cortex

Relative expression values as log₂ for gap junction proteins in zona glomerulosa (ZG, n=20) and zona fasciculata (ZF, n=21) of adrenal cortex of same patients. Horizontal line at y=2 represents the minimum threshold level of detection in the array. (Shaikh et al., 2015; Zhou et al., 2015).

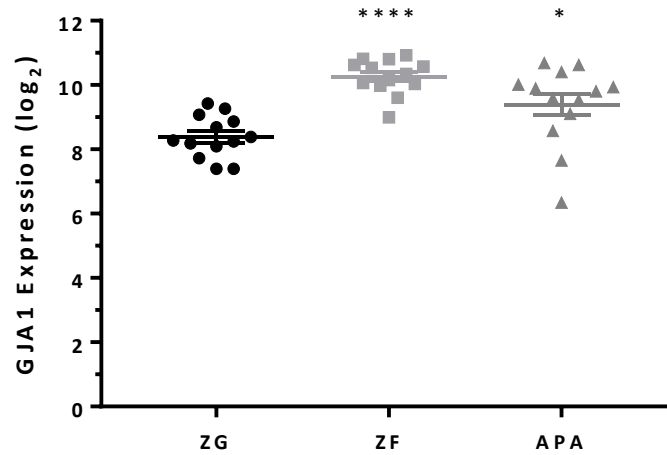


Fig. 47 Microarray expression analysis of GJA1 in adrenal cortex and APAs

Relative expression values as \log_2 for GJA1 in zona glomerulosa (ZG), zona fasciculata (ZF) and aldosterone producing adenomas (APA) from same patients (n=13, One-way ANOVA, ****P<0.0001, *P=0.0102 compared to ZG). (Shaikh et al., 2015; Zhou et al., 2015).

5.2.7 Case report of patient 184, *CADM1* mutant APA

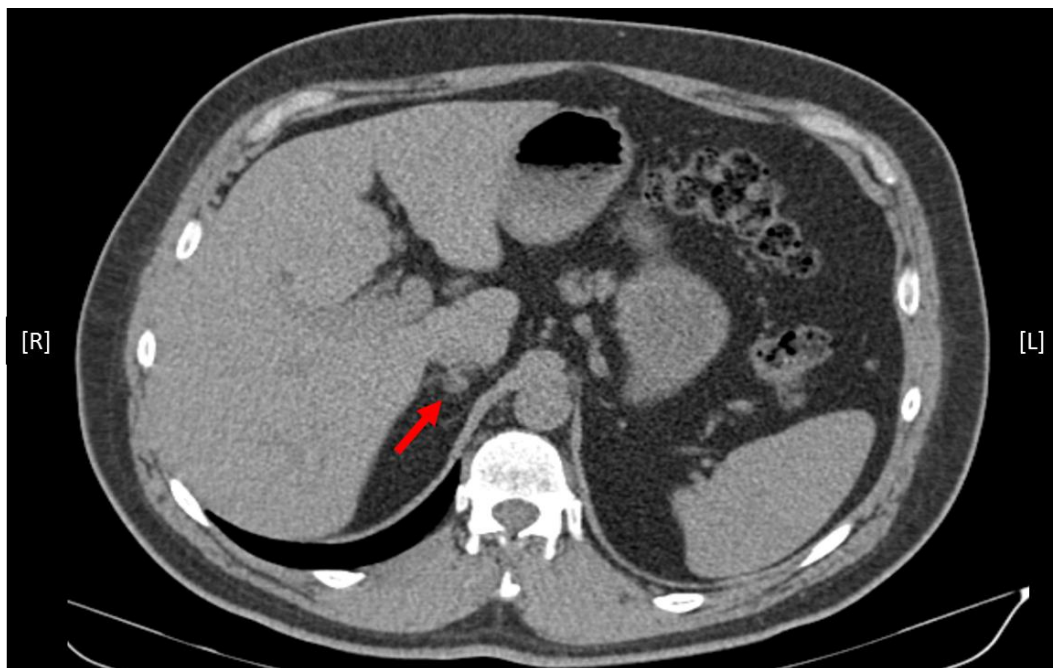
The patient with the *CADM1* mutant APA was a 46 year old male, who presented with low renin hypertension with blood pressure of 164/116 mmHg, not managed despite being on 4 anti-hypertensive drugs - bisoprolol, lacidipine and losartan/hydrochlorothiazide. Patient's aldosterone-renin-ratio (ARR) was found to be fluctuating on several occasions. Readings at two visits were 1) plasma aldosterone 147 μ mol/L and renin 11mU/L; and 2) plasma aldosterone **647** μ mol/L and renin 5mU/L.

Abdominal CT scan revealed normal left adrenal but presence of a 13mm adenoma on the right adrenal (Fig. 48). The findings were confirmed by adrenal vein sampling (AVS) for lateralisation to right adrenal with aldosterone-to-cortisol ratio of >12.4 compared to 1.9 for left adrenal vein (Table 22).

Table 22: AVS results of patient 184

Vein	Cortisol (nmol/L)	Aldosterone (μ mol/L)	Aldosterone/Cortisol (x1000)
IVC	1,701	1,803	2.5
Right adrenal	15,365	>190,000	>12.4
Left adrenal	21,436	41,070	1.9

a.



b.

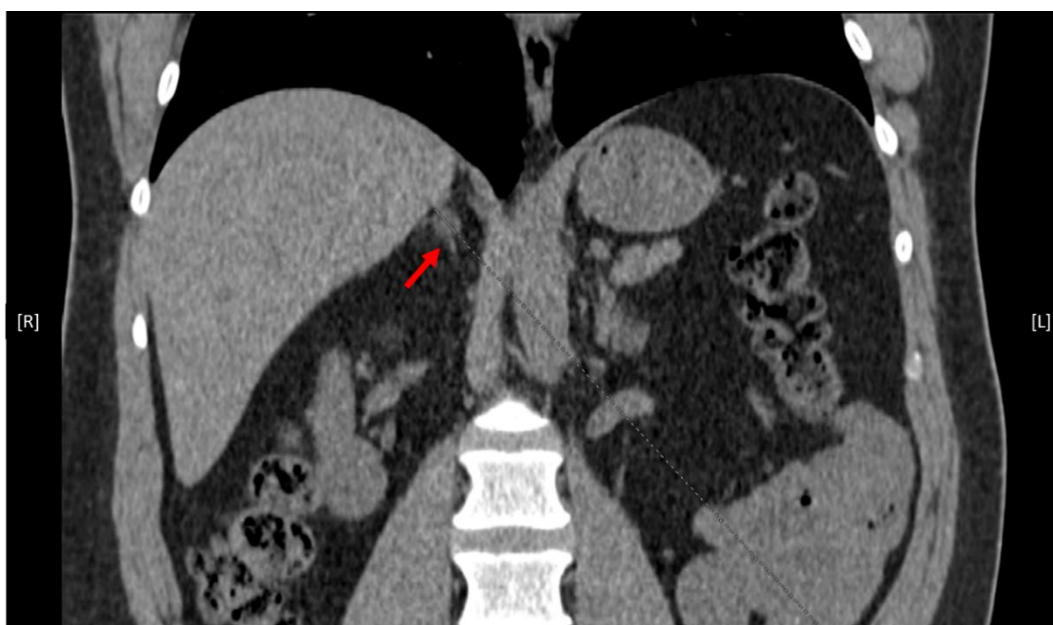


Fig. 48: Abdominal CT scan of patient 184.

a. Axial view, and b. Coronal view of patient 184's abdominal CT scans. Presence of an adenoma on right adrenal gland is indicated by red arrows.

With this successful lateralisation and diagnosis of primary aldosteronism, the patient underwent right adrenalectomy. Removed adrenal was dissected by pathologists to identify the adenoma (Fig. 49). A yellow/brown cortical nodule measuring 6x6mm was identified. Rest of the adrenal also appeared to be finely nodular with nodules less than 1mm in diameter.

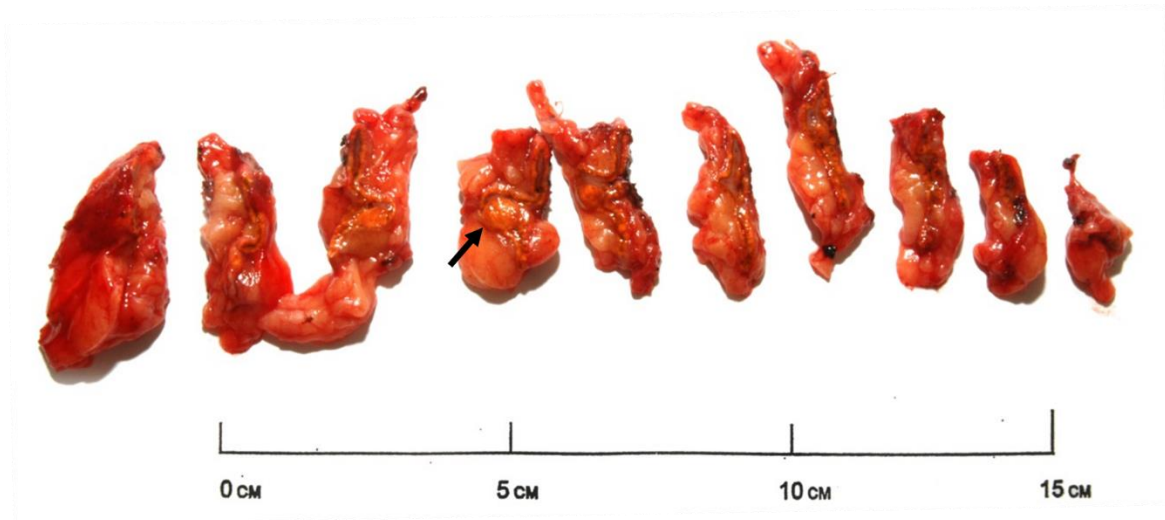


Fig. 49: Sliced right adrenal of patient 184. Adenoma is indicated by black arrow.

Haematoxylin and eosin (H&E) staining and immunohistochemistry for CYP11B1, CYP11B2 and KCNJ5 on the FFPE sections of adenoma and adjacent normal tissue was done at the Human Tissue Bank, Addenbrooke's Hospital (Fig. 50). Adenoma mostly stained positive for CYP11B2, with a few patches of cells negative. Two APCCs were also detected by positive CYP11B2 staining. The pattern was similar for KCNJ5 staining, but reciprocal for CYP11B1 as expected. On microscopic investigations, the nodule/APA appeared to contain a mix of lipid-rich (ZF-like) and lipid-depleted (ZG-like) cells with presence of spironolactone bodies in the ZG-like regions (Fig. 51). APCCs also showed many spironolactone bodies, but ZG of the adjacent normal cortex was negative for these and CYP11B2 expression.

Post adrenalectomy, the patient was completely cured of hypertension without any anti-hypertensive medications, with the reading of 121/88mmHg blood pressure, 27mU/L renin and 143pmol/L aldosterone.

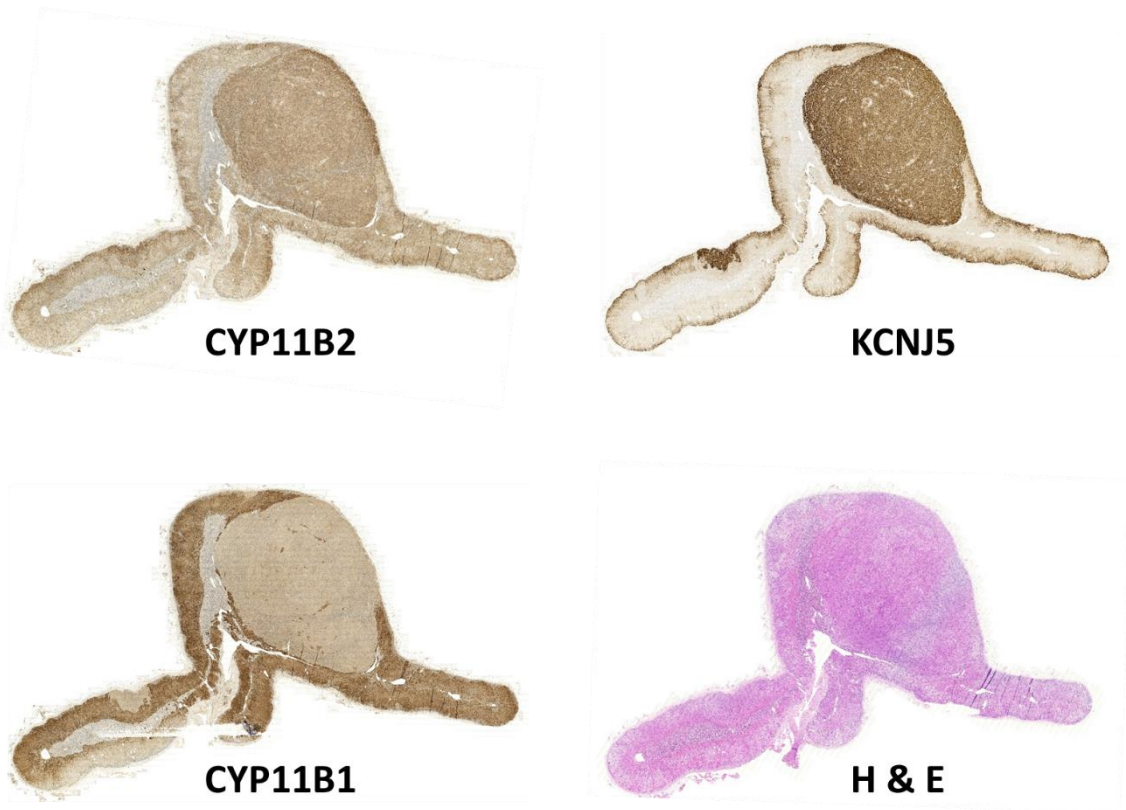
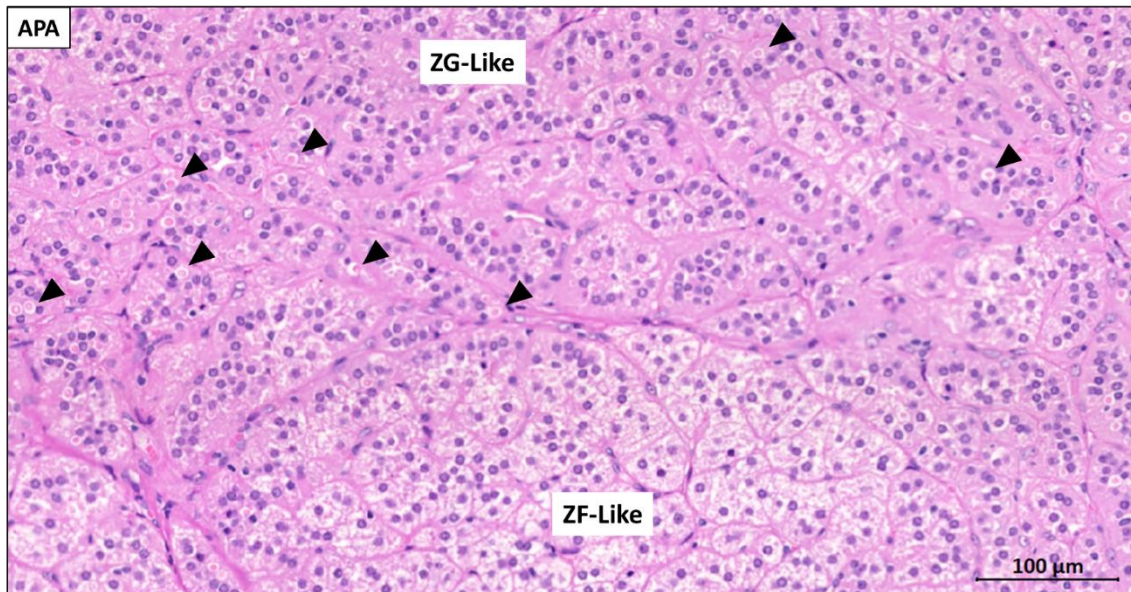


Fig. 50: Immuno-staining for CYP11B2, KCNJ5 & CYP11B1 and H&E staining for patient 184 tumour and adjacent normal adrenal.

(Courtesy: Dr Alison Marker, Department of Pathology, Addenbrooke's Hospital)

a.



b.

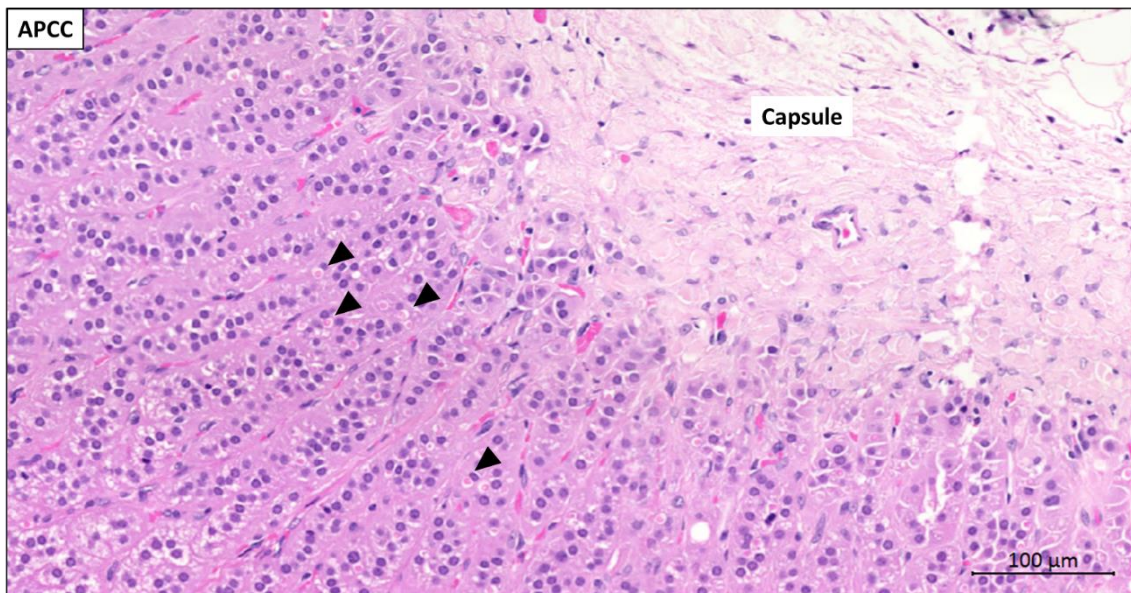


Fig. 51: H&E staining for APA and APCC in adrenal section of 184.

a. H&E staining for APA shows mix of ZG-like and ZF-like regions with spironolactone bodies in the ZG-like region (black arrow heads). b. Similar enrichment of spironolactone bodies was seen in the APCC within the adrenal cortex.

5.2.8 Aims and Hypotheses

Main aim for this part of my PhD was to investigate the role of CADM1 in aldosterone producing adrenal cells and the effect of somatic mutations we discovered.

Before investigating the effects of mutations on CADM1 function, its expression in human adrenal tissues was analysed. In vitro studies were carried out by shRNA mediated CADM1 silencing in H295R cells to investigate how endogenous CADM1 regulated aldosterone secretion.

As discussed earlier, the two somatic mutations found in CADM1 localised in the transmembrane domain of the protein changing uncharged amino acids, glycine (G) and valine (V) to negatively charged aspartate residue (D). It was hypothesised that these aspartate substitutions in the transmembrane α -helix would lead to mis-folding of the protein preventing its normal translocation to the plasma membrane. This loss of CADM1 expression on the cell surface would result in loss of cellular adhesion and interaction supporting adenoma formation and hyper aldosterone secretion.

If the mutations prove to be functional, by at least influencing (increasing) aldosterone secretion compared to the WT, this would be the first study of a cell adhesion protein in physiological aldosterone secretion in normal adrenal ZG and pathological condition of primary aldosteronism.

5.3 Materials and methods

5.3.1 RNA extraction from FFPE sections of 184NT

Due to unavailability of RNALater samples for the normal or APA tissue of patient 184, RNA was extracted from FFPE tissue blocks. 10 sections of 4 μ m thickness each for normal tissue and APA tissue block were cut and collected separately in 2ml centrifuge tubes. Sections were deparaffinised in 1ml xylene by vigorous vortexing for 10sec. Dissolved sections were centrifuged at full speed for 2min. supernatant was discarded and pellet was washed in 100% ethanol for complete removal of residual xylene. Sections were centrifuged again and supernatant discarded. Pellet was air dried at room temperature for complete evaporation of ethanol. From these deparaffinised sections RNA was extracted using RNeasy FFPE Kit (73504, Qiagen) according to manufacturer's instructions. DNase treated RNA was finally eluted in 30 μ l nuclease-free water and concentration was estimated by Nanodrop.

5.3.2 RT-PCR primers and conditions

To study CADM1 expression in H295R cells and human adrenal tissues, primers specific to CADM1 cDNA were designed and are listed in the Table 23. PCRs were setup under conditions described earlier (Section 2.1.5) using GoTaq polymerase with TD_68_60 PCR program.

Table 23: List of CADM1 RT primers.

Primer Name	Location on mRNA/cDNA	Sequence
6F	Exon 6	GCTTGAGTTAACATGTGAAGCCATCG
7-8F	Boundary of exon 7 & 8	GCTGTATGTATACGATCCCCCACC
9-10R	Boundary of exon 9 & 10	AGTGAAGTATGTACCTTTATGTCTGGC
Int7R	Intron after exon 7	CCAACTGGTTTTTGATTTTCAACTTGACC
9F	Exon 9	ATCCCGAGCAGGTGAAGAAGG

5.3.3 CADM1 cloning and mutagenesis

Full length cDNA sequence for CADM1 open reading frame was amplified from H295R cDNA as template using Q5 DNA polymerase. 5' primer contained CACC sequence followed by Flag-tag sequence upstream of CADM1 start codon and 3' primer contained Myc-tag sequence downstream of last coding amino acid of CADM1 (Table 24). Amplified product was cloned into the gateway cloning entry vector, pENTR using directional TOPO cloning technology (pENTR™/D-TOPO™ Cloning Kit, K240020, Invitrogen) according to manufacturer's instructions.

Table 24: CADM1 cloning primers.

CADM1 cloning primer	Primer sequence (5' → 3')
Topo-Flag-CADM1-F	CACCATGGATTACAAGGATGACGACGATAAGGGATCCATGGCGAGTGTAGTGCTG
Myc-CADM1-R	GCATGAATTCCTACAGATCTTCTTCGCTAATCAGTTTCTGTTTCGATGAAGTACTCTTCTTTCTTCG

Topo ligation reaction was transformed into TOP10 chemically competent E.coli and positive clones were selected on LB agar plates containing kanamycin. pENTR clones for CADM1 were minipreped and sequence verified. All clones corresponded to SP4 isoform of CADM1 which was then used as template to prepare SP1 isoform by a mutagenesis reaction using Q5 site-directed mutagenesis kit (NEB). Mutagenesis primers were designed using NEBaseChanger online tool (NEB) to insert 33bp sequence corresponding to exon 9A (Table 25). Both CADM1-SP4/SP1-pENTR plasmids were used to make the 2 mutant constructs for G379D and V380D, following the same procedure. Finally WT and 2 mutant constructs for SP4 and SP1 CADM1 isoforms in pENTR vector were ready for gateway cloning reaction.

Table 25: CADM1 mutagenesis primers

Mutagenesis primer	Primer Sequence
Ins-Ex9A-F	gaaccagcagttcacgATTCCCGAGCAGGTGAAG
Ins-Ex9A-R	tgtcgtcgcggtgtgtCTGTGATGATGGTAAGGATG
G379D-F	GTGATCGGTGaCGTCGTGGCG
G379D-R	GGCATGATCCACTGCCCTG
V380D-F	ATCGGTGGCGaCGTGGCGGTG
V380D-R	CACGGCATGATCCACTGCC

pENTR constructs were used for transfer of cloned cDNAs into pLOC vector in a *attL/attR* recombination reaction using LR Clonase II enzyme mix (11791020, Invitrogen) according to manufacturer's instructions. Recombined plasmids reaction was transformed into Stable competent cells (NEB) and selected on LB agar plates containing ampicillin. Positive clones were minipreped and sequence verified. Clones with correct sequences were maxipreped and used for preparing lentivirus by transfection of HEK293T cells. The PuroR-pLOC construct described earlier was used as the transfection control empty vector (EV) in this study.

5.3.4 CADM1 shRNA cloning

21bp long shRNA sequences for scrambled (non-targeting control) or specific to CADM1 (Fig. 52) were inserted in the pLVTH vector using Q5 site-directed mutagenesis kit (NEB).

Mutagenesis primers were designed using NEBaseChanger online tool (NEB) to insert shRNA, consisting of sense, loop and antisense sequences into the vector (Table 26).



Fig. 52: Sequences for scrambled (a) and CADM1 (b) shRNAs in pLVTH

Table 26: CADM1 shRNA cloning primers

Primer Name	Primer sequence
scrambled-F	tccaacgaggttattacgtaaggtattTTTTGGAAAAGCTTATCGATAC
scrambled-R	tccaacgaggttattacgtaaggtatccGGGGATCTGTGGTCTCAT
shCADM1-F	tccaattgtagaggataagtcacatctgtTTTTGGAAAAGCTTATCGATAC
shCADM1-R	tccaattgtagaggataagtcacatctgccGGGGATCTGTGGTCTCAT

Mutagenesis KLD reaction was used to transform NEB Stable E.coli and selected on LB agar plates containing ampicillin. Positive clones were miniprep and sequence verified. Clones with correct sequences were maxiprep and used for preparing lentivirus by transfection of HEK293T cells.

5.3.5 Cell culture media concentration

In the experiments to study CADM1 ectodomain shedding in H295R, cell culture supernatants were western blotted for α -NTF levels using anti-CADM1-NT (3E1) antibody. Transduced cells were cultured in phenol-red and serum free DMEM F-12/HAM media for 24hr. Conditioned media was collected and concentrated using Amicon Ultra-0.5 Centrifugal Filter Units with Ultracel-30 membrane (Millipore). Filtration units containing 500 μ l supernatants were centrifuged at 14,000xg for 10min at 4°C to concentrate samples by a factor of 22. Concentrated supernatants were collected and diluted with 4X Bolt™ LDS Sample Buffer (B0007, ThermoFisher) for gel electrophoresis and western blotting.

5.3.6 Western blotting

According to the experiment and availability of total protein after protein assay, 10-40µg cell lysate protein or 15-20µl concentrated cell culture media was diluted with the 4X Bolt™ LDS Sample Buffer (B0007, ThermoFisher) and 10X Bolt® Sample Reducing Agent (B0009, ThermoFisher). Samples were incubated at 37°C for 5 min before running on Bolt® 10% Bis-Tris Plus Gels (ThermoFisher) in Bolt® MES SDS Running Buffer at 165V for 30-35min at room temperature.

For western blotting, gels were removed from gel-casting plates, equilibrated in the Tris-Glycine transfer buffer containing 10% methanol and 0.05% SDS for 10min before setting up the transfer stacks. PVDF-FL membrane with no auto-fluorescence were activated in 100% methanol for 15sec and equilibrated in the transfer buffer for 5min. Protein transfer was set up at 60V for 1hr in cold room.

PVDF membranes with transferred proteins were blocked in 5% fat-free milk-TBS solution for 1hr at room temperature and incubated with primary antibodies diluted in 5% milk-TBST (with 0.1% Triton X-100) overnight at 4°C. Two primary antibodies from different species (mouse, rabbit or chicken) were used at the same time at this step as species-specific secondary antibodies conjugated with either IRDye 680RD or IRDye 800CW fluorophores were used for detection by Odyssey scanner, Li-Cor. Membranes incubated with primary antibodies were washed in TBST 3 times for 5min each at room temperature and incubated with secondary antibodies diluted in 5% milk-TBST for 1hr. Membranes were washed again in TBST for 30min and rinsed in deionised water before scanning for protein detection using 700nm and 800nm channels in the Odyssey scanner. Resulting images were analysed with ImageStudio Lite software (Li-Cor).

5.4 Results

5.4.1 *CADM1* transcripts in H295R cells, human adrenal and APAs

Expression of different *CADM1* transcripts was tested in H295R cells followed by semi-quantitative analysis in APAs and adjacent normal adrenals by RT-PCRs. Relative expression levels of total *CADM1* were also tested in paired normal and APA samples by qPCRs. Finally *CADM1* protein localisation in the FFPE section of normal adrenal and APA samples was studied using immunohistochemistry.

5.4.1.1 *CADM1* expression in H295R cells

CADM1 primers specific for targeted regions in the cDNA sequence were used for PCR and product sizes could differentiate between alternatively spliced transcripts' expression in H295R cells. It was found that *CADM1* expression was easily detectable in cDNA of H295R cells (Fig. 53). Primer pair, 6F + 9-10R amplified products corresponding to transcripts SP4 and SP1 (Lane 1), but most predominantly SP4 that translates into an isoform 442 amino acids in length. This expression pattern was confirmed by another pair of primers, 7-8F + 9-10R (Lane 3) with shorter products for all isoforms. Transcript SP1 translates into a 453 amino acid long isoform. In addition to these two membrane localised isoforms of *CADM1*, positive amplification in Lane 2 with primer pair 6F + Int7R (where Int7R lies in the intronic sequence between exon 7 and 8) confirmed the expression of soluble/secreted isoform SP5 of *CADM1*.

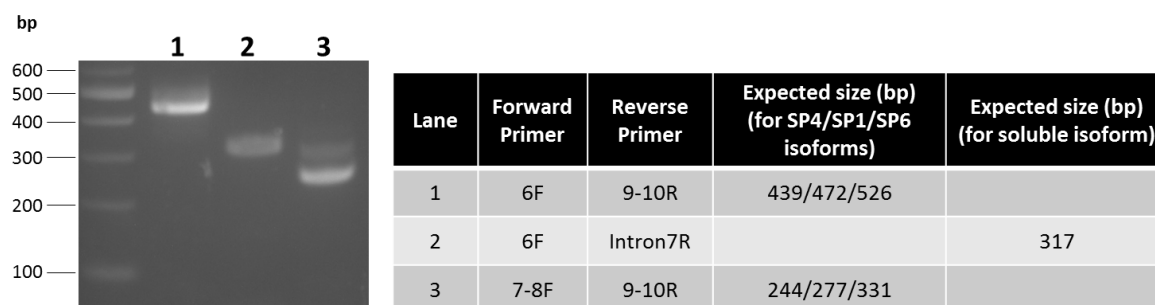


Fig. 53: RT-PCR for *CADM1* expression in H295R cells.

5.4.1.2 *CADM1* expression in human adrenal and APAs

RT-PCRs for paired normal (N) and APA (T) cDNA samples were performed using primers 7-8F + 9-10R. This was to verify if expression pattern of *CADM1* isoforms in these samples follows that in H295R cells. SP4 isoform was found to be the most predominant of all membrane localised *CADM1* isoforms in normal adrenals and APAs as well. All APAs used in this analysis had the somatic mutations in *KCNJ5*, *CACNA1D* or *CTNNB1* as indicated in the Fig. 54.

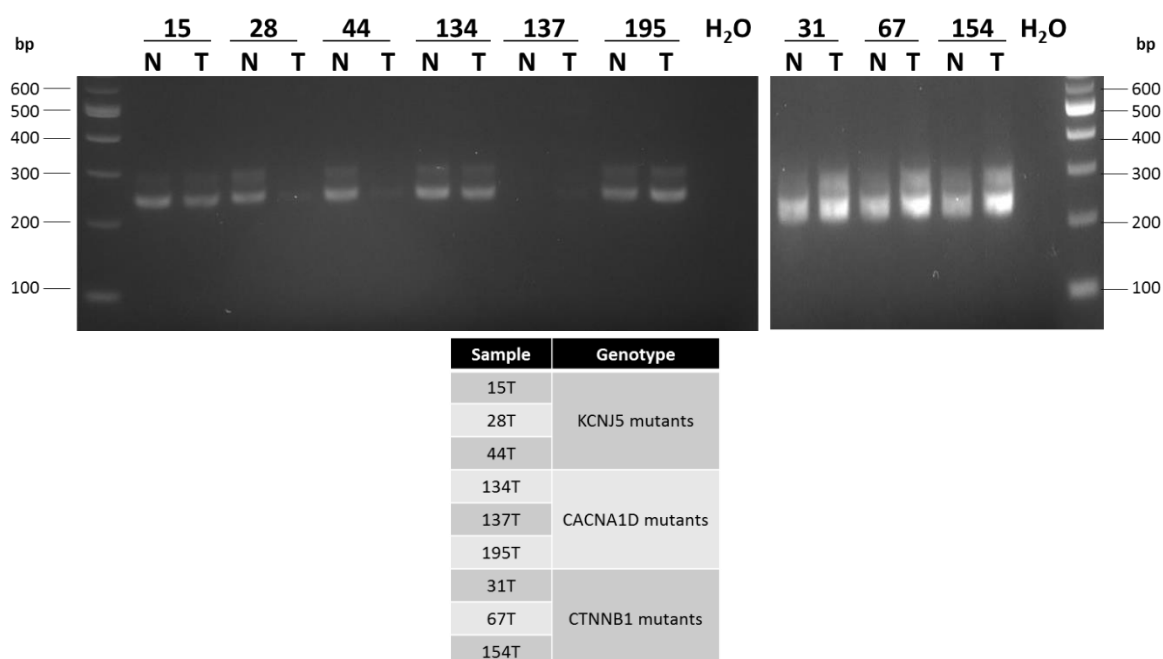


Fig. 54: RT-PCR for CADM1 expression in human normal adrenal and APA samples.

RT-PCR for CADM1 expression using primers 7-8F + 9-10R to amplify membrane localised CADM1 isoforms. Paired normal (N) and APA (T) cDNAs were used as template for PCRs. Patient IDs are indicated above each pair and the mutant gene for each APA is shown in the table.

5.4.2 CADM1 protein localisation in human adrenal and APAs

FFPE sections of human adrenal of patients who underwent adrenalectomy because of diagnosis of pheochromocytoma or primary aldosteronism due to APAs were immunostained using antibodies against CADM1 C-terminal or CYP11B2. Serial sections were stained for 2 proteins to minimise the histological and structure variations.

Typically not much CYP11B2 staining was observed in the ZG, except for intense staining in random small clusters of cells that have been previously defined as aldosterone producing cell clusters, APCCs. As expected all APAs tested stained positively for CYP11B2 with some patches of cells low in expression. Interestingly, strong CADM1 staining on plasma membrane was observed throughout ZG and APCCs (Fig. 55, Fig. 56). No differences were observed in CADM1 staining patterns in normal adrenals next to pheochromocytoma or APAs. ZF and adrenal medulla also expressed high levels of CADM1.

Within APAs CADM1 expression followed the expression pattern of CYP11B2. Small patches of cells negative for CYP11B2 also expressed lower levels of CADM1 (Fig. 57). No differences were found in the pattern of CADM1 expression in patient 184's APA and adjacent normal tissue (Fig. 58).

5.4.2.1 Normal adrenal and APCCs

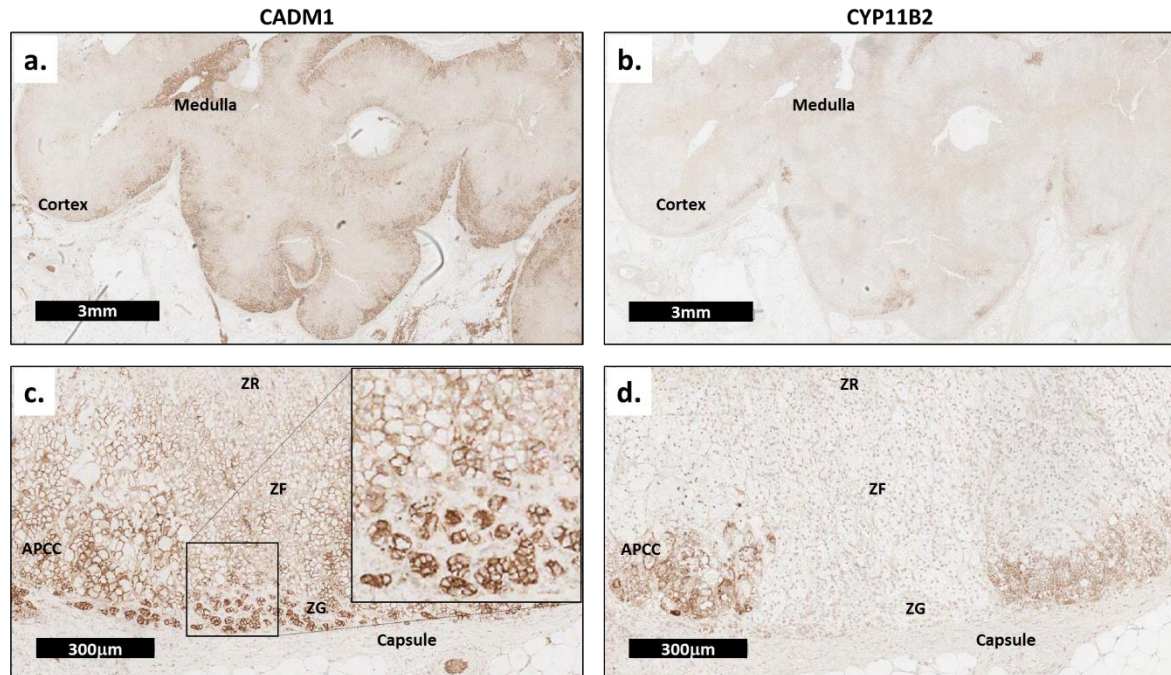


Fig. 55: Immunohistochemistry for CADM1 and CYP11B2 in normal adrenal gland.

Representative image for serial FFPE sections of normal adrenal gland of patients with pheochromocytoma stained with anti-CADM1 (a & c) and anti-CYP11B2 (b & d) antibodies (n=3). Low magnification images for both antibodies (a & b) show overall staining pattern in adrenal cortex and medulla. Higher power images (c & d) show staining pattern in ZG, ZF, ZR and APCCs (aldosterone-producing cell clusters) within the adrenal cortex. Scale bars are also shown.

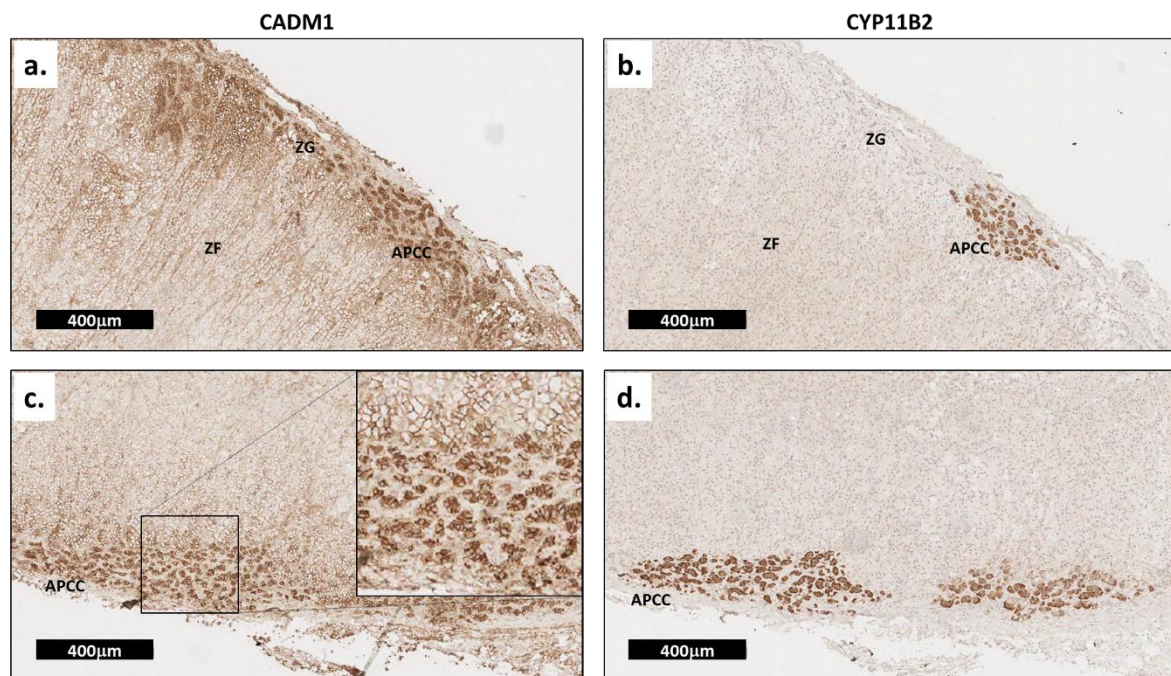


Fig. 56: Immunohistochemistry for CADM1 and CYP11B2 in adrenal cortex next to APA.

Representative image for serial FFPE sections of normal adrenal gland of patients with APA stained with anti-CADM1 (a & c) and anti-CYP11B2 (b & d) antibodies (n=5). Scale bars are also shown.

5.4.2.2 APAs

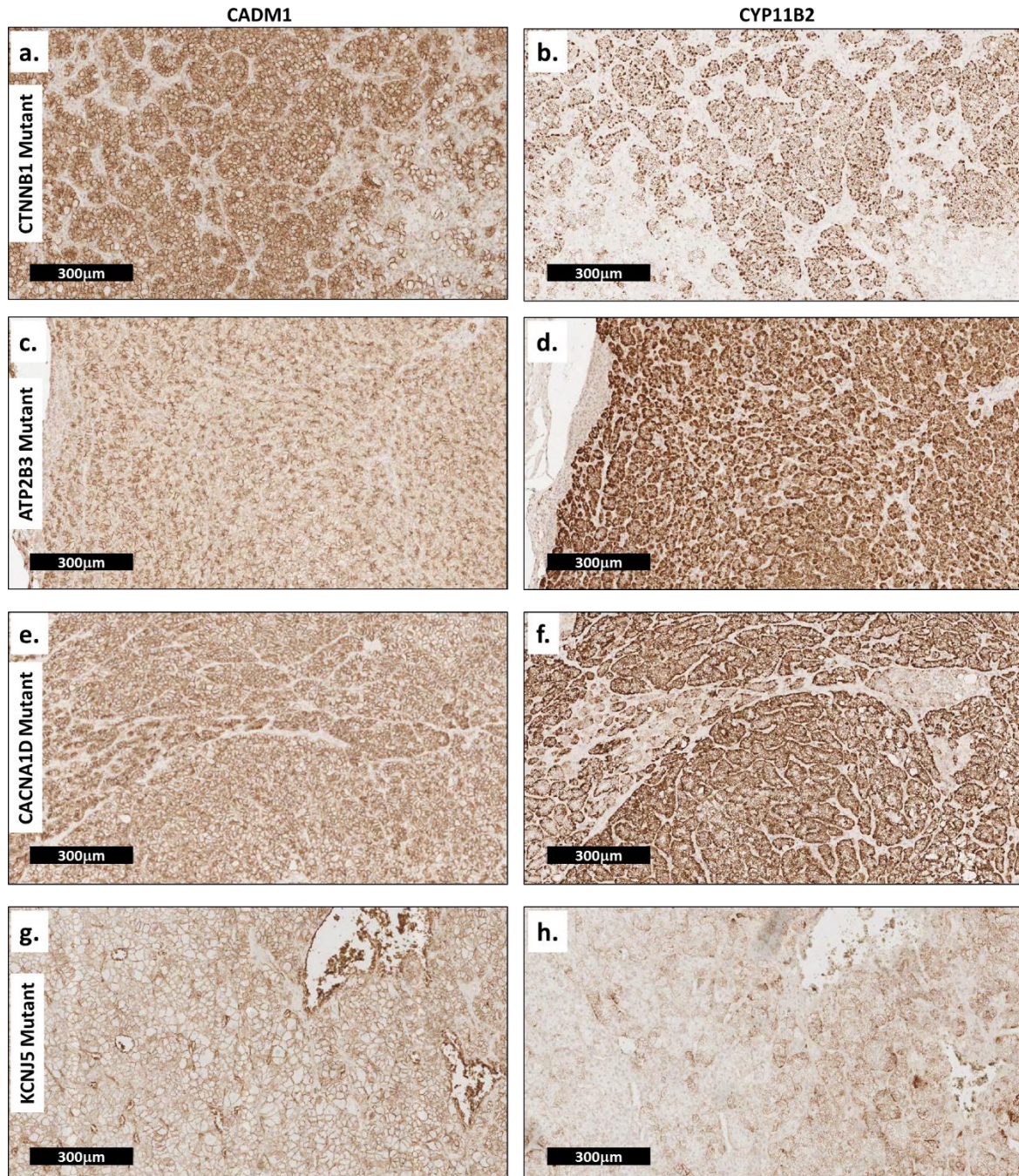


Fig. 57: Immunohistochemistry for CADM1 and CYP11B2 in APAs.

Representative image for serial FFPE sections of APAs with indicated mutations stained with anti-CADM1 (a, c, e & g) and anti-CYP11B2 (b, d, f & h) antibodies (n=5).

5.4.2.3 Patient 184

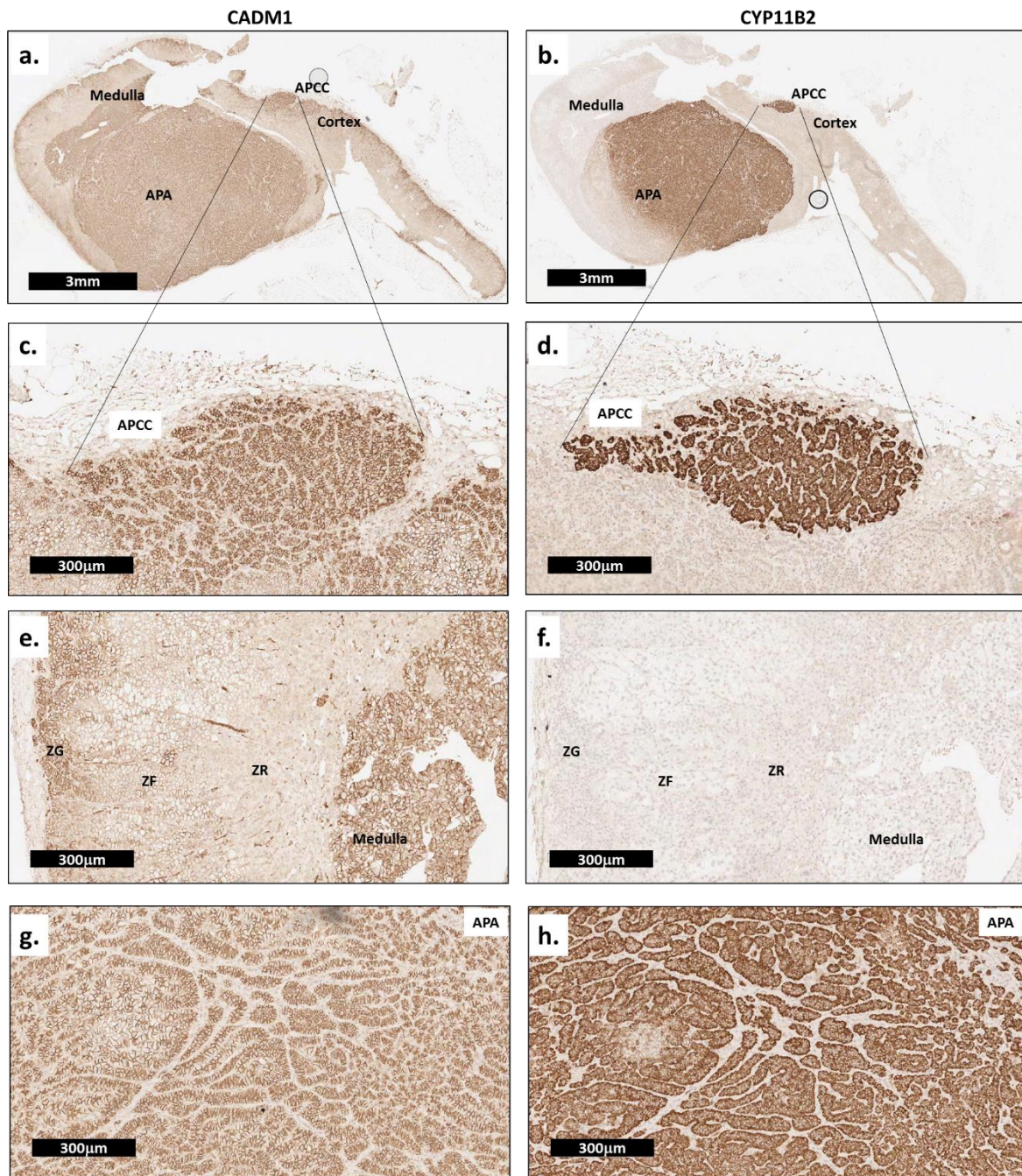


Fig. 58: Immunohistochemistry for CADM1 and CYP11B2 in patient 184's adrenal sections.

Serial FFPE sections of CADM1 mutant APA and adjacent normal adrenal stained with anti-CADM1 (a, c, e & g) and anti-CYP11B2 (b, d, f & h) antibodies. Low magnification images for both antibodies (a & b) show overall staining pattern. Higher power images (c - h) show regions ZG, ZF, ZR, medulla (e & f); APCC (c & d) and the APA (g & h). Scale bars are also shown.

5.4.3 Confirmation of mutant allele expression in 184T cDNA

cDNA from APA sample of patient 184 was sequenced to confirm the expression of mutant allele of CADM1 at the mRNA level. RNA samples available for patient 184 adjacent normal adrenal and APA were sourced from FFPE sections. CADM1 cDNA was amplified using primers 9F and 9-10R (Section 5.3.2) targeting only 146bp amplicon, small enough to be amplified given the quality of cDNA from these samples. Sanger sequencing revealed mutant allele (c. 1139 T>A, p. V380D) expression in the APA sample (Fig. 59). Though it is not a quantitative measure, but height of peaks for the wild-type and mutant alleles at cDNA position 1139 appeared approximately in similar proportion to that in the APA gDNA sample (Fig. 41). This confirms that the mutation does not result in gene deletion or silencing, which rules out the loss of tumour suppressor role of CADM1 to be the cause of APA formation.

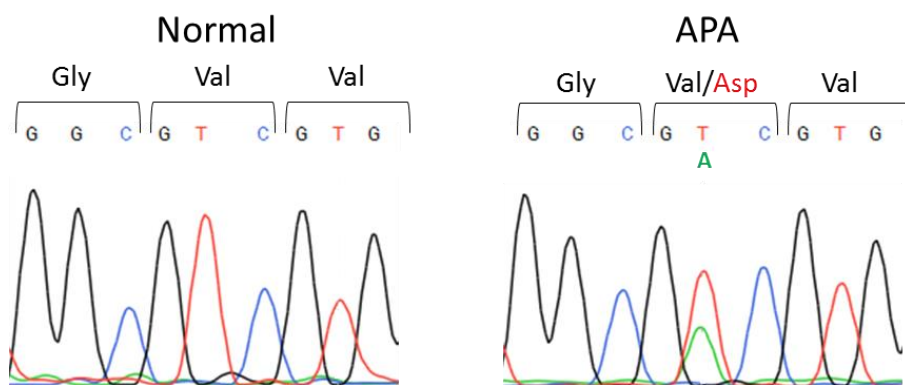


Fig. 59: Chromatograms for CADM1 sequencing in the cDNA of patient 184 normal adrenal and APA samples showing expression of mutant allele, c. 1139 T>A.

5.4.4 Mutant CADM1 proteins are processed differentially by proteases

H295R cells transduced with equal transducing units of lentivirus for wild-type or mutant CADM1 in two isoforms, SP4 and SP1 were analysed for protein expression and susceptibility to processing by endogenous proteases of α -, β - or γ -secretase families. Whole cell lysates and cell culture media were western blotted using specific antibodies towards intracellular C-terminal and extracellular Ig-domains in N-terminal of CADM1. In addition to CADM1 antibodies, cell lysates were also immuno-blotted with the anti-Myc antibody as all constructs were tagged with Myc sequence on the C-terminal of CADM1 coding sequence.

Myc antibody detected WT and both mutant CADM1 proteins in the two isoforms tested. Full-length glycosylated and non-glycosylated forms of the protein were detected across all samples, but no further processed fragments were detected. Despite equal transduction efficiency in all samples, as revealed by equal tGFP expression, total CADM1-V380D expression was relatively lower as compared to CADM1-WT (Fig. 60a). No such dramatic effect was seen for other mutant, CADM1-G379D. Due to high endogenous CADM1 expression in H295R cells, the over-expression of CADM1-WT and mutant proteins was not as obvious when blotted with the CADM1-CT antibody, except for the α -C terminal fragment (α -CTF) that is produced by the action of γ -secretase (Fig. 60b). H295R cells overexpressing CADM1-WT contained α -CTF as two bands (doublet) compared to that from the endogenous CADM1. In both isoforms of CADM1, bigger of the two bands in α -CTF from CADM1-G379D seemed slightly smaller but at higher levels than that from CADM1-WT. α -CTF from CADM1-V380D seemed to be present only as a single band similar to that produced by endogenous CADM1.

Due to lower levels of CADM1-V380D protein seen in the cell lysates it was tested if this was due to increased ectodomain shedding of V380D mutant by the proteases producing more α -NTF in the supernatant. Media collected from the transduced cells was concentrated and blotted for detection of α -NTF using CADM1-NT (3E1) antibody. No more ectodomain shedding was found in the CADM1-G379D than that in CADM1-WT (Fig. 60c), but the levels of α -NTF in CADM1-V380D expressing cells were much lower than the CADM1-WT and comparable to the endogenous α -NTF as seen in the empty vector lane. It was concluded even though CADM1-V380D protein was glycosylated and probably translocates to the plasma membrane but not as efficiently as the WT or the G379D mutant protein and was less stable and degraded at higher rate.

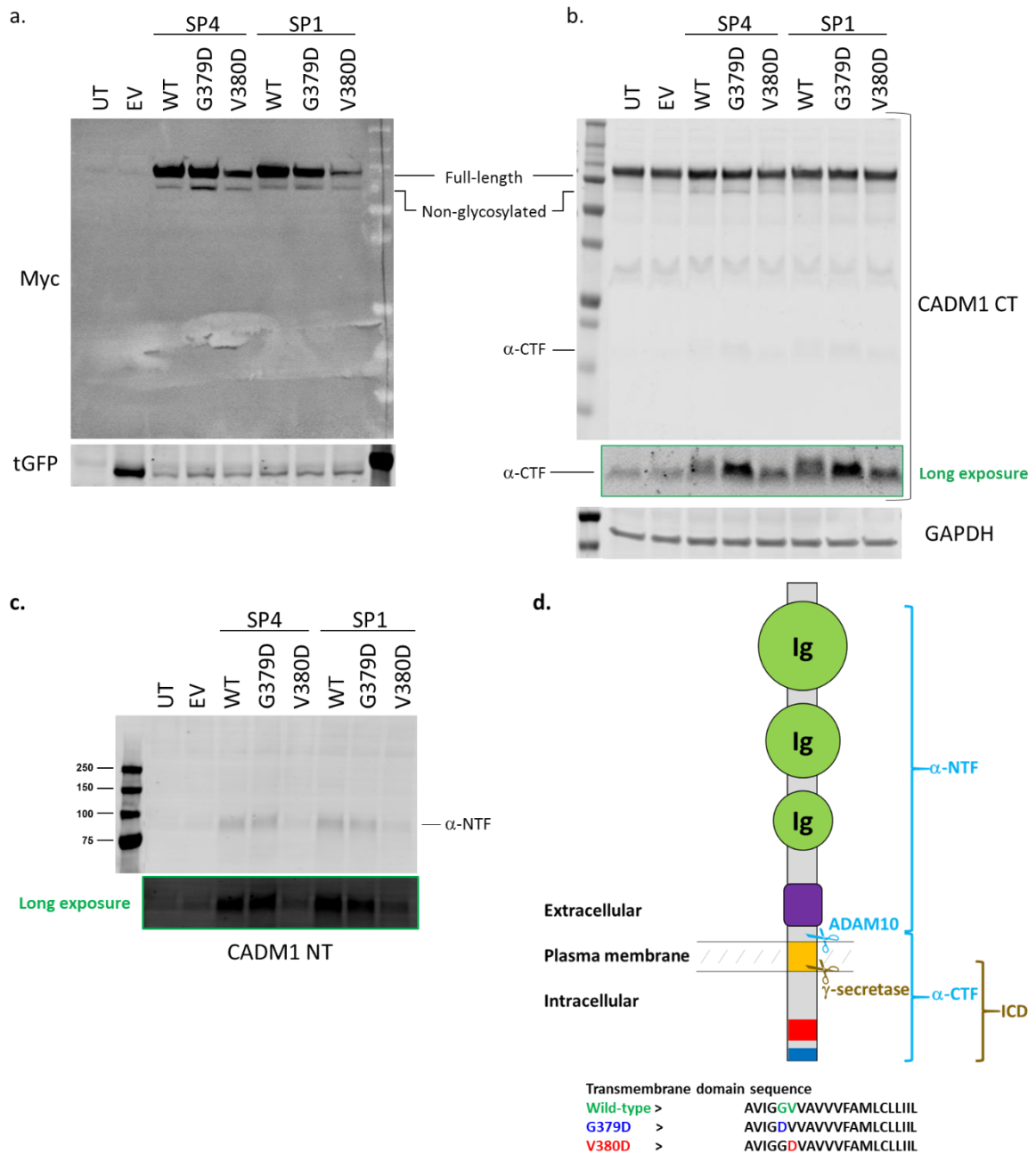


Fig. 60: Western blot analysis for expression of CADM1 WT or mutants in transduced H295R cells. Immunoblot for whole cell-lysate from transduced H295R cells using **a.** anti-Myc and anti-tGFP antibodies; and **b.** anti-CADM1 CT and anti-GAPDH antibodies. **c.** Immunoblot for concentrated cell-culture supernatant using anti-CADM1 NT antibody (n=3). **d.** Schematic representation of CADM1 protein structure showing various domains and cleavage fragments generated by action of proteases, ADAM10 and γ -secretase. UT: Un-transduced, EV: Empty-vector, WT: Wild-Type, NTF: N-terminal fragment, CTF: C-terminal fragment, ICD: intracellular domain. Transmembrane domain amino acid sequence for WT and mutants, G379D and V380D is also shown.

5.4.5 Mutant CADM1 upregulates aldosterone synthesis

5.4.5.1 CYP11B2 mRNA & aldosterone secretion

H295R cells transduced with lentivirus for CADM1-WT or mutants in the two isoforms were tested for aldosterone synthase, CYP11B2 expression and aldosterone secretion. 72hrs post-transduction, cells were starved overnight in serum-free media and replaced with fresh serum-free media for another 24hrs. This conditioned media was analysed for aldosterone levels and cells were harvested for RNA extraction and qPCRs for CADM1 and CYP11B2.

CADM1 qPCR data revealed comparable levels of transduction for all constructs and was about 10-fold higher CADM1 expression compared to un-transduced and empty-vector controls (Fig. 61a). Overexpression of CADM1-WT led to no changes in CYP11B2 mRNA or aldosterone secretion compared to the controls (Fig. 61b). Interestingly both mutants, CADM1-G379D and CADM1-V380D upregulated CYP11B2 expression by approximately 12-folds and 15-22 folds, respectively, compared to controls and CADM1-WT. The corresponding increase in aldosterone secretion ranged from 2.6-fold for CADM1-G379D to 3.7-fold for CADM1-V380D (Fig. 61c). No significant differences were found between the CADM1 isoforms SP4 and SP1 for any of the WT or mutant constructs.

5.4.5.2 Immunocytochemistry for CADM1 and CYP11B2

The significant upregulation of CYP11B2 mRNA in the H295R cells expressing mutant CADM1 was investigated by confocal imaging in order to establish the relation between CADM1 genotype and CYP11B2 expression at cellular level. This experiment would also show if there is any direct correlation between CYP11B2 expression and higher CADM1-WT expression as observed in ZG cells of adrenal cortex and APCCs (Section 5.4.1). H295R cells grown on coverslips were transduced with lentivirus for CADM1-WT or mutants, which were fixed and immuno-stained with anti-CYP11B2 and anti-CADM1-NT (3E1) antibodies 72hrs after transduction.

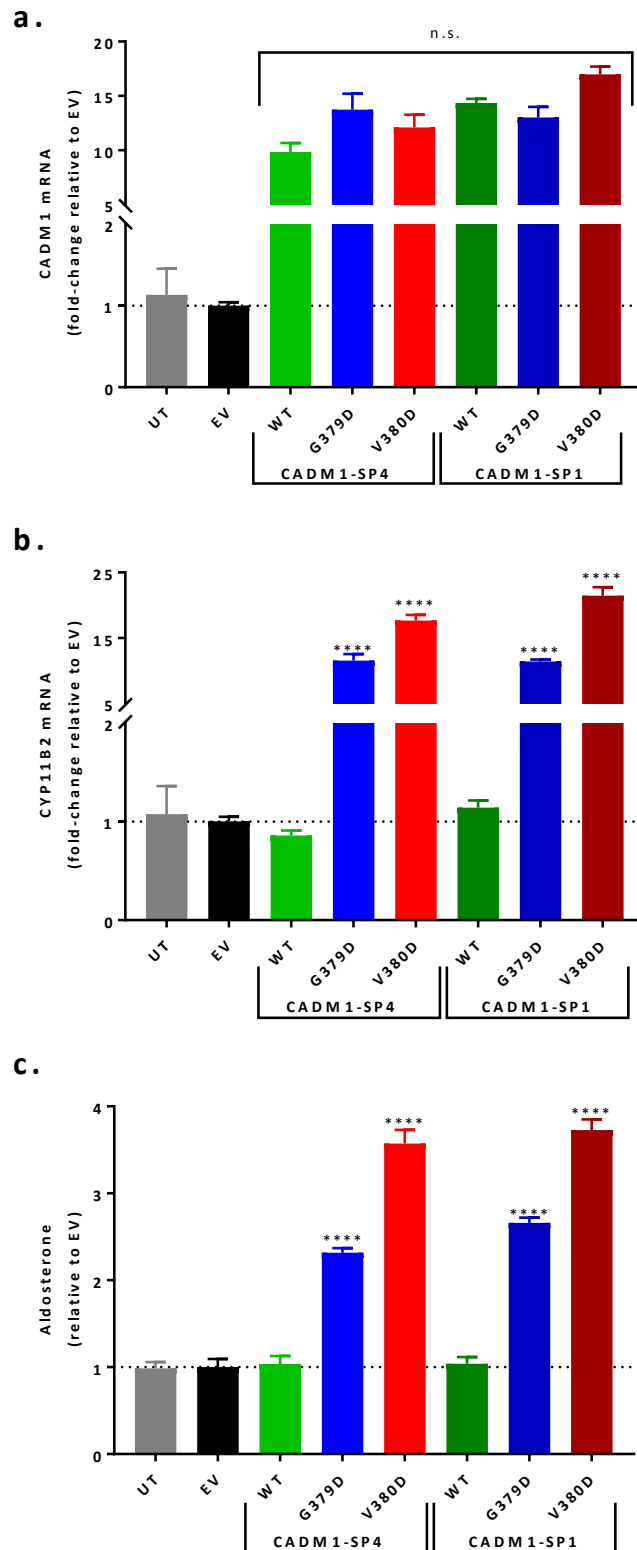


Fig. 61: Mutant CADM1 upregulates CYP11B2 mRNA expression and aldosterone secretion.
a. Estimation of relative CADM1 mRNA expression to show equal transduction efficiency for all constructs **b.** Relative CYP11B2 mRNA expression in the transduced cells. **c.** Corresponding aldosterone assay (n=4 in quadruplicate). (One-way ANOVA, ****P<0.0001, compared to EV). Error bars represent s.e.m.

Transduced cells were distinguished from the un-transduced cells by turbo-GFP (tGFP) expression which was mainly in the nuclei. This was due to the presence of nuclear localisation signal (NLS) sequence present on 5' end of tGFP sequence in the pLOC vectors. Overexpression of CADM1 constructs was confirmed by brighter staining with anti-CADM1-NT antibody in the tGFP positive cells compared to the adjoining untransduced cells (Fig. 62). In accordance with the qPCR results for CYP11B2 (Fig. 61b), immuno-staining with anti-CYP11B2 antibody did not give any positive signal above background in the cells expressing only CADM1-WT, whether endogenous or overexpressing. Notably, cells expressing either of the mutant CADM1 at moderate levels showed upregulated CYP11B2 expression by higher staining confirming the qPCR mRNA results (Fig. 62). Interestingly, this upregulated CYP11B2 staining was only observed in the cells expressing moderate levels of mutant CADM1 and not in those with very high levels of mutant CADM1 as indicated by intense nuclear tGFP levels.

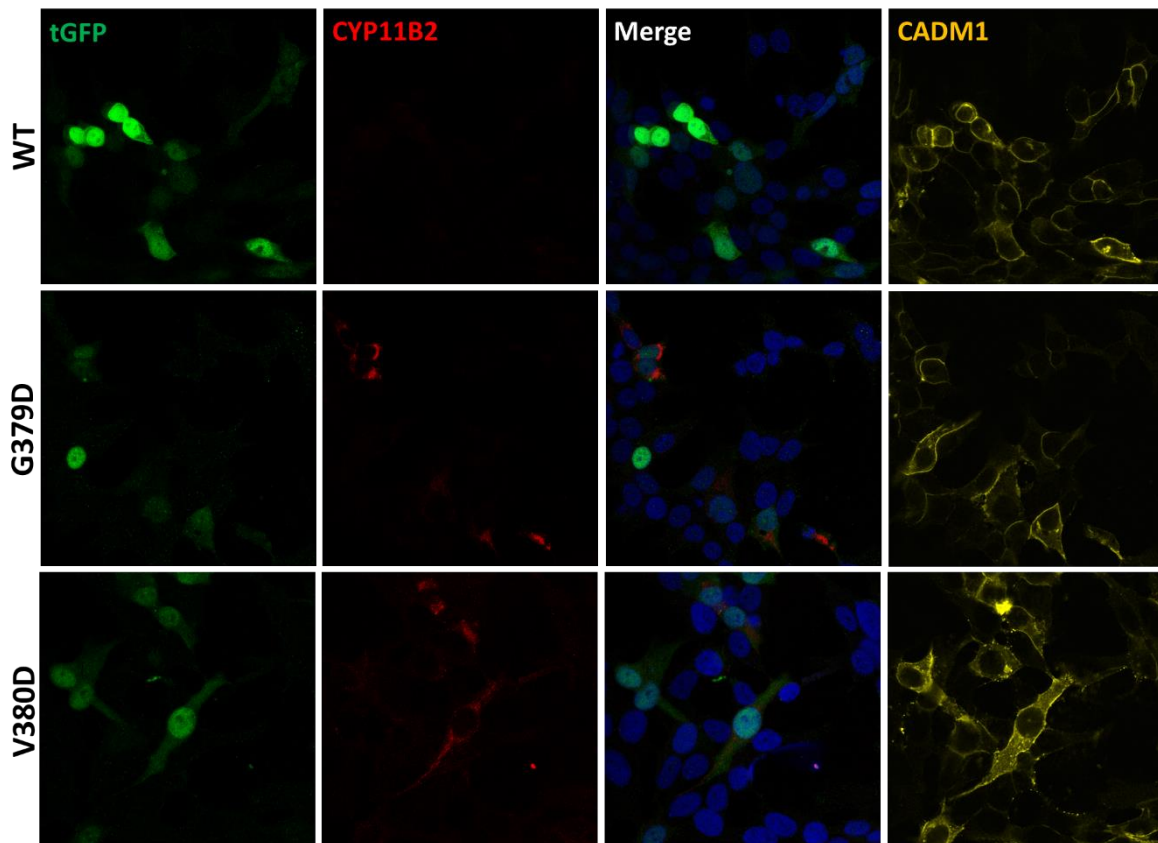


Fig. 62: Confocal images for H295R cells transduced with CADM1-SP4 WT or mutants, G379D or V380D.

Transduced H295R cells were fixed and immuno-stained with anti-tGFP (green), anti-CYP11B2 (red) and anti-CADM1-NT (3E1) (yellow) antibodies. Nuclei were stained with DAPI (blue). Merge of transduced cells and CYP11B2 expression is shown to represent the correlation between mutant CADM1 expression and CYP11B2 upregulation in the transduced cells.

5.4.5.3 Angiotensin II stimulation on *CADM1* mutants

Angiotensin II stimulation effects were studied in the H295R cells expressing WT or mutant *CADM1* to test if the presence of mutant *CADM1* has any direct effect on the angiotensin II stimulation pathway of aldosterone secretion. Comparison of fold-change increase in *CYP11B2* mRNA and aldosterone secretion in the presence of angiotensin II revealed no significant differences between the untransduced, transduction control cells and cells over-expressing WT or mutant *CADM* in either isoforms (Fig. 63).

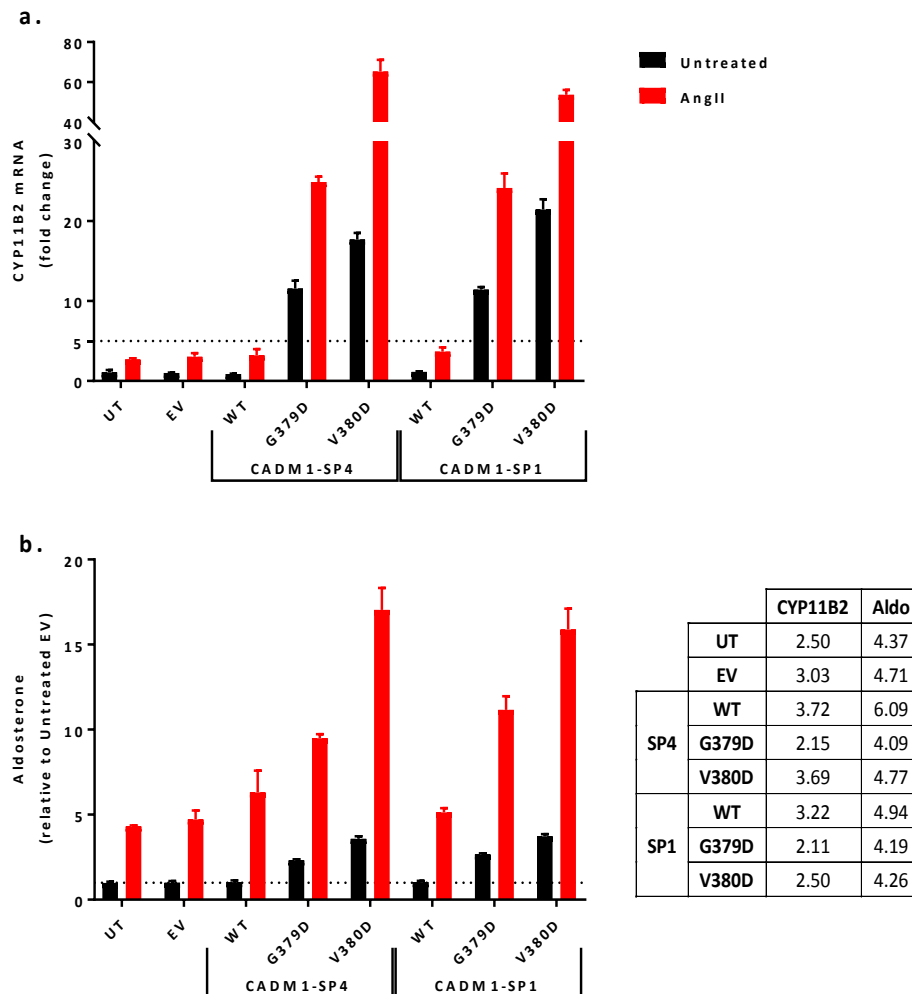


Fig. 63: Angiotensin II stimulation on H295R cells expressing *CADM1*-WT or mutants.

Transduced H295R cells were starved with serum-free media overnight before 24hr treatment with either PBS (black bars, Untreated) or 10nM Angiotensin II (red bars, AngII). **a.** *CYP11B2* mRNA expression in transduced H295R cells. **b.** Aldosterone secretion from transduced H295R cells. Error bars represent s.e.m. (n=2 in quadruplicate). Table shows the fold increase in *CYP11B2* expression and aldosterone secretion under angiotensin II stimulation.

5.4.5.4 *CADM1-WT attenuates mutant-induced aldosterone secretion*

To replicate the CADM1 WT and mutant dosage as it would be in the mutant APA and study its effect on aldosterone secretion, H295R cells were transduced with “either WT or mutant CADM1” or “a mixture of mutant and WT CADM1”. Total number of lentiviral particles transduced in various conditions was kept uniform by supplementing with control lentivirus (EV).

qPCR for CADM1 revealed a dose dependent increase in expression only in the cells transduced with CADM1-WT (EV + WT vs WT + WT in Fig. 64a). Total CADM1 expression in the cells transduced with mutant CADM1 in the presence or absence of CADM1-WT remain unchanged (EV + G379D/V380D vs WT + G379D/V380D in Fig. 64a). Despite increased dose-dependent CADM1-WT expression, no change in CYP11B2 expression or aldosterone secretion was observed as compared to the transduction control cells (EV/WT + WT vs EV + EV in Fig. 64 b & c). Interestingly, over-expression of CADM1-WT in the cells transduced with mutant CADM1 reduced the effect of mutations on the upregulation of CYP11B2 expression and aldosterone synthesis (EV + G379D/V380D vs WT + G379D/V380D in Fig. 64 b & c). These results suggested the dominant negative effect of CADM1 mutants on aldosterone upregulation.

5.4.6 *Aldosterone secretion is not regulated by ICD of CADM1*

γ -secretase, a protease is responsible for intra-membrane processing of CADM1 α -CTF to release intracellular domain (ICD) into the cytoplasm. Effect of LY-411,575 a potent inhibitor of γ -secretase activity was tested for endogenous and over-expressed CADM1 α -CTF levels and inhibition on aldosterone secretion in H295R cells.

5.4.6.1 *Effect of γ -secretase inhibition on endogenous CADM1 processing and aldosterone secretion*

H295R cells were treated with LY-411,575 in a dose range of 0.1-100 μ M for 24hr period. Conditioned cell culture media was collected for aldosterone assay and whole cell protein extracts were prepared for western blotting with anti-CADM1-CT antibody.

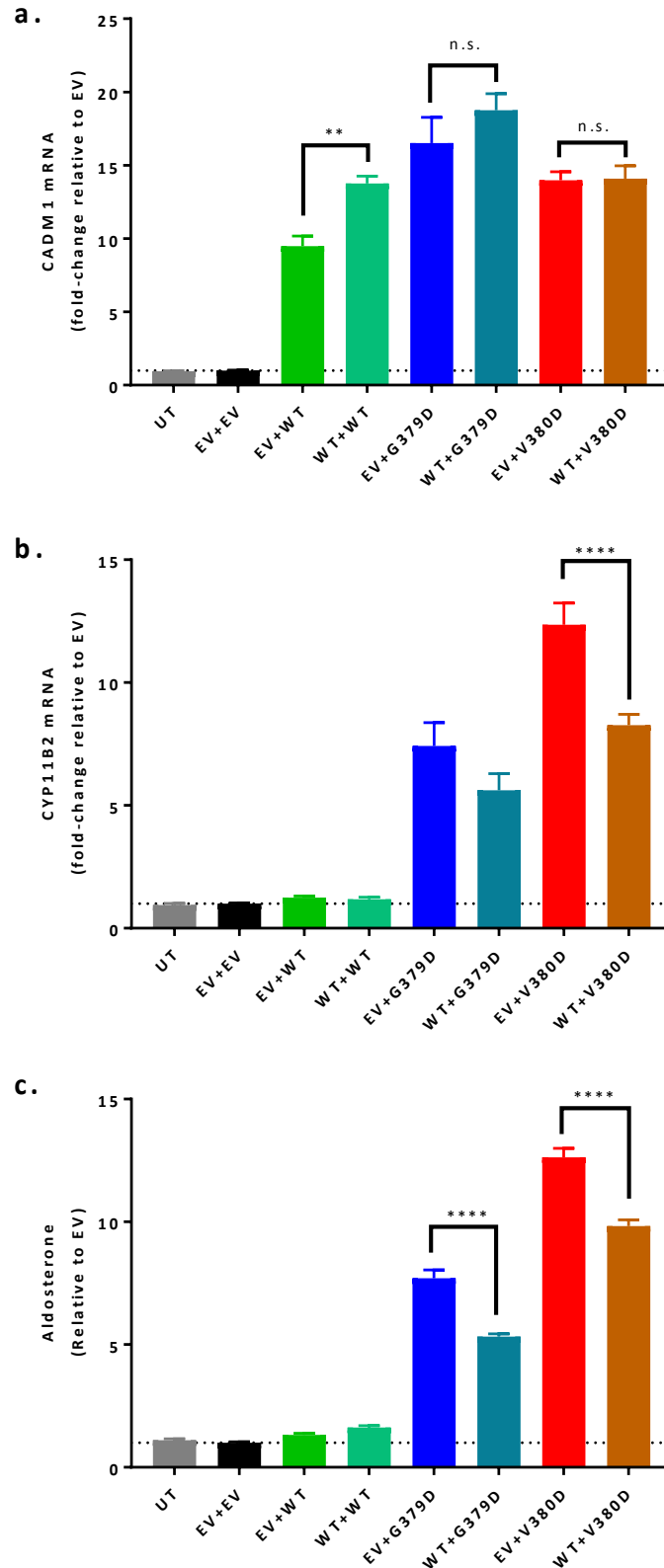


Fig. 64: CADM1-WT reduces the effects of mutants on CYP11B2 and aldosterone upregulation.

a. Estimation of relative CADM1 mRNA expression to show transduction efficiency for all constructs. **b.** Relative CYP11B2 mRNA expression in the transduced cells. **c.** Corresponding aldosterone assay. (n=2 in quadruplicate). (One-way ANOVA, **P=0.0061, ****P<0.0001). Error bars represent s.e.m.

It was found that γ -secretase inhibition led to accumulation of α -CTF at the lowest concentration of 0.1 μ M LY-411,575 tested, indicating reduced cleavage of α -CTF by γ -secretase inhibition to produce ICD (Fig. 65a). Aldosterone assay revealed that γ -secretase inhibition by LY-411,575 at this concentration or even 10-fold higher, 1 μ M is not sufficient to induce any inhibitory effect on aldosterone secretion from H295R cells and only significant reduction of about 60% in aldosterone was observed at 100 μ M LY-411,575 (Fig. 65b). These results imply that endogenous CADM1 does not exert its effect on aldosterone secretion via its ectodomain shedding followed by generation of ICD by γ -secretase.

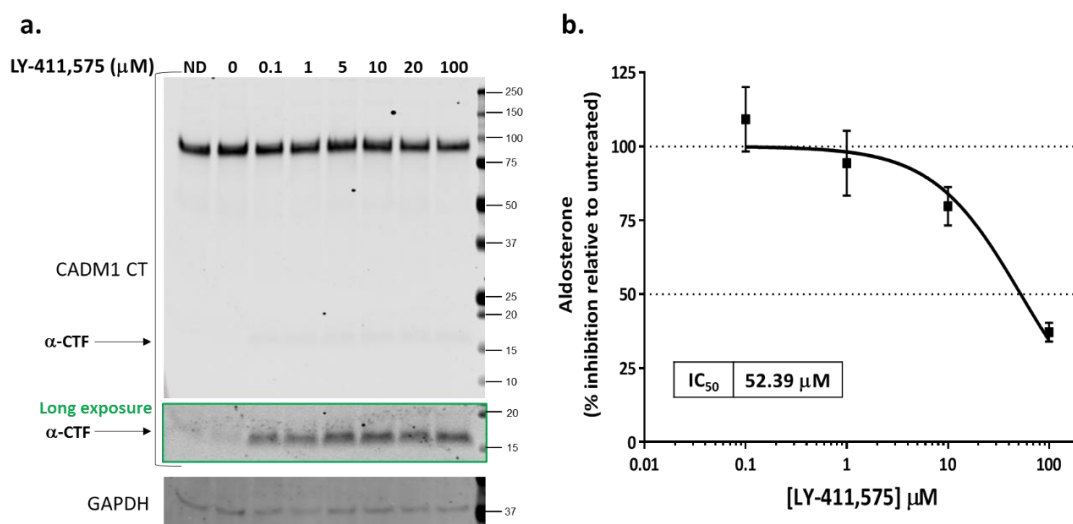


Fig. 65: Effect of γ -secretase inhibitor, LY-411,575 on α -CTF of CADM1 and aldosterone secretion from H295R cells.

a. Immuno-blot using anti-CADM1 CT antibody on cell lysates of H295R cells treated with LY-411,575 with indicated μ molar concentrations used. Untreated samples were either not exposed to DMSO (ND: no DMSO) or 0.1% DMSO (n=2). **b.** Dose curve of LY-411,575 effect on aldosterone secretion. At every tested concentration of LY-411,575 percent inhibition of aldosterone from untreated samples is represented. Error bars represent s.e.m.

5.4.6.2 Effect of γ -secretase inhibition on overexpressed CADM1 and aldosterone secretion

Following the effect of LY-411,575 on the processing of α -CTF from endogenous CADM1, similar treatments were performed on H295R cells transduced to overexpress CADM1 WT or mutants. The 2 lowest concentrations, 0.1 and 1 μ M of LY-411,575 were tested as significant inhibition of γ -secretase was observed.

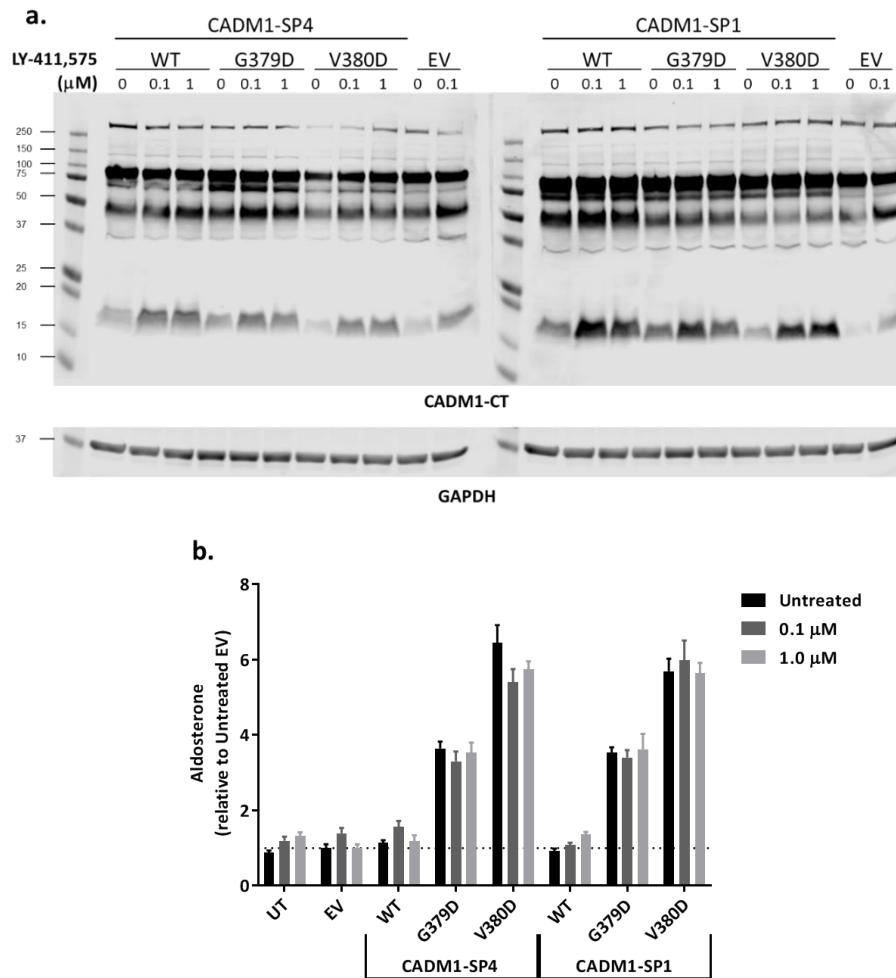


Fig. 66: γ -secretase inhibition in H295R cells overexpressing CADM1-WT or mutants.

a. Immuno-blot using anti-CADM1 CT antibody on cell lysates of transduced H295R cells treated with 0.1 or 1 μM LY-411,575. Untreated cells (0 μM) were treated with DMSO only. **b.** Effect of LY-411,575 treatment on aldosterone secretion from transduced cells is represented as relative to untreated empty-vector cells. No significant differences in aldosterone secretion was found with LY-411,575 treatment at either concentration compared to untreated cells expressing CADM1 WT or mutants ($n=2$). Error bars represent s.e.m.

It was found that LY-411,575 efficiently inhibited processing of α -CTF to ICD in all CADM1 WT or mutant expressing cells (Fig. 66a). Aldosterone assay in overexpressing cell treated with LY-411,575 revealed no inhibition in aldosterone secretion compared to untreated cells even in the cells transduced with the mutant CADM1 (Fig. 66b). These results imply, as with endogenous CADM1 which is WT, neither of the mutants in both isoforms upregulate aldosterone synthesis and secretion via increased shedding or generation of ICD translocating to mitochondria, the site of aldosterone synthesis.

5.4.7 Mutant CADM1 disrupts inter cellular adhesion

H295R cells were transduced with lentivirus for WT or mutant CADM1 and fixed for immunostaining with CADM1-CT antibody. Confocal imaging revealed significant differences in the morphology of cells overexpressing mutant CADM1 compared to the WT CADM1 expressing cells. Cells expressing high levels of mutant protein appeared rounded and less adhered to adjacent cells (Fig. 67), whereas no such loss of cell-cell adhesion was observed in the cells expressing endogenous or transduced WT CADM1.

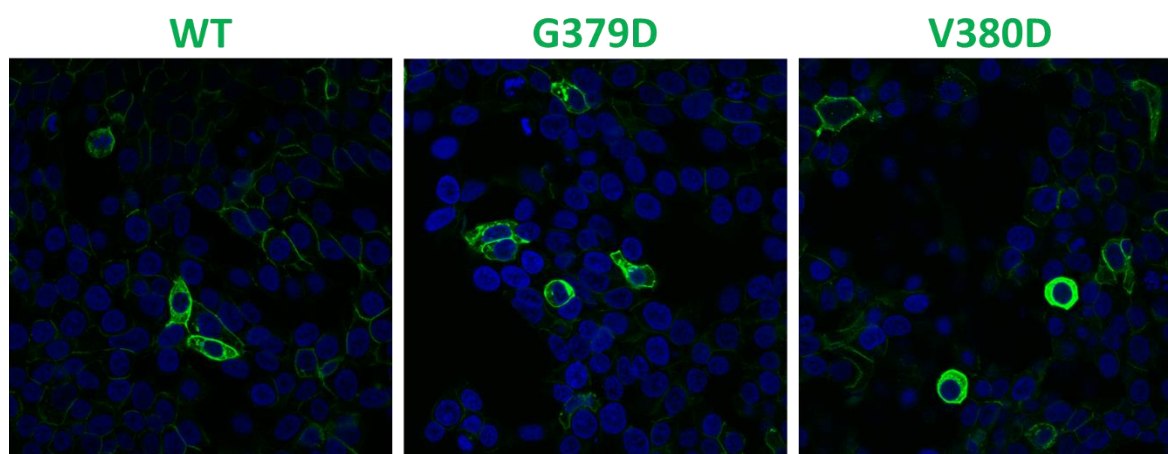


Fig. 67: Sub-cellular localisation of overexpressed CADM1-WT or mutants in H295R cells.

Confocal images for H295R cells over-expressing WT or mutant CADM1-SP4 and immuno-stained using CADM1-CT antibody (green). Nuclei were stained with DAPI (blue) in mounting media.

To replicate this observation from H295R cells, HEK293 cells were transfected with pLOC plasmids for CADM1 WT or mutants using PEI. 48hrs from transfection, live cells were imaged for distribution of tGFP expressing cells as the indicator of cells transfected with WT or mutant CADM1 (or empty vector). It was observed that cells transfected with WT CADM1 clustered together compared to those transfected with empty vector. Very few transfected cells were observed to be present on their own without clustering. The number of individual cells in mutant transfected wells was observed to be significantly higher with fewer and smaller clusters compare to the WT wells (Fig. 68). H295R cells grown in suspension, with lower cellular adhesion were found to secrete significantly more aldosterone than those cultured in adherent cell culture plates (Fig. 69), suggesting cellular adhesion is critical for controlled aldosterone production.

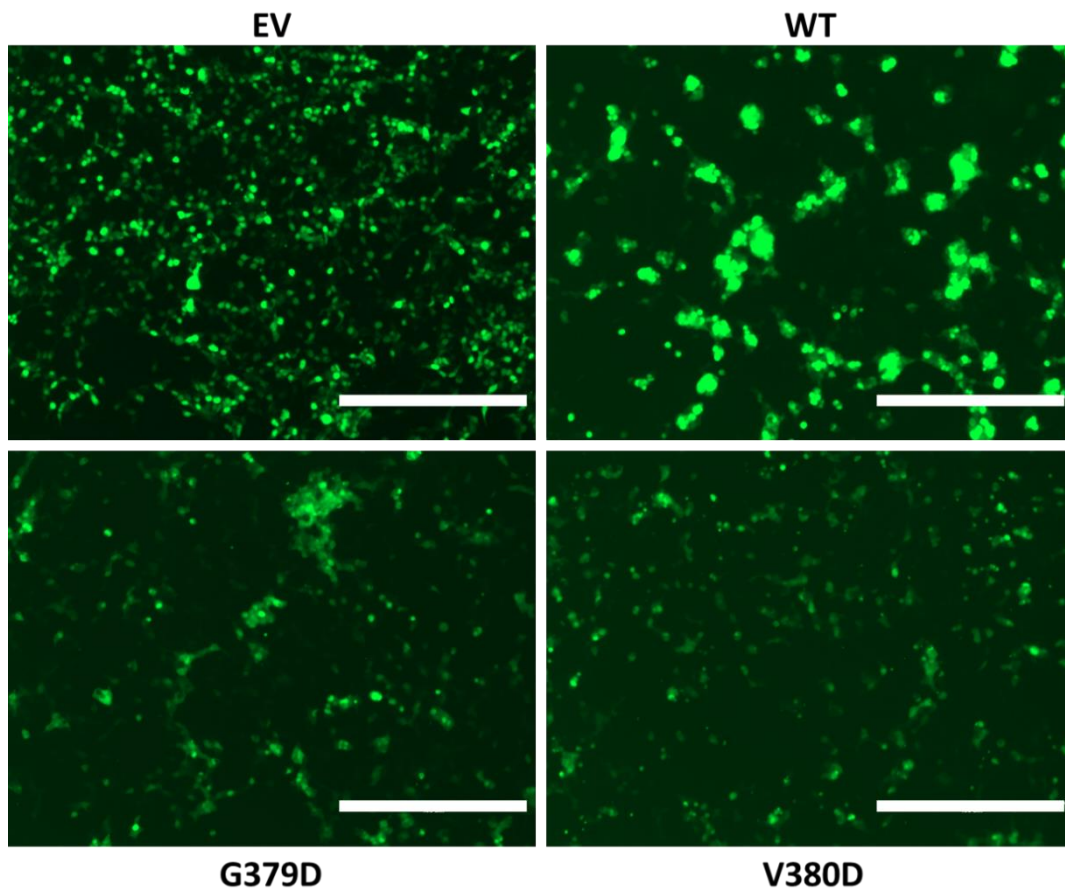


Fig. 68: Loss of cell-cell adhesion in HEK293 cells expressing mutant CADM1.

Fluorescent images for HEK293 cells transfected with pLOC constructs of empty vector (EV), WT or mutant CADM1. The tGFP in pLOC localised to nuclei representing distribution of CADM1 expressing cells. Scale bars = 400 μ m.

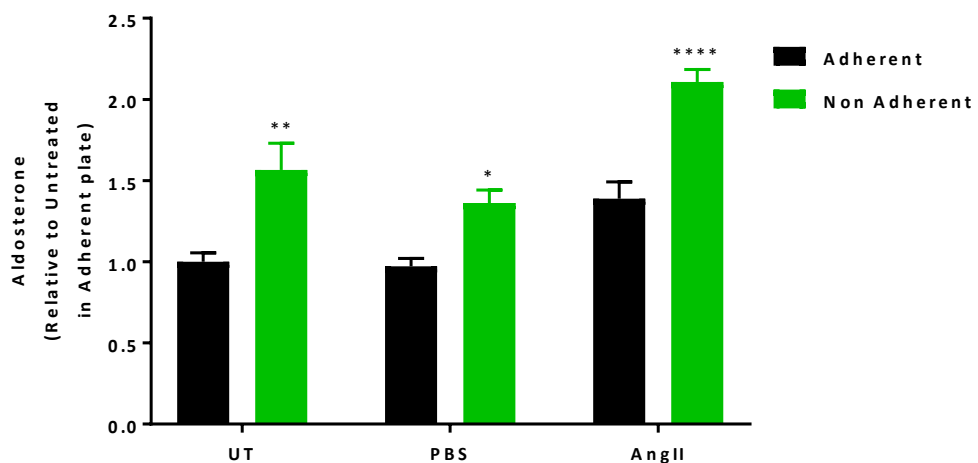


Fig. 69: Aldosterone secretion from H295R cells cultured in monolayer or suspension.

Equal number of H295R cells were plated in serum-free media only (UT), or in the presence of either PBS or 10nM AngII for 24hrs and aldosterone levels were measured. (Two-way ANOVA, *P=0.0251, **P=0.0010, ****P<0.0001 for Non-adherent vs Adherent culture plates). (n=2 in quadruplicate) Error bars represent s.e.m.

5.4.8 CADM1 silencing downregulates aldosterone synthesis

To study the normal physiological function of CADM1 in adrenal cortex, studying the effects of CADM1 knockdown was essential. H295R cells were transduced with the lentivirus for either non-targeting scrambled shRNA or a shRNA sequencing specific for CADM1 mRNA. Efficiency of CADM1 knockdown and its effect on aldosterone secretion and CYP11B2 expression were analysed.

5.4.8.1 CADM1 mRNA and protein

GFP fluorescence was used as the measure of transduction efficiency and over 90% of H295R cells were found to be GFP positive in both conditions of non-targeting or CADM1 shRNA. qPCR for CADM1 revealed about 80% knockdown of CADM1 mRNA in cells transduced with shCADM1 compared to those with the non-targeting shRNA (Fig. 70a). CADM1 protein knockdown was confirmed by western blot (Fig. 70b) and confocal imaging (Fig. 70c) using CADM1 antibodies.

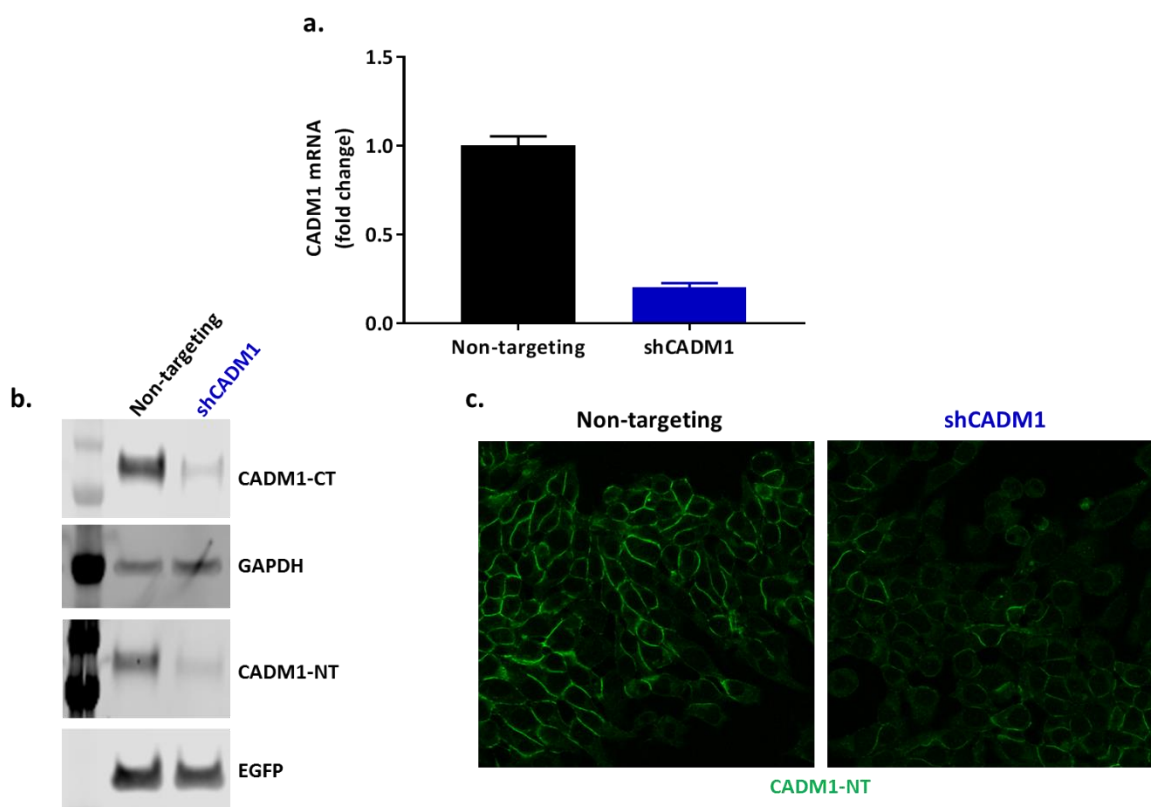


Fig. 70: Silencing of CADM1 in H295R cells using shRNA lentivirus.

a. qPCR for CADM1 mRNA fold change in cells transduced with shRNA lentivirus. 18s rRNA was used as housekeeping gene for normalising CADM1 C_t values. Error bars represent s.e.m. **b.** Whole cell lysate was immunoblotted using CADM1-CT and NT antibodies showing reduction in CADM1 protein in the wells transduced with CADM1 specific shRNA. Immuno-blot for GAPDH was used as loading control and EGFP as transduction efficiency. **c.** H295R cells grown on coverslips were transduced and fixed for immunostaining with CADM1-NT antibody. (n=3).

5.4.8.2 CYP11B2 mRNA and aldosterone secretion

Aldosterone synthesis and secretion were downregulated in the absence of CADM1. qPCRs showed a significant decrease in the CYP11B2 mRNA levels by 50% in the cells transduced with shCADM1 compared to controls (Fig. 71a) and corresponding reduction in aldosterone secretion by 40% was observed (Fig. 71b).

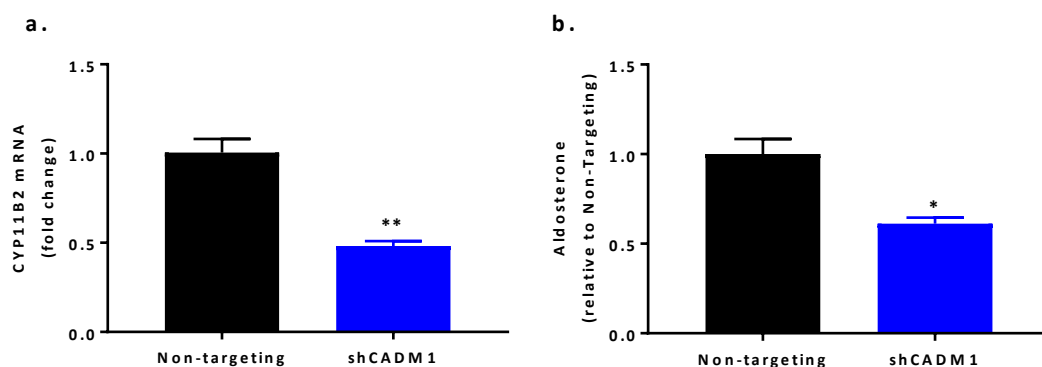


Fig. 71: Effect of CADM1 knockdown on aldosterone synthesis in H295R cells.

a. qPCR for CYP11B2 mRNA (t test, P value = 0.0029, ** $P \leq 0.01$) and **b.** Aldosterone secretion (t test, P value = 0.013, * $P \leq 0.05$) in H295R cells transduced with Non-targeting and CADM1 shRNA (n=3 in quadruplicate). Error bars represent s.e.m.

5.4.8.3 Abatement of AngII response in silenced cells

Effect of angiotensin II stimulation on aldosterone synthesis and secretion were analysed in the CADM1 silenced H295R cells. It was found the cells with CADM1 knockdown were less responsive to angiotensin stimulation as revealed by statistically non-significant upregulation of CYP11B2 mRNA (Fig. 72a). 2 fold increase in CYP11B2 in presence of AngII in the non-targeting cells was reduced to 1.6-fold in CADM1 silenced cells, which was not significant compared to untreated cells. Corresponding aldosterone secretion in CADM1 silenced cells on angiotensin II stimulation was significantly reduced to only 3.8-fold of untreated as compared to nearly 8-fold in non-targeting cells (Fig. 72b).

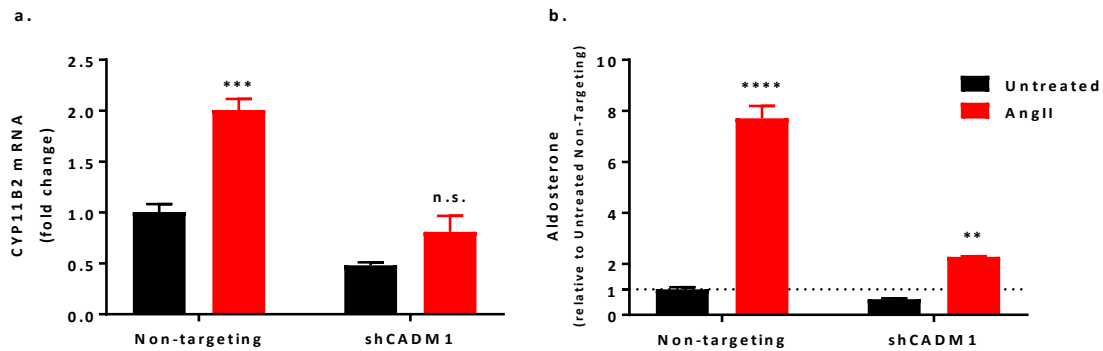


Fig. 72: Angiotensin II treatment of CADM1 silenced cells.

H295R cells transduced with scrambled (Non-targeting) or CADM1 (shCADM1) shRNA lentivirus were either untreated (PBS only, black bars) or treated with 10nM AngII (red bars). **a.** CYP11B2 mRNA (Two-way ANOVA, ***P value = 0.0003 for non-targeting; and not significant, n.s. P value = 0.1079 for shCADM1, AngII vs Untreated) and **b.** aldosterone secretion (Two-way ANOVA, ****P value < 0.0001 for non-targeting; and **P value = 0.0031 for shCADM1, AngII vs Untreated) were estimated and are expressed as fold change relative to Non-targeting untreated samples (n=2 in triplicate). Error bars represent s.e.m.

5.4.9 Possible link between CADM1 & a gap junction protein, Connexin-43

5.4.9.1 Increased Cx43 in silenced cells

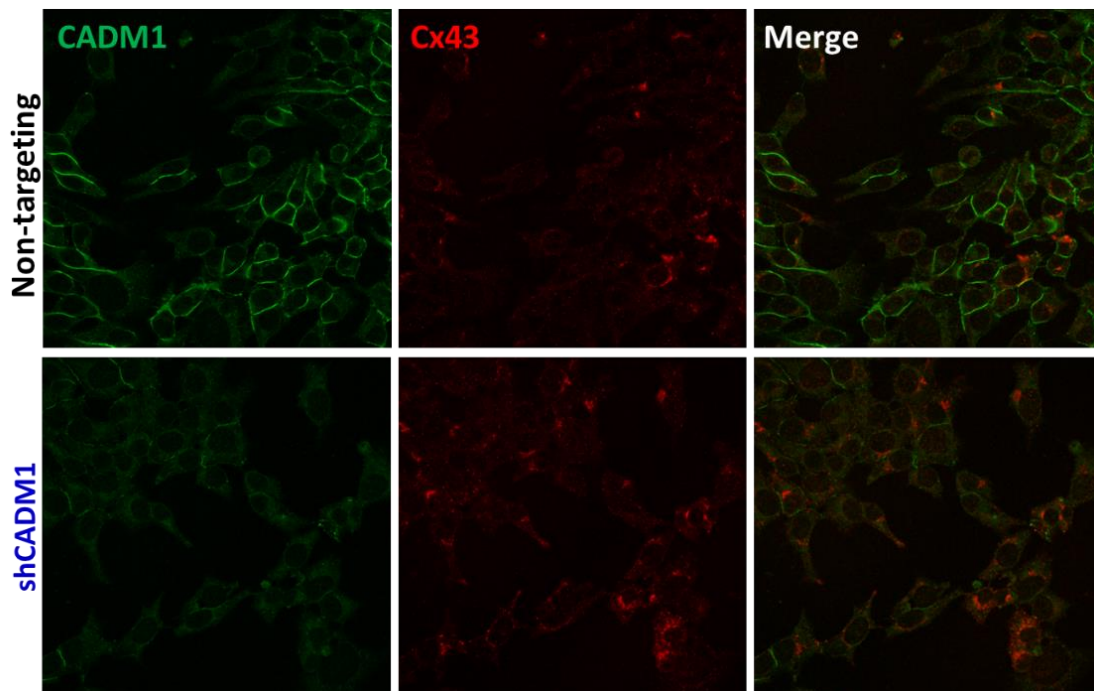
In order to investigate if knockdown of CADM1 has an effect on localisation of connexin-43, similar to that reported for Cx36 in mouse pancreatic cells (Ito et al., 2012), H295R transduced with shRNA for CADM1 were co-stained for CADM1 and Cx43. Not much overall expression of Cx43 was observed in the H295R cells and hardly any on the cell membrane (top panel in Fig. 73a). In the cells with CADM1 knockdown, increase in overall and membranous expression of Cx43 expression was observed (bottom panel in Fig. 73a), which was confirmed by western blotting (Fig. 73b). This increase in Cx43 protein levels was seen at the mRNA level as well in the RNAseq analysis (Section 5.4.11).

5.4.9.2 Para-nuclear expression in ZG, APCCs and APAs

FFPE section of dissected adrenal gland from patient 184 were co-stained for expression of Cx43 and CADM1-NT and visualised using fluorescently tagged anti-rabbit and anti-chicken secondary antibodies respectively. Another section was also stained for CYP11B2 expression and visualised using anti-mouse secondary antibody. As expected, Cx43 was found to be highly expressed at the plasma membranes in ZF of the adrenal cortex, but appeared to be expressed at very low levels in ZG (Fig. 74). The localisation of Cx43 in ZG was not membranous, but more like cytoplasmic aggregates near nuclei. This punctate para-nuclear aggregation of Cx43, possibly in endoplasmic reticulum or Golgi apparatus, was even more evident in the APCCs which express CADM1 at relatively higher levels than ZG. Again, high

CADM1 expression in APAs is observed with impaired Cx43 trafficking to the membranes and stuck in the para-nuclear organelles (Fig. 75).

a.



b.

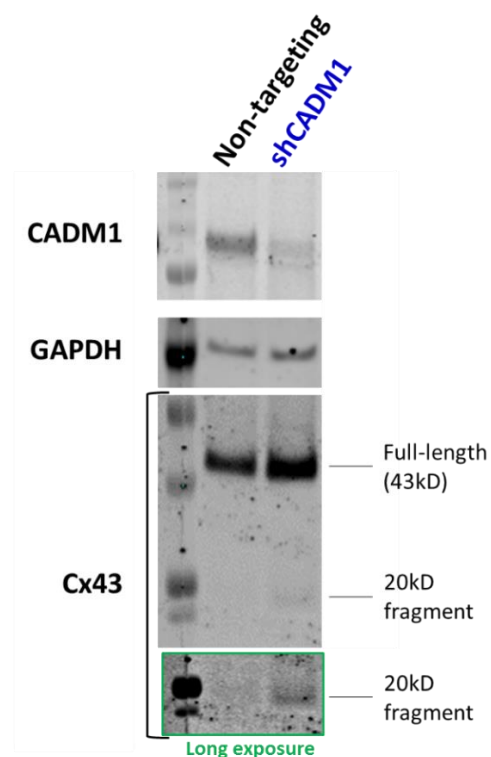


Fig. 73: Expression of connexin-43 in CADM1 silenced H295R cells.

H295R cells transduced with lentivirus for non-targeting or CADM1 specific shRNAs were a. immuno-stained with CADM1-NT (green) and Cx43 (red) antibodies; and b. whole-cell lysate was western-blotted (n=2).

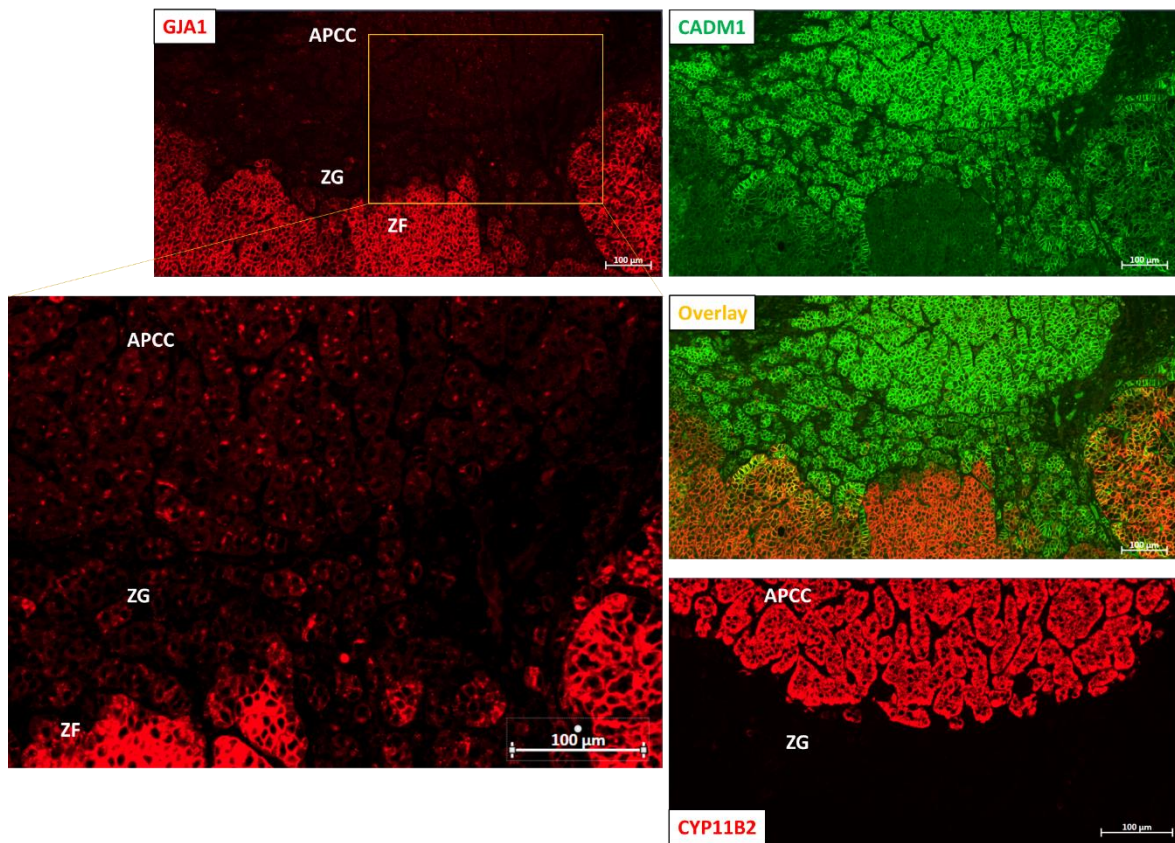


Fig. 74: Immunofluorescence for GJA1, CADM1 and CYP11B2 expression in adrenal cortex and APCC (n=5).

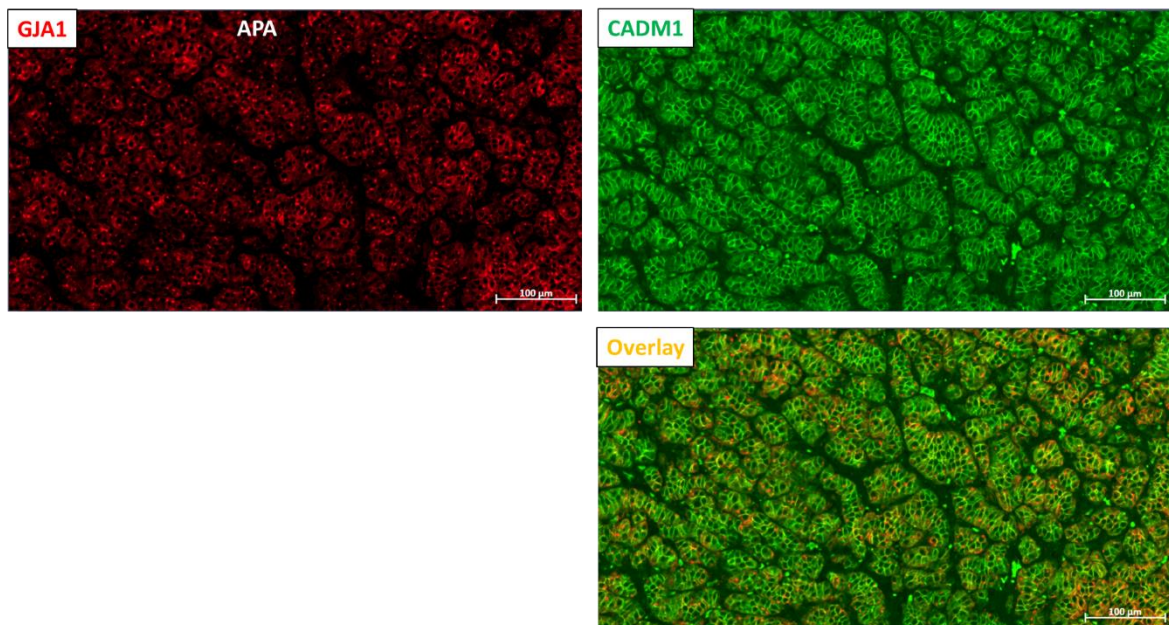


Fig. 75: Immunofluorescence for GJA1 and CADM1 expression in APAs (n=5).

5.4.9.3 Effect of AngII & PMA treatment on Cx43 levels

H295R cells were treated with 10nM angiotensin II or 200ng/ml PMA (phorbol 12-myristate 13- acetate) to study their effect on Cx43 expression in relation to aldosterone and CYP11B2 expression. PMA is a transient activator of protein kinase C, shown to increase ectodomain shedding of CADM1 (Nagara et al., 2012) and also shown here by reduced signal for full length CADM1 in PMA treated cells (Fig. 77b). Both AngII and PMA stimulation increased aldosterone secretion and CYP11B2 expression as expected (Fig. 76 a & b). Co-staining for CYP11B2 and Cx43 revealed downregulation of Cx43 in response to AngII stimulation, particularly in the cells showing higher CYP11B2 expression (Fig. 77a). This reduction in Cx43 protein levels in AngII treated cells was confirmed by western blot (Fig. 77b), despite minute increase in GJA1 transcription (Fig. 76d). PMA treatment led to significant increase in Cx43 protein levels (Fig. 77) and upregulated GJA1 transcription was observed (Fig. 76d).

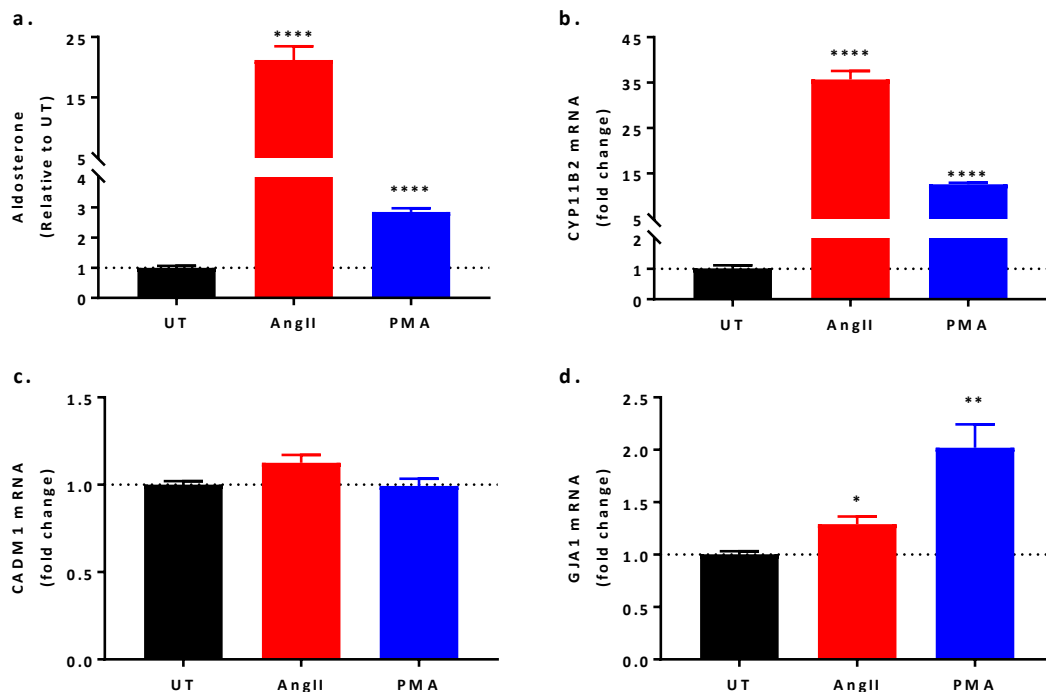


Fig. 76: Aldosterone secretion and transcriptional analysis of H295R cells treated with Angiotensin II and PMA.

H295R cells were treated with AngII or PMA for 24hrs and **a.** aldosterone secretion, and qPCRs for **b.** CYP11B2, **c.** CADM1 and **d.** GJA1 were analysed. All values for both treatments are represented as relative to untreated (UT) samples. (2-tailed T-test, *P=0.0112, **P=0.0039, ****P<0.0001 for AngII/PMA compared to UT) (n=2 in quadruplicate). Error bars represent s.e.m.

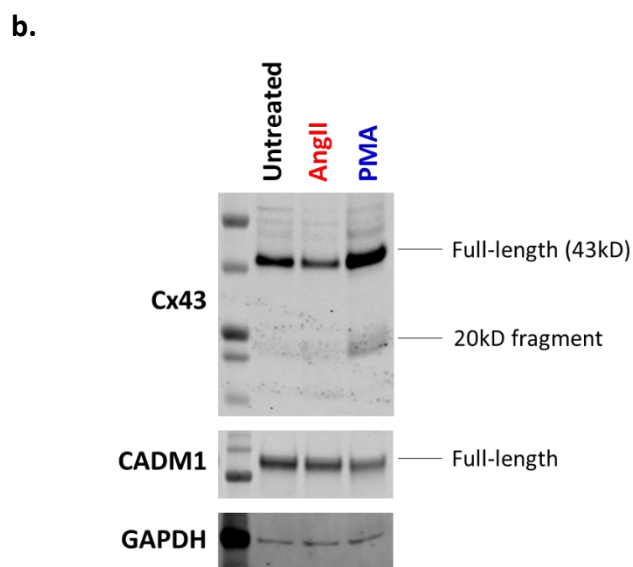
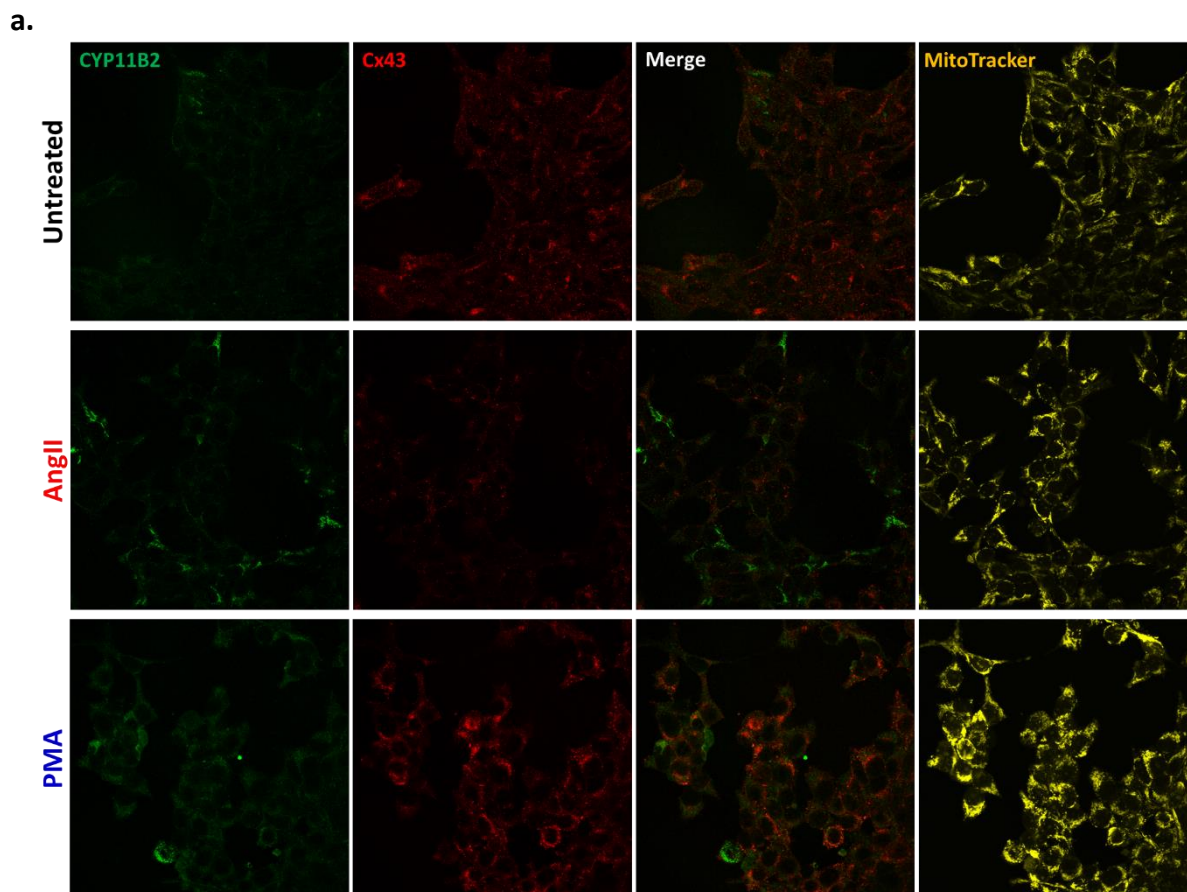


Fig. 77: Effect of Angiotensin II and PMA on expression of connexin-43 in H295R cells.
 H295R cells treated with AngII or PMA were **a.** stained with mitochondrial marker (MitoTracker, yellow) and immuno-stained with CYP11B2 (green) and Cx43 (red) antibodies; and **b.** whole-cell lysate was western-blotted for Cx43 and CADM1 levels (n=2).

5.4.10 RNAseq for CADM1-WT vs mutants overexpressing H295R cells

Transcriptome analysis, by RNAseq for H295R cells transduced with lentivirus for CADM1 WT and mutants in both isoforms SP4 and SP1 was done. There were very few interesting genes that were significantly differentially expressed in cells overexpressing CADM1-WT compared to the control cells. *CYP11B2* was one of the top genes upregulated (up to 31-fold) in cells expressing mutant CADM1 in both isoforms, with no change in the WT expressing cells along with its transcriptional regulatory gene, *NR4A2* (Fig. 78). Some other genes involved in early steps of steroidogenesis like *STAR* and *HSD3B2* were also upregulated in the presence of mutant CADM1 by at least 2-folds. Mutant CADM1 not only upregulated aldosterone synthase, but also led to 6-10 fold increase in the *CYP11B1* expression but whether it is in response to upregulated adrenocorticotrophic hormone (ACTH) receptor, *MC2R* (8-13 fold) and accessory protein, *MRAP* (6.5-8.5 fold) cannot be commented.

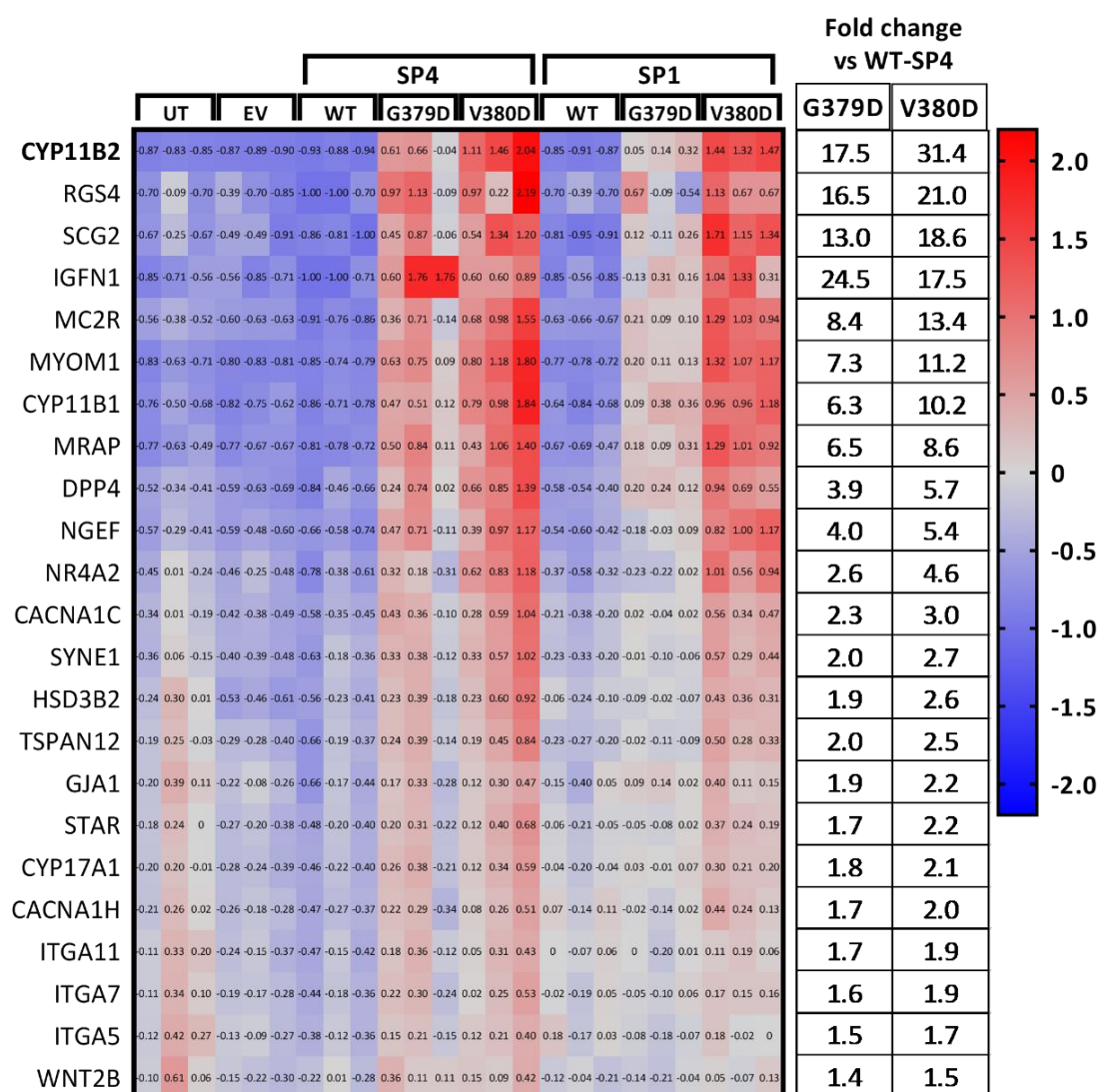


Fig. 78: Heatmap for selected genes differentially expressed in H295R cells expressing CADM1-mutants.

Heatmap shows selected 23 top genes significantly upregulated in the presence of CADM1-mutants compared to CADM1-WT (n=3 per group). Student's two-tailed T-test with P<0.05 and fold change, FC≥2 vs WT.

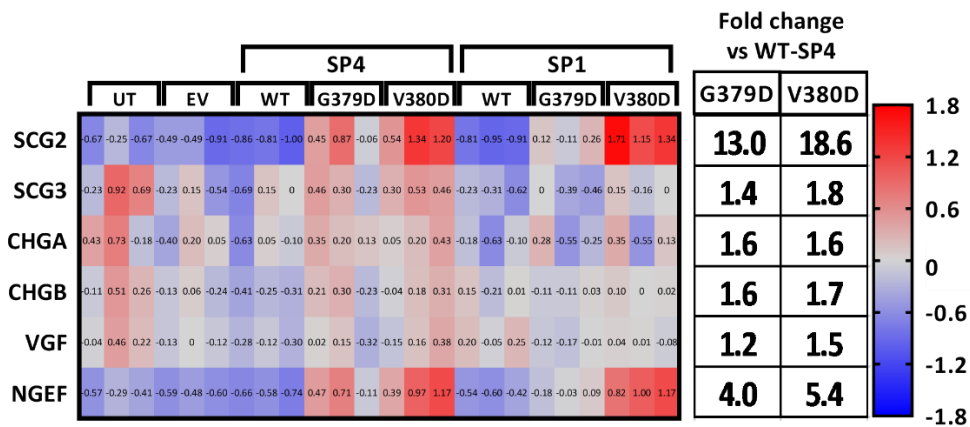


Fig. 79: Heatmap for granin family of genes differentially expressed in H295R cells expressing CADM1-mutants.

5.4.11 RNAseq for CADM1 silenced H295R cells

Transcriptome analysis, by RNAseq for H295R cells where CADM1 expression was knocked down using shRNA, revealed a large number of significantly differentially expressed genes - compared to the control cells transduced with non-targeting shRNA. CADM1 knockdown led to the downregulation of approximately 70% of the pool of significantly different genes, suggesting its critical role in normal cell physiology (Fig. 80).

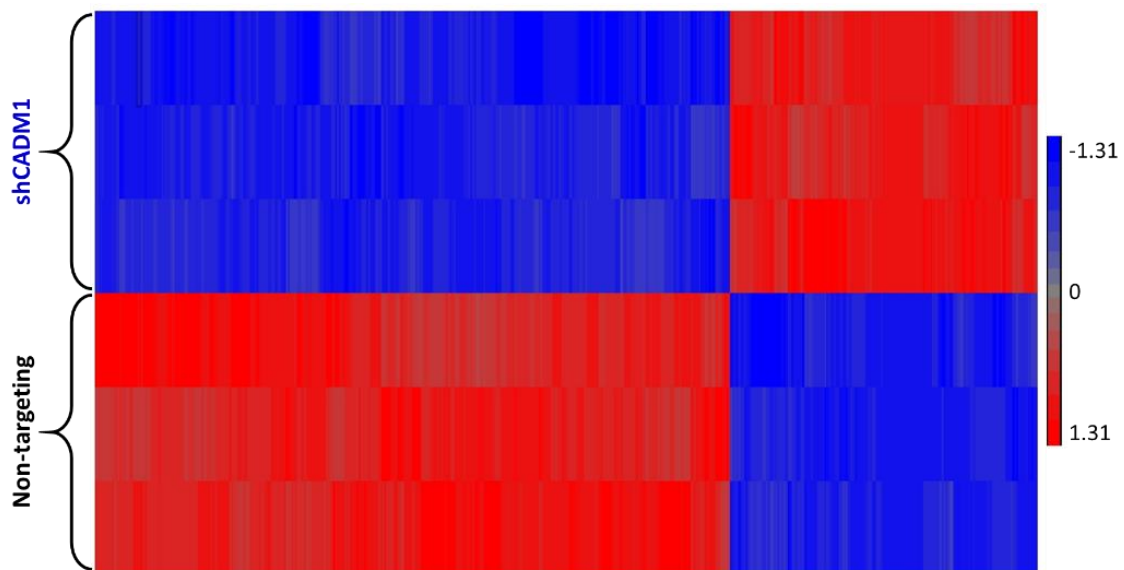


Fig. 80: Heatmap for genes significantly differentially expressed in H295R cells with CADM1 knockdown compared to control shRNA cells.

Hierarchical clustering of gene RPKM, with false discovery rate, FDR<0.05 and no cut-off for fold change between 2 groups. Number of genes represented, n=739.

In addition to confirmation of *CYP11B2* downregulation and *GJA1* upregulation in shCADM1 cells, as shown previously (Sections 5.4.8.2 & 5.4.9.1), some other genes relevant for cell-adhesion and steroidogenesis are represented in Fig. 81. Several integrin genes were downregulated in shCADM1 cells, except for *ITGA8* that was 2-fold upregulated in the absence of CADM1. No change in *CYP11B1* expression was observed. Interestingly, expression of a pro-survival factor, *BCL2* (B-cell lymphoma 2) was downregulated in shCADM1 cells by ~40%.

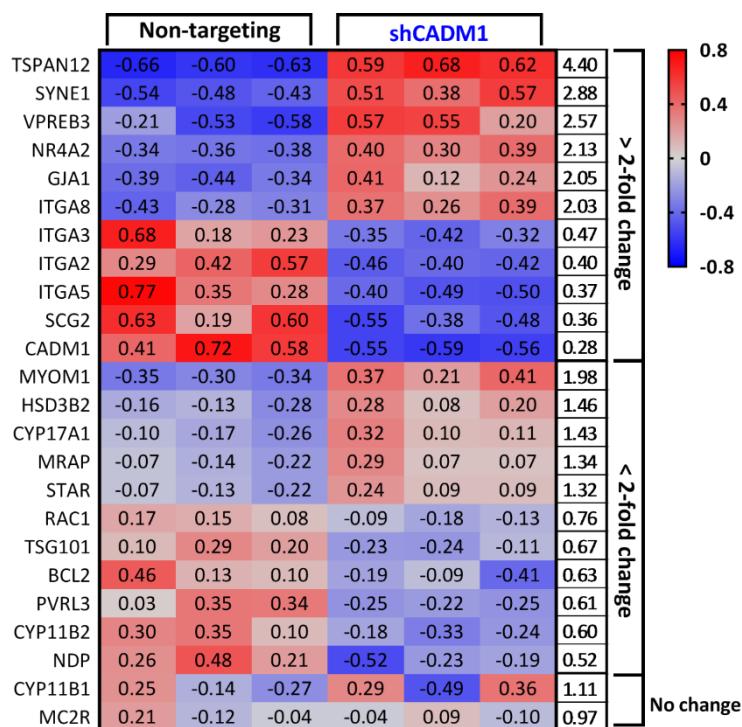


Fig. 81: Heatmap for selected genes differentially expressed in H295R cells with CADM1 knockdown compared to control shRNA cells.

Heatmap shows some selected top genes significantly upregulation in the shCADM1 cells compared to control shRNA (non-targeting) cells (n=3 per group). Student's two-tailed T-test with $P < 0.05$ and fold change indicated.

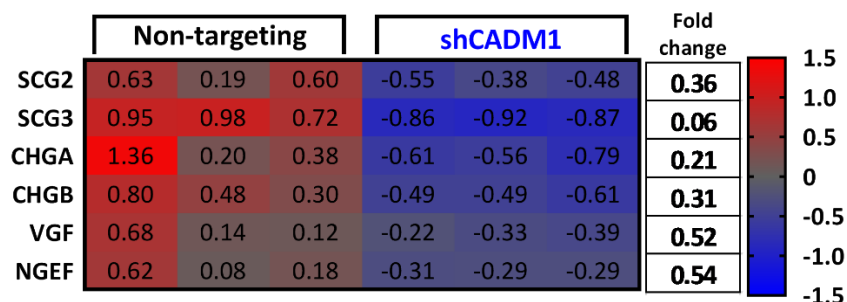


Fig. 82: Heatmap for granin family of genes differentially expressed in H295R cells with CADM1 knockdown compared to control shRNA cells.

5.4.12 RNAseq for *CADM1* APA vs other ZG-like APAs

RNAseq analysis for 3 pairs of adjacent normal and APA was done. The 3 APAs used here were *CADM1* (184T), *ATP2B3* (192T) and *CACNA1D* (195T) mutants. Analysis for the gene expression in 184T versus average of 192T and 195T is shown in Fig. 83. Most of the differentially expressed genes from previous 2 experiments were found to be upregulated in 184T, but only a few, *AQP2*, *TMEM110*, *TSPAN12*, *VPREB3* and *MYOM1* were more than 2-fold higher as compared to the average of other 2 APAs. It is important to note that we might be missing signals from many genes like those in the granin family due to adrenal medulla contaminating of our RNA prep of APA samples. For example, *SCG2* that is highly expressed in adrenal medulla, showed no difference in its expression in three APAs in the study but was differentially expressed in H295R cells expressing mutant *CADM1* or silenced *CADM1* (Fig. 79 & Fig. 82).

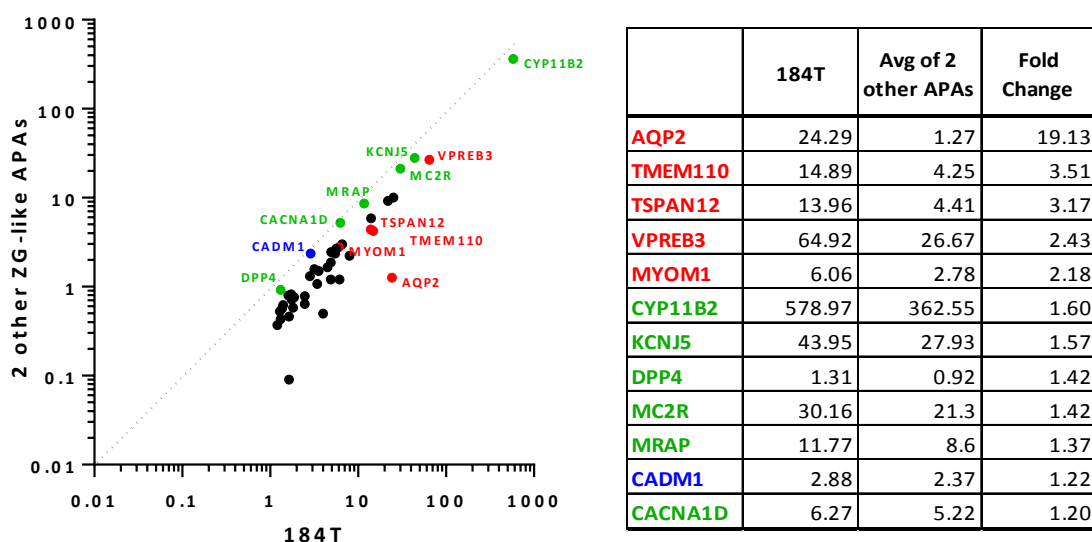


Fig. 83: Dot-plot for genes' expression in *CADM1* mutant, 184T versus average of 2 other ZG-like APAs.

Dot-plot represents common genes that were more than 2-fold upregulated in 184T compared to its adjacent normal and the average of 192T & 195T. Fold change compared to the 2 other APAs is shown in the table. Genes potentially be significantly higher in *CADM1* mutant tumour are shown in red, and other genes that are not 2-fold higher but relevant to adrenal/aldosterone physiology are shown in green.

AQP2 encodes a protein aquaporin-2, a water channel which is expressed in response to vasopressin (anti-diuretic hormone), exclusively on the apical membranes of renal collecting tubules (Nielsen et al., 1995). Here *AQP2* increases water reabsorption by collecting duct cells. Aldosterone on the other hand, has an opposite effect by decreasing apical *AQP2* expression *in vitro* (Hasler et al., 2003) and *in vivo* model of *CYP11B2* knockout mice (Makhanova et al., 2006). Unexpectedly, our lab found upregulated expression of *AQP2* by >2-fold in {1} APAs vs adjacent normal adrenal glands (Azizan et al., 2012a) and {2} *CACNA1D/ATP1A1* mutant vs

KCNJ5 mutant APAs (Azizan et al., 2013). Transcriptome analysis of *CADM1* mutant APA (184T) revealed exceptionally high expression of *AQP2* compared to the other 2 APAs that were *CACNA1D* and *ATP1A1* mutants (Fig. 83 & Table 27). This was confirmed by immunohistochemistry for *AQP2* expression easily detected in 184T, with little or no positivity in the 2 other APAs (Fig. 84, IHC done by Wanfeng Zhao). In addition to some membranous staining, *AQP2* appeared to be aggregated in cell inclusion bodies in 184T (Fig. 84a), whereas such inclusion bodies in other APAs do not show *AQP2* expression (Fig. 84 b & c).

Table 27: AQP2 expression from RNAseq analysis of 3 APAs/Normal pairs

Sample ID	Normal	APA	184T/Average
184	0.93	24.29	19.13
192	0.05	2.16	
195	0.17	0.38	

Though H295R cells do not express any *AQP2* and no change was observed in cells overexpressing *CADM1*-WT SP1 and SP4 isoforms, but a few reads for *AQP2* expression (1-4 reads) were detected in *CADM1*-V380D expressing H295R cells in RNAseq analysis (Table 28). Due to no or very low read counts, no statistical analysis could be done and only the raw data is shown here. These results are consistent with high *AQP2* expression in 184T, harbouring V380D mutation. If *AQP2* upregulation proves to be a true and direct effect of *CADM1* mutation, it might be exploited to further explore *CADM1*'s role in APAs.

Table 28: AQP2 expression from RNAseq analysis of H295R cells overexpressing *CADM1*

		No. of reads	Average
Untransfected		0, 2, 0	0.67
Empty Vector		0, 0, 0	0.00
SP4	WT	0, 0, 0	0.00
	G379D	1, 0, 0	0.33
	V380D	2, 4, 1	2.33
SP1	WT	0, 0, 0	0.00
	G379D	1, 1, 0	0.67
	V380D	1, 1, 0	0.67

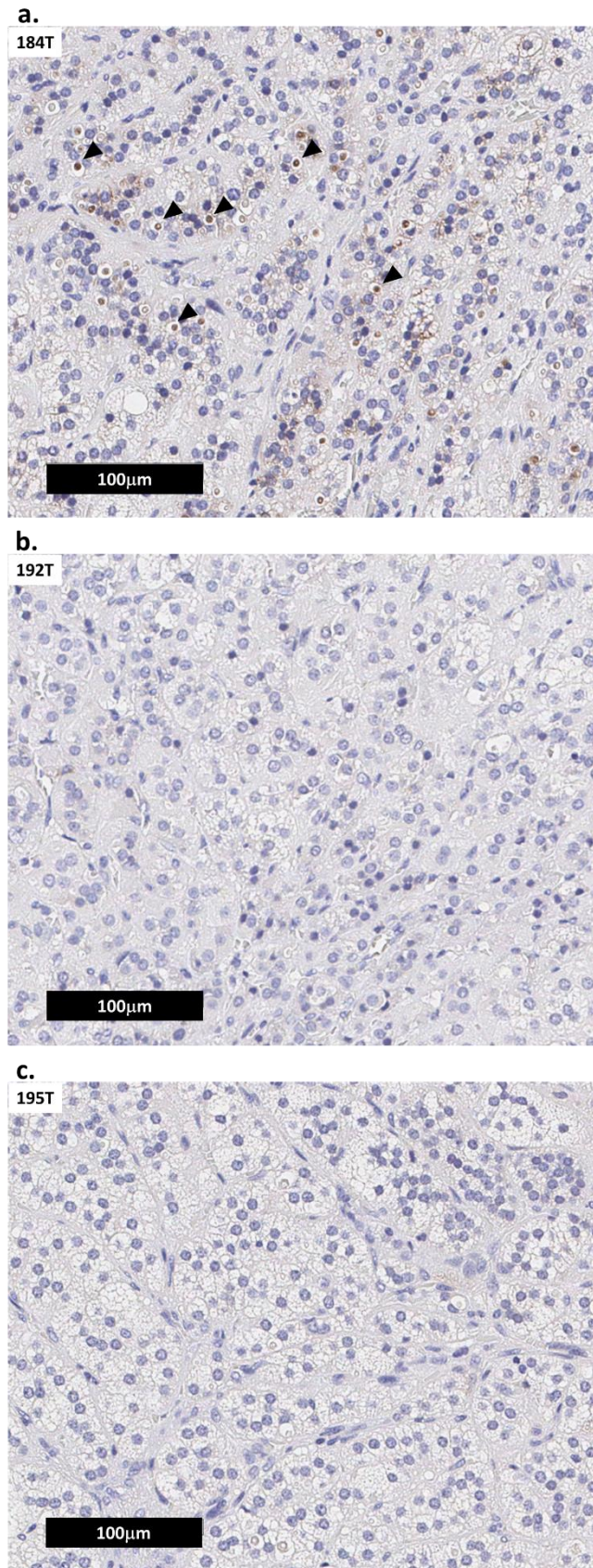


Fig. 84: Immunohistochemistry for AQP2 in APAs

IHC for AQP2 in the three APAs for which RNASeq was performed. **a.** CADM1 mutant APA 184T. **b.** & **c.** Two other ZG-like APAs - 192T and 195T. Arrow heads indicate cell inclusion bodies positive for AQP2. Scale bar is shown. (This staining was performed by Wanfeng Zhao at Human Tissue Bank, Addenbrooke's Hospital).

5.5 Discussion

With the discovery of mutations in *CADM1*, a tumour suppressor gene, it was hypothesized that these mutations would have a pathogenic role due to the loss of function resulting in increased tumour cell proliferation and autonomous aldosterone secretion. To investigate this hypothesis and study the role of *CADM1* in aldosterone secretion in normal and pathogenic tissues, I started with analysing *CADM1* expression levels and localisation in the normal adrenals and APAs. RT-PCR and immunohistochemistry for *CADM1* showed its high expression in the human adrenals, APAs and adrenocortical carcinoma derived cell line, H295R cells. Transcripts expression analysis in all – H295R cells and human adrenal tissue samples showed *CADM1*-SP4 to be the most predominant isoform in the samples tested (Fig. 53 & Fig. 54) as is the case with other tissues like brain, testis, mast cells etc. Isoform with constitutively shed ectodomain, SP1 and the secreted/soluble isoform with retained intron, SP5 are also expressed in these tissues (Fig. 53). Soluble isoform has been shown to function in a self-antagonistic manner by inhibiting trans-homophilic *CADM1* interaction between adjacent cells (Koma et al., 2004). Effects of soluble isoform expression in H295R cells is not known and was not investigated in this study.

Immunohistochemistry for *CADM1* localisation in normal adrenal sections revealed intense staining in the zona glomerulosa of adrenal cortex. There was easily detectable expression in zona fasciculata and adrenal medulla (Fig. 55 a & c, & Fig. 58e). In all these regions *CADM1* localised to cell membranes and no intracellular staining for cleaved products was observed (Fig. 55c & Fig. 56c). Interestingly, aldosterone producing cell clusters (APCCs) in adrenal cortex as defined by high *CYP11B2* expression, normally not seen in the continuous ZG layer (Fig. 55 b & d; Fig. 56 b & d; Fig. 58 b & d) showed highly upregulated expression of *CADM1* (Fig. 55 a & c; Fig. 56 a & c; Fig. 58 a & c). Similarly, *CADM1* is expressed in APAs in the pattern similar to that of *CYP11B2* that is, mostly homogenous with some patches negative for both *CYP11B2* and *CADM1* (Fig. 57 & Fig. 58). These findings suggest that *CADM1* plays an important role in aldosterone secretion.

Despite the introduction of negatively charged aspartate residue in the transmembrane domain of *CADM1* mutants, heterologous expression of WT and mutants in H295R cells, both mutants could translocate to the plasma membranes (Fig. 62 & Fig. 67). Western blots with the Myc antibody showed both mutant proteins were glycosylated efficiently as indicated by relatively similar proportions of 2 bands for all samples (Fig. 60a). This blot also revealed lower protein expression for V380D as compared to the WT or the second mutant G379D irrespective of the isoforms SP4 or SP1. This was not due to the excessive shedding of ectodomain and further proteolytic processing of *CADM1*-V380D as no increase in the α -NTF levels in the supernatant was observed (Fig. 60c). α -NTF for *CADM1*-V380D reflected the total

protein levels in cell lysates. Surprisingly there were no differences seen in the protein levels or ectodomain shedding for the WT protein in 2 isoforms expressed in H295R cells, when SP1 is supposed to be constitutively shed. It could probably be that H295R cells do not express or are unable to secrete the protease, ADAM10 or similar, required for the constitutive shedding into the media.

The differences in the number and sizes of α -CTF fragments generated in cells expressing WT or mutant CADM1 as shown by western blotting using anti-CADM1 CT antibody (Fig. 60b), suggest different cleavage sites of ectodomain shedding by ADAM10. Though it is not possible to conclude this without 3D structure modelling of WT and mutant proteins, evidences are there in literature that ADAM10 and other proteases in the family proteolytically cleave membrane proteins at a fixed distance from cell surface rather than by recognising a specific amino acid sequence (Hayashida et al., 2010). It is speculated that the mutations within the transmembrane domain of CADM1 change the angle at which ectodomain is exposed on the cell surface leading to differences in the sizes of α -CTFs generated compared to the WT. There are no reports of phosphorylation of CADM1 or cleaved α -CTFs, but presence of putative phosphorylation sites suggests this is possibly a regulatory mechanism which can be affected by the presence of mutations in CADM1. Difference between the number and sizes of α -CTF fragments generated from the 2 mutants suggest different impact the 2 variants in adjacent residues have on CADM1 structure and possibly the downstream mechanisms.

Increased aldosterone secretion and CYP11B2 upregulation by both mutants suggested a gain-of-function phenotype as no change is seen with the overexpression of CADM1-WT compared to the control cells (Fig. 61). The effect of 2 mutations on aldosterone synthesis differed significantly from each other with V380D expression resulting in the most extreme phenotype despite the least total protein expression. These results imply very different mechanisms the two mutations might be functioning with. Immunofluorescence of transduced cells for CYP11B2 was in accordance with the qPCR analysis that no staining for CYP11B2 expression was observed in H295R cells expressing CADM1-WT, but only in the ones expressing mutant V380D mutant more than G379D (Fig. 62).

To investigate if the intracellular domain (ICD) of CADM1 does play a role in aldosterone secretion, possibly by translocating to mitochondria like in lung epithelial cells (Hagiya et al., 2015), a γ -secretase inhibitor LY-411,575 was used to block γ -secretase mediated proteolytic processing of α -CTF to generate ICD. Treating H295R cells with LY-411,575 resulted in accumulation of α -CTF suggesting effective inhibition of γ -secretase activity at the concentration of 0.1 μ M (Fig. 65a), though no reduction in aldosterone secretion was observed below 10 μ M LY-411,575 (Fig. 65b). It can be concluded that ICD of endogenous

CADM1 does not play a role in aldosterone secretion, and any inhibition observed at 10 μ M or higher LY-411,575 concentrations is non-specific and via CADM1 independent pathways. Similar observations from LY-411,575 treatment were seen on H295R cells overexpressing WT or mutant CADM1 (Fig. 66) which suggests that CADM1 perhaps regulate aldosterone secretion by an alternative pathway.

Immunofluorescence for CADM1 localisation in H295R cells' monolayer is very asymmetric and shows membranous staining only where a cell is in contact with another cell (Fig. 70c) suggesting a critical role in cell-cell adhesion and possibly inter-cell communication in this cell line as well. This inter-cellular adhesion seems to be lost in cells expressing CADM1 mutants as suggested by rounded morphology with no or little cell-cell contact (Fig. 67). This loss of cellular adhesion is probably due to inability of mutant CADM1 to form trans-homo/heterophilic interaction with CADM1 on the cell surface of neighbouring cells. This phenomenon appeared to be more prominent in V380D expressing cells than those expressing G379D mutant CADM1. The difference in the degree of their effect on cell adhesion also supports much higher upregulation of aldosterone secretion in V380D than in G379D mutant CADM1 expressing H295R cells. Similar loss of cell-cell adhesion was also very obvious in the HEK293 cells transfected with either mutant CADM1 compared to that seen in the case of overexpressed CADM1-WT (Fig. 68). It is believed that CADM1-mutants, G379D and V380D lead to loss-of-function for CADM1's adhesion properties resulting in gain-of-function phenotype in stimulating aldosterone secretion. Interestingly, co-transduction of WT and mutant CADM1 showed attenuated aldosterone secretion as compared to the mutant alone (Fig. 64). This suggested a dominant negative effect of mutant CADM1 on aldosterone because of its sensitivity to CADM1-WT dosage. On the other hand, mutant CADM1 induced aldosterone upregulation was not additionally potentiated by angiotensin II treatment and remained limited to 2-3 fold increase irrespective of CADM1 genotype (Fig. 63). These observations suggest aldosterone secretion "in response to angiotensin II stimulation" and "due to loss of cellular adhesion in the presence of mutant CADM1" are two independent pathways.

This theory is supported by the two *in vitro* observations. Firstly, higher aldosterone secretion from H295R cells cultured in suspension in the low attachment vessels (cells are less in contact with each other) as compared to when cell are adhered to the surface (Fig. 69). Secondly, elevated levels of aldosterone secretion usually seen from dispersed primary adrenal cortical cells that contain less than 5% cells of zona glomerulosa origin. In primary cell culture, loss of glomeruli entity means loss of intercellular adhesion and communication resulting in each cell to make aldosterone autonomously rather than in a regulated manner within a glomerulus of ZG. The loss of pace making activity of a glomerulus is not only executed via Ca²⁺ as the second

messenger (Hu et al., 2012) but also adhesion molecules like CADM1 in a Ca²⁺ independent manner.

Apart from studying the effects of mutations on CADM1 function in pathological condition, I investigated the role endogenous CADM1 plays in regulation of aldosterone secretion under “normal” conditions. Though overexpression of CADM1-WT showed no effect on aldosterone or CYP11B2 expression, its knockdown resulted in downregulation of aldosterone synthesis and secretion in H295R cells (Fig. 71). Absence of CADM1 also resulted in lower responsiveness of H295R cells to angiotensin II mediated aldosterone stimulation (Fig. 72). The reason for contrasting effects of CADM1 dosage and its mutational status on H295R cells’ responsiveness to angiotensin II treatment is probably that the minimum threshold level of CADM1 is required for normal physiological aldosterone secretion. Above this threshold/basal level the mutant CADM1 functions as antagonist for adhesion lifting the regulatory checkpoint that CADM1 imposes under normal conditions.

Transcriptome analysis of H295R cells overexpressing CADM1 WT or mutants showed a very few genes to be downregulated in mutant expressing cells and most were upregulated (Fig. 78). Interestingly, many of the upregulated genes in mutant expressing cells were also upregulated in the CADM1 silenced cells – *MYOM1*, *TSPAN12*, *GJA1*, *SYNE1*, *MRAP* and steroidogenesis enzymes *STAR*, *HSD3B2*, *NR4A2*, *CYP17A1* etc. with an exception of *CYP11B2* expression which goes in opposite directions that is upregulated in mutant cells but downregulated in shCADM1 cells (Fig. 78 & Fig. 81). Most of granin family proteins also followed this pattern of opposite direction, being upregulated in the presence of mutant CADM1 and down in CADM1 silenced H295R cells (Fig. 79 & Fig. 82).

Another surprising exception was the expression of *CYP11B1*, which remained unchanged in CADM1 silenced cells but was 6-10 fold upregulated in mutant expressing cells (Fig. 78 & Fig. 81). These observation suggests mutants function in a way similar to reducing absolute availability of CADM1 in the cells by their inhibitory effects on cell adhesion as in the case of silenced cells.

GJA1, the highest of all gap junction proteins in adrenal (Fig. 46), was upregulated in CADM1 silenced cells (Fig. 73 & Fig. 81) and also in mutant CADM1 expressing H295R cells (Fig. 78). A 20kD transcript of *GJA1* translated from an internal start site has been reported to function as an auxiliary trafficking protein for the full-length Cx43 to the plasma membrane forming functional gap junction channels (Smyth and Shaw, 2013). Western blots showed an increase in full-length Cx43 and the 20kD fragment levels as well in shCADM1 cells (Fig. 73). Increased

Cx43 mRNA and protein in H295R cells treated with PMA (Fig. 76 & Fig. 77) was observed. PMA increases CADM1 ectodomain shedding resulting in lesser full-length CADM1 on cell surface and fewer inter-cellular adhesion points. This inverse membranous expression of CADM1 and Cx43 was also obvious in the immunohistochemistry of human adrenal sections. In ZF with relatively less CADM1 expression, Cx43 localises to cell membranes (Fig. 74). Complementarily, CADM1 rich regions of ZG, APAs and APCCs show no membranous localisation of Cx43. All Cx43 appears to be accumulated in para-nuclear aggregates which is possibly the endoplasmic reticulum or Golgi apparatus (Fig. 74 & Fig. 75). These observations suggest CADM1 probably prevents gap junctional intercellular communications (GJIC) by reducing the number of functional intercellular channels between adjacent cells through which small molecules are shared. Additionally, downregulation of *TSG101* was observed in transcriptome analysis of shCADM1 cells (Fig. 81). *TSG101* (tumour susceptibility gene 101), encodes for one of the proteins involved in ubiquitin mediated lysosomal degradation of Cx43 inhibiting its recycling to plasma membrane (Leithe et al., 2009). It is also speculated that the possible changes in angulation of ectodomain of the mutant CADM1 prevents neighbouring cells to come close enough at optimum distance required to form functional connexions. In conclusion, CADM1 might play a role in regulating GJIC by increasing Cx43 degradation, either by supporting expression of TSG101 or by regulating 20kD isoform expression to limit its membrane trafficking. So far, the link between CADM1 and Cx43 has only been reported in skin wound healing process where they interact indirectly via a common interacting protein, CASK (Márquez-Rosado et al., 2012).

Similar to the studies in nephropathic kidneys and CADM1 silencing experiments in renal tubular cells (Kato et al., 2018), 40% downregulation of *BCL2*, a pro-survival/anti-apoptotic gene in shCADM1 cells was found, suggesting CADM1's role in supporting H295R cell survival.

TSPAN12, a member of tetraspanin family of proteins contains 4 transmembrane domains. It acts as a co-receptor for ligand *NDP* (norrin) binding to its receptor *FZD4* (frizzled 4) inducing the signalling pathway which results in the protection of β -catenin from degradation (Knoblich et al., 2014; Lai et al., 2017). Elevated nuclear β -catenin recruits *TCF/LEF* and other transcriptional factors independently of Wnt signalling. The observations of 2-fold downregulated NDP expression in the absence of CADM1, with possible 4.4-fold compensatory increase in *TSPAN12* are supported by previous reports of increased β -catenin signalling implicated in the development of adrenal cancers and hyper aldosterone secretion in APAs (Berthon et al., 2010, 2014; Teo et al., 2015). RNAseq for mutant vs WT CADM1 expressing H295R cells (Fig. 78) and 184T vs other 2 APAs (Fig. 83), respectively showed 2-2.5 and >3 fold higher *TSPAN12* expression. This might be explained by *TSPAN12*'s role in supporting primary tumour growth but inhibiting metastasis (Knoblich et al., 2014).

CHAPTER 6

CHAPTER 6 - CONCLUSIONS

Candidate gene screening and whole exome sequencing of APAs in our cohort revealed different rates of prevalence for mutated genes in the APAs investigated to that reported in the literature for other cohorts. CACNA1D gene was found to be the most commonly mutated gene followed by the KCNJ5. This was due to the presence of large number of small APAs that could be diagnosed by PET-CT using C¹¹-metomidate at the Addenbrooke's Hospital. We believe that small APAs could be undetected in adrenal CT scans or MRI, and therefore PET-CT would be more efficient in diagnosis and management of PA.

Increased calcium influx via mutant Ca_v1.3 does lead to hyper aldosterone secretion in H295R cells. Apart from its conventional function of voltage-gated calcium channel, we found evidence of its role as a transcription factor mediated by calpain cleaved intracellular c-terminal. Nuclear translocation of cleaved Ca_v1.3's c-terminal appeared to regulate aldosterone synthesis and secretion. Aldosterone synthase, CYP11B2 expression was found to be downregulated in the adrenals of Ca_v1.3 knockout mice. This finding was critical to establish the significant role that Ca_v1.3 plays in the physiological regulation of aldosterone synthesis and not just when mutated in the APAs. Moreover, the discovery of Ca_v1.3 selective 3 tool compounds at ■■■ proved to be immensely promising as at least one of these, compound B, could inhibit aldosterone secretion both in H295R and in the primary adrenal cells. More primary cells/tissues are needed for testing the effects of compound B on aldosterone regulation, which can be developed further into a drug for treating PA patients not just with the CACNA1D mutated APAs but any APAs.

We discovered novel somatic mutations in cell adhesion molecule 1, CADM1 in 2 APAs in Cambridge and Munich cohorts. Expression of mutant CADM1 was found to have a dominant effect by increasing aldosterone synthesis in the H295R cells. This is perhaps due to the disruption of physiological intercellular adhesion necessary for controlled aldosterone secretion. Overexpression of wild-type CADM1 does not affect aldosterone levels but maintenance of basal CADM1 expression is essential for sustained aldosterone secretion. CADM1 might be involved in regulation of gap-junctional intercellular communications by inhibiting membrane trafficking of connexin-43. RNAseq experiments revealed a large number of genes differentially expressed in presence of mutant CADM1 or silenced CADM1. Future studies on some of the top genes, like aquaporin-2 (AQP2) would enhance our understanding of the significant role CADM1 plays in physiological and pathological conditions of aldosterone secretion. This study again highlights the significance of intercellular adhesion and communication in ZG of adrenal cortex for sustained and regulated aldosterone secretion.

Appendix

Buffer recipes

1. Ca²⁺ bath solution
10mM CaCl₂, 150mM TEA-Br, 3mM KCl, 1mM NaHCO₃, 1mM MgCl₂, 10mM HEPES, 4mM Glucose, pH 7.4 using Tris Base (pH7-9).
2. Ba²⁺ bath solution
10mM BaCl₂, 150mM TEA-Br, 3mM KCl, 1mM NaHCO₃, 1mM MgCl₂, 10mM HEPES, 4mM Glucose, pH 7.4 using Tris Base (pH7-9).
3. Cs internal solution
140mM CsOH, 140mM Aspartic acid, 5mM EGTA, 2mM MgCl₂, 0.1mM CaCl₂, 2mM K₂ATP, 10mM HEPES, pH 7.2 with 3M CsOH.
4. Cell lysis buffer
50mM Tris, 0.15M NaCl, 1mM EGTA, 1mM EDTA, 1mM sodium orthovanadate, 50mM NaF, 10mM sodium pyrophosphate, 10mM glycerol-2-phosphate, 1% Triton X-100, pH 7.5

REFERENCES

- Åkerström, T., Willenberg, H.S., Cupisti, K., Ip, J., Backman, S., Moser, A., Maharjan, R., Robinson, B., Iwen, K.A., Dralle, H., et al. (2015). Novel somatic mutations and distinct molecular signature in aldosterone-producing adenomas. *Endocr. Relat. Cancer* *22*, 735–744.
- Allen, T.J., and Mikala, G. (1998). Effects of temperature on human L-type cardiac Ca²⁺ channels expressed in *Xenopus* oocytes. *Pflügers Arch. Eur. J. Physiol.* *436*, 238–247.
- Allinen, M., Peri, L., Kujala, S., Lahti-Domenici, J., Outila, K., Karppinen, S.M., Launonen, V., and Winqvist, R. (2002). Analysis of 11q21-24 loss of heterozygosity candidate target genes in breast cancer: Indications of TSLC1 promoter hypermethylation. *Genes Chromosom. Cancer* *34*, 384–389.
- Azizan, E. a B., Lam, B.Y.H., Newhouse, S.J., Zhou, J., Kuc, R.E., Clarke, J., Happerfield, L., Marker, A., Hoffman, G.J., and Brown, M.J. (2012a). Microarray, qPCR, and KCNJ5 sequencing of aldosterone-producing adenomas reveal differences in genotype and phenotype between zona glomerulosa- and zona fasciculata-like tumors. *JCEM* *97*, 819–829.
- Azizan, E. a B., Murthy, M., Stowasser, M., Gordon, R., Kowalski, B., Xu, S., Brown, M.J., and O’Shaughnessy, K.M. (2012b). Somatic mutations affecting the selectivity filter of KCNJ5 are frequent in 2 large unselected collections of adrenal aldosteronomas. *Hypertension* *59*, 587–591.
- Azizan, E.A.B., Poulsen, H., Tuluc, P., Zhou, J., Clausen, M. V., Lieb, A., Maniero, C., Garg, S., Bochukova, E.G., Zhao, W., et al. (2013). Somatic mutations in ATP1A1 and CACNA1D underlie a common subtype of adrenal hypertension.
- Baig, S.M., Koschak, A., Lieb, A., Gebhart, M., Dafinger, C., Nürnberg, G., Ali, A., Ahmad, I., Sinnegger-Brauns, M.J., Brandt, N., et al. (2011). Loss of Ca(v)1.3 (CACNA1D) function in a human channelopathy with bradycardia and congenital deafness. *Nat. Neurosci.* *14*, 77–84.
- Barrett, P.Q., Guagliardo, N.A., Klein, P.M., Hu, C., Breault, D.T., and Beenhakker, M.P. (2016). Role of voltage-gated calcium channels in the regulation of aldosterone production from zona glomerulosa cells of the adrenal cortex. *J. Physiol.* *594*, 5851–5860.
- Bergström, M., Bonasera, T. a, Lu, L., Bergström, E., Backlin, C., Juhlin, C., and Långström, B. (1998). In vitro and in vivo primate evaluation of carbon-11-etomidate and carbon-11-metomidate as potential tracers for PET imaging of the adrenal cortex and its tumors. *J. Nucl. Med.* *39*, 982–989.
- Bergström, M., Juhlin, C., Bonasera, T.A., Sundin, A., Rastad, J., Akerström, G., and Långström, B. (2000). PET imaging of adrenal cortical tumors with the 11beta-hydroxylase tracer 11C-metomidate. *J. Nucl. Med.* *41*, 275–282.
- Berthon, A., Sahut-Barnola, I., Lambert-Langlais, S., de Joussineau, C., Damon-Soubeyrand, C., Louiset, E., Taketo, M.M., Tissier, F., Bertherat, J., Lefrançois-Martinez, A.-M., et al. (2010). Constitutive beta-catenin activation induces adrenal hyperplasia and promotes adrenal cancer development. *Hum. Mol. Genet.* *19*, 1561–1576.
- Berthon, A., Drelon, C., Ragazzon, B., Boulkroun, S., Tissier, F., Amar, L., Samson-Couterie, B., Zennaro, M.-C., Plouin, P.-F., Skah, S., et al. (2014). WNT/β-catenin signalling is activated in

aldosterone-producing adenomas and controls aldosterone production. *Hum. Mol. Genet.* **23**, 889–905.

Beuschlein, F., Boulkroun, S., Osswald, A., Wieland, T., Nielsen, H.N., Lichtenauer, U.D., Penton, D., Schack, V.R., Amar, L., Fischer, E., et al. (2013). Somatic mutations in ATP1A1 and ATP2B3 lead to aldosterone-producing adenomas and secondary hypertension. *Nat. Genet.* **45**, 440–444.

Biederer, T. (2006). Bioinformatic characterization of the SynCAM family of immunoglobulin-like domain-containing adhesion molecules. *Genomics* **87**, 139–150.

Biederer, T., Sara, Y., Mozhayeva, M., Atasoy, D., Liu, X., Kavalali, E.T., and Südhof, T.C. (2002). SynCAM, a synaptic adhesion molecule that drives synapse assembly. *Science* (80-). **297**, 1525–1531.

Boles, K.S., Barchet, W., Diacovo, T., Cella, M., and Colonna, M. (2005). The tumor suppressor TSLC1/NECL-2 triggers NK-cell and CD8+ T-cell responses through the cell-surface receptor CRTAM. *Blood* **106**, 779–786.

Boulkroun, S., Beuschlein, F., Rossi, G.P., Golib-Dzib, J.F., Fischer, E., Amar, L., Mulatero, P., Samson-Couterie, B., Hahner, S., Quinkler, M., et al. (2012). Prevalence, clinical, and molecular correlates of KCNJ5 mutations in primary aldosteronism. *Hypertension* **59**, 592–598.

Briet, M., and Schiffrin, E.L. (2010). Aldosterone: Effects on the kidney and cardiovascular system. *Nat. Rev. Nephrol.* **6**, 261–273.

Buraei, Z., and Yang, J. (2010). The β subunit of voltage-gated Ca²⁺ channels. *Physiol. Rev.* **90**, 1461–1506.

Burton, T.J., Mackenzie, I.S., Balan, K., Koo, B., Bird, N., Soloviev, D. V., Azizan, E.A.B., Aigbirhio, F., Gurnell, M., and Brown, M.J. (2012). Evaluation of the Sensitivity and Specificity of 11 C-Metomidate Positron Emission Tomography (PET)-CT for Lateralizing Aldosterone Secretion by Conn's Adenomas. *JCEM* **97**, 100–109.

Cens, T., Restituito, S., Galas, S., and Charnet, P. (1999). Voltage and calcium use the same molecular determinants to inactivate calcium channels. *J. Biol. Chem.* **274**, 5483–5490.

Chang, C.-C., Cao, S., Kang, S., Kai, L., Tian, X., Pandey, P., Dunne, S.F., Luan, C.-H., Surmeier, D.J., and Silverman, R.B. (2010). Antagonism of 4-substituted 1,4-dihydropyridine-3,5-dicarboxylates toward voltage-dependent L-type Ca²⁺ channels Ca V 1.3 and Ca V 1.2. *Bioorg. Med. Chem.* **18**, 3147–3158.

Chien, A.J., Carr, K.M., Shirokov, R.E., Rios, E., and Hosey, M.M. (1996). Identification of palmitoylation sites within the L-type calcium channel beta2a subunit and effects on channel function. *J. Biol. Chem.* **271**, 26465–26468.

Choi, M., Scholl, U.I., Yue, P., Björklund, P., Zhao, B., Nelson-Williams, C., Ji, W., Cho, Y., Patel, A., Men, C.J., et al. (2011). K⁺ channel mutations in adrenal aldosterone-producing adenomas and hereditary hypertension. *Science* (80-). **331**, 768–772.

Cohen, C.J., McCarthy, R.T., Barrett, P.Q., and Rasmussen, H. (1988). Ca channels in adrenal glomerulosa cells: K⁺ and angiotensin II increase T-type Ca channel current. *PNAS* **85**, 2412–

2416.

Conn, J.W. (1955). Primary aldosteronism, a new clinical syndrome. *J. Lab. Clin. Med.* *45*, 3–17.

Faraji, F., Pang, Y., Walker, R.C., Nieves Borges, R., Yang, L., and Hunter, K.W. (2012). *Cadm1* Is a Metastasis Susceptibility Gene That Suppresses Metastasis by Modifying Tumor Interaction with the Cell-Mediated Immunity. *PLoS Genet.* *8*.

Fernandes-Rosa, F.L., Williams, T.A., Riester, A., Steichen, O., Beuschlein, F., Boulkroun, S., Strom, T.M., Monticone, S., Amar, L., Meatchi, T., et al. (2014). Genetic spectrum and clinical correlates of somatic mutations in aldosterone-producing adenoma. *Hypertension* *64*, 354–361.

Fernandes-Rosa, F.L., Daniil, G., Orozco, I.J., Göppner, C., El Zein, R., Jain, V., Boulkroun, S., Jeunemaitre, X., Amar, L., Lefebvre, H., et al. (2018). A gain-of-function mutation in the *CLCN2* chloride channel gene causes primary aldosteronism. *Nat. Genet.* *50*, 355–361.

Findeisen, F., and Minor, D.L. (2009). Disruption of the IS6-AID linker affects voltage-gated calcium channel inactivation and facilitation. *J. Gen. Physiol.* *133*, 327–343.

Fogel, A.I., Li, Y., Giza, J., Wang, Q., Lam, T.K.T., Modis, Y., and Biederer, T. (2010). N-glycosylation at the SynCAM (Synaptic Cell Adhesion Molecule) immunoglobulin interface modulates synaptic adhesion. *J. Biol. Chem.* *285*, 34864–34874.

Fujita, E., Kouroku, Y., Ozeki, S., Tanabe, Y., Toyama, Y., Maekawa, M., Kojima, N., Senoo, H., Toshimori, K., and Momoi, T. (2006). Oligo-astheno-teratozoospermia in mice lacking RA175/TSLC1/SynCAM/IGSF4A, a cell adhesion molecule in the immunoglobulin superfamily. *Mol. Cell. Biol.* *26*, 718–726.

Fujita, E., Dai, H., Tanabe, Y., Zhiling, Y., Yamagata, T., Miyakawa, T., Tanokura, M., Momoi, M.Y., and Momoi, T. (2010). Autism spectrum disorder is related to endoplasmic reticulum stress induced by mutations in the synaptic cell adhesion molecule, *CADM1*. *Cell Death Dis.* *1*, e47.

Fukuhara, H., Kuramochi, M., Fukami, T., Kasahara, K., Furuhata, M., Nobukuni, T., Maruyama, T., Isogai, K., Sekiya, T., Shuin, T., et al. (2002). Promoter methylation of *TSLC1* and tumor suppression by its gene product in human prostate cancer. *Jpn. J. Cancer Res.* *93*, 605–609.

Funder, J.W., Carey, R.M., Fardella, C., Gomez-Sanchez, C.E., Mantero, F., Stowasser, M., Young, W.F., and Montori, V.M. (2008). Case detection, diagnosis, and treatment of patients with primary aldosteronism: an endocrine society clinical practice guideline. *JCEM* *93*, 3266–3281.

Funder, J.W., Carey, R.M., Mantero, F., Murad, M.H., Reincke, M., Shibata, H., Stowasser, M., and Young, W.F. (2016). The Management of Primary Aldosteronism: Case Detection, Diagnosis, and Treatment: An Endocrine Society Clinical Practice Guideline. *J. Clin. Endocrinol. Metab.* *101*, 1889–1916.

Furuno, T., Ito, A., Koma, Y.-I., Watabe, K., Yokozaki, H., Bienenstock, J., Nakanishi, M., and Kitamura, Y. (2005). The spermatogenic Ig superfamily/synaptic cell adhesion molecule mast-cell adhesion molecule promotes interaction with nerves. *J. Immunol.* *174*, 6934–6942.

Galibert, L., Diemer, G.S., Liu, Z., Johnson, R.S., Smith, J.L., Walzer, T., Comeau, M.R., Rauch, C.T., Wolfson, M.F., Sorensen, R.A., et al. (2005). Nectin-like protein 2 defines a subset of T-cell zone dendritic cells and is a ligand for Class-I-restricted T-cell-associated molecule. *J. Biol. Chem.* *280*, 21955–21964.

Ganguly, A. (1992). Cellular origin of aldosteronomas. *Clin. Investig.* *70*, 392–395.

Giangreco, A., Jensen, K.B., Takai, Y., Miyoshi, J., and Watt, F.M. (2009). Necl2 regulates epidermal adhesion and wound repair. *Development* *136*, 3505–3514.

Gomez-Ospina, N., Tsuruta, F., Barreto-Chang, O., Hu, L., and Dolmetsch, R. (2006). The C terminus of the L-type voltage-gated calcium channel Ca(V)1.2 encodes a transcription factor. *Cell* *127*, 591–606.

Gomez-Ospina, N., Panagiotakos, G., Portmann, T., Pasca, S.P., Rabah, D., Budzillo, A., Kinet, J.P., and Dolmetsch, R.E. (2013). A promoter in the coding region of the calcium channel gene CACNA1C generates the transcription factor CCAT. *PLoS One* *8*, e60526.

Gomez-Sanchez, C.E., Qi, X., Velarde-Miranda, C., Plonczynski, M.W., Parker, C.R., Rainey, W., Satoh, F., Maekawa, T., Nakamura, Y., Sasano, H., et al. (2014). Development of monoclonal antibodies against human CYP11B1 and CYP11B2. *Mol. Cell. Endocrinol.* *383*, 111–117.

Gomyo, H., Arai, Y., Tanigami, A., Murakami, Y., Hattori, M., Hosoda, F., Arai, K., Aikawa, Y., Tsuda, H., Hirohashi, S., et al. (1999). A 2-MB sequence-ready contig map and a novel immunoglobulin superfamily gene IGSF4 in the LOH region of chromosome 11q23.2. *Genomics* *62*, 139–146.

Hagiyama, M., Inoue, T., Furuno, T., Iino, T., Itami, S., Nakanishi, M., Asada, H., Hosokawa, Y., and Ito, A. (2013). Increased expression of cell adhesion molecule 1 by mast cells as a cause of enhanced nerve-mast cell interaction in a hapten-induced mouse model of atopic dermatitis. *Br. J. Dermatol.* *168*, 771–778.

Hagiyama, M., Yoneshige, A., Inoue, T., Sato, Y., Mimae, T., Okada, M., and Ito, A. (2015). The intracellular domain of cell adhesion molecule 1 is present in emphysematous lungs and induces lung epithelial cell apoptosis. *J. Biomed. Sci.* *22*, 67.

Hahner, S., Stuermer, A., Kreissl, M., Reiners, C., Fassnacht, M., Haenscheid, H., Beuschlein, F., Zink, M., Lang, K., Allolio, B., et al. (2008). [123I]Iodometomidate for molecular imaging of adrenocortical cytochrome P450 family 11B enzymes. *JCEM* *93*, 2358–2365.

Han, T.S., Walker, B.R., Arlt, W., and Ross, R.J. (2014). Treatment and health outcomes in adults with congenital adrenal hyperplasia. *Nat. Rev. Endocrinol.* *10*, 115–124.

Hardege, I., Xu, S., Gordon, R.D., Thompson, A.J., Figg, N., Stowasser, M., Murrell-Lagnado, R., and O'Shaughnessy, K.M. (2015). Novel Insertion Mutation in KCNJ5 Channel Produces Constitutive Aldosterone Release From H295R Cells. *Mol. Endocrinol.* *29*, 1522–1530.

Hasler, U., Mordasini, D., Bianchi, M., Vandewalle, A., Féraillé, E., and Martin, P.-Y. (2003). Dual influence of aldosterone on AQP2 expression in cultured renal collecting duct principal cells. *J. Biol. Chem.* *278*, 21639–21648.

Hayashida, K., Bartlett, A.H., Chen, Y., and Park, P.W. (2010). Molecular and cellular mechanisms of ectodomain shedding. *Anat. Rec.* *293*, 925–937.

Hell, J.W., Westenbroek, R.E., Breeze, L.J., Wang, K.K., Chavkin, C., and Catterall, W. a (1996). N-methyl-D-aspartate receptor-induced proteolytic conversion of postsynaptic class C L-type calcium channels in hippocampal neurons. *Proc. Natl. Acad. Sci. U. S. A.* *93*, 3362–3367.

Hu, C., Rusin, C.G., Tan, Z., Guagliardo, N.A., and Barrett, P.Q. (2012). Zona glomerulosa cells of the mouse adrenal cortex are intrinsic electrical oscillators. *JCI* *122*, 2046–2053.

Huang, H., Tan, B.Z., Shen, Y., Tao, J., Jiang, F., Sung, Y.Y., Ng, C.K., Raida, M., Köhr, G., Higuchi, M., et al. (2012). RNA editing of the IQ domain in Ca(v)1.3 channels modulates their Ca²⁺-dependent inactivation. *Neuron* *73*, 304–316.

Huang, H., Yu, D., and Soong, T.W. (2013). C-Terminal Alternative Splicing of CaV1.3 Channels Distinctively Modulates Their Dihydropyridine Sensitivity. *Mol. Pharmacol.* *84*, 643–653.

Huang, H., Ng, C.Y., Yu, D., Zhai, J., Lam, Y., and Soong, T.W. (2014). Modest CaV1.342-selective inhibition by compound 8 is β -subunit dependent. *Nat. Comm* *5*, 4481.

Hulme, J.T., Konoki, K., Lin, T.W.-C., Gritsenko, M.A., Camp, D.G., Bigelow, D.J., and Catterall, W.A. (2005). Sites of proteolytic processing and noncovalent association of the distal C-terminal domain of CaV1.1 channels in skeletal muscle. *Proc. Natl. Acad. Sci. U. S. A.* *102*, 5274–5279.

Hulme, J.T., Yarov-Yarovoy, V., Lin, T.W.-C., Scheuer, T., and Catterall, W. a (2006). Autoinhibitory control of the CaV1.2 channel by its proteolytically processed distal C-terminal domain. *J. Physiol.* *576*, 87–102.

Hundemer, G.L., Curhan, G.C., Yozamp, N., Wang, M., and Vaidya, A. (2017). Cardiometabolic outcomes and mortality in medically treated primary aldosteronism: A retrospective cohort study. *Lancet Diabetes Endocrinol.* *6*, 51–59.

Inoue, T., Hagiwara, M., Yoneshige, A., Kato, T., Enoki, E., Maenishi, O., Chikugo, T., Kimura, M., Satou, T., and Ito, A. (2014). Increased ectodomain shedding of cell adhesion molecule 1 from pancreatic islets in type 2 diabetic pancreata: Correlation with hemoglobin A1c levels. *PLoS One* *9*.

Ito, A., Jippo, T., Wakayama, T., Morii, E., Koma, Y., Onda, H., Nojima, H., Iseki, S., and Kitamura, Y. (2003a). SgIGSF: a new mast-cell adhesion molecule used for attachment to fibroblasts and transcriptionally regulated by MITF. *Blood* *101*, 2601–2608.

Ito, A., Ichiyanagi, N., Ikeda, Y., Hagiwara, M., Inoue, T., Kimura, K.B., Sakurai, M.A., Hamaguchi, K., and Murakami, Y. (2012). Adhesion molecule CADM1 contributes to gap junctional communication among pancreatic islet α -cells and prevents their excessive secretion of glucagon. *Islets* *4*, 49–55.

Ito, T., Shimada, Y., Hashimoto, Y., Kaganoi, J., Kan, T., Watanabe, G., Murakami, Y., and Imamura, M. (2003b). Involvement of TSLC1 in progression of esophageal squamous cell carcinoma. *Cancer Res.* *63*, 6320–6326.

Kang, S., Cooper, G., Dunne, S.F., Dusel, B., Luan, C.-H., Surmeier, D.J., and Silverman, R.B. (2012). CaV1.3-selective L-type calcium channel antagonists as potential new therapeutics for Parkinson's disease. *Nat. Comm* *3*, 1146.

Kato, T., Hagiwara, M., Takashima, Y., Yoneshige, A., and Ito, A. (2018). Cell adhesion

molecule-1 shedding induces apoptosis of renal epithelial cells and exacerbates human nephropathies. *Am. J. Physiol. Renal Physiol.* *314*, F388–F398.

Kawano, S., Ikeda, W., Kishimoto, M., Ogita, H., and Takai, Y. (2009). Silencing of ErbB3/ErbB2 signaling by immunoglobulin-like Necl-2. *J. Biol. Chem.* *284*, 23793–23805.

Kim, D.-I., Kang, M., Kim, S., Lee, J., Park, Y., Chang, I., and Suh, B.-C. (2015). Molecular Basis of the Membrane Interaction of the β_2 Subunit of Voltage-Gated Ca^{2+} Channels. *Biophys. J.* *109*, 922–935.

Knoblich, K., Wang, H.X., Sharma, C., Fletcher, A.L., Turley, S.J., and Hemler, M.E. (2014). Tetraspanin TSPAN12 regulates tumor growth and metastasis and inhibits β -catenin degradation. *Cell. Mol. Life Sci.* *71*, 1305–1314.

Koma, Y., Ito, A., Wakayama, T., Watabe, K., Okada, M., Tsubota, N., Iseki, S., and Kitamura, Y. (2004). Cloning of a soluble isoform of the SgIGSF adhesion molecule that binds the extracellular domain of the membrane-bound isoform. *Oncogene* *23*, 5687–5692.

Koma, Y.I., Furuno, T., Hagiwara, M., Hamaguchi, K., Nakanishi, M., Masuda, M., Hirota, S., Yokozaki, H., and Ito, A. (2008). Cell Adhesion Molecule 1 Is a Novel Pancreatic-Islet Cell Adhesion Molecule That Mediates Nerve-Islet Cell Interactions. *Gastroenterology* *134*, 1544–1554.

Kreissl, M.C., Schirbel, A., Fassnacht, M., Haenscheid, H., Verburg, F.A., Bock, S., Saeger, W., Knoedler, P., Reiners, C., Buck, A.K., et al. (2013). ^{123}I iodometomidate imaging in adrenocortical carcinoma. *JCEM* *98*, 2755–2764.

Kuramochi, M., Fukuhara, H., Nobukuni, T., Kanbe, T., Maruyama, T., Ghosh, H.P., Pletcher, M., Isomura, M., Onizuka, M., Kitamura, T., et al. (2001). TSLC1 is a tumor-suppressor gene in human non-small-cell lung cancer. *Nat. Genet.* *27*, 427–430.

Kutner, R.H., Zhang, X.Y., and Reiser, J. (2009). Production, concentration and titration of pseudotyped HIV-1-based lentiviral vectors. *Nat Protoc* *4*, 495–505.

Lai, M.B., Zhang, C., Shi, J., Johnson, V., Khandan, L., McVey, J., Klymkowsky, M.W., Chen, Z., and Junge, H.J. (2017). TSPAN12 Is a Norrin Co-receptor that Amplifies Frizzled4 Ligand Selectivity and Signaling. *Cell Rep.* *19*, 2809–2822.

Leithe, E., Kjenseth, A., Sirnes, S., Stenmark, H., Brech, A., and Rivedal, E. (2009). Ubiquitylation of the gap junction protein connexin-43 signals its trafficking from early endosomes to lysosomes in a process mediated by Hrs and Tsg101. *J. Cell Sci.* *122*, 3883–3893.

Lenzini, L., Rossitto, G., Maiolino, G., Letizia, C., Funder, J.W., and Rossi, G.P. (2015). A meta-analysis of somatic KCNJ5 K^{+} channel mutations in 1636 patients with an aldosterone-producing adenoma. *J. Clin. Endocrinol. Metab.* *100*, E1089–E1095.

Li, J., Zhang, Z., Bidder, M., Funk, M.C., Nguyen, L., Goodfellow, P.J., and Rader, J.S. (2005). IGSF4 promoter methylation and expression silencing in human cervical cancer. *Gynecol. Oncol.* *96*, 150–158.

Lieb, A., Ortner, N., and Striessnig, J. (2014). C-terminal modulatory domain controls coupling of voltage-sensing to pore opening in Cav1.3 L-type Ca^{2+} channels. *Biophys. J.* *106*, 1467–1475.

- Lu, L., Sirish, P., Zhang, Z., Woltz, R.L., Li, N., Timofeyev, V., Knowlton, A. a., Zhang, X.-D., Yamoah, E.N., and Chiamvimonvat, N. (2015). Regulation of Gene Transcription by Voltage-gated L-type Calcium Channel, Cav1.3. *J. Biol. Chem.* *290*, 4663–4676.
- Lung, H.L., Cheng, Y., Kumaran, M.K., Liu, E.T.-B., Murakami, Y., Chan, C.Y., Yau, W.L., Ko, J.M.Y., Stanbridge, E.J., and Lung, M.L. (2004). Fine mapping of the 11q22-23 tumor suppressive region and involvement of TSLC1 in nasopharyngeal carcinoma. *Int. J. Cancer* *112*, 628–635.
- Makhanova, N., Sequeira-Lopez, M.L.S., Gomez, R.A., Kim, H.S., and Smithies, O. (2006). Disturbed homeostasis in sodium-restricted mice heterozygous and homozygous for aldosterone synthase gene disruption. *Hypertension* *48*, 1151–1159.
- Mangoni, M.E., Couette, B., Bourinet, E., Platzer, J., Reimer, D., Striessnig, J., and Nargeot, J. (2003). Functional role of L-type Cav1.3 Ca²⁺ channels in cardiac pacemaker activity. *PNAS* *100*, 5543–5548.
- Marcantoni, A., Vandael, D.H.F., Mahapatra, S., Carabelli, V., Sinnegger-Brauns, M.J., Striessnig, J., and Carbone, E. (2010). Loss of Cav1.3 channels reveals the critical role of L-type and BK channel coupling in pacemaking mouse adrenal chromaffin cells. *J. Neurosci.* *30*, 491–504.
- Márquez-Rosado, L., Singh, D., Rincón-Arano, H., Solan, J.L., Lampe, P.D., Marquez-Rosado, L., Singh, D., Rincon-Arano, H., Solan, J.L., and Lampe, P.D. (2012). CASK (LIN2) interacts with Cx43 in wounded skin and their coexpression affects cell migration. *J. Cell Sci.* *125*, 695–702.
- Masuda, M., Kikuchi, S., Maruyama, T., Sakurai-Yageta, M., Williams, Y.N., Ghosh, H.P., and Murakami, Y. (2005). Tumor suppressor in lung cancer (TSLC)1 suppresses epithelial cell scattering and tubulogenesis. *J. Biol. Chem.* *280*, 42164–42171.
- Masuda, M., Maruyama, T., Ohta, T., Ito, A., Hayashi, T., Tsukasaki, K., Kamihira, S., Yamaoka, S., Hoshino, H., Yoshida, T., et al. (2010). CADM1 interacts with Tiam1 and promotes invasive phenotype of human T-cell leukemia virus type I-transformed cells and adult T-cell leukemia cells. *J. Biol. Chem.* *285*, 15511–15522.
- Mattsson, C., and Young, W.F. (2006). Primary aldosteronism: Diagnostic and treatment strategies. *Nat. Clin. Pract. Nephrol.* *2*, 198–208.
- McGee, A.W., Nunziato, D.A., Maltez, J.M., Prehoda, K.E., Pitt, G.S., and Bredt, D.S. (2004). Calcium channel function regulated by the SH3-GK module in beta subunits. *Neuron* *42*, 89–99.
- Milliez, P., Girerd, X., Plouin, P.F., Blacher, J., Safar, M.E., and Mourad, J.J. (2005). Evidence for an increased rate of cardiovascular events in patients with primary aldosteronism. *J. Am. Coll. Cardiol.* *45*, 1243–1248.
- Mimae, T., Hagiwara, M., Inoue, T., Yoneshige, A., Kato, T., Okada, M., Murakami, Y., and Ito, A. (2014). Increased ectodomain shedding of lung epithelial cell adhesion molecule 1 as a cause of increased alveolar cell apoptosis in emphysema. *Thorax* *69*, 223–231.
- Miranda-Laferte, E., Ewers, D., Guzman, R.E., Jordan, N., Schmidt, S., and Hidalgo, P. (2014). The N-terminal domain tethers the voltage-gated calcium channel β 2e-subunit to the plasma

membrane via electrostatic and hydrophobic interactions. *J. Biol. Chem.* **289**, 10387–10398.

Mizutani, K., Kawano, S., Minami, A., Waseda, M., Ikeda, W., and Takai, Y. (2011). Interaction of nectin-like molecule 2 with integrin $\alpha 6\beta 4$ and inhibition of disassembly of integrin $\alpha 6\beta 4$ from hemidesmosomes. *J. Biol. Chem.* **286**, 36667–36676.

Moiseeva, E.P., Leyland, M.L., and Bradding, P. (2012). CADM1 isoforms differentially regulate human mast cell survival and homotypic adhesion. *Cell. Mol. Life Sci.* **69**, 2751–2764.

Moiseeva, E.P., Roach, K.M., Leyland, M.L., and Bradding, P. (2013). CADM1 Is a Key Receptor Mediating Human Mast Cell Adhesion to Human Lung Fibroblasts and Airway Smooth Muscle Cells. *PLoS One* **8**, 1–8.

Monticone, S., Hattangady, N.G., Nishimoto, K., Mantero, F., Rubin, B., Cicala, M.V., Pezzani, R., Auchus, R.J., Ghayee, H.K., Shibata, H., et al. (2012). Effect of KCNJ5 mutations on gene expression in aldosterone-producing adenomas and adrenocortical cells. *JCEM* **97**, 1567–1572.

Monticone, S., Hattangady, N.G., Penton, D., Isales, C.M., Edwards, M.A., Williams, T.A., Sterner, C., Warth, R., Mulatero, P., and Rainey, W.E. (2013). A novel Y152C KCNJ5 mutation responsible for familial hyperaldosteronism type III. *JCEM* **98**, 1861–1865.

Monticone, S., Else, T., Mulatero, P., Williams, T. a, Rainey, W.E., and Willia (2014). Understanding primary aldosteronism: impact of next generation sequencing and expression profiling. *Mol. Cell. Endocrinol.* **399C**, 311–320.

Monticone, S., Bandulik, S., Stindl, J., Zilbermint, M., Dedov, I., Mulatero, P., Allgaeuer, M., Lee, C.R., Stratakis, C.A., Williams, T.A., et al. (2015). A case of severe hyperaldosteronism caused by a de novo mutation affecting a critical salt bridge Kir3.4 residue. *JCEM* **100**, E114-8.

Monticone, S., D’Ascenzo, F., Moretti, C., Williams, T.A., Veglio, F., Gaita, F., and Mulatero, P. (2017). Cardiovascular events and target organ damage in primary aldosteronism compared with essential hypertension: a systematic review and meta-analysis. *Lancet Diabetes Endocrinol.* **6**, 41–50.

Mulatero, P., Stowasser, M., Loh, K.C., Fardella, C.E., Gordon, R.D., Mosso, L., Gomez-Sanchez, C.E., Veglio, F., and Young, W.F. (2004). Increased diagnosis of primary aldosteronism, including surgically correctable forms, in centers from five continents. *J. Clin. Endocrinol. Metab.* **89**, 1045–1050.

Murakami, Y. (2005). Involvement of a cell adhesion molecule, TSLC1/IGSF4, in human oncogenesis. *Cancer Sci.* **96**, 543–552.

Murakami, Y., Nobukuni, T., Tamura, K., Maruyama, T., Sekiya, T., Arai, Y., Gomyou, H., Tanigami, A., Ohki, M., Cabin, D., et al. (1998). Localization of tumor suppressor activity important in nonsmall cell lung carcinoma on chromosome 11q. *PNAS* **95**, 8153–8158.

Murray, S.A., Davis, K., Fishman, L.M., and Bornstein, S.R. (2000). Alpha1 connexin 43 gap junctions are decreased in human adrenocortical tumors. *J Clin Endocrinol Metab* **85**, 890–895.

Nagara, Y., Hagiya, M., Hatano, N., Futai, E., Suo, S., Takaoka, Y., Murakami, Y., Ito, A., and

- Ishiura, S. (2012). Tumor suppressor cell adhesion molecule 1 (CADM1) is cleaved by a disintegrin and metalloprotease 10 (ADAM10) and subsequently cleaved by γ -secretase complex. *Biochem. Biophys. Res. Commun.* *417*, 462–467.
- Nakahata, S., and Morishita, K. (2012). CADM1/TSLC1 is a novel cell surface marker for adult T-cell leukemia/lymphoma. *J. Clin. Exp. Hematop.* *52*, 17–22.
- Nakamura, Y., Kitada, M., Satoh, F., Maekawa, T., Morimoto, R., Yamazaki, Y., Ise, K., Gomez-Sanchez, C.E., Ito, S., Arai, Y., et al. (2015). Intratumoral heterogeneity of steroidogenesis in aldosterone-producing adenoma revealed by intensive double- and triple-immunostaining for CYP11B2/B1 and CYP17. *Mol. Cell. Endocrinol.* 1–7.
- Namkung, Y., Skrypnik, N., Jeong, M.J., Lee, T., Lee, M.S., Kim, H.L., Chin, H., Suh, P.G., Kim, S.S., and Shin, H.S. (2001). Requirement for the L-type Ca(2+) channel α (1D) subunit in postnatal pancreatic beta cell generation. *JCI* *108*, 1015–1022.
- Nanba, K., Chen, A.X., Omata, K., Vinco, M., Giordano, T.J., Else, T., Hammer, G.D., Tomlins, S.A., and Rainey, W.E. (2016). Molecular Heterogeneity in Aldosterone-Producing Adenomas. *JCEM* jc.2015-3239.
- Nielsen, S., Chou, C.L., Marples, D., Christensen, E.I., Kishore, B.K., and Knepper, M.A. (1995). Vasopressin increases water permeability of kidney collecting duct by inducing translocation of aquaporin-CD water channels to plasma membrane. *Proc. Natl. Acad. Sci. U. S. A.* *92*, 1013–1017.
- Okamura, T., Nakajima, Y., Katano-Toki, A., Horiguchi, K., Matsumoto, S., Yoshino, S., Yamada, E., Tomaru, T., Ishii, S., Saito, T., et al. (2017). Characteristics of Japanese aldosterone-producing adenomas with KCNJ5 mutations. *Endocr. J.* *64*, 39–47.
- Ortner, N.J., Bock, G., Vandael, D.H.F., Mauersberger, R., Draheim, H.J., Gust, R., Carbone, E., Tuluc, P., and Striessnig, J. (2014). Pyrimidine-2,4,6-triones are a new class of voltage-gated L-type Ca(2+) channel activators. *Nat. Comm* *5*, 3897.
- Payet, M.D., Durroux, T., Bilodeau, L., Guillon, G., and Gallo-Payet, N. (1994). Characterization of K⁺ and Ca²⁺ ionic currents in glomerulosa cells from human adrenal glands. *Endocrinology* *134*, 2589–2598.
- Pinggera, A., Lieb, A., Monteleone, S., Brown, M.J., Liedl, K.R., Tuluc, P., and Striessnig, J. (2014). Human Cav1.3 (CACNA1D) calcium channel mutations associated with hyperaldosteronism or autism risk. In Program No. 2012.12 2014 Neuroscience Meeting Planner., p. Available at: <http://www.abstractsonline.com/Plan/>.
- Pinggera, A., Lieb, A., Benedetti, B., Lampert, M., Monteleone, S., Liedl, K.R., Tuluc, P., and Striessnig, J. (2015). CACNA1D de novo mutations in autism spectrum disorders activate Cav1.3 L-type calcium channels. *Biol. Psychiatry* *77*, 816–822.
- Pinggera, A., Mackenroth, L., Rump, A., Schallner, J., Beleggia, F., Wollnik, B., and Striessnig, J. (2017). New gain-of-function mutation shows CACNA1D as recurrently mutated gene in autism spectrum disorders and epilepsy. *Hum. Mol. Genet.* *26*, 2923–2932.
- Platzer, J., Engel, J., Schrott-Fischer, A., Stephan, K., Bova, S., Chen, H., Zheng, H., and Striessnig, J. (2000). Congenital deafness and sinoatrial node dysfunction in mice lacking class

D L-type Ca²⁺ channels. *Cell* 102, 89–97.

Powlson, A.S., Gurnell, M., and Brown, M.J. (2015). Nuclear imaging in the diagnosis of primary aldosteronism. *Curr. Opin. Endocrinol. Diabetes. Obes.* 22, 150–156.

Quinn, S.J., Cornwall, M.C., and Williams, G.H. (1987). Electrical properties of isolated rat adrenal glomerulosa and fasciculata cells. *Endocrinology* 120, 903–914.

Rainey, W.E., Bird, I.M., and Mason, J.I. (1994). The NCI-H295 cell line: a pluripotent model for human adrenocortical studies. *Mol. Cell. Endocrinol.* 100, 45–50.

Rainey, W.E., Saner, K., and Schimmer, B.P. (2004). Adrenocortical cell lines. *Mol. Cell. Endocrinol.* 228, 23–38.

Reimer, E.N., Walenda, G., Seidel, E., and Scholl, U.I. (2016). CACNA1H M1549V mutant calcium channel causes autonomous aldosterone production in HAC15 cells and is inhibited by Mibefradil. *Endocrinology* en.2016-1170.

Rossi, G.P., Bernini, G., Caliumi, C., Desideri, G., Fabris, B., Ferri, C., Ganzaroli, C., Giacchetti, G., Letizia, C., Maccario, M., et al. (2006). A prospective study of the prevalence of primary aldosteronism in 1,125 hypertensive patients. *J. Am. Coll. Cardiol.* 48, 2293–2300.

Samak, G., Narayanan, D., Jaggar, J.H., and Rao, R. (2011). CaV1.3 Channels and Intracellular Calcium Mediate Osmotic Stress-induced N-terminal c-Jun Kinase Activation and Disruption of Tight Junctions in Caco-2 Cell Monolayers. *J. Biol. Chem.* 286, 30232–30243.

Sasaki, H., Nishikata, I., Shiraga, T., Akamatsu, E., Fukami, T., Hidaka, T., Kubuki, Y., Okayama, A., Hamada, K., Okabe, H., et al. (2005). Overexpression of a cell adhesion molecule, TSLC1, as a possible molecular marker for acute-type adult T-cell leukemia. *Blood* 105, 1204–1213.

Satoh, H., Lamb, P.W., Dong, J.T., Everitt, J., Boreiko, C., Oshimura, M., and Barrett, J.C. (1993). Suppression of tumorigenicity of A549 lung adenocarcinoma cells by human chromosomes 3 and 11 introduced via microcell-mediated chromosome transfer. *Mol. Carcinog.* 7, 157–164.

Savard, S., Amar, L., Plouin, P.-F., and Steichen, O. (2013). Cardiovascular Complications Associated With Primary Aldosteronism: A Controlled Cross-Sectional Study. *Hypertension* 62, 331–336.

Scharinger, A., Eckrich, S., Vandael, D.H., Schönig, K., Koschak, A., Hecker, D., Kaur, G., Lee, A., Sah, A., Bartsch, D., et al. (2015). Cell-type-specific tuning of Cav1.3 Ca²⁺-channels by a C-terminal automodulatory domain. *Front. Cell. Neurosci.* 9, 1–18.

Scholl, U.I., Nelson-Williams, C., Yue, P., Grekin, R., Wyatt, R.J., Dillon, M.J., Couch, R., Hammer, L.K., Harley, F.L., Farhi, A., et al. (2012). Hypertension with or without adrenal hyperplasia due to different inherited mutations in the potassium channel KCNJ5. *PNAS* 109, 2533–2538.

Scholl, U.I., Goh, G., Stölting, G., de Oliveira, R.C., Choi, M., Overton, J.D., Fonseca, A.L., Korah, R., Starker, L.F., Kunstman, J.W., et al. (2013). Somatic and germline CACNA1D calcium channel mutations in aldosterone-producing adenomas and primary aldosteronism. *Nat. Genet.* 45, 1050–1054.

Scholl, U.I., Olting, G.S., Nelson-Williams, C., Vichot, A.A., Choi, M., Loring, E., Prasad, M.L.,

- Goh, G., Carling, T., Juhlin, C., et al. (2015). Recurrent gain of function mutation in calcium channel CACNA1H causes early-onset hypertension with primary aldosteronism. *Elife* 4.
- Scholl, U.I., Stölting, G., Schewe, J., Thiel, A., Tan, H., Nelson-Williams, C., Vichot, A.A., Jin, S.C., Loring, E., Untiet, V., et al. (2018). CLCN2 chloride channel mutations in familial hyperaldosteronism type II. *Nat. Genet.*
- Schroder, E., Byse, M., and Satin, J. (2009). L-type calcium channel C terminus autoregulates transcription. *Circ. Res.* 104, 1373–1381.
- Shaikh, L.H., Zhou, J., Teo, A.E.D., Garg, S., Neogi, S.G., Figg, N., Yeo, G.S., Yu, H., Maguire, J.J., Zhao, W., et al. (2015). LGR5 activates non-canonical Wnt-signaling and inhibits aldosterone production in the human adrenal. *JCEM* jc.2015-1734.
- Singh, A., Gebhart, M., Fritsch, R., Sinnegger-Brauns, M.J., Poggiani, C., Hoda, J.-C., Engel, J., Romanin, C., Striessnig, J., and Koschak, A. (2008). Modulation of voltage- and Ca²⁺-dependent gating of CaV1.3 L-type calcium channels by alternative splicing of a C-terminal regulatory domain. *J. Biol. Chem.* 283, 20733–20744.
- Smyth, J.W., and Shaw, R.M. (2013). Autoregulation of connexin43 gap junction formation by internally translated isoforms. *Cell Rep.* 5, 611–618.
- Spät, A. (2004). Glomerulosa cell—a unique sensor of extracellular K⁺ concentration. *Mol. Cell. Endocrinol.* 217, 23–26.
- Spät, A., and Hunyady, L. (2004). Control of aldosterone secretion: a model for convergence in cellular signaling pathways. *Physiol. Rev.* 84, 489–539.
- Stowasser, M., and Gordon, R.D. (2003). Primary aldosteronism. *Best Pract. Res. Clin. Endocrinol. Metab.* 17, 591–605.
- Stowasser, M., and Gordon, R.D. (2016). Primary Aldosteronism: Changing Definitions and New Concepts of Physiology and Pathophysiology Both Inside and Outside the Kidney. *Physiol. Rev.* 96, 1327–1384.
- Surmeier, D.J., Guzman, J.N., Sanchez-Padilla, J., and Goldberg, J.A. (2011). The origins of oxidant stress in Parkinson's disease and therapeutic strategies. *Antioxid. Redox Signal.* 14, 1289–1301.
- Taguchi, R., Yamada, M., Nakajima, Y., Satoh, T., Hashimoto, K., Shibusawa, N., Ozawa, A., Okada, S., Rokutanda, N., Takata, D., et al. (2012). Expression and mutations of KCNJ5 mRNA in Japanese patients with aldosterone-producing adenomas. *J. Clin. Endocrinol. Metab.* 97, 1311–1319.
- Takahashi, S.X., Mittman, S., and Colecraft, H.M. (2003). Distinctive modulatory effects of five human auxiliary β 2 subunit splice variants on L-type calcium channel gating. *Biophys. J.* 84, 3007–3021.
- Teo, A.E.D., Garg, S., Haris Shaikh, L., Zhou, J., Karet Frankl, F.E., Gurnell, M., Happerfield, L., Marker, A., Bienz, M., Azizan, E.A.B., et al. (2015). Pregnancy, Primary Aldosteronism, and Adrenal CTNNB1 Mutations. *N. Engl. J. Med.* 150923140040009.
- Tunny, T.J., Gordon, R.D., Klemm, S. a, and Cohn, D. (1991). Histological and biochemical

distinctiveness of atypical aldosterone-producing adenomas responsive to upright posture and angiotensin. *Clin. Endocrinol. (Oxf)*. *34*, 363–369.

Vallath, S., Sage, E.K., Kolluri, K.K., Lourenco, S.N., Teixeira, V.S., Chimalapati, S., George, P.J., Janes, S.M., and Giangreco, A. (2016). CADM1 inhibits squamous cell carcinoma progression by reducing STAT3 activity. *Sci. Rep.* *6*, 24006.

Wakayama, T., Ohashi, K., Mizuno, K., and Iseki, S. (2001). Cloning and characterization of a novel mouse immunoglobulin superfamily gene expressed in early spermatogenic cells. *Mol. Reprod. Dev.* *60*, 158–164.

Wakayama, T., Koami, H., Ariga, H., Kobayashi, D., Sai, Y., Tsuji, A., Yamamoto, M., and Iseki, S. (2003). Expression and functional characterization of the adhesion molecule spermatogenic immunoglobulin superfamily in the mouse testis. *Biol. Reprod.* *68*, 1755–1763.

Wakayama, T., Sai, Y., Ito, A., Kato, Y., Kurobo, M., Murakami, Y., Nakashima, E., Tsuji, A., Kitamura, Y., and Iseki, S. (2007). Heterophilic binding of the adhesion molecules poliovirus receptor and immunoglobulin superfamily 4A in the interaction between mouse spermatogenic and Sertoli cells. *Biol. Reprod.* *76*, 1081–1090.

Wang, B., Li, X., Zhang, X., Ma, X., Chen, L., Zhang, Y., Lyu, X., Tang, Y., Huang, Q., Gao, Y., et al. (2015). Prevalence and Characterization of Somatic Mutations in Chinese Aldosterone-Producing Adenoma Patients. *Medicine (Baltimore)*. *94*, e708.

van der Weyden, L., Arends, M.J., Chausiaux, O.E., Ellis, P.J., Lange, U.C., Surani, M.A., Affara, N., Murakami, Y., Adams, D.J., and Bradley, A. (2006). Loss of TSLC1 Causes Male Infertility Due to a Defect at the Spermatid Stage of Spermatogenesis. *Mol. Cell. Biol.* *26*, 3595–3609.

Willenberg, H.S., Schott, M., Saeger, W., Tries, A., Scherbaum, W.A., and Bornstein, S.R. (2006). Expression of connexins in chromaffin cells of normal human adrenals and in benign and malignant pheochromocytomas. *Ann. N. Y. Acad. Sci.* *1073*, 578–583.

Williams, M.E., Feldman, D.H., McCue, A.F., Brenner, R., Velicelebi, G., Ellis, S.B., and Harpold, M.M. (1992). Structure and functional expression of $\alpha 1$, $\alpha 2$, and β subunits of a novel human neuronal calcium channel subtype. *Neuron* *8*, 71–84.

Williams, T.A., Monticone, S., Morello, F., Liew, C.C., Mengozzi, G., Pilon, C., Asioli, S., Sapino, A., Veglio, F., and Mulatero, P. (2010). Teratocarcinoma-derived growth factor-1 is upregulated in aldosterone-producing adenomas and increases aldosterone secretion and inhibits apoptosis in vitro. *Hypertension* *55*, 1468–1475.

Wu, V.C., Huang, K.H., Peng, K.Y., Tsai, Y.C., Wu, C.H., Wang, S.M., Yang, S.Y., Lin, L.Y., Chang, C.C., Lin, Y.H., et al. (2015). Prevalence and clinical correlates of somatic mutation in aldosterone producing adenoma-Taiwanese population. *Sci. Rep.* *5*, 1–10.

Wu, V.C., Wang, S.M., Chueh, S.C.J., Yang, S.Y., Huang, K.H., Lin, Y.H., Wang, J.J., Connolly, R., Hu, Y.H., Gomez-Sanchez, C.E., et al. (2017). The prevalence of CTNNB1 mutations in primary aldosteronism and consequences for clinical outcomes. *Sci. Rep.* *7*, 1–10.

Xie, C.B., Shaikh, L.H., Garg, S., Tanriver, G., Teo, A.E.D., Zhou, J., Maniero, C., Zhao, W., Kang, S., Silverman, R.B., et al. (2016). Regulation of aldosterone secretion by Cav1.3. *Sci. Rep.* *6*, 24697.

- Xu, W., and Lipscombe, D. (2001). Neuronal Ca(V)1.3 α (1) L-type channels activate at relatively hyperpolarized membrane potentials and are incompletely inhibited by dihydropyridines. *J. Neurosci.* *21*, 5944–5951.
- Yageta, M., Kuramochi, M., Masuda, M., Fukami, T., Fukuhara, H., Maruyama, T., Shibuya, M., and Murakami, Y. (2002). Direct association of TSLC1 and DAL-1, two distinct tumor suppressor proteins in lung cancer. *Cancer Res.* *62*, 5129–5133.
- Yamada, D., Yoshida, M., Williams, Y.N., Fukami, T., Kikuchi, S., Masuda, M., Maruyama, T., Ohta, T., Nakae, D., Maekawa, A., et al. (2006). Disruption of spermatogenic cell adhesion and male infertility in mice lacking TSLC1/IGSF4, an immunoglobulin superfamily cell adhesion molecule. *Mol. Cell. Biol.* *26*, 3610–3624.
- Yamaguchi, H., Okuda, M., Mikala, G., Fukasawa, K., and Varadi, G. (2000). Cloning of the β 2a subunit of the voltage-dependent calcium channel from human heart: cooperative effect of α 2 δ and β 2a on the membrane expression of the α 1C subunit. *Biochem. Biophys. Res. Commun.* *267*, 156–163.
- Yoneshige, A., Hagiya, M., Inoue, T., Mimae, T., Kato, T., Okada, M., Enoki, E., and Ito, A. (2015). Increased ectodomain shedding of cell adhesion molecule 1 as a cause of type II alveolar epithelial cell apoptosis in patients with idiopathic interstitial pneumonia. *Respir. Res.* *16*, 1–12.
- Young, W.F. (2003). Minireview: Primary Aldosteronism—Changing Concepts in Diagnosis and Treatment. *Endocrinology* *144*, 2208–2213.
- Young, W.F. (2007). Primary aldosteronism: Renaissance of a syndrome. *Clin. Endocrinol. (Oxf)*. *66*, 607–618.
- Zheng, F.-F., Zhu, L.-M., Nie, A.-F., Li, X.-Y., Lin, J.-R., Zhang, K., Chen, J., Zhou, W.-L., Shen, Z.-J., Zhu, Y.-C., et al. (2015). Clinical Characteristics of Somatic Mutations in Chinese Patients With Aldosterone-Producing Adenoma. *Hypertension* *65*, 622–628.
- Zhiling, Y., Fujita, E., Tanabe, Y., Yamagata, T., Momoi, T., and Momoi, M.Y. (2008). Mutations in the gene encoding CADM1 are associated with autism spectrum disorder. *Biochem. Biophys. Res. Commun.* *377*, 926–929.
- Zhou, J., Shaikh, L.H., Neogi, S.G., McFarlane, I., Zhao, W., Figg, N., Brighton, C. a., Maniero, C., Teo, A.E.D., Azizan, E. a B., et al. (2015). DACH1, a Zona Glomerulosa Selective Gene in the Human Adrenal, Activates Transforming Growth Factor- β Signaling and Suppresses Aldosterone Secretion. *Hypertension* *65*, 1103–1110.